IDAHO TRANSPORTATION DEPARTMENT

RESEARCH REPORT

Combining In-situ and Remote Sensing-Based Monitoring Methods to Improve the Efficiency and Accuracy of Landslide Monitoring Activities

RP 311

By

Donna M. Delparte, Ph.D., James Mahar, Ph.D., LPG, PG, PHG,

Ashley Butterworth, B.S., Matt Belt, M.S., Betty Brown, B.S., Dana Drinkall, M.S.

Idaho State University

Prepared for

Idaho Transportation Department

ITD Research Program, Planning and Development Services

Highways Division

April 2025

Disclaimer

This document is disseminated under the sponsorship of the Idaho Transportation Department and the United States Department of Transportation in the interest of information exchange. The State of Idaho and the United States Government assume no liability of its contents or use thereof.

The contents of this report reflect the view of the authors, who are responsible for the facts and accuracy of the data presented herein. The contents do not necessarily reflect the official policies of the Idaho Transportation Department or the United States Department of Transportation.

The State of Idaho and the United States Government do not endorse products or manufacturers. Trademarks or manufacturers' names appear herein only because they are considered essential to the object of this document.

This report does not constitute a standard, specification or regulation.

Technical Report Documentation Page

1. Report No. FHWA-ID-25-311	2. Government Accession No.	3. Recipient's Catalog No.
4. Title and Subtitle Combining In-situ and Remote Sensing-Based Monitoring Methods to Improve the Efficiency and Accuracy of Landslide Monitoring Activities		5. Report Date February 2025 6. Performing Organization Code RP311
7. Author(s): Donna M. Delparte, https://orcid.org/0000-0002-9107-5117 James Mahar, https://orcid.org/0009-0000-1751-9712 Ashley Butterworth, https://orcid.org/0009-0006-6114-2127 Matt Belt, https://orcid.org/0000-0003-0372-1260 Dana Drinkall, https://orcid.org/0000-0003-2107-6429 Betty Brown, https://orcid.org/0009-0009-7436-8389		8. Performing Organization Report No. Fund: 220572 Index: RGEO4G
9. Performing Organization Name and Address Idaho State University 921 S 8th Ave, Pocatello, ID 83209		10. Work Unit No. (TRAIS) 11. Contract or Grant No. T002986
12. Sponsoring Agency Name and Address Idaho Transportation Department (SPR) Highways Division, Planning and Development Services, Research Program PO Box 7129 Boise, ID 83707-7129		13. Type of Report and Period Covered [Final or Interim] Report 05/08/2023 - 02/08/2025 14. Sponsoring Agency Code RP-311
15. Supplementary Notes Project performed in cooperation with the Idaho Transportation Department and Federal Highway Administration.		
16. Abstract Repeat LiDAR or photogrammetry surveys for conducting temporal and spatial studies of mass movements are an emerging part of landslide hazard monitoring research, including the use of sensors aboard small Unmanned Aircraft Systems (UAS). The ability to measure change at a site over time can be an important asset in identifying slopes that pose a significant hazard to people and infrastructure, especially when paired with on-site inclinometer data. Data acquisition of LiDAR with UAS provides numerous benefits compared to other traditional airborne or terrestrial platforms. Our overall research approach was to collect and integrate geotechnical, landslide geometry, displacement, weather and surface site condition data with UAS remotely sensed data for evaluation of landslide hazards at four landslide areas. Accurate repeat LiDAR studies can be difficult to achieve due to inherent issues from using different platforms and sensors including the use of different vertical datum such as geoids or ellipsoid reference systems, poor co-registration of flightlines, differences in data quality, resolution, or georeferencing software, classification changes, and changes in post processing steps. This study provides recommendations for data acquisition and processing protocols to overcome registration limitations, reduce uncertainty in change detection models, and describe best practices for monitoring landslide movement and characterization.		
17. Key Words Landslides, change detection, Unmanned Aircraft Systems, UAS, M3C2, LiDAR, photogrammetry	18. Distribution Statement Copies available from the ITD Research Program	
19. Security Classification (of this report) Unclassified	20. Security Classification (of this page) Unclassified	21. No. of Pages 167 / 22. Price None

Acknowledgments

The authors gratefully acknowledge Idaho Transportation Department's Research Program for the funding that made this project possible. In addition, we thank the Technical Advisory Committee for their input and suggestions during the project.

Technical Advisory Committee

Each research project is overseen by a Technical Advisory Committee (TAC), which is led by an Idaho Transportation Department (ITD) project sponsor and project manager. The TAC is responsible for monitoring project progress, reviewing deliverables, ensuring that study objectives are met, and facilitating implementation of research recommendations, as appropriate. ITD's Research Program Manager appreciates the work of the following TAC members in guiding this research study.

- Project Sponsor: Chad Clawson, P.E., State Construction & Materials Engineer
- Project Manager: Shawn Enright, P.G., Engineering Geologist, ITD District Six

TAC Members:

- Greydon Wright, P.E., Operations Manager, ITD District Five
- Nikolas Stevens, P.G., Engineering Geologist, ITD District One
- Anne Rector, GIS Analyst II, ITD District Six
- Jet Johnstone, Geographic Information Systems Analyst III, ITD HQ GIS
- Mark Hayes, P.E., Staff Engineer Res A, ITD District Six
- Tyler Coy, P.E., Geotechnical Engineer, ITD HQ
- Amanda Laib, Senior Research Analyst, ITD Research Program
- Darrell Hanners, P.L.S., Land Surveyor, ITD District Five
- Garrett Speeter, P.G., Geologist, ITD District Two
- Zach Lifton, Ph.D., P.G., Hazards Geologist, Idaho Geological Survey
- FHWA-Idaho Advisor: Ed Miltner, P.E., Structures Engineer, FHWA- Idaho Division

Table of Contents

List of Tables

List of Figures

List of Abbreviations and Acronyms

23 CFR 420	Code of Federal Regulations, Title 23, Part 420
AGL	Above Ground Level
C2C	Cloud to Cloud Distance Calculation
C2M	Cloud-to-Mesh Distance Calculation
D2M	Quantum System's oblique five camera system
FAA	Federal Aviation Administration
FHWA	Federal Highway Administration
FOV	Field of View
GCP	Ground Control Point
GPS	Global Positioning System
IMU	Inertial Measurement Unit
ISU	Idaho State University
ITD	Idaho Transportation Department
NDAA	National Defense Authorization Act
M3C2	Multiscale Model-to-Model Cloud Comparison
PPK	Post Processed Kinematic
RD&T	Research, development, and technology transfer
RGB	Red, green, blue optical camera
RMS	Root Mean Square
SP&R	State Planning & Research (FHWA)
SfM	Structure from Motion
TAC	Technical Advisory Committee
UAS	Unmanned Aircraft Systems
UAV	Unmanned Aerial Vehicle
USCS	Unified Soil Classification System
USGS	United States Geological Survey
VTOL	Vertical Takeoff and Landing

Executive Summary

Idaho State University (ISU), in collaboration with Idaho Transportation Department (ITD), conducted a comprehensive research study aimed at enhancing the monitoring and management of landslide hazards that threaten critical transportation infrastructure. The focus of this report was the integration of in-situ geotechnical instrumentation with advanced remote sensing technologies to develop a more precise, efficient, and cost-effective approach for assessing slope instability along transportation corridors. With landslides posing ongoing threats to infrastructure, public safety, and economic stability, the research investigated how combining traditional ground-based measurements with Unmanned Aircraft Systems (UAS) equipped with LiDAR and photogrammetry sensors can improve early detection and hazard assessment and track slope instability.

Field investigations were conducted at landslide-prone sites across southeastern Idaho, with sites selected based on historical movement, geological diversity, vegetation cover, and existing ITD instrumentation. At each location, repeated UAS surveys generated high-resolution topographic data, that were analyzed alongside ground-based inclinometer measurements, prior UAS LiDAR datasets and LiDAR acquired from manned aircraft. A suite of change detection methods – including DEM differencing (DoD), cloud-to-cloud (C2C), cloud-to-mesh (C2M), and Multiscale Model-to-Model Cloud Comparison (M3C2) – were utilized to quantify surface movement over time and ensure the accuracy of the data.

The findings underscore the value of UAS-based LiDAR for landslide monitoring, particularly its ability to deliver detailed terrain data at low cost and risk while accessing otherwise hazardous or remote areas. To overcome challenges associated with aligning multi-temporal datasets, especially when comparing different sensor types or coordinate systems, this research offers standardized workflows for data acquisition, processing, and co-registration. These workflows offer a repeatable and scalable framework for future monitoring efforts.

A key recommendation from this report is the implementation of routine annual UAS surveys at all identified landslide-prone areas, with increased monitoring frequency at high-risk sites. Notably, the Swan Valley East site was identified as an area of immediate concern due to ongoing surface movement and the absence of a dewatering system. The researchers recommend the installation of dewatering wells and continued monitoring to reduce the risk of future instability. UAS observations played a crucial role in identifying this issue during the relatively short duration of the study.

This project highlights the importance of integrating advanced remote sensing technologies with traditional geotechnical monitoring to support more resilient infrastructure planning and public safety initiatives. Building internal capacity within ITD to acquire, manage, process, and interpret remote sensing data—alongside establishing standardized procedures—will be essential for ensuring long-term geohazard preparedness and effective infrastructure management.

1. Introduction

Background

Recognizing, monitoring, and mitigating landslide risks is crucial for developing effective strategies in prediction, mitigation, and response against their potentially devastating consequences, especially along transportation corridors. Landslides, according to the United States Geological Survey (USGS) Landslide Handbook (2008), are the downslope movement of organic material, soil, and rock due to gravity. This phenomenon ranges from minor rockfalls to colossal events with the power to reshape entire landscapes (Campforts et al. 2022). Landslides vary in their occurrence and magnitude and can be triggered by various factors. Geological conditions play an essential role, with the composition and structure of the terrain impacting slope stability. Climatic elements, such as heavy rainfall or rapid snowmelt, can also trigger landslide events. Human activities, categorized as anthropogenic influences, can contribute to or increase landslide risks, thereby emphasizing the interplay between nature and human impact on the stability of slopes (Kaushal et al. 2025).

The susceptibility of an area to landslides is influenced by geological factors such as rock type, soil composition, thickness of and type of underlying unconsolidated materials, and slope gradient. Competent rocks are commonly less susceptible to mass movement than unconsolidated materials such as alluvium (Sarkar and Kanungo 2004; Wachal and Hudak 2000). This is due to unconsolidated materials generally having less friction and cohesion which allows greater infiltration of water, thereby reducing the shear strength (Wachal and Hudak 2000). Low-cohesion sand, gravel, and clay compositions are particularly vulnerable to landslides due to a combination of factors including friction between particles, attraction between particles, density of particle packing, moisture content and historical stresses when compared to high-cohesion materials such as solid rock (Yu et al. 2021). Additionally, the slope gradient of an area is a critical factor in assessing landslide potential. Steeper slopes inherently pose a greater susceptibility to mass movements, as the gravitational force is stronger when compared to lower angle slopes. Understanding these geological intricacies is essential for accurately evaluating and predicting landslide susceptibility to reduce potential risk by informed decision-making in land use planning.

Recognizing the diverse range of natural triggers underscores the dynamic and interconnected nature of landslide occurrences, highlighting the importance of a comprehensive approach to understanding and mitigating landslide events. Various natural factors, including but not limited to, heavy rainfall, earthquakes, volcanic eruptions, fire, snowmelt, and fluctuations in groundwater levels can function as triggers for landslides. Intense rainfall, for instance, has the capacity to saturate the soil, reducing its stability and consequently inducing landslides (Sidle and Bogaard 2016). Earthquakes, on the other hand, can cause widespread mass movements of soil and rock (Youd 1985). Volcanic eruptions contribute to landslide risk by releasing ash and other debris which can alter terrain stability by loading extra material to a slope or increasing its slope angle (Schuster and Wieczorek 2018). Fire disturbance can remove stabilizing vegetative cover, heightening the potential for landslide activity (Rengers et al. 2020). Snowmelt and shifts in groundwater levels saturate the soil, causing instability (Miao et al. 2019).

Human activities also contribute to slope instability: deforestation, extraction, mining, road construction, and improper land use are the main determinants. Deforestation, for instance, can result

in soil erosion and the depletion of vegetation cover, rendering slopes more vulnerable to landslides (Alexander 1992). Mining activities weaken the structural integrity of both soil and rock thus increasing instability leading to landslide events (Pankow et al. 2014). Roadway construction projects on marginally stable slopes can undermine, overload, or increase filtration that can contribute to landslide events (Swanson and Dyrness 1975; Tanyaş et al. 2022). These anthropogenic factors emphasize the need for sustainable land management practices and responsible development to mitigate the natural and human-induced factors contributing to slope instability and associated landslide hazards.

Motivation

Highways constitute vital elements within the transportation network, serving as crucial links between cities, towns, and key destinations. They facilitate the movement of people, goods, and vehicles across large distances, contributing significantly to various societal and economic functions. Despite their importance, highways are susceptible to devastating impacts from landslides, which can impede or block roadways, disrupting regular traffic flow, and causing road closures. This, in turn, leads to delays, diversions, and challenges for both commuters and transportation services. Landslides can thus hinder the movement of people and goods, which can negatively influence business and agricultural production (Kjekstad and Highland 2009; Schuster and Highland 2001). Businesses reliant on the affected transportation routes may encounter disruptions in their supply chains, impacting trade and commerce.

On average, landslides annually cause around 25 deaths and 1.5 billion dollars of damage a year to infrastructure across the United States (Tetra Tech 2023), although the figure can vary widely from year to year (Froude and Petley 2018; Mirus et al. 2020). Critical infrastructure and transportation routes across the US are at risk from these dangerous and potentially deadly geohazards. Additionally, landslides pose a threat to the integrity of road infrastructure, including pavement, bridges, and culverts. The force exerted by shifting soil and rock can cause extensive damage to road surfaces and compromise supporting structures, demanding extensive repairs and maintenance efforts. These repairs incur extra costs and potential disruptions in the availability of transportation routes (Frazier and Nichols 2015; Tetra Tech 2023). Unstable terrain increases the likelihood of accidents, injuries, damages, or even fatalities for motorists, pedestrians, and nearby structures. Prioritizing the safety of individuals traveling on highways affected by landslides is paramount.

Unmanned Aircraft Systems (UAS), commonly referred to as drones, are now widely used to survey natural phenomena including landslides (Sun et al. 2024). One of the primary advantages of UAS lies in their ability to enhance cost efficiency. UAS are useful across a diverse range of applications, leveraging their capability to access remote or hazardous areas, collect data, and execute tasks that were once considered impossible or impractical. UAS and advanced sensors are becoming indispensable in landslide detection and prevention efforts (Syzdykbayev, Karimi, and Karimi 2020; Eker, Aydın, and Hübl 2018; Booth, McCarley, and Nelson 2020; Hung et al. 2019). Equipped with remote sensing and imaging technologies, drones can survey and analyze terrains prone to landslides, facilitating early detection and allowing for timely intervention. This capability enhances the overall effectiveness of landslide prevention strategies and contributes to minimizing the potential impact on communities and ecosystems.

Sensors, such as LiDAR, have revolutionized geohazard modeling, monitoring, and management (Zielke 2024). High resolution LiDAR point cloud data has the ability to penetrate vegetation with multiple returns, which is useful for studying hazards such as mass movements (Jaboyedoff et al. 2012). The multi-return nature of LiDAR compared to single return sensors (i.e., RGB photogrammetry) allows the sensor to penetrate vegetation and reveal the topography below. Furthermore, repeat LiDAR surveys for temporal and spatial studies of mass movements have been a growing part of landslide hazard monitoring research, such as the use of LiDAR sensors aboard UAS (Hung et al. 2019; Stumvoll et al. 2022; Sun et al. 2024). The ability to measure change at a site over a period of years, as multiple studies have shown (Mora et al. 2018; Booth, McCarley, and Nelson 2020; Hung et al. 2019), can be an important asset in identifying slopes that pose a significant hazard to people and infrastructure.

Project Goals

The overarching goal of this project was to assess the feasibility and benefits of monitoring landslide activity through the integration of in-situ instrumentation and using best practices for remote sensing. The research approach was to collect and integrate geotechnical, landslide geometry, displacement, weather and surface site condition data for evaluation of landslide hazards that could impact Idaho Transportation Department (ITD) assets at four landslide areas identified by the study team and ITD. The initial stage of the investigation allowed our team to research and catalogue the existing site-specific data in ArcGIS Pro software, including detailed maps of the surface topography along with scarps, vegetation and seepage areas to complete the initial site evaluation and landslide characterization of the site. The geotechnical data included soil and rock types, geologic structures, groundwater conditions, and seismicity at the site. The intent was to develop a model of the existing subsurface conditions both inside and outside the areas of movement, including site-specific surface/borehole information available from ITD. Periodic site visits were made for repeat UAS surveys to assess changes in slope conditions. ITD partners collected instrumentation data so that our team could create displacement/time plots related to ground motion/precipitation data. Pairing this data was helpful in assessing the present and future stability of a slope. We have modeled the geometry of the landslide study areas including 3-dimensional projections of the landslide and summarized/superimposed the available displacement/geotechnical data. Despite the growth in use of UAS for remote sensing observations, there is no standardized approach and limited guidance for selecting the best platform, sensors, processing software, etc. to monitor landslide susceptible slopes. Furthermore, there are limited studies on how to pair in-situ instrumentation with remotely sensed information from UAS.

Specifically, the following objectives from the ITD project RFP were to:

a) Compare in-situ landslide movement measurements with remote sensing-based measurements.

b) Develop realistic accuracy estimates for remote sensing-based change detection.

c) Create a list of remote sensing tools and their applications for a given landslide scenario.

d) Research and summarize best practices and recommendations for using remote sensing tools alongside in-situ instrumentation to reduce costs and improve public safety.

e) Develop a list of minimum processing and quality criteria for various data types (e.g., publicly available LIDAR, UAS photogrammetry, UAS LIDAR, and thermal imagery) for the purpose of remote monitoring of landslide movement and characterization.

2. Landslide Investigation Using UAS and Remote Sensing

Unmanned Aircraft Systems (UAS) and Landslide Mapping and Monitoring

Data acquisition with UAS provides numerous benefits compared to other traditional airborne or terrestrial platforms. A UAS can not only autonomously fly more remote and hazardous sites, thereby avoiding exposure of personnel to potential dangers, but it is also a more efficient and cost-effective platform than airplanes or satellites (Hung et al. 2019). Airborne platforms are more expensive to operate due to aviation fuel costs and aviator fees; as well as requiring higher flight altitudes and more time for flight planning (Carey et al. 2019; Resop, Lehmann, and Cully Hession 2019). Whereas, a UAS flight is more flexible to schedule, is compact for travel to areas far from an airport, relies on rechargeable batteries instead of aviation fuel, and often has lower remote pilot fees since the remote pilot certification is quicker and cheaper to obtain than a pilot's license (Carey et al. 2019).

Despite the increase in UAS LiDAR data availability and reduction in sensor size, accurate repeat LiDAR studies can be difficult to achieve as the technology changes over time and the sensors and georeferencing techniques evolve. Using older, already collected and processed UAS LiDAR or manned aircraft LiDAR data poses numerous problems with vendors who typically use their own proprietary processing methods, making alignment of point clouds difficult (Okyay et al. 2019; Booth, McCarley, and Nelson 2020; Cucchiaro et al. 2020). These inherent issues from using different platforms and sensors include the use of different vertical datum such as geoids or ellipsoid reference systems, poor co-registration of flightlines, differences in data quality, resolution, or georeferencing software, classification changes, and changes in post processing steps (Schaffrath, Belmont, and Wheaton 2015; Okyay et al. 2019; Cucchiaro et al. 2020). Intrinsic differences such as these can lead to problems with vertical or horizontal biases and poor uncertainty measurements that under or overestimating change, which is a concern when studying geohazards (Schaffrath, Belmont, and Wheaton 2015; Bernard, Lague, and Steer 2021).

Projects using existing LiDAR data such as Booth et al.'s (2020) landslide study in California, often encounter these problems, necessitating the reprocessing of datasets and their alignment to avoid critical errors. One method of correcting differing geoid or ellipsoid issues is to calculate the difference between the two using software tools developed by the National Oceanic and Atmospheric Administration's (NOAA). The National Geodetic Survey (NGS) Coordinate Conversion and Transformation Tool (NCAT) and the vertical datum transformation tool (vdatum) that allows for point data transformation between coordinate systems (Cooper et al. 2013; Schaffrath, Belmont, and Wheaton 2015). To check for horizontal bias, x and y coordinates of well-defined structures can be identified in both datasets to see how well they match up (Schaffrath, Belmont, and Wheaton 2015). However, there are issues with this solution at sites where ground control points cannot be used, either due to dense vegetation or hazardous conditions. Another common issue in repeat LiDAR studies that affects the accuracy of the measurements is different threshold models to quantify uncertainty. A common correction is to use a spatially variable error model that combines the influence of various parameters such as point density and slope into a fuzzy inference system. This system of quantifying

uncertainty in a model differs from a rule-based system since the input and output categories are represented as fuzzy numbers, allowing overlap in areas of ambiguity (Schaffrath, Belmont, and Wheaton 2015).

Even after reprocessing LiDAR data with the same georeferencing system, poor co-registration of the flights can still cause alignment issues (Schaffrath, Belmont, and Wheaton 2015; Daehne and Corsini 2013). The issue of poor co-registration has multiple solutions; the common way to address this problem is to use the original GPS ground control or equivalent points and LiDAR data to recalibrate the new raw data (Corsini et al. 2013; Schaffrath, Belmont, and Wheaton 2015). Other common tools to correct for co-registration used in repeat LiDAR studies include a Bayesian approach to realign the flight strips for both flights, the mathematical Generalized Procrustes Analysis, or the plane structure based 4-point Congruent sets technique (Cucchiaro et al. 2020; Fotsing, Nziengam, and Bobda 2020; BayesMap Solutions LLC 2020). In areas where ground control points cannot be placed, recalibration can be difficult. There are multiple algorithms that can be used for the registration of point clouds without ground control points. Methods such as the "Align" tool in Cloud Compare require the user to manually identify multiple sets of equivalent points before a fine registration (iterative closest point algorithm) can be used (CloudCompare 2016; Kuçak, Erol, and Erol 2022; Booth et al. 2018; Cucchiaro et al. 2020; Gressin et al. 2013).

While these common issues with repeat LiDAR are briefly discussed in studies, the detailed procedures for reprocessing and aligning UAS LiDAR, UAS photogrammetry point clouds, or manned aircraft LiDAR are often missing. This lack of standardized procedures for processing and co-registering UAS LiDAR data can make repeat LiDAR efforts using older datasets incredibly difficult (Eitel et al. 2016; Cucchiaro et al. 2020). In this study, we strive to create an accurate and repeatable workflow for processing LiDAR data to measure change at mass movement sites.

Pre-Flight Field Data Gathering

Survey and Ground Control

Ground control points are necessary to georeference geospatial products such as photogrammetry and LiDAR surveys. Image-space coordinates collected by scanners are transformed to an absolute coordinate system through known locations of ground control points (GCPs) (Westoby et al., 2012). GCPs are features clearly visible in point cloud surveys and exist as two types:

1. Permanent

Permanent ground control points are stationary objects that consist of clearly defined intersections or points. Examples include building corners, road intersections, or survey benchmarks. Surveys collected in this study utilize observation wells and benchmarks as other permanent ground control points.

2. Temporary

Suitable permanent ground control points may not exist in certain survey sites, such as in remote or rural areas. Temporary targets can be placed for ground control at any desired location within the

survey site. Targets used in this study are high-contrast mesh squares with defined centroids that are easy to detect in point cloud surveys (Figure 2.1). For LiDAR surveys, the LiDAR Mesh targets (Figure 2.1) are easily identifiable in LiDAR point clouds and aid in alignment and registration.

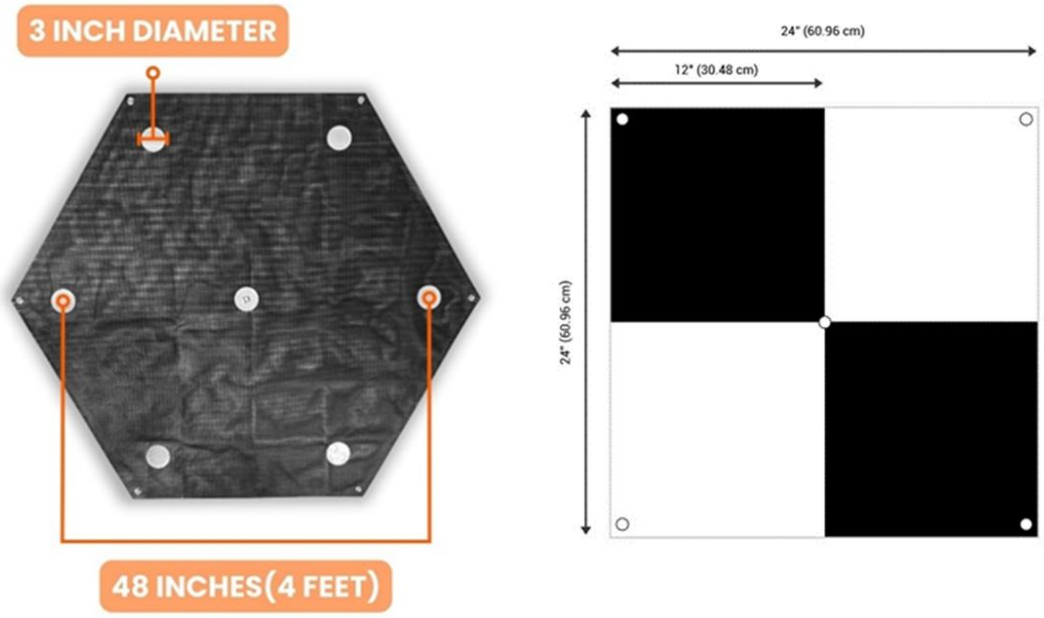

Figure 2.1 Temporary Ground Control Targets. LiDAR Mesh Target (left) and Checkered UAS Ground Control (right) from Sky High Bull's-Eye, Birmingham, Alabama

While only four GCPs are generally required for georeferencing, additional GCPs will typically yield greater accuracy. In this study a combination of permanent GCPs (where applicable) and multiple temporary GCPs were utilized. GCPs for topographic surveys should prioritize placement of survey points across the vertical range of terrain features (i.e. placements that include lowest and highest elevations) and typically be placed in the shape of a die or with a minimum of corner extents covered (James et al. 2017; Davidson et al. 2019; Awasthi et al. 2020; Zimmerman, Jansen, and Miller 2020). After placement, GCP locations are recorded with survey-grade, base and rover GPS systems (Emlid RS2 units) and processed either with a Post-processed Kinematic (PPK) or Real-time Kinematic (RTK) approach to provide accurate locations. Although a stratified random placement of GCPs was found to provide better accuracy than a systematic placement for photogrammetric UAS surveys (Oniga et al. 2020) another study found that a systematic placement provided better results when UAS sidelap between flight paths was reduced to 75% (Rangel, Gonçalves, and Pérez 2018). Higher altitude flights require fewer GCP placements, yet poorly placed GCPs (not easily viewable from the UAS, placed on too soft ground, obstructed from overhanging obstacles, and not visible in a minimum of 4 images) resulted in poor accuracy overall (Zimmerman, Jansen, and Miller 2020). For this study we used a minimum of 20 permanent and temporary ground control points per study site. All temporary ground control were secured in place for the duration of the study.

Automated ground control points that can be laid out and a button pushed to record GPS location is another option for the time-consuming process of placing and surveying ground control positions at a site. For example, Aeropoints (manufactured by Propeller), are 20 x 20 x 1-inch-thick board with a checkboard pattern and solar panel for power that can be placed for 10-45 minutes at a site to automatically record coordinate locations and through a network of targets and correction sites, provide 1 cm accuracy. Some UAS platforms, such as the WingtraOne or the Trinity Pro, can be interfaced directly to the network and fewer GCPs are required for accurate UAS image processing. However, it is unlikely that the panel would be left in-situ for long-term monitoring.

Remote Sensing Data Acquisition

Platforms and Sensors

To cover the spatial extents of our areas (>1.25 km^2 or 0.49 mi^2), we selected a vertical take-off and landing (VTOL) fixed wing UAS to perform the majority of flights. We used both the Trinity F90+ and the Trinity™ Pro made by Quantum Systems GMBH (Figure 2.2). The Trinity™ Pro (Quantum Systems 2024) is a National Defense Authorization Act (NDAA) compliant UAS that is approved for data acquisition over federal lands and for use by federal agencies. NDAA compliant drones meet strict national defense regulatory standards and exclude those made in or manufactured with key components from China, Russia, North Korea, or Iran (H.R.2670 - 118th Congress 2024). The maximum flight time for the Trinity is 90 minutes, with a cruising speed of 38 mph, and maximum flight coverage area of 2.5 mi^2 (Quantum Systems 2024). The VTOL capabilities of the platform allows users to take off and land in tight spaces. The Trinity is equipped with an interchangeable payload bay that can accommodate a suite of sensor payloads. For this study, we utilized the YellowScan Q240 LiDAR system (Yellowscan 2021), a geomatics grade, high-speed scanning LiDAR sensor (Figure 2.2). We flew the Trinty with the Q240 at 100 m or 328 ft above ground with a terrain following flight pattern to facilitate data collection at 50-100 points per m^2. The sensor is equipped with a geomatics grade GPS with an estimated precision of 1.8-2.5 cm (Yellowscan 2021). This sensor provided LiDAR coverage of all project sites in 2024.

A second sensor for the Trinity was used for flights in 2023. This sensor payload was used for flights in 2023 due to a delay in receiving the Q240 LiDAR sensor. Although this sensor provides exceptional coverage of sloped features, it cannot penetrate forest canopy in comparison to the Q240 LiDAR sensor. The D2M Oblique sensor is equipped with five high-resolution, multi-directional cameras (Quantum Systems 2023). With one nadir and four oblique 26 MP cameras. The sensor is capable of collecting highly detailed images from rugged terrain surfaces. Flown at 120 m AGL the sensor provides a resolution of 1.8 cm/px.

(image sources: https://www.yellowscan.com/wp-content/uploads/2021/03/Trinity-F90-with-QUBE240-LIDAR-1-1024x493.jpg and https://www.duncan-parnell.com/quantum-systems-oblique-d2m-five-lens-rgb-camera)

Figure 2.2 Quantum Systems Trinity F90+ with YellowScan Qube 240 LiDAR and D2M Oblique Camera Payloads

Mission Planning

For UAS mission planning we used Quantum System's Qbase software (Quantum Systems 2021). Qbase allows users to create autonomous flight missions by creating a polygon or flight area over a selected site using satellite imagery as a backdrop to aid in identifying the area of interest. The user can pre-program their flight line overlap, flight height, sensor payload, and select options for terrain following. During flight operations the remote pilot can interactively monitor in-flight progress and aircraft status. With the Quantum Systems D2M Oblique payload we flew at an above ground altitude of 100 m to 120 m and an overlap between flight paths of 70-75%. We selected advanced terrain following to maintain the aircraft height above ground level (AGL). On occasion, for less complex terrain, we flew 100-120 m above the max height of the flight leg.

For the Q240 LiDAR sensor, Qbase allows for flight planning maneuvers for inertial measurement unit (IMU) calibration before and after LIDAR data collection. The calibration procedure ensures that the LiDAR point cloud data and IMU data are correctly aligned. The IMU records the aircraft's motion, orientation and combined with the geomatics grade GPS onboard, the aircraft position. Once the calibration was complete the data acquisition over the study site was flown at 100-120 m AGL (following terrain), with a 50-65% overlap between flight paths and concluded with a final calibration pattern.

Data Acquisition

Permission from landowners was secured by ITD before flight operations. Launching and landing sites were selected by choosing a location free from obstacles and hazards. Before flight operations, a Notice to Airmen (NOTAM) was issued for the flight area and timeframe. Further, we alerted private airfields near flight areas of our operating location and times. At the launch site, a safety assessment was made before conducting any flights.

Before flight operations we setup a geomatics grade Trimble R10 base station to collect GPS data during the entire flight operation. The base station was essential for post-processing LiDAR data. The short baseline between the base station and GPS/IMU system onboard the Q240 LiDAR aids in improving accuracy. Following a manufacturer's checklist for UAS inspection and setup along with safety checks, we launched our UAS after the flight plan was loaded. An FAA certified remote pilot and at least one visual observer performed the flight operations. During flights, Qbase software allowed operators to view the flight status and aircraft performance. Additionally, the Qbase software allowed the integration of a uAvioni pingUSB device to monitor air traffic in the area and alert the team of any potential conflict with manned aircraft. Post flight operations maintenance checks were performed and then the UAS was disassembled.

Data Processing and Analysis

Photogrammetry / Structure from Motion Processing

To process imagery from the D2M Oblique five camera system, we used Agisoft Metashape v. 2.1.4 software (Agisoft LLC 2023) to create point clouds in LAS 1.4 format, digital elevation models (DEM), and orthomosaics. Agisoft Metashape is one of several structure from motion (SfM) software packages that combines photogrammetry principles with computer vision to process UAS images into seamless models. Prior to importing individual cameras into Agisoft, we post-processed camera positions using Qbase software. Using corrected GPS base station data and recorded flight logs from our UAS platform, we then performed PPK processing to correct the GPS locations more precisely for each camera position. This corrected position updated the camera positions for Agisoft Metashape processing. We utilized the recommended processing steps (Agisoft 2024) from the software manufacturer to stitch together the images we acquired in combination with ground control point coordinate locations to produce our final products. To classify the point cloud from our D2M sensor, we utilized LASGround in LAStools software (Rapidlasso GmbH 2023).

LiDAR

To address the common repeat LiDAR issues, we used the following workflow (Figure 2.3). It combines four different software packages for post processing LiDAR data: CloudStation v. 2403.0.1-b1de7940

(YellowScan, France), Applanix POSPac UAV v. 8.4 (Trimble, USA), BayesStripAlign v. 2.25 (BayesMap Solutions, USA), and LAStools (Rapidlasso, Germany). The first step was to extract flight data from the UAS and from our Trimble R10 base station. The LiDAR associated files from the Yellowscan Q240 LiDAR include the point cloud data collected during the flight and a T04 file that contains inertial measurement unit (IMU) and GPS information in Applanix (Trimble) binary format. The Trimble R10 base station has T02 files with positions recorded during the flight operations. We use the T02 and T04 files to create a Smoothed Best Estimated Trajectory (SBET) file for each of the flights with PosPac UAV. PosPac UAV software uses the IMU and global navigation satellite system (GNSS) data to georeference the flight data. Since we placed our R10 Trimble base station over an unknown reference location at the sites for a minimum of two hours, we used Trimble's CenterPoint RTX Post-Processing service to accurately reference the position of the base station. Once we processed the Q240 and base station data files and adjusted the base station location to the corrected position, we ran the GNSS-Inertial Processor in POSPac to compute the smoothed best estimate trajectory from the raw data. The trajectories were then exported as SBET files, which we used in Yellowscan's propriety CloudStation software to generate LAS files of the pointclouds. CloudStation also allows the use of ground control points in processing the georeferenced point cloud data. Further, we colorized the point cloud in CloudStation by using orthomosaics captured during flights with the D2M Oblique sensor. As a final step in CloudStation, we performed an automated point cloud classification to identify noise, ground, vegetation, and other features in the point cloud. The point cloud was export in LAS 1.4 format.

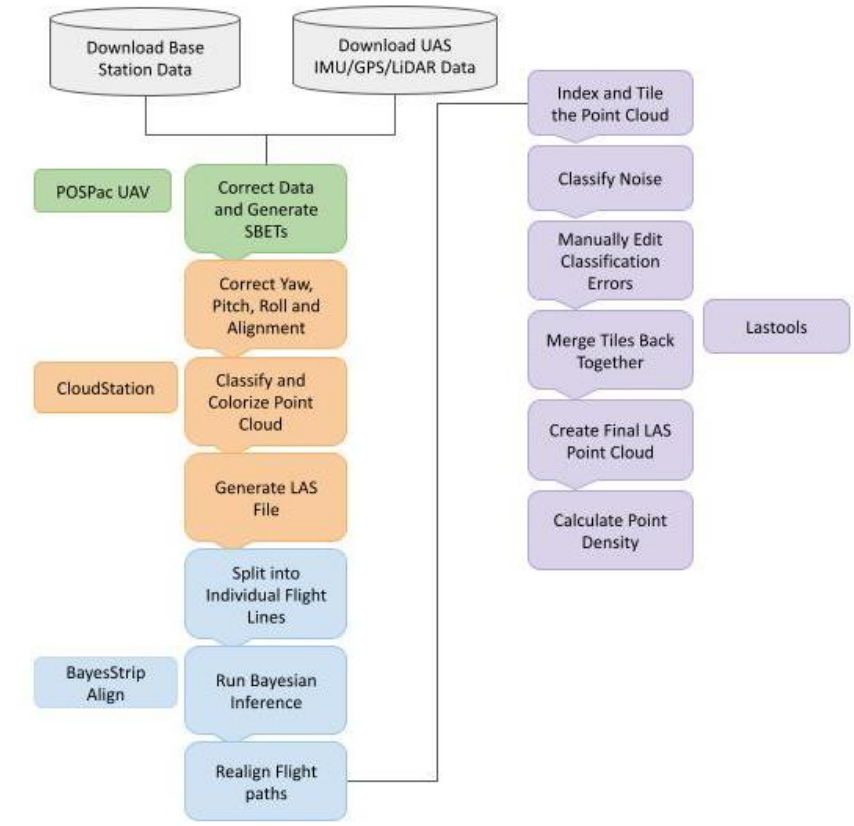

Figure 2.3 LiDAR Data Processing Workflow

Strip Alignment and Point Cloud Classification Adjustment

Although CloudStation runs a LiDAR strip alignment processing step, we choose to fine tune the alignment exported from CloudStation to increase the accuracy of the data and remove bias influencing repeat LiDAR analysis. As CloudStation provides a good strip alignment, this is a step that could be removed from the workflow, but we found that BayesStripAlign did improve our cloud alignment. BayeStripAlign splits the flight up into individual flightpaths before running a Bayesian inference to align the flight strips and correct geometric errors (BayesMap Solutions 2024). Bayes StripAlign works to correct the absolute and relative geometric errors of LiDAR swaths that can be due to issues such as IMU altitude and position errors. This method uses LAS files with timestamps as well as the SBET trajectory files we created. Once input into the program, the timestamps were used to register overlapping flight lines and correct errors with the flight including low or high frequency IMU drifts, boresight misalignment, lever arm errors, or internal geometry miscalibration (BayesMap Solutions 2024). Using Bayes StripAlign software, we first cut each site into individual strips of flightlines before realigning the cuts from the applied corrections to create the new point clouds with improved accuracy. The uncertainty of the point clouds for each campaign were further improved by assigning a larger weight to more accurate points (BayesMap Solutions 2024). The flight lines were then realigned and exported as a new point cloud. This process, paired with the use of the geodetic grade GPS and PPK processing,

reduced the root-mean squared (RMS) error for the point clouds. This improvement from the initial CloudStation alignment was recorded in accuracy assessment report files for all flights.

The newly aligned point clouds were then imported into and processed with Rapidlasso's LASTools to correct any ground / vegetation classification errors in the point cloud. This classification process required multiple steps. First, we ran the LASindex tool that creates and appends a file containing the spatial indexing information for the point cloud (Rapidlasso GmbH 2023). The next step was to divide the site into tiles for ease of processing with LAStiles, creating 100 m^2 tiles with 10 m buffers. Once the site was tiled with the LAStile tool, we ran the LASnoise tool to classify any noise present in the cloud using the default settings. With the LASview tool we were then able to manually edit any points in the clouds that were misclassified during the CloudStation classification process and save these edited tiles as Lay files. Before continuing to process the sites, the LASlayers tools converted the Lay files into Laz files. Then we merged the tiles into one point cloud using the LASmerge tool; we exported the merged cloud as a LAS file. All point clouds from each flight were exported from LAStools to WGS84 UTM 12N with WGS84(1762) for analysis, as this was the default coordinate system used by the aircraft and sensors.

Change Detection Analysis

Once point clouds are properly aligned, Figure 2.4 and Table 2.1 highlights various change detection methods to capture geomorphic changes, such as the Digital Elevation Model of Difference (DoD), Cloud-to-Cloud (C2C), Cloud-to-Model (C2M), and M3C2 (Andresen and Schultz-Fellenz 2023; Esposito et al. 2017; Sun et al. 2024). The DEM of difference method (DoD) uses two rasters of elevation data and subtracts one of these rasters from the other to calculate the difference. Since this method projects the point cloud onto the two-dimensional x-y plane, the change detected in this method is one dimensional only along the z-axis (DiFrancesco, Bonneau, and Hutchinson 2020). This method, while computationally efficient, lacks accuracy when it comes to complex terrain where the surface orientation is greatly varied (DiFrancesco, Bonneau, and Hutchinson 2020). The C2M method compares a point cloud to a triangulated mesh surface of a second point cloud. The distance is calculated from each point in the cloud to the nearest point on the surface mesh (Cignoni, Rocchini, and Scopigno 1998). For this reason, the accuracy of this method is dependent on the quality of the triangulated surface.

There are two methods of comparing point clouds: the cloud-to-cloud (C2C) change detection and the Multiscale model-to-model cloud comparison (M3C2). For C2C, the distance is measured between the points from one cloud to the nearest point of another cloud (Girardeau-Montaut et al. 2005). Due to the arbitrary nature of simply using the closest point, the C2C method requires dense point clouds and low surface roughness. Furthermore, this method has one major drawback in that it does not calculate sign direction, which is necessary for identifying erosion or deposition. However, a variation on C2C, known as the multiscale model-to-model cloud comparison (M3C2) is ideal for measuring material loss and gain (Lague, Brodu, and Leroux 2013; Bernard, Lague, and Steer 2021). The M3C2 method is a direct comparison between two point clouds collected at different times, using an algorithm that calculates distance of a normal vector. Instead of limiting itself to just the nearest point in the next cloud, the vector is calculated using the points nearest neighbors. This method avoids the uncertainty of vertical height that is often intrinsic to using DEM-to-DEM analysis (Esposito et al. 2017). The Multiscale Model-to-Model Cloud Comparison (M3C2) is a widely used method for distance computation to evaluate 3D changing features in point clouds. It operates by computing distances within a locally oriented search

cylinder. When the projection diameter of M3C2 becomes larger than the changing area on a rock or hill slope, change cannot be identified. For this study we used a combination of all of these methods to detect change between flight dates using CloudCompare v. 2.14 (2015) software.

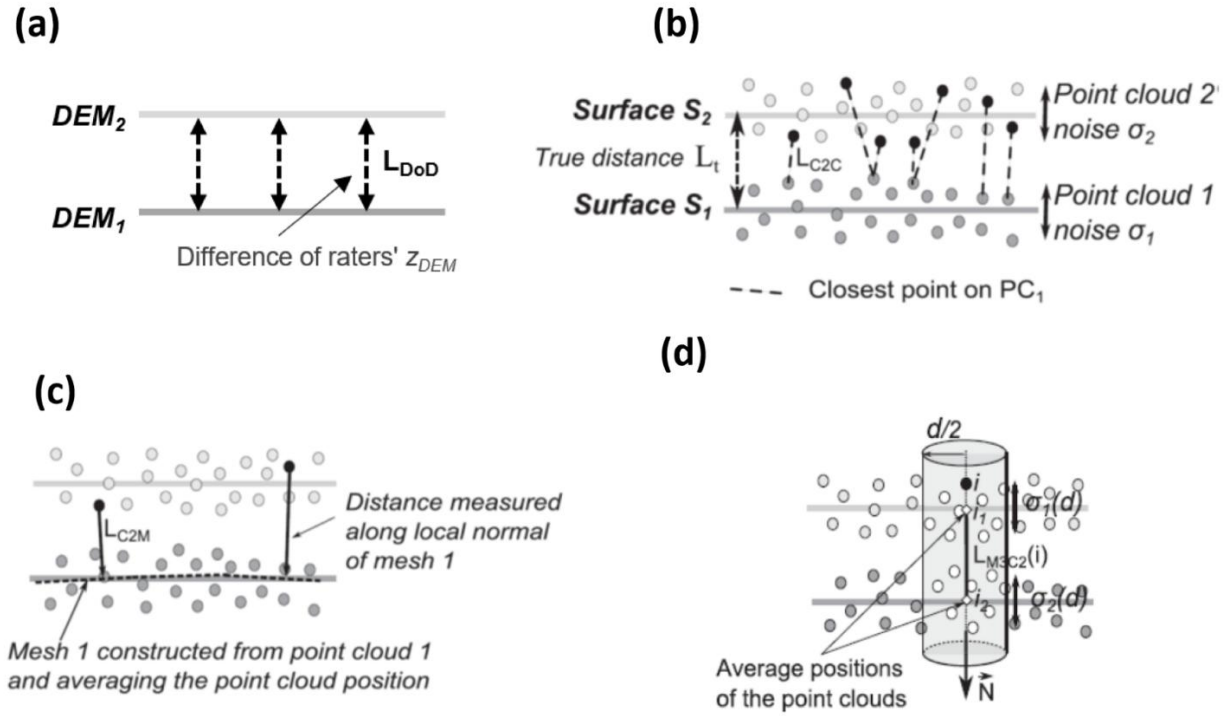

Figure 2.4 Common Change Detection Methods. (a) Differencing of DEMs (DoD), with distances computed vertically. (b) Cloud-to-cloud (C2C) distances are computed based on closest point distance. (c) Cloud-to-mesh (C2M) is computed between closest points along the local normal of the mesh. (d) Multiscale Model-to-Model Cloud Comparison (M3C2) is computed through a cylindrical axis, which gives a mean distance along the normal direction (Adapted from Sun et al. 2024; Andresen and Schultz-Fellenz 2023; Lague, Brodu, and Leroux 2013)

Table 2.1 Change Detection Approaches

Method	**Reference**
DEM of Difference (DoD)	(Wheaton 2008)
Cloud-To-Cloud (C2C) distance	(Girardeau-Montaut et al. 2005)
Cloud-To-Mesh (C2M) distance	(Cignoni, Rocchini, and Scopigno 1998)
Multiscale Model-to-Model Cloud Comparison (M3C2)	(Lague, Brodu, and Leroux 2013)

3. Landslide Site Characterization

Site Selection of Landslide Slopes

Four landslide areas were selected by ITD for this project representing a cross-section of diverse slope parameters. General locations are shown in Figure 3.1 and described in Table 3.1 of this report.

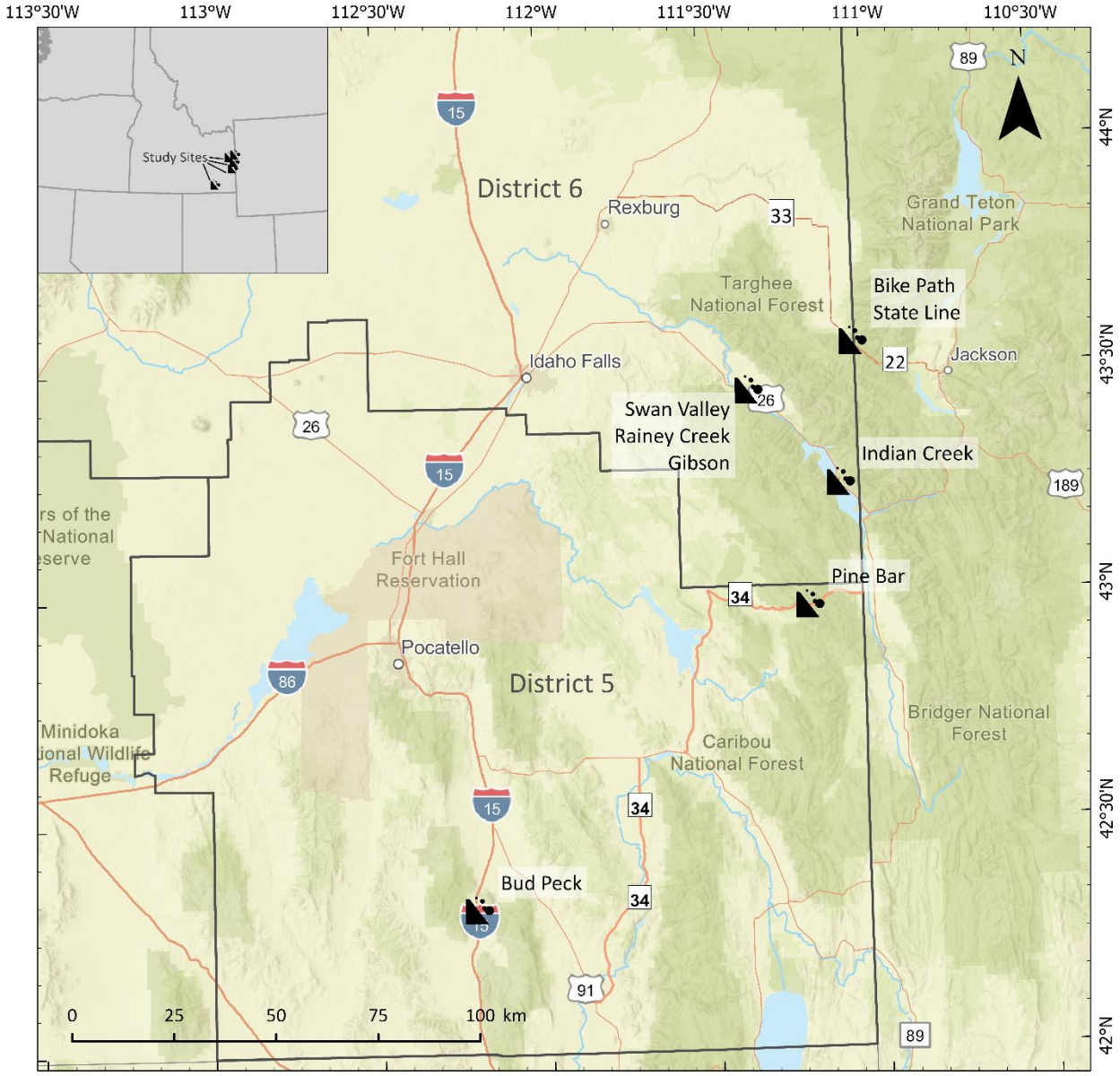

Figure 3.1 Landslide Study Area Locations in Eastern Idaho

Four main areas of investigation are located in Idaho Transportation Department (ITD) Districts 5 and 6 and are identified and described as follows in Table 3.1. Swan Valley East, Rainey Creek, and Gibson sites are adjacent to each other and have been grouped as part of a larger Swan Valley Landslide Complex.

The study areas are located along Interstate 15, US Highway 26, and State Highway 34 where historical landslide activity has occurred. The criteria used in selecting the sites include:

- Historical landslide events
- Vegetation cover
- Exposed areas (bare earth)
- Densely forested areas
- ITD existing instrumentation

The Swan Valley and Indian Creek sites are in ITD District 6, whereas the Pine Bar and Bud Peck landslide slide areas are in District 5. Further, in District 6, ISU researchers also conducted a one-time UAS LiDAR survey along State Highway 33 in June 2024 in response to active slide events (Bike Path and State Line).

All sites have manned aircraft LiDAR available at the Quality Level (QL) 1 or 2 and were flown between 2017-2020. QL 1 LiDAR data has a minimum of 8 recorded x, y, and z points per square meter and typically provides a 0.5 m resolution digital elevation model (DEM). QL2 LiDAR has a minimum of 2 points recorded per square meter and a DEM resolution of 1 m. In comparison, ISU's UAS LiDAR data is >80 pts per meter squared and is able to produce DEMs at >0.10 m.

Table 3.1 Landslide Study Site Descriptions

ITD Sites	Highway	Mile Post	Site Coordinates	Number of Inclinometers	Comments
Swan Valley East	US - 26	373.85 - 374.27	111°23'53"-111°22'05"W 43°27'16"-43°26'53"N	5	A large historic landslide was reactivated 30 years ago when the roadway was realigned. Surficial slumping and smaller slides occur in this location almost every year near inclinometer LT-4 and LT-5.
Rainey Creek	US - 26	374.8 - 375.2	111°22'51"-111°22'09"W 43°27'7"-43°26'51"N	2	Large slide area has been mitigated twice. Initial signs of movement observed in the area during study period. Mitigation measures employed were unloading the head scarp area on the western side and installing a large shot rock shear buttress on the eastern flank of the complex.
Gibson	US - 26	375.9 - 376.3	111°22'24"-111°20'42"W 43°27'33"-43°27'11"N	1	Smaller, active slide in a historic large slide complex. Movement has been increasing slowly during the last few years. Cracks have formed in the pavement. Partially mitigated with light weight fill resulting in reduced movement rates. ITD plans to install another inclinometer below the roadway.
Indian Creek Slide Complex	US - 26	397.9 - 399.0	111°6'45"-111°5'20"W 43°14'33"-43°14'03"N	3	Movement has occurred in at least one instrumented location and in several nearby areas without instrumentation. Road closing landslide occurred and mitigated near LT33 in the 1960's and again in the late 1990's. An underdrain system was installed but movement still occurs in random areas.
Pine Bar Slide	SH - 34	104.1 - 104.35	111°12'43"-111°11'58"W 42°58'39"-42°58'18"N	4	Large landslide complexes with previous failures on the eastern margin above monitoring points. Instrument results indicate slow movement. Some indication that the slide mass contains varied areas of movement.
Bud Peck Slide	I - 15	22.6 - 22.8	112°13'53"-112°12'37"W 42°19'51"-42°18'57"N	9	No current movement. Potentially mitigated with horizontal drains installed in 2002. Embankment failure and loss of northbound lane of I-15 in 1983. Reconstructed embankment with light weight fill using locally sourced Pumice and horizontal drains. Slight movements detected and raised ground water storage in 2001 prompted additional instrumentation and deeper horizontal drains installed in 2002. No movements since 2002.

Source: Idaho Transportation Department (2024)

Swan Valley Landslide Complex

Study Area Overview

The Swan Valley Landslide Complex is located in the Eastern Snake River Plain along US Highway 26 on the north side of the South Fork of the Snake River (Figure 3.2). The section lies between mile markers 373.85 and 376.3. The study area is approximately 4.75 km^2 (1.8 mi^2) along US 26 and lies between longitudes 111°23' 53’’W and 111° 20' 42’’W and latitudes 43° 27' 33'' N and 43° 26' 51''N. The area is generally south-facing with the uplands characterized by agricultural fields, transitioning to a steeper topography covered with sagebrush, grass, and forb cover on slopes adjacent to the river. Elevation ranges between 1605 to 1750 m (5265 to 5742 ft). Evidence of historic hillslope movement and landslide activity is visible along slopes both above and below the highway. The study area was divided into three individual sites as follows:

- Swan Valley East
- Rainey Creek
- Gibson

Evidence of mudflows and scarps were observed near the bottom of the slopes on the north side of the highway. Swan Valley East had one mudflow during the ITD-ISU 2023 – 2024 investigation period. ITD has eight inclinometers across the Swan Valley East, Rainey Creek, and Gibson sites to monitor slope movements at depth in the complex slide area (Figure 3.2).

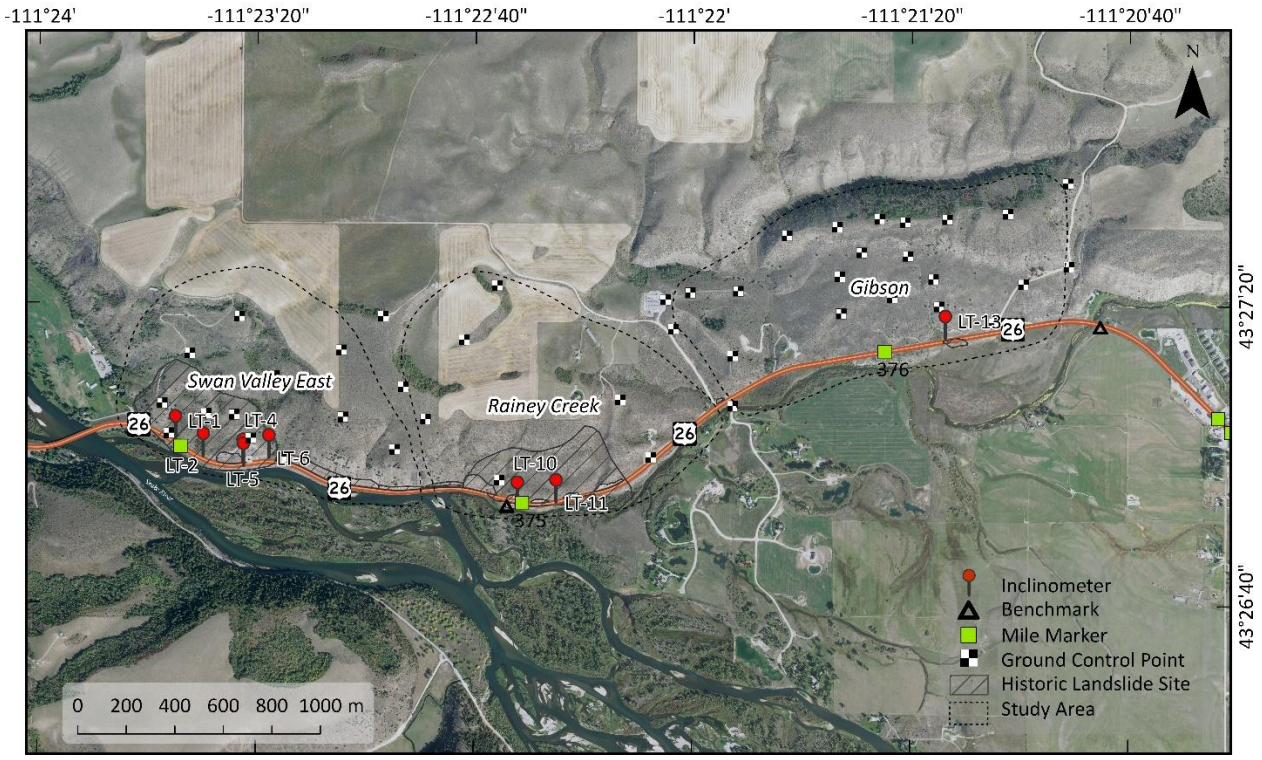

Figure 3.2 Swan Valley Landslide Complex Study Area

Geologic Conditions Overview

Dossett et al. (2012) identify five basic soil/rock formations in the Swan Valley Complex area (Figure 3.3):

- Loess (Ql)
- Alluvium (Qal)
- Landslide Debris (Qls)
- Basalt (Qbar/Tbs)
- Tuff (Qyh)

The upland area above the slopes is mantled with loess (Ql) described as a structureless silt (Dossett et al., 2012). Loess is reported to be as much as 80 ft thick and underlain by a volcanic sequence consisting of Quaternary age Antelope Flat Basalt, Huckleberry Ridge Tuff and Tertiary age Swan Valley Basalt. The formations exposed on the slopes are described by Dossett et al. (2012) as consisting of black columnar vesicular basalt (Qbar and Tbs) and devitrified rhyolitic ash-flow tuff (Qyh) (Figure 3.3).

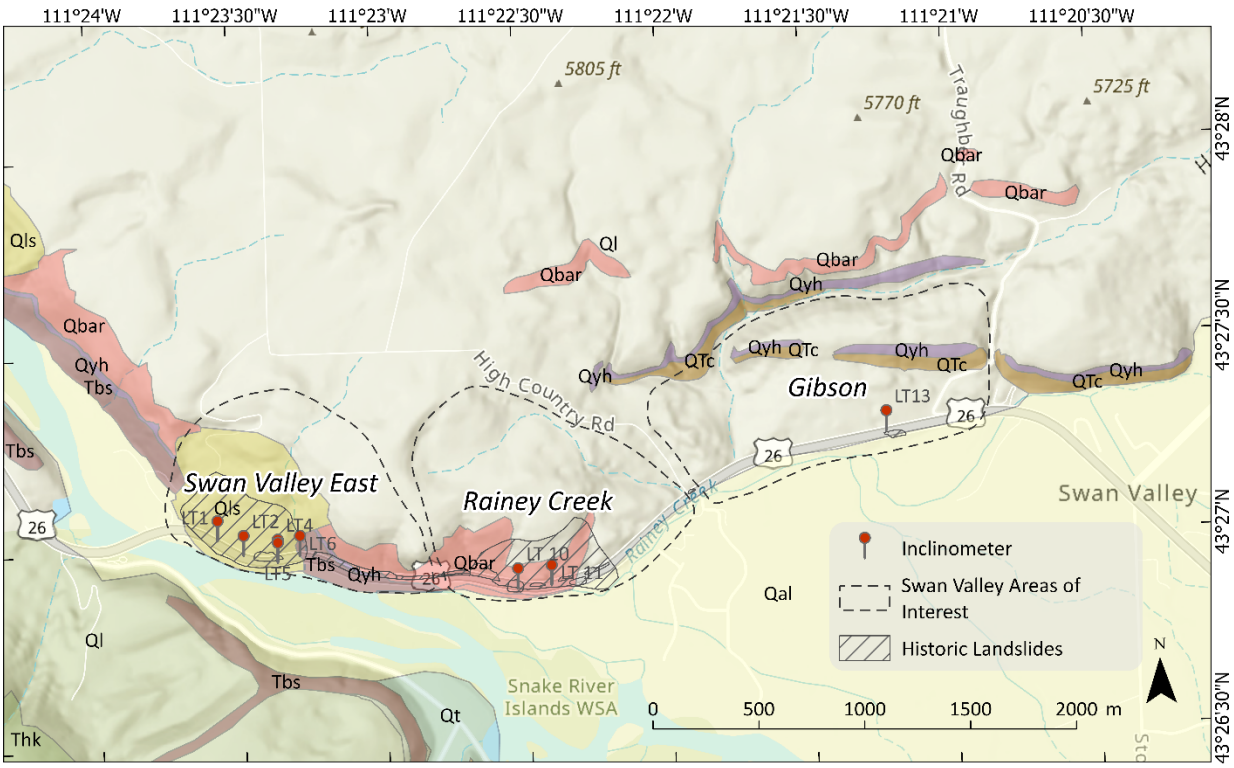

Qyh - Huckleberry Ridge Tuff: Light gray to grayish-pink crystal rich welded devitrified rhyolitic ash-flow tuff with well-developed eutaxitic fabric. Columnar jointing is common. Non-flattened white and pink pumices present in some localities. As much as 80 ft thick.

Qt - Travertine: Light-cream to gray, thin bedded (1/4 to 2 inches), vuggy calcium carbonate spring deposits. Deposited in low mounds and cones mostly along the Snake River fault.

Qbar - Basalt of Antelope Flat, Rim Facies: dark-gray to black vesicular basalt. Containing phenocrysts of olivine and plagioclase. As much as 100 feet thick. Columnar jointing

Ql - Loess: Light yellow to yellow-gray well-sorted structureless silt. As much as 80 feet thick.

Qls - Landslide deposits

QTc - not described

Tbs - Basalt of Swan Valley: Dark-gray to black, weathered brown to green, vesicular basalt. As much as 200 ft thick. Columnar jointing and massive flows are common. Red cinder and volcanic breccia layers are intercalated with the lava flows near the Swan Valley bridge. Variable-oriented jointing patterns found in some areas. Pillows and rosette-style jointing are absent. Dips about 10 degrees to the northeast near Conant Valley.

Thk - Kilgore Tuff: Dark grey to light purple, crystal-rich, devitrified to lithophysal welded tuff containing tan and dark brown flattened pumice fragments.

Thb - Blacktail Creek Tuff: Dark gray to purple crystal-rich, highly devitrified welded ash-flow tuff containing flattened pumice fragments.

Qal - Alluvium: Unconsolidated, well sorted silt, sand, and gravel deposits along stream courses. Includes older terrace gravels along the Snake River.

Adapted from Dossett et al. 2012.

Figure 3.3 Geology of the Swan Valley Landslide Complex (Adapted from Dossett et al. 2012)

The Antelope Flat Formation also contains mixed layers of basalt fragments and older quartzite. Pillow basalt, together with interflow debris, occur on the same stratigraphic horizon as the Huckleberry Ridge Tuff. The older Basalt of Swan Valley is present on both sides of the Snake River in the Swan Valley East and Rainey Creek areas but appears to be absent in the Gibson slopes near the highway on the east side of the complex. Morgan and McIntosh (2005) postulate that volcanic activity and associated uplift and faults started in Swan Valley roughly 16 million years ago. Analysis of paleomagnetic and volcanic data

indicate that eruptions occurred every 100,000 years. Geologic mapping in the study area indicates periodic uplift along northwest-trending faults, leading to erosion, river incision and deposition of sediments.

Deposits of sand, unconsolidated silt, and gravel in past and present channels of the South Fork of the Snake River are found on the valley floor. The gravel contains basalt fragments below the surface of the riverbank. Only one location in the Swan Valley study area has a fault (Morgan and McIntosh, 2005). A 28-meter (92-ft) high scarp along a basalt flow shows initial surface ruptures along Pine Creek. Age dating indicates that the flow is 1.5 million years old. The late Quaternary loess overlying the basalt does not show evidence of fault displacement. Henderson et al. (2023) mapped two normal faults bordering Swan Valley: the Grand Valley Fault on the northeast side and the Snake River Fault on the southwest side of the graben.

The rock and soil types bordering the landslides on the north side of Swan Valley along US-26 are primarily Pleistocene basalt overlain by loess in the highlands and Quaternary alluvial deposits in the Snake River Valley floor (Jobin and Schroeder, 1964). Based on a literature review, most of the landslides in the highland areas are not active. Areas showing active movement tend to advance by minimal creep. The landslides that post-date the loess deposits are now generally inactive, although instances of reactivation can still be detected as observed in the present study.

UAS Surveys of the Swan Valley Landslide Complex

The ISU Department of Geosciences conducted aerial flights in the Swan Valley Complex area six times during the two-year investigation period (Table 3.2). The initial aerial survey was performed on 19 July 2023 and the last survey on 03 October 2024. In May 2024, an additional survey was conducted on an active flow area in Swan Valley East using a multi-copter platform equipped with an RGB camera. Approximately 61 ground control points were used across the Swan Valley East, Rainey Creek, and Gibson sites. Eight of the ground control points were stationary objects such as survey benchmarks and well coverings. The remainder were cross-style mesh GCPS or metal pans with black and white markings that were left out for the duration of the study and surveyed twice, in the spring of 2023 and the spring of 2024.

Table 3.2 Swan Valley Landslide Complex Drone Surveys

Area	Sensor	Date
Swan Valley East and Rainey Creek	D2M - Oblique	07-19-2023 / 07-21-2023
Swan Valley East and Rainey Creek	Q240 - LiDAR	06-20-2024
Swan Valley East and Rainey Creek	Q240 - LiDAR	10-03-2024
Swan Valley East (only)	Phantom 4 Pro	05-31-2024
Gibson	D2M	07-21-2023
Gibson	Q240 - LiDAR	06-08-2024
Gibson	Q240 - LiDAR	10-03-2024

Swan Valley Complex Inclinometers/Boring Logs

Inclinometers

A total of 8 inclinometers have been installed by ITD in the three study areas comprising the Swan Valley Landslide Complex (see Table 3.3, Table 3.4, Table 3.5 and Figure 3.2). Initial measurement dates vary between 25 and 26 September 2017. Most of the inclinometers were placed along US-26 adjacent to areas of active movement. ITD inclinometer designations, coordinate locations/elevations, and depths are summarized in Table 3.3.

Table 3.3 Swan Valley East Inclinometers

Inclinometer	Location (Lat/Long)	Ground Surface Elevation	Total Depth	Status
LT-1	43.450493 / -111.39301	5287 ft / 1611 m	48 ft / 14.6 m	Operational
LT-2	43.449854 / -111.391592	5297 ft / 1614 m	48 ft / 14.6 m	Operational
LT-4	43.449635 / -111.389541	5301 ft / 1615 m	48 ft / 14.6 m	Operational
LT-5	43.449493 / -111.389541	5294 ft / 1613 m	49 ft / 14.9 m	Operational
LT-6	43.449805 / -111.388246	5297 ft / 1614 m	38 ft / 11.6 m	Operational

Table 3.4 Rainey Creek Inclinometers

Inclinometer	Location (Lat/Long)	Ground Surface Elevation	Total Depth	Status
LT-10	43.448088 / -111.375581	5297 ft / 1614 m	48 ft / 14.6 m	Operational
LT-11	43.448185/ -111.373614	5297 ft / 1614 m	48 ft / 14.6 m	Operational

Table 3.5 Gibson Slide Area Inclinometer

Inclinometer	Location (Lat/Long)	Ground Surface Elevation	Total Depth	Status
LT-13	43.454302 / -111.353814	5317 ft / 1621 m	48 ft / 14.6 m	Operational

Boring Logs

Geotechnical boring logs were prepared by Landslide Technology of Portland Oregon for the inclinometer installations authorized by ITD. Two-inch OD standard split spoon samples were taken at 5-ft intervals. Blow counts were recorded for each 6-in. interval of drive for a total sample length of 18-in. Soil descriptions include color and moisture and for coarse grained soils: visual percentages of grain size, grain shape, density and mineralogy. Plasticity, consistency (strength) and the presence of organics were provided for the fine-grained soils. Samples were visually classified under the Unified Soil Classification

System (USCS) and interpretations made on the origins of the individual layers. Water contents were provided in the logs using a graphical format across from the soil samples. Groundwater levels and dates recorded during drilling were also included in the logs.

Split spoon and continuous HQ-triple tube cores were taken where rock was encountered in the bore hole. Rock type, color, degree of weathering and strength (described using hardness terms) were recorded in the logs. Joint properties include spacing, planarity, staining, and mineral filling. Core recovery and Rock Quality Designation (RQD) were displayed in graphical format for each core run. Core photos are attached to the some of the reports. ITD boring logs of all inclinometer holes are provided in Appendix A of this report.

Swan Valley East

Overview

Swan Valley East contains a major landslide area primarily above and to a lesser extent below US-26 along the edge of the Snake River (identified as Qls, landslide deposits, in Figure 3.5). One small area in the eastern part of the past landslide area underwent additional movement during the investigation period near mile-marker 374.2 and within the area marked as Qls (landslide deposits) in Figure 3.5. All of the present slide activity in the Swan Valley East area occurred on the hillside above (north) of US-26. Moreover, there was no evidence of damage or movement along the roadway surface. The flow stopped in the ditch on the north side and did not reach the highway.

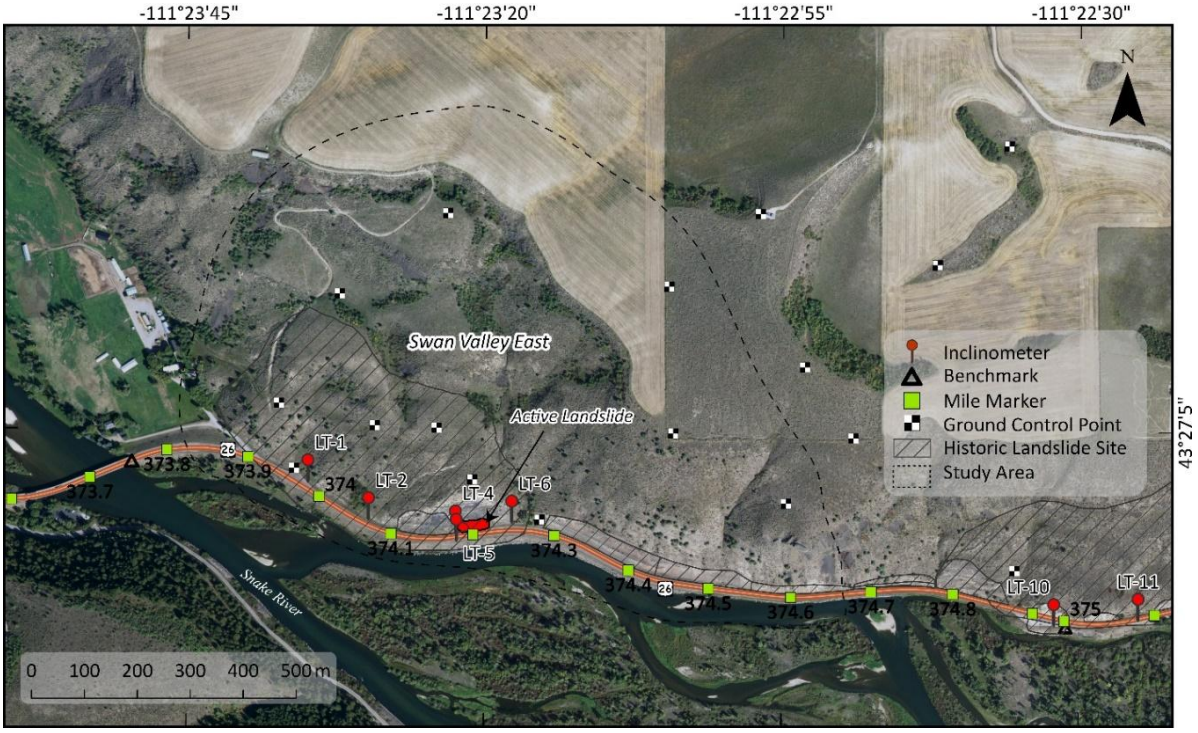

Figure 3.4 Swan Valley East Landslide Study Site

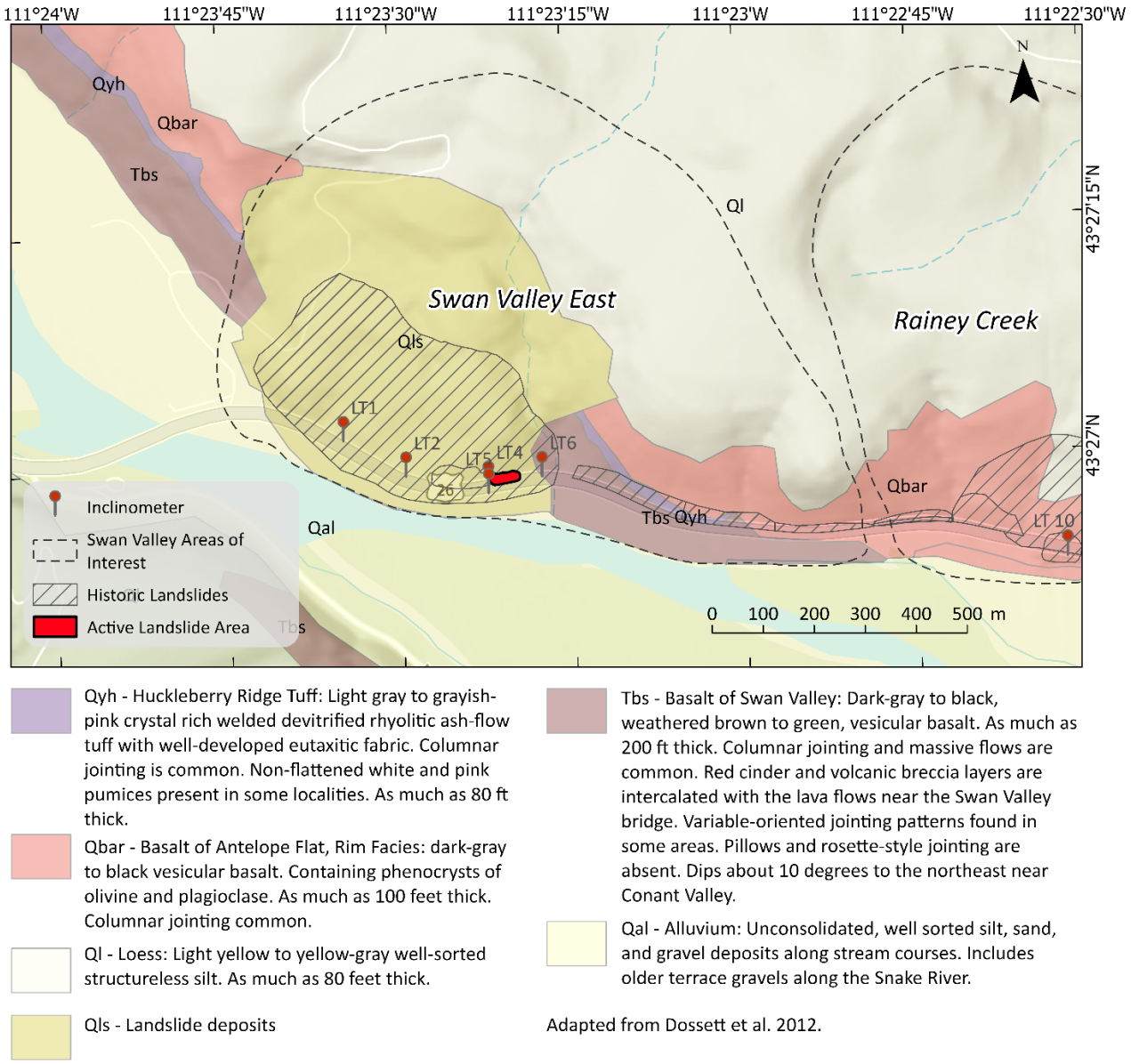

Qyh - Huckleberry Ridge Tuff: Light gray to grayish-pink crystal rich welded devitrified rhyolitic ash-flow tuff with well-developed eutaxitic fabric. Columnar jointing is common. Non-flattened white and pink pumices present in some localities. As much as 80 ft thick.

Qbar - Basalt of Antelope Flat, Rim Facies: dark-gray to black vesicular basalt. Containing phenocrysts of olivine and plagioclase. As much as 100 feet thick. Columnar jointing common.

Ql - Loess: Light yellow to yellow-gray well-sorted structureless silt. As much as 80 feet thick.

Qls - Landslide deposits

Tbs - Basalt of Swan Valley: Dark-gray to black, weathered brown to green, vesicular basalt. As much as 200 ft thick. Columnar jointing and massive flows are common. Red cinder and volcanic breccia layers are intercalated with the lava flows near the Swan Valley bridge. Variable-oriented jointing patterns found in some areas. Pillows and rosette-style jointing are absent. Dips about 10 degrees to the northeast near Conant Valley.

Qal - Alluvium: Unconsolidated, well sorted silt, sand, and gravel deposits along stream courses. Includes older terrace gravels along the Snake River.

Adapted from Dossett et al. 2012.

Figure 3.5 Geology of the Swan Valley East Landslide Study Area (Adapted from Dossett et al. 2012)

UAS Surveys and Hillslope Movement

The overall elevation changes in Swan Valley East determined in the ISU Photogrammetry/LiDAR surveys between July 2023 and June 2024 are shown in Figure 3.6. Areas in red indicate upward or positive movement and in blue downward displacement. Magnitudes of movement are indicated by the color intensity on the right side of the figure. The area in white are trees which inhibited photogrammetry and LiDAR elevation (Z-direction) measurements.

The displacement patterns indicate erosion in the valley on the east side of the study area and below the highway just above the South Fork of the Snake River. Two local areas of slide movement (uphill side in red and downhill side in blue) were detected between Inclinometers LT1-LT2 and LT4/LT5-LT6 (Figure 3.6). Other than the local mudflow, there was no evidence of slope movement during the period except for the displacement data obtained in the LiDAR surveys.

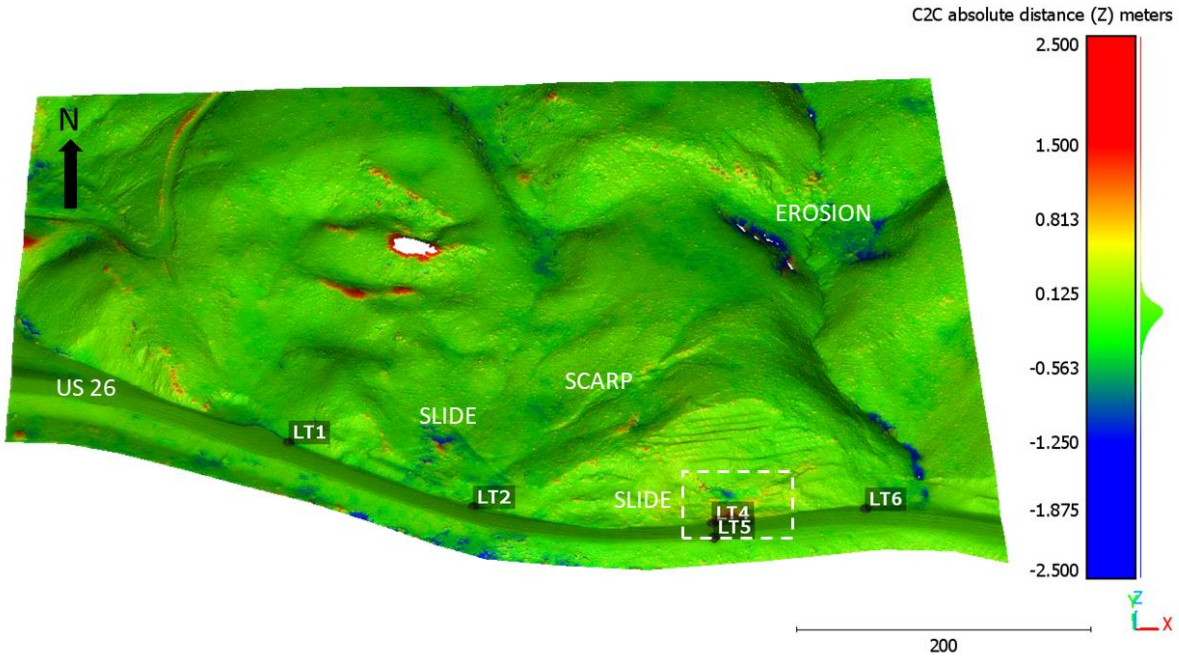

Figure 3.6 Swan Valley East Change Detection July 2023 to June 2024

A close-up of the active landslide on the east side of study area detected between the July 2023 and June 2024 LiDAR surveys is shown in Figure 3.7. Based on the movement pattern, the affected area is approximately 150 ft (46 m) wide and 105 ft (32 m) upslope. A scarp is noticeable at the top of the slide and hummocky ground is present in and near the toe (Figure 3.8 and Figure 3.9). The scarp at the top of the slide has a maximum downward displacement of 8 ft (2.4 m). The corresponding maximum heave near the toe of the slope is approximately 4.5 ft (1.4 m). The inflection point is roughly 32 ft (10 m) from the north edge of the highway. The profile view of the slide (Figure 3.9

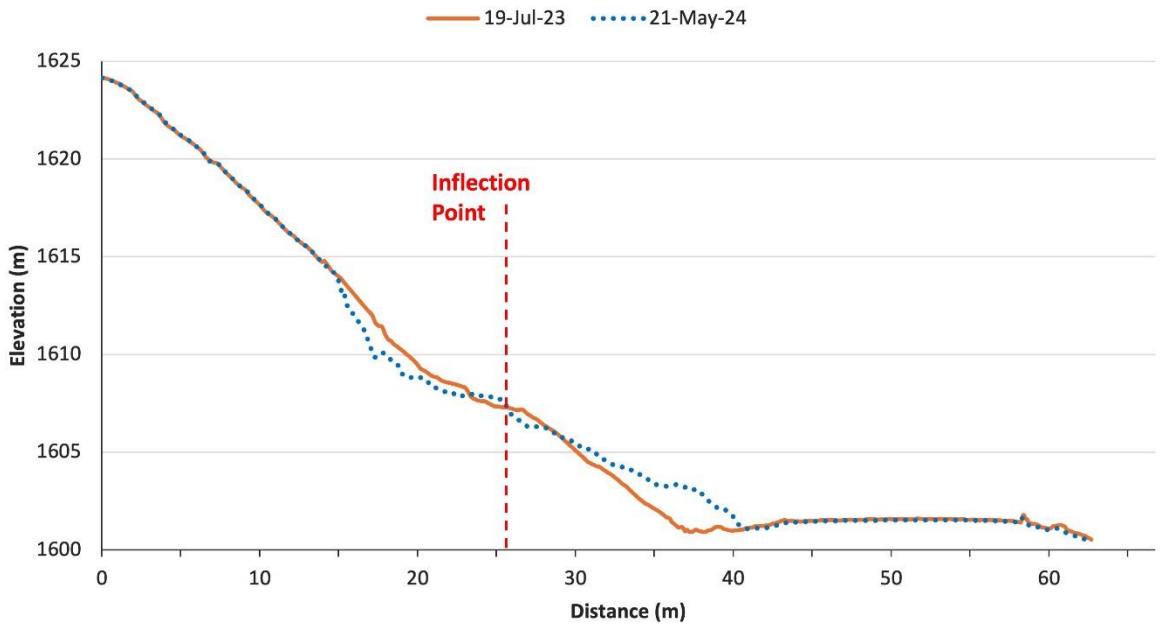

)

shows a classic hummocky topography near the toe of the slope with little or no displacement affecting the road.

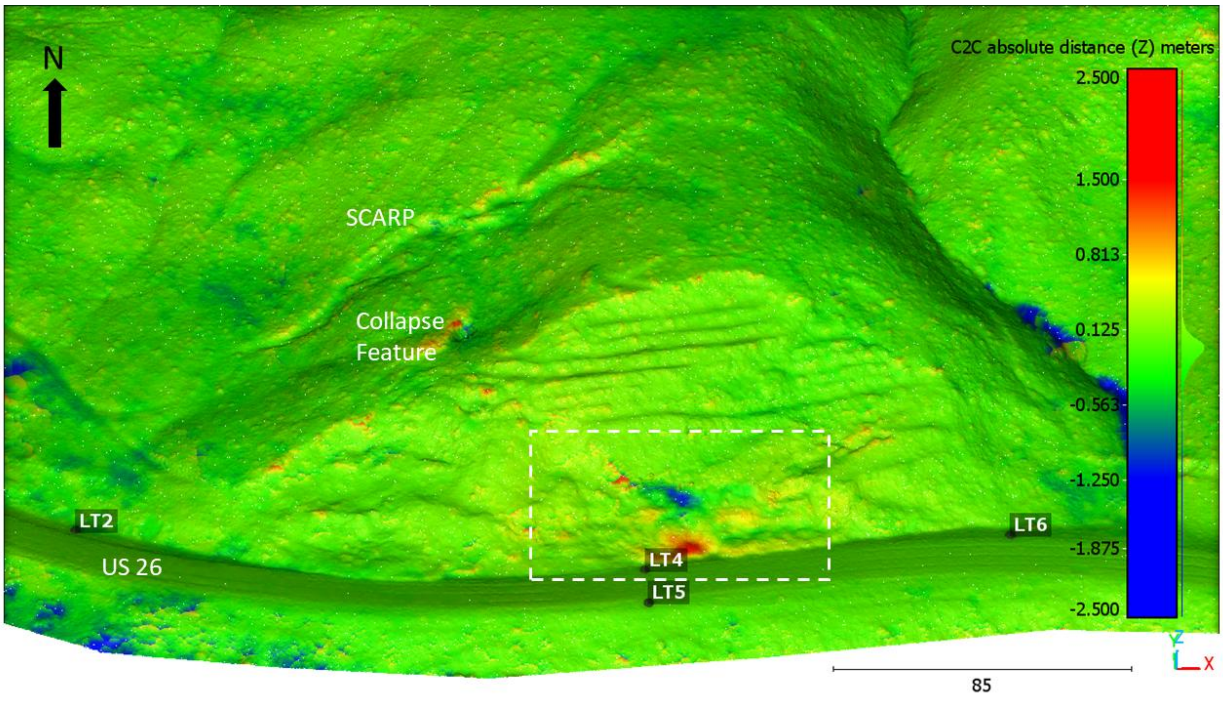

Figure 3.7 Active Slide Area Change Detection July 2023 to June 2024 (white dashed box)

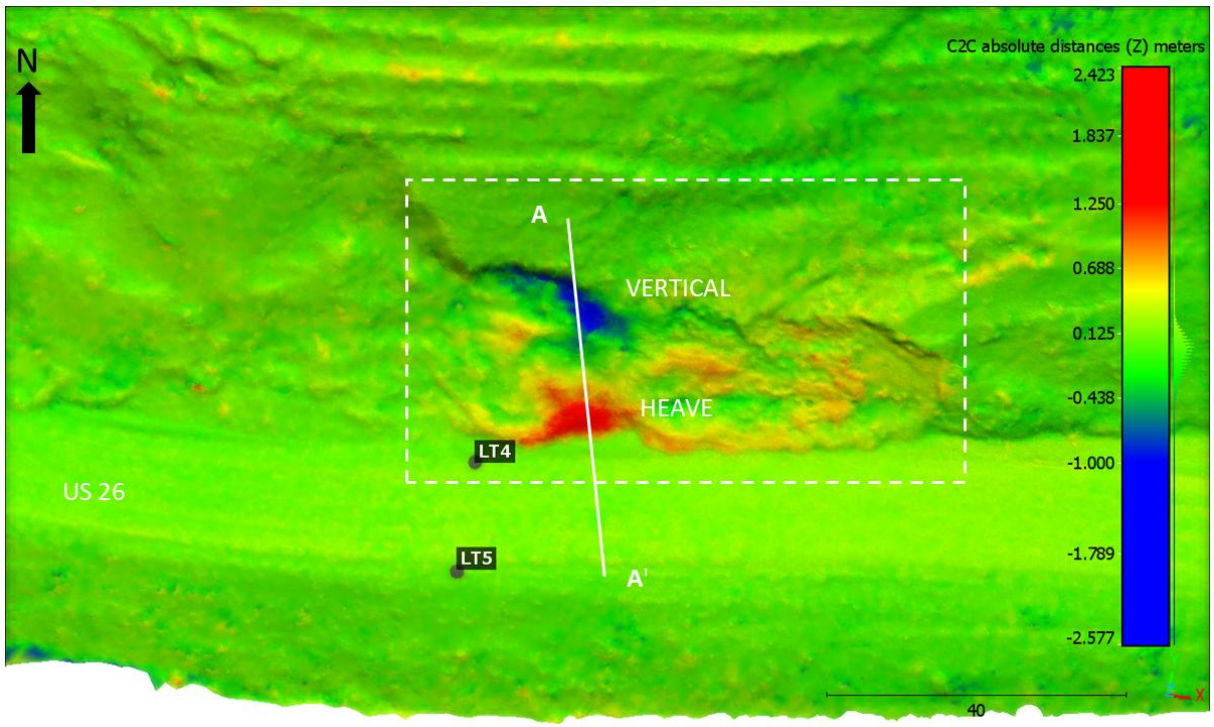

Figure 3.8 Active Slide Area Change Detection July 2023 to June 2024 with Profile Line

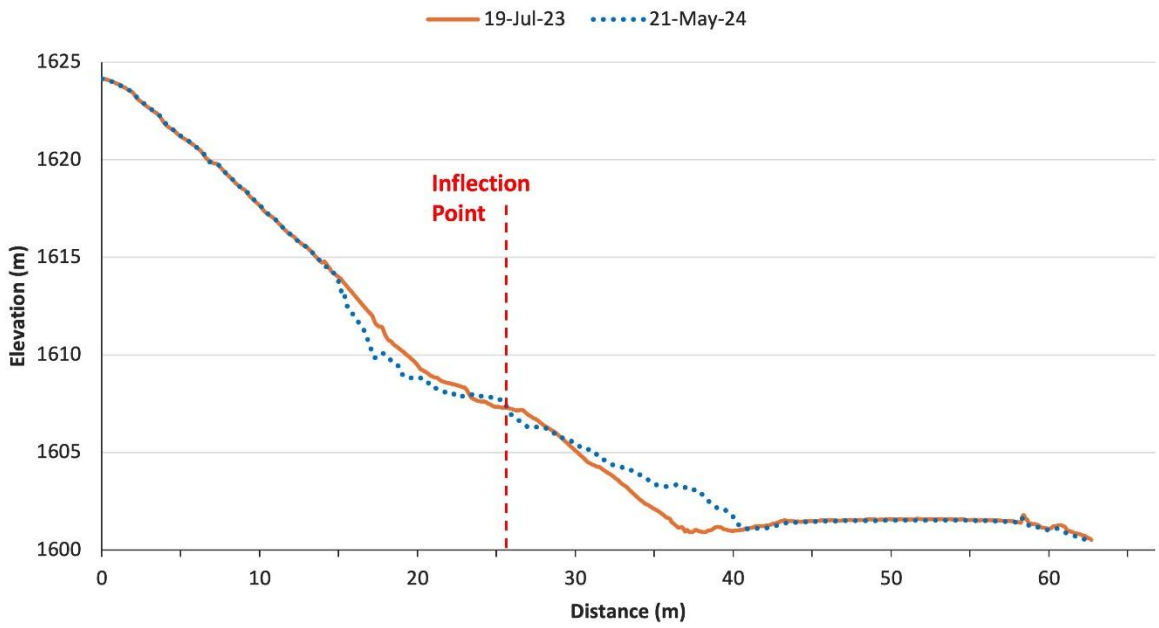

Figure 3.9 East View of Slope Profile in Maximum Displacement Cross Section (A-A')

A discontinuous linear feature is noted in the UAS air photos approximately 850 ft (260 m) above the active slide area and is a positive indicator of a much larger future slide that could impact the highway (Figure 3.11). The UAS survey also revealed a major collapse feature along an intermediate scarp between the active slide area and the upper scarp 850 ft (260 m) above the road (Figure 3.11). Such features form as a result of lateral displacement and opening/collapse of the ground surface along the movement zone. The depressions serve as an active area of infiltration in which the surface water is collected on the slope, flows underground and saturates the downslope portion of the slide area leading to slope failures and mud flows. Review of past air photos shows the same depression in the slope in 2020, but is absent in 1987. These depressions should be identified and infilled to reduce pore pressures acting along surfaces of sliding.

Study of the complete UAS photo indicates that the eastern portion of the upper scarp is somewhat discontinuous but intermittently present between the trace visible in Figure 3.11 and the valley further to the east more than 1000 ft (300 m) across the slope. The conditions revealed in the UAV surveys are responsible for the present landslide above US-26 and pose very serious future highway safety concerns. Clearly the conditions and stability should be investigated further and remediated as needed.

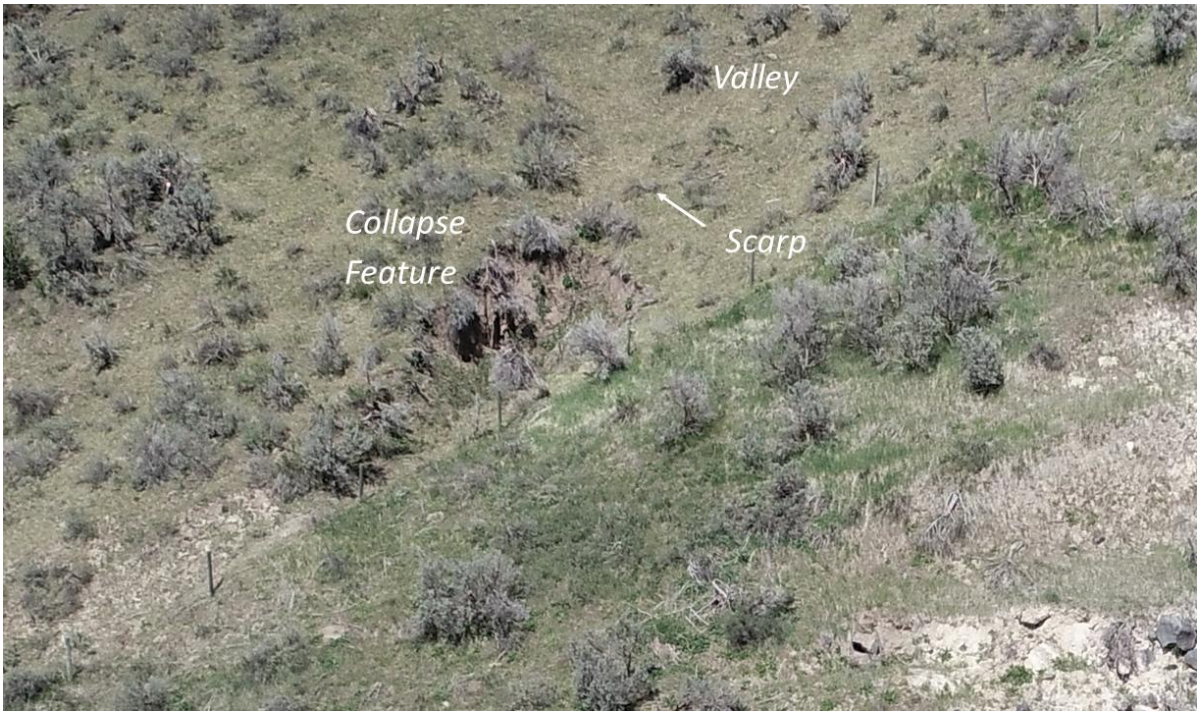

Figure 3.10 Collapse Feature above Active Landslide Area

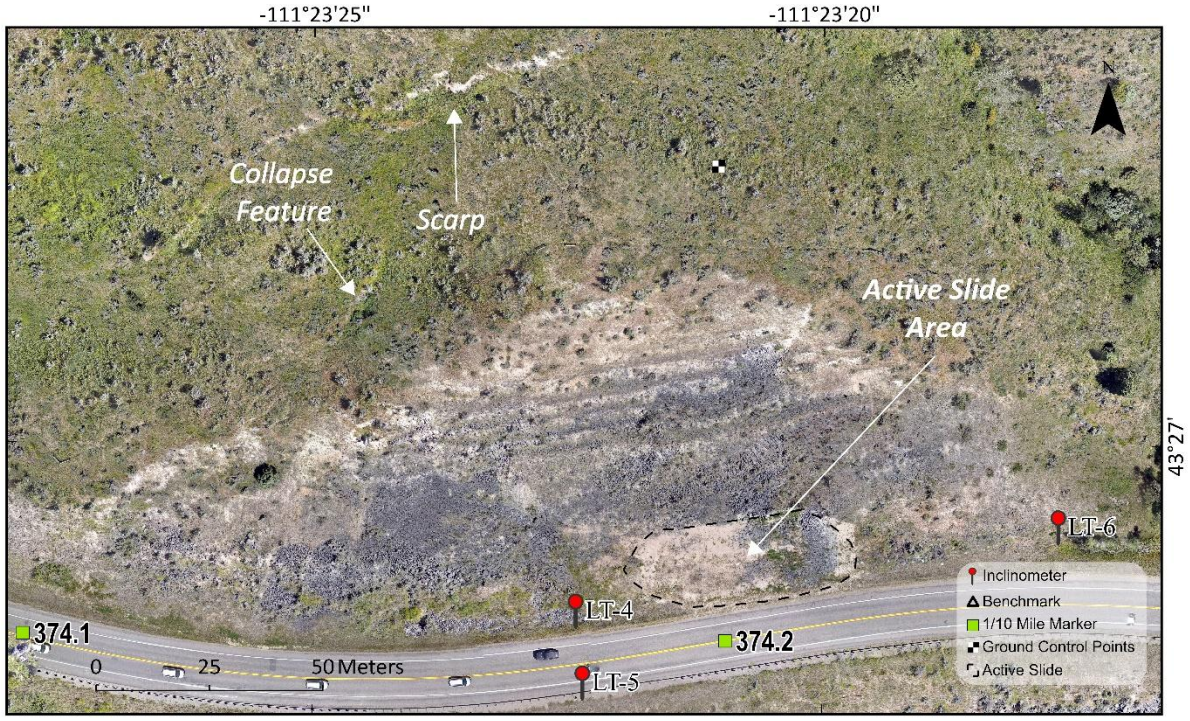

Figure 3.11 Swan Valley East Active Slide Area with Scarps and Collapse Feature

Swan Valley East Inclinometers

In 2017, a total of five Slope Indicator inclinometers (LT1, LT2, LT4, LT5 and LT6) were installed by ITD to measure lateral displacements in the Swan Valley East Landslide Area adjacent to the highway. All of the inclinometers were placed near the toe of the slope. Casings were installed to depths of 38 to 49 ft below the ground surface and were grouted from the end caps to the surface. Initial baseline readings at 2-ft depth intervals were taken by ITD personnel on 25 and 26 September 2017 and on the following dates during the active ITD-ISU field investigation period.

- 06 July 2023
- 24 April 2024
- 30 May 2024
- 01 October 2024
- 07 November 2024

The active landslide in Swan Valley East is located between Inclinometers LT4/LT5 on the west side and LT6 on the east side of the area (Figure 3.7). The bore holes containing the inclinometers are located between US-26 mile-markers 374.1 and 374.3 and were drilled to a depth of approximately 50 ft. The inclinometers are located outside the active area of movement and do not show significant lateral displacement during the two-year study period.

The displacement data from LT4 closest to the active slide is typical for the period (Figure 3.12). In Figure 3.12, the A-axis, upslope-downslope axial displacement at depth is plotted against the corresponding boring log. The inclinometer data in the B-axis direction is not included in the diagram because the measured displacement is parallel with the slope. (The B-axis data and remaining inclinometer plots are given in Appendix A of this report.) The absence of inclinometer movement in the closest inclinometers is consistent with the displacement pattern obtained in the 2023-2024 LiDAR surveys.

Subsurface Profile Adjacent to the Active Slide Area in Swan Valley East

The subsurface profile on the upslope (north) side of the roadway (in Borings LT4 and LT6) adjacent to the active slide area consists of 10.8 to 18 ft of colluvium, respectively, over decomposed to slightly weathered basalt (Figure 3.12). In Bore Hole LT4, the colluvium is a very dense silty, sandy GRAVEL (GW) with a trace of clay. The gravel recovered in the 1-3/8-in. ID split spoon sampler is up to 1 in. in size. The one N-value at a depth of 5 ft is 57 blows/ft indicative of a very dense, undisturbed gravel. The colluvium is only 11 ft thick and is present above decomposed basalt with refusal N-values and a water level at elevation 5257.5 ft below the contact.

On the east end beyond the active slide area, the colluvium is described in the log of LT6 as soft, slightly sandy, slightly clayey SILT (ML) with numerous zones of angular decomposed rock fragments, occasional ash and carbonized organics (see Appendix A). Refusal blow counts were recorded in split spoon samples taken at depths of more than 5 ft below the ground surface. On 9 December 2017, ground water was logged at elevation 5267.9 ft in Boring LT6 in the lower portion of the colluvium. The water levels in both borings were roughly 17.1 and 17.5 ft below the ground surface.

Tertiary Swan Valley Basalt was encountered below the soil in both upslope borings and is described in the inclinometer logs as decomposed to slightly weathered rock. The top of rock was encountered at elevation 5264.2 ft in LT4 and 5267.0 ft in LT6. In Bore Hole LT4, the upper 14.3 ft of rock is described as decomposed basalt: black, hard, sandy, slightly clayey to clayey SILT (ML) with numerous rock fragments up to 1 in. in size (Figure 3.12). The decomposed rock was sampled with a standard split spoon: refusal values (50/1 in. to 50/2 in.) were recorded in the 14-ft decomposed rock interval. The decomposed basalt is absent in Bore Hole LT6 east of the active slide area. The basalt below the colluvium or decomposed rock is described as dark gray, hard, vesicular, slightly to moderately weathered, very highly to highly fractured, with smooth to rough planar fractures dipping at angles of 40 to 60^{o}. Core recovery in the basalt was 100%; RQD values ranged between 20 and 91%.

Nothing in the boring logs north of the highway (LT4 and LT6) indicate the presence of past slide activity.

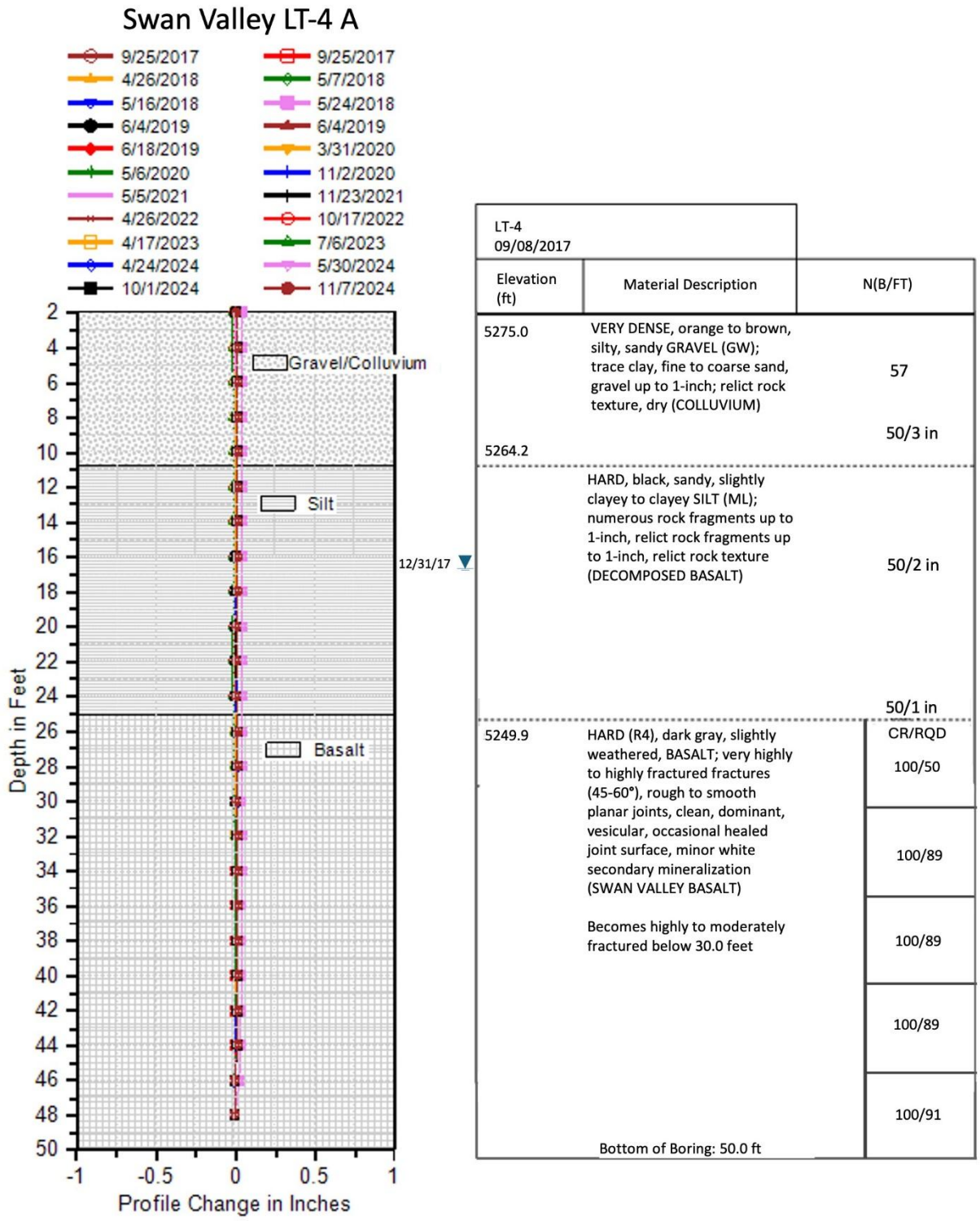

Figure 3.12 Inclinometer Displacements and Corresponding Log of Boring LT-4 West of the 2023-2024 Active Slide Area

The log of Boring LT5 on the south side of the road across from LT4 shows 27 ft of embankment fill, above 11 ft of colluvium underlain by at least 12.4 ft of alluvium (see Appendix A). Unlike LT4, no rock (basalt) was encountered in the bore hole. The fill in LT5 is described as a soft to medium stiff, brown to gray, slightly sandy, slightly clayey to clayey SILT (ML) with occasional rock fragments and ash. Standard penetration values in the fill between depths of 15 and 26 ft are 3 to 10 blows/ft. The low N-values are the result of past slope movement and/or poor compaction during construction of the roadway embankment. The 11 ft of colluvium beneath the fill is described as very dense, gray to brown, slightly silty, sandy GRAVEL (GW) with angular rock fragments. The description is similar to the colluvium present in Bore Hole LT4. The alluvium below a depth of 38 ft (elevation 5227 ft) is described as medium dense to dense, brown to gray, sandy GRAVEL (GW) with particles up to 3/4-in. in size. Groundwater was encountered in the alluvium at the time of drilling at approximate elevation 5223 ft.

Slope Movement West of the Active Slide Area

Lateral displacement at depth was recorded in Inclinometer LT2 east of the active slide area prior to and during the study period (Figure 3.13). The displacement-depth plot shows rigid body lateral movement of approximately 0.3 in (0.7 cm) to a depth of 24 ft during the 6 July 2023 to 7 November 2024 measurement period (Figure 3.13). The lateral movement continues downward in shear to a depth of 30 ft. The log of Boring LT2 shows the failure zone in the lower colluvium described as brown silty CLAY (CL) with a trace of sand. The standard penetration value of 5 blows/ft indicates a medium stiff clay and the lower value is consistent with shear strain in the colluvium.

In December 2017, the groundwater table was at and just above the base of the movement zone in the lower colluvial formation. The colluvium in which the movement is taking place is resting on a sandy GRAVEL (GW) with a trace of clay described in the boring log as LANDSLIDE/SLIDE DEBRIS. The LiDAR data indicated no measurable movement during the study period even though the inclinometer showed a total displacement of 0.3 in (0.7 cm) at and below the ground surface. The incremental slope movement 0.3 in (0.9 cm) has not reached the 2 cm (0.8 in) horizontal and 3 cm (1.2 in) vertical thresholds for measurable displacement in the LiDAR survey.

It is apparent that both the inclinometer, LiDAR data and photography along with groundwater water levels and pavement damage are invaluable in monitoring the stability of the slopes along ITD assets. The subsurface depth/geometry of the slide area are needed using inclinometers placed in and below the moving slope to fully develop any remedial measures needed for stabilizing the slopes.

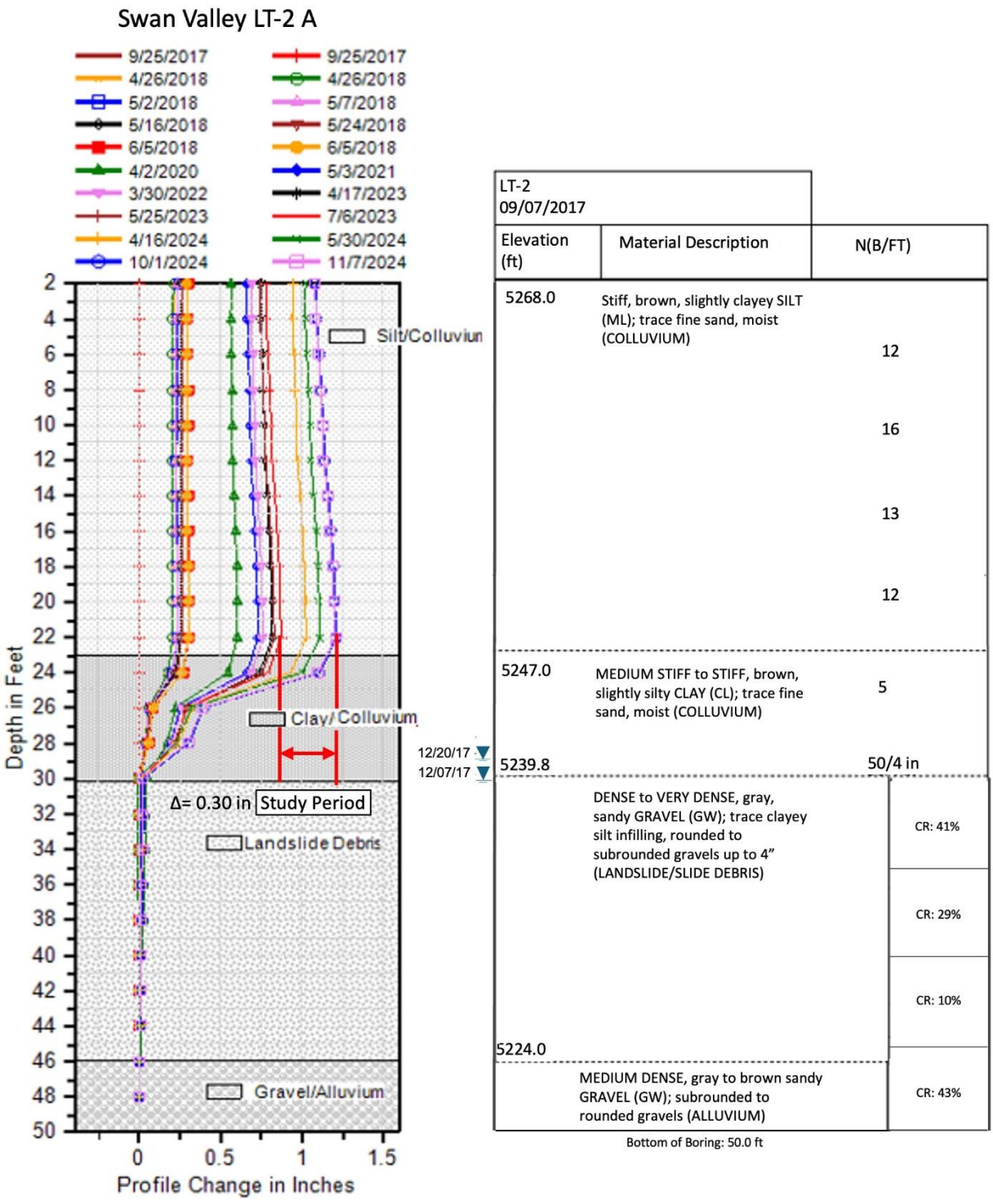

Figure 3.13 Inclinometer displacements and corresponding log of Boring LT2 west of the 2023-2024 active slide area in Swan Valley East (red lines with arrows indicate study period)

Swan Valley Precipitation Records During the 2023-2024 Investigation Period

Daily precipitation records for the Swan Valley area were obtained from the NOAA Swan Valley, ID weather station (Figure 3.14). The weather station is located within 5 miles of the Swan Valley Landslide Complex consisting of Swan Valley East, Rainey Creek and Gibson landslide study sites. Study period limits are shown as vertical red lines in the figure. Between the July 2023 and May-June 2024 drone surveys, the slope movement at the Swan Valley East site consisted of a mud flow and adjacent landslides. The slide did not intersect US-26; there is no record of the specific date(s) on which the slope movement occurred.

Based on the precipitation data, the slope movements east of Inclinometers LT4/LT5 most likely occurred during the February to early March 2024 time period. The total precipitation during this period at the gauge location was an approximate 3.3 in. with a 1.86 in. rainfall event in the first week of March. The displacement-time plot of the upslope-downslope A-axis (LT-2A) in Inclinometer LT2 also shows a significant increase in the magnitude and rate of ground surface movement during the same time period (Figure 3.15). Although there are no contemporaneous records of the slope movement, the local mudslide between Inclinometers LT4 and LT6 is an index that the heavy rainfall during this period was the likely cause of the slope movement event.

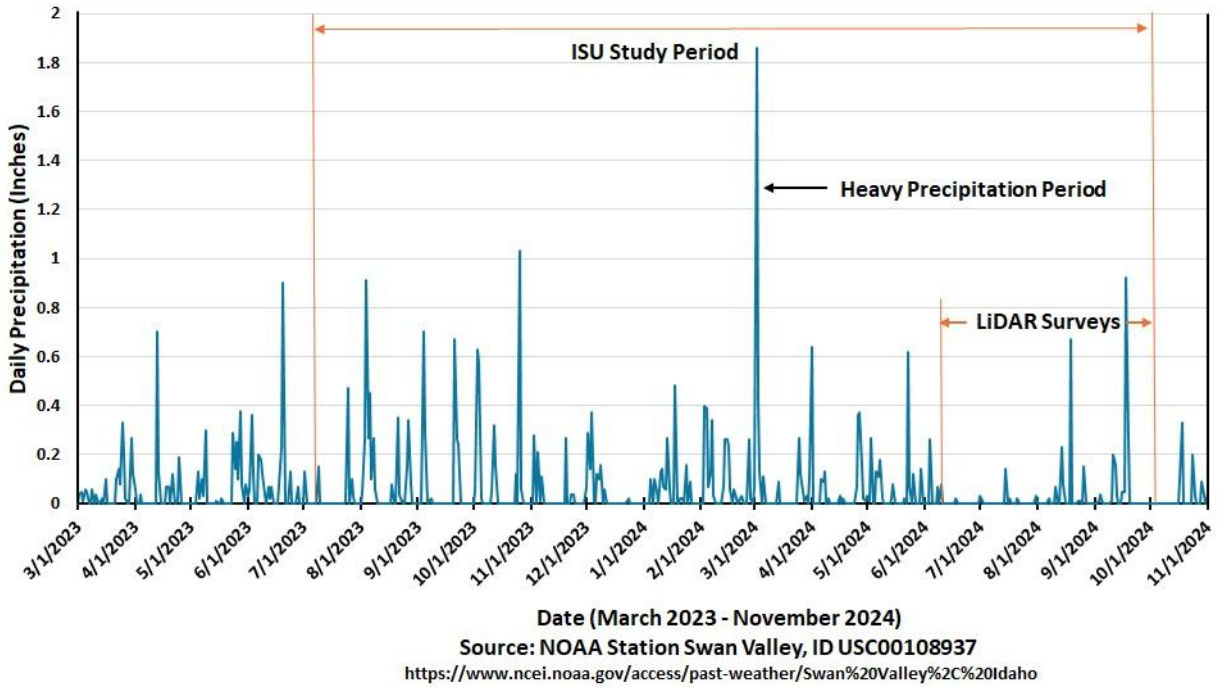

Figure 3.14 Swan Valley precipitation record for the duration of the study period

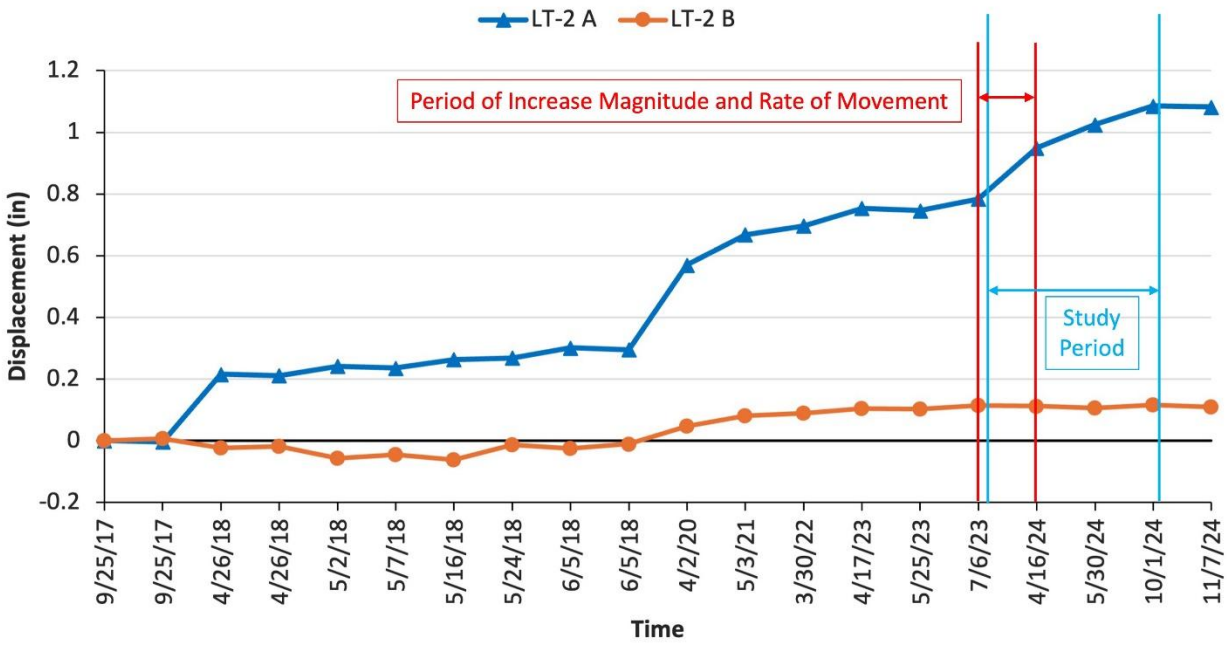

Figure 3.15 Near-Surface Swan Valley East LT-2 inclinometer time-displacement measurements

Seismic Events During the 2023-2024 Investigation Period

Figure 3.16 and Table 3.6 highlight the seismic events during the investigation period. Two events in the 3.5 to 3.9 magnitude range occurred within 50 km (31 miles) of the study site in late 2023 (October and December).

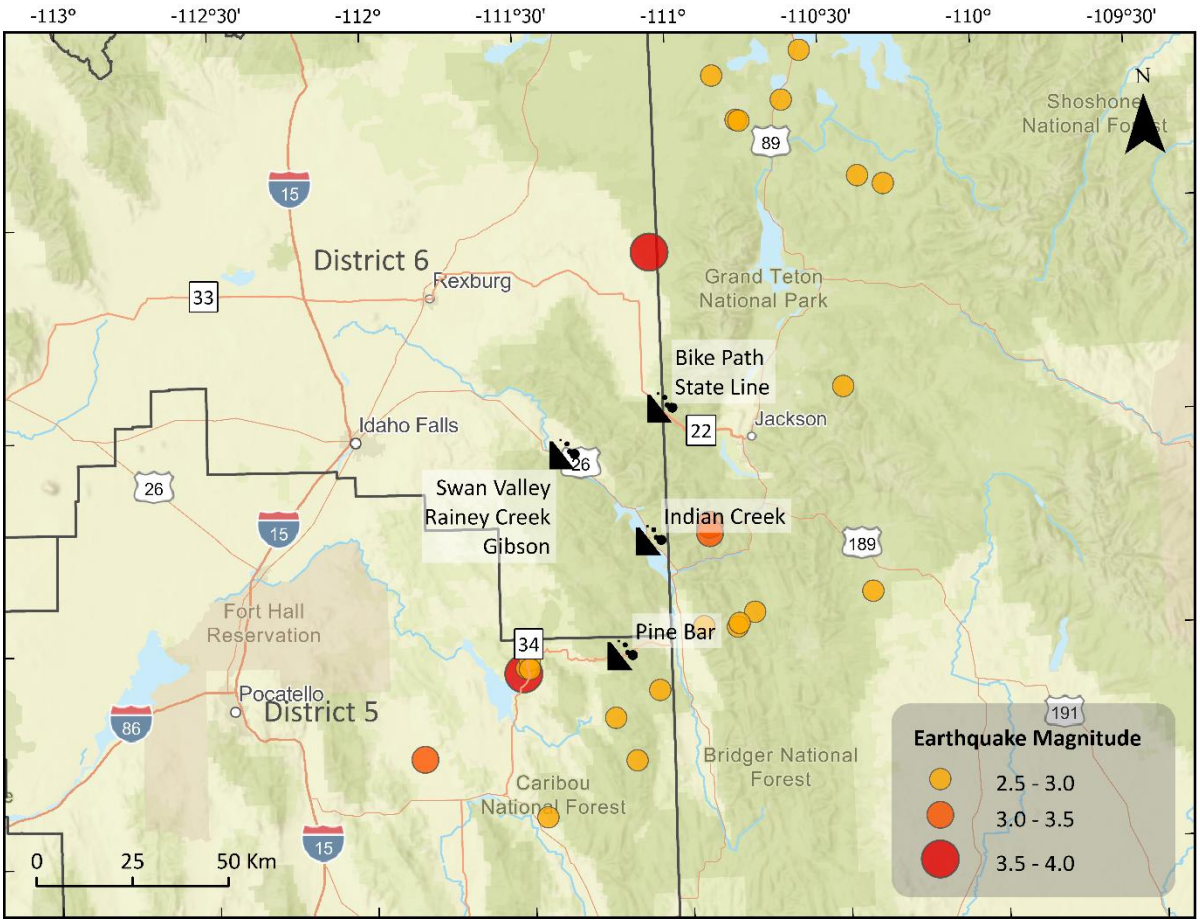

Figure 3.16 Seismic Events During the 2023-2024 Swan Valley Investigation

Table 3.6 Seismic Activity ≥ 2.5 Magnitude and within 50 kilometers of the Swan Valley Area during the Study Period

Date	Latitude	Longitude	Depth	Magnitude
8/29/2024	43.0382	-110.938	0.568	2.7
8/9/2024	43.2757	-110.908	8.704	3.1
8/2/2024	43.2558	-110.908	9.392	3.1
4/13/2024	42.8305	-111.229	5	2.6
12/8/2023	43.92	-111.072	9.987	**3.9**
10/26/2023	43.0677	-110.773	5	2.8
10/14/2023	42.9529	-111.511	6.487	2.7
10/14/2023	42.9716	-111.499	5	2.7
10/13/2023	42.9403	-111.52	0.327	**3.6**
10/13/2023	42.951	-111.5	1.524	2.7
8/15/2023	42.8924	-111.086	1.207	2.9
6/18/2023	43.0344	-110.83	5	2.6
6/16/2023	43.0428	-110.824	9.43	2.6

Rainey Creek Slide Area

Overview

The Rainey Creek slide area is located along Rainey Creek between the Swan Valley East and Gibson study areas. The section lies along US-26 between mile markers 374.8 to 375.5. The Rainey Creek site includes a large area of past landslide activity above and to a lesser extent below US-26 (Figure 3.17). Long sections of Rainey Creek have been pushed south as a result of past landslide movement. Two inclinometers LT-10 and LT-11 were installed by ITD on the south side of the highway to monitor slope movement. There was no evidence of slope landslide activity or roadway damage during the ITD-ISU 2023 to 2024 investigation period.

Figure 3.17 Location and identification of Rainey Creek Study Area in the Swan Valley Complex

UAS Change Detection in the Rainey Creek Study Area

The ISU Department of Geoscience conducted aerial surveys for the entire Swan Valley Complex including Rainey Creek three times during the two-year investigation period (Table 3.2). Comparison of the July 2023 and June 2024 LiDAR surveys show no measurable movement during the study period. (Figure 3.18).

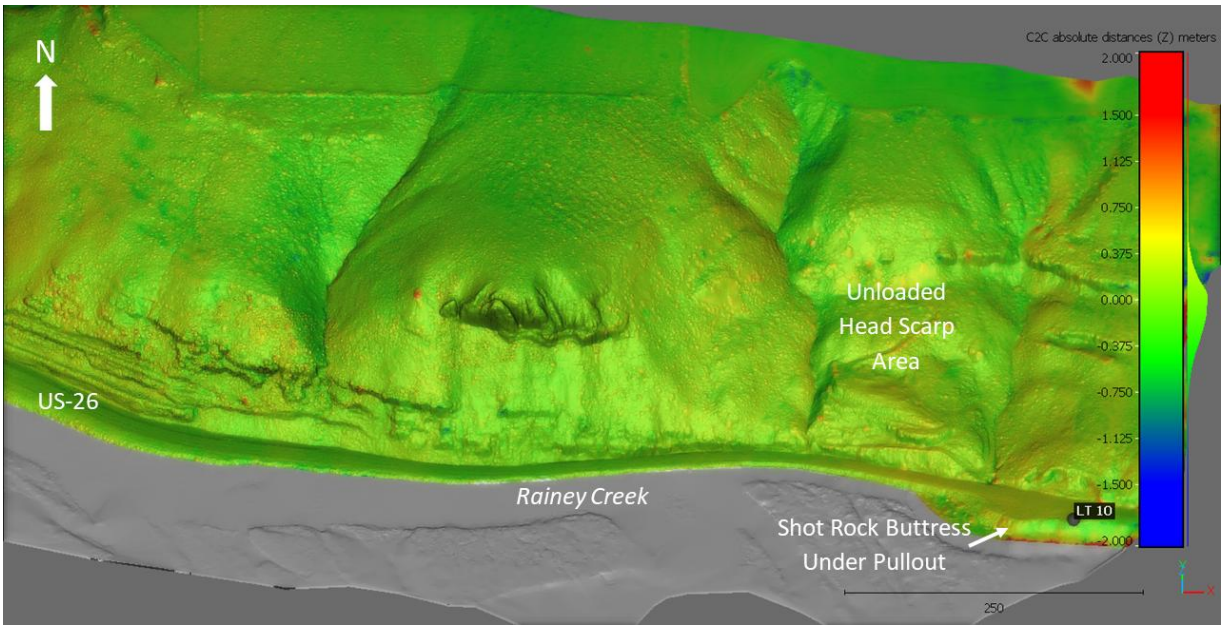

Figure 3.18 Rainey Creek Change Detection - July 2023 to October 2024

Rainey Creek Geologic Conditions

Based on the geologic map published by Dossett et al., 2012, the Rainey Creek site contains two basic quaternary formations:

- wind-blown silt (loess): Qi

- Antelope Flat Basalt: Qbar (Figure 3.3).

Dorssett et al (2012) describe the loess as a structureless silt and the Antelope Flat Basalt as

"Dark-gray to black vesicular basalt. Containing phenocrysts of olivine and plagioclase. As much as 100 ft thick. Columnar jointing common."

Quaternary alluvium (Qal) is also present in the slide area below (south of) the road.

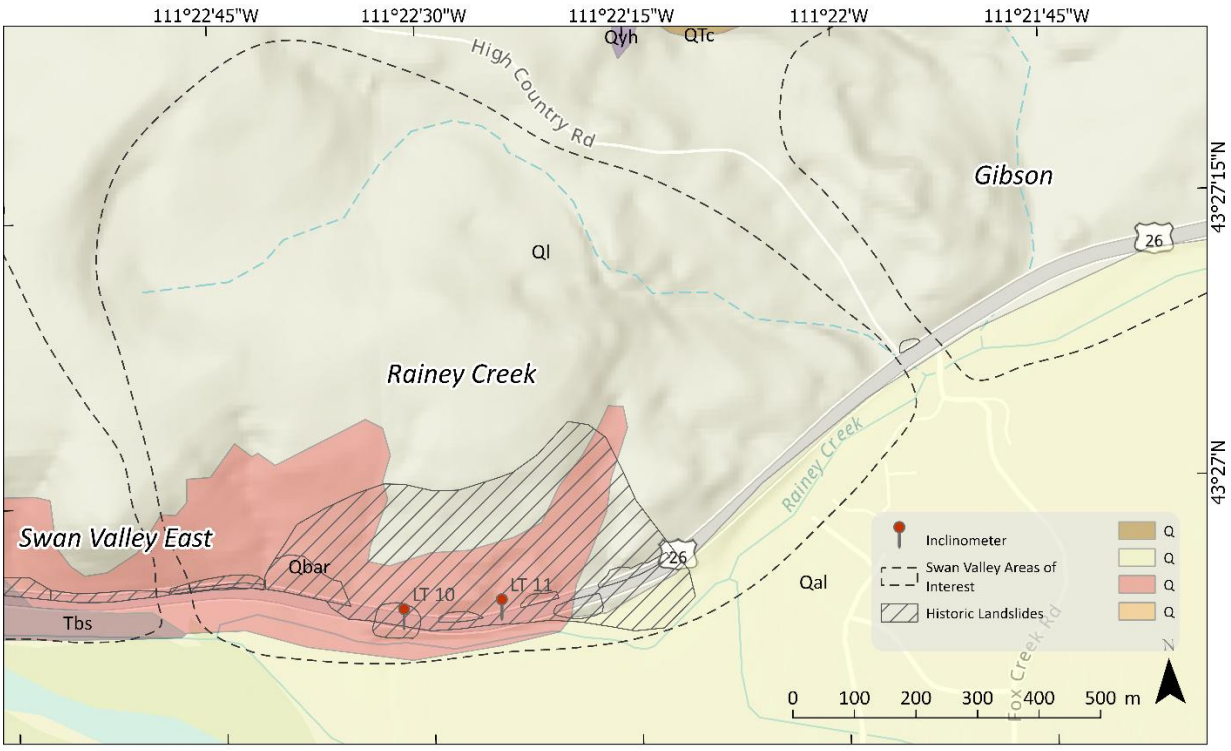

Qyh - Huckleberry Ridge Tuff: Light gray to grayish-pink crystal rich welded devitrified rhyolitic ash-flow tuff with well-developed eutaxitic fabric. Columnar jointing is common. Non-flattened white and pink pumices present in some localities. As much as 80 ft thick.

Qbar - Basalt of Antelope Flat, Rim Facies: dark-gray to black vesicular basalt. Containing phenocrysts of olivine and plagioclase. As much as 100 feet thick. Columnar jointing common.

Ql - Loess: Light yellow to yellow-gray well-sorted structureless silt. As much as 80 feet thick.

Tbs - Basalt of Swan Valley: Dark-gray to black, weathered brown to green, vesicular basalt. As much as 200 ft thick. Columnar jointing and massive flows are common. Red cinder and volcanic breccia layers are intercalated with the lava flows near the Swan Valley bridge. Variable-oriented jointing patterns found in some areas. Pillows and rosette-style jointing are absent. Dips about 10 degrees to the northeast near Conant Valley.

Qal - Alluvium: Unconsolidated, well sorted silt, sand, and gravel deposits along stream courses. Includes older terrace gravels along the Snake River.

Adapted from Dossett et al. 2012.

Figure 3.19 Geologic map of Rainey Creek Study Area (Adapted from Dossett et al. 2012)

Rainey Creek Instrumentation

Subsurface Conditions on the South Side of the Previous Slide Area

In September 2017, ITD installed two inclinometers (LT-10 and LT-11) in the Rainey Slide Area (Table 3.7). Both inclinometers were placed along the highway at or near the toe of the slope. Bore Holes LT-10 and LT-11 were drilled to depths of 50 and 40.1 ft, respectively. Both borings encountered fill and rock. In the log of LT-10, the basalt was placed in the Tertiary Swan Valley Formation (Tbs) and not the quaternary Antelope Flat Formation (Qbar) as shown on the geologic map (Figure 3.19).

Table 3.7 Inclinometer locations and status in the Rainey Creek Study Area

Inclinometer	Location (Lat/Long)	Ground Surface Elevation	Total Depth	Status
LT-10	43.448088/ -111.375581	5260 ft	48 ft	Operational
LT-11	43.448185/ -111.373614	5295 ft	38 ft	Operational

LT-10 and LT-11 Boring Logs

The basic subsurface profile in the past slide area consists of fill with and without underlying colluvium on rock. FILL 18 to 20 ft thick was encountered at both bore hole locations. In Bore Hole LT-10, the FILL is described as a soft to very soft, brown, clayey SILT to silty CLAY (CL-ML) with trace fine sand and moist to dry (Figure 3.20). Standard Penetration Test N-values were very low (2, 5 and 10 blows/ft) and water contents high (between 20 and 59%). The log of Boring LT-11 shows a similar upper layer profile except the N-values in the FILL are slightly higher (13, 6 and 7 blows/ft). Decomposed BRECCIA was encountered below the FILL in LT-10. The BRECCIA is a dense to very dense, dry, slightly clayey, silty sandy GRAVEL with angular sand and gravel rock fragments and scattered ash layers. All standard penetration N-values in the 14-ft thick BRECCA layer are at refusal (50 blows/1 to 3 in.). In LT-10, hard, dark gray, slightly weather BASALT was encountered at a depth of 34 ft. The BASALT contains closely spaced, smooth to rough, planar fractures dipping at angles of 40 to 60°. Clay fillings and secondary minerals were logged along the fracture surfaces. Core recovery is 100% and RQD 70 and 50%. The log shows a ground-water level at 34 ft at the time of drilling (10 September 2017).

In Bore Hole LT-11, an 11-ft thick layer of COLLUVIUM was encountered between the FILL and the underlying DECOMPOSED BRECCIA. The COLLUVIUM is a brown, slightly sandy, clayey SILT (ML) with scattered rock fragments up to 1 in. in size and occasional wood debris. A Standard Penetration Test N-value of 6 blows/ft was recorded at the top of the COLLUVIUM. The DECOMPOSED BRECCIA below the COLLUVIUM is a gray, silty sandy GRAVEL (GP) in a cemented volcanic ash matrix with angular fragments up to 3/4 in. in size. The unit is dry, no water levels were recorded in the log at the time of drilling the borehole.

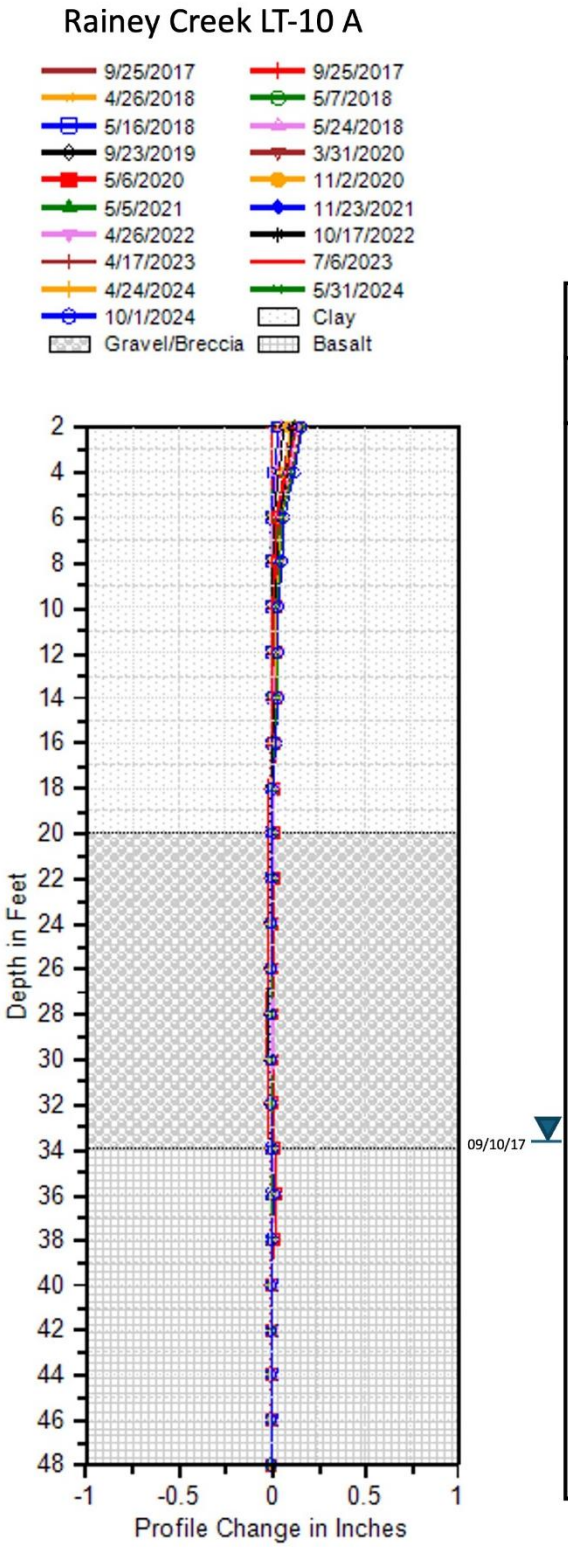

LT-10
09/10/2017

Elevation	Material Description	N (Blows/ft)
5260	VERY SOFT to SOFT, brown, Clayey SILT to silty CLAY (CL-ML); trace fine sand, slightly moist to dry (EMBANKMENT FILL)	2 5 10
5240	DENSE to VERY DENSE, slightly clayey, silty sandy GRAVEL; angular sand-to gravel-sized rock fragments, scattered ash layers, dry (DECOMPOSED BRECCIA)	50/2 in 50/3 in 50/1 in 50/1 in
5226	HARD, dark gray, slightly weathered BASALT; highly fractured fractures (40-60°), smooth to rough planar, clay infilling and secondary mineralization on fractured surfaces, dominant (SWAN VALLEY BASALT)	REC/RQD 100/70 100/50

Bottom of Boring: 50 ft

Figure 3.20 Inclinometer Displacements and Log of Boring LT 10 in Rainey Creek Study Area

Inclinometer Measurements

Inclinometers LT-10 and LT-11 were installed in the Rainey Creek Study Area and initial readings taken in September 2017. The bottoms of the casings are at depths of 48 ft in LT-10 and 38 ft in LT-11. Subsequent readings were made on the following dates during the ITD-ISU field investigation period.

- 06 July 2023
- 24 April 2024
- 30 May 2024
- 01 October 2024

Both inclinometers show lateral downslope movement with displacements of less than 0.1 at the roadway surface during the monitoring period (Figure 3.21). The incremental slope movement did not reach the 2 cm (0.8 in.) horizontal and 3 cm (1.2 in.) vertical thresholds for measurable displacement in the Rainey Creek LiDAR survey.

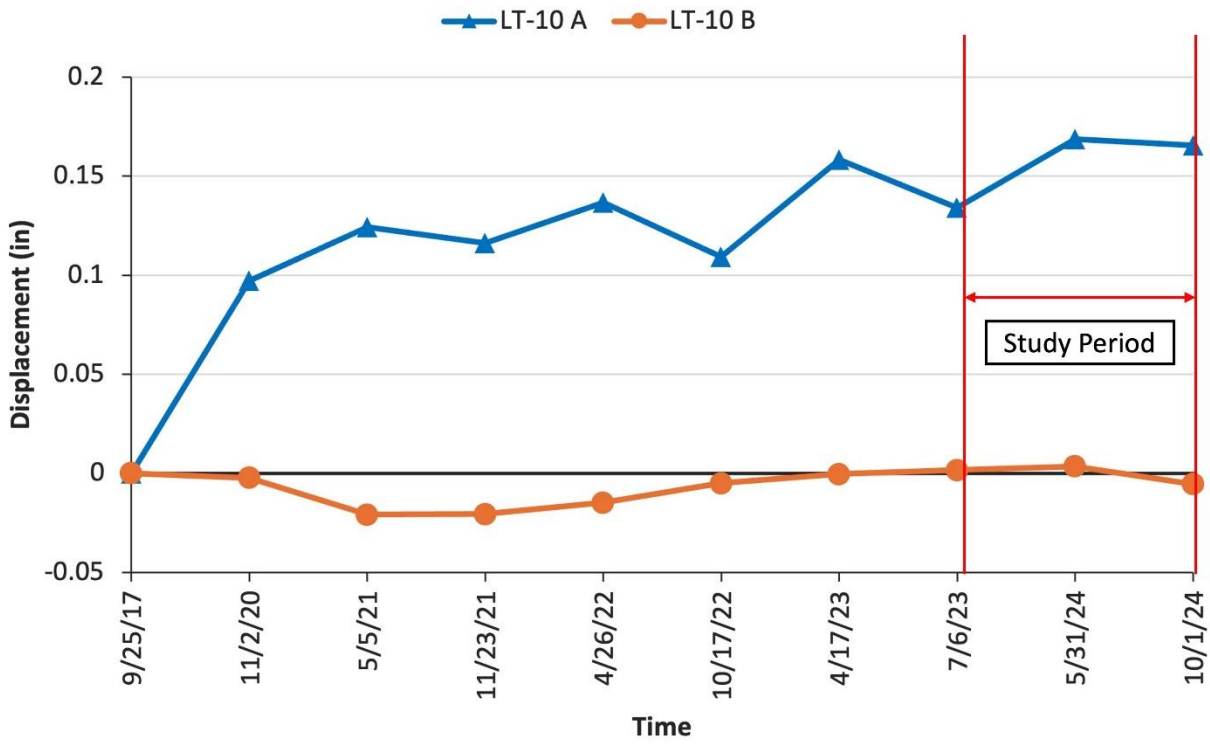

Figure 3.21 Near-Surface Displacement-Time Plot for Rainey Creek Inclinometer LT-10. Red lines with the arrow indicate the study period

Gibson Slide Area

Overview

The Gibson slide area is located on the far east end of the Swan Valley Complex and north of Rainey Creek (Figure 3.22). The overall dimensions of the site are approximately 2.3 km (1.4 miles) by 1.3 km (0.81 miles) and the area is geographically bounded by longitudes 111°22'24" W and 111°20'42" W and latitudes 43°27'00" N and 43°27'11" N. The long axis of the site trends east-northeast and the Gibson area is located at mile marker 376 on the Swan Valley Highway (US-26). The slope above the slide area contains basalt and tuff outcrops. The Rainey Creek channel in the center and on the east side of the site has been pushed south as a result of past landslide activity. The landscape consists of agricultural land and pasture typical of the remaining Swan Valley Complex. One inclinometer (LT-13) with groundwater monitoring capability was placed by ITD along the road.

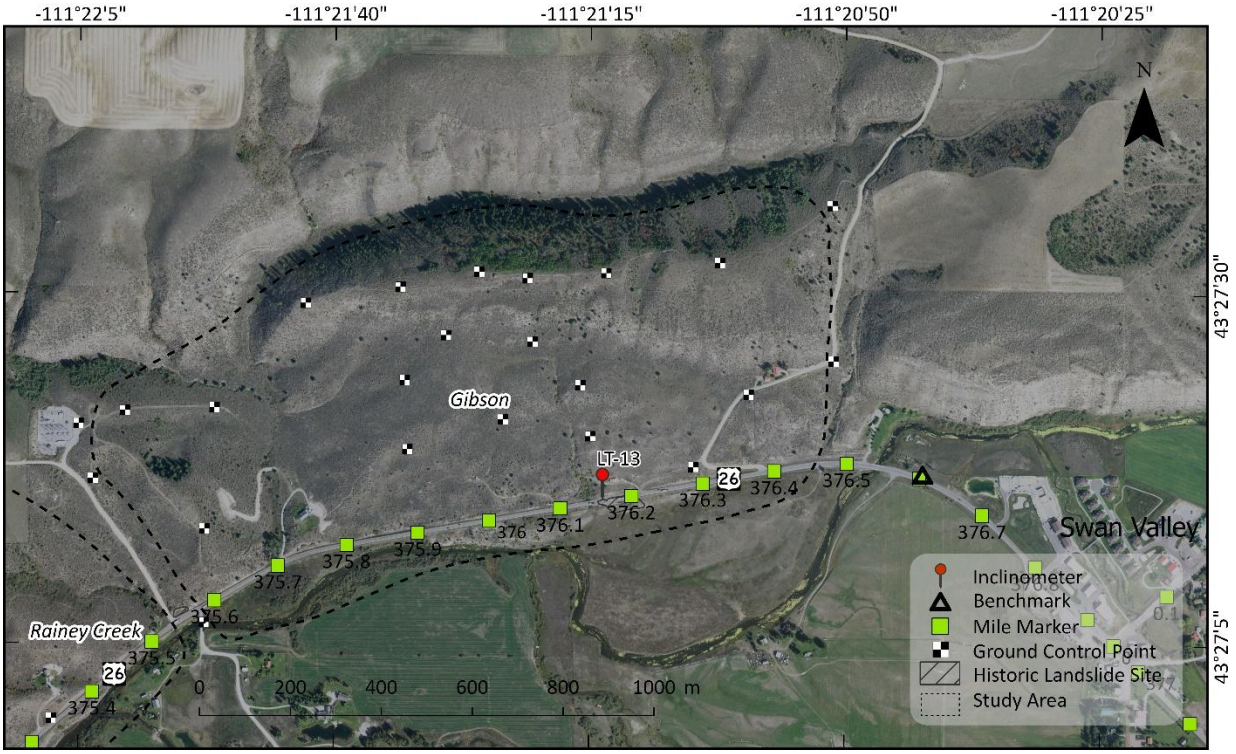

Figure 3.22 Location and Identification of the Gibson Slide Area in Swan Valley Complex along US-26

UAS Aerial Surveys of Gibson Slide Area

ISU Geosciences first surveyed the Gibson area on 21 July 2023 (Table 3.8). Subsequent surveys were carried out in June and October 2024.

Table 3.8 UAS Surveys of the Gibson Landslide Area

Platform / Sensor	Date
Trinity F90+ / D2M Oblique RGB 5 Camera	07-21-2023
Trinity Pro / Q240 - LiDAR	06-08-2024
Trinity Pro / Q240 - LiDAR	10-03-2024

To perform the aerial surveys, 24 ground control points were established across the site (Figure 3.16).

Gibson Landslide Terrain and Change Detection

The ground surface terrain mapped in the October 2024 survey is shown in Figure 3.23. The topographic lobe west of Inclinometer LT-13 along with the hummocky topography suggest past slope movement beneath and adjacent to US-26. The ground surface elevation changes between the 2023 and 2024 surveys in Figure 3.24 indicate some erosion in the intermittent stream channels on both sides of US-26 and Rainey Creek. There is no indication of slope movement in Gibson based on the Photogrammetry/LiDAR surveys during the study period.

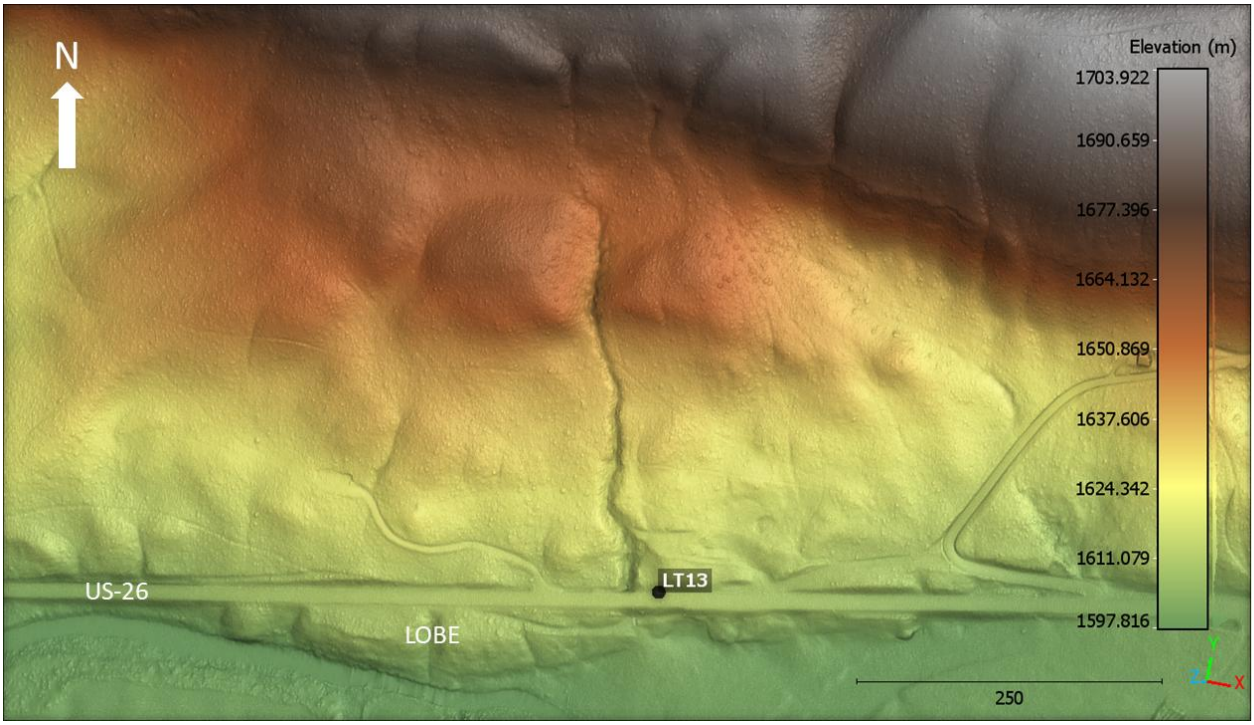

Figure 3.23 LiDAR October 2024 Elevation for Gibson Survey Area

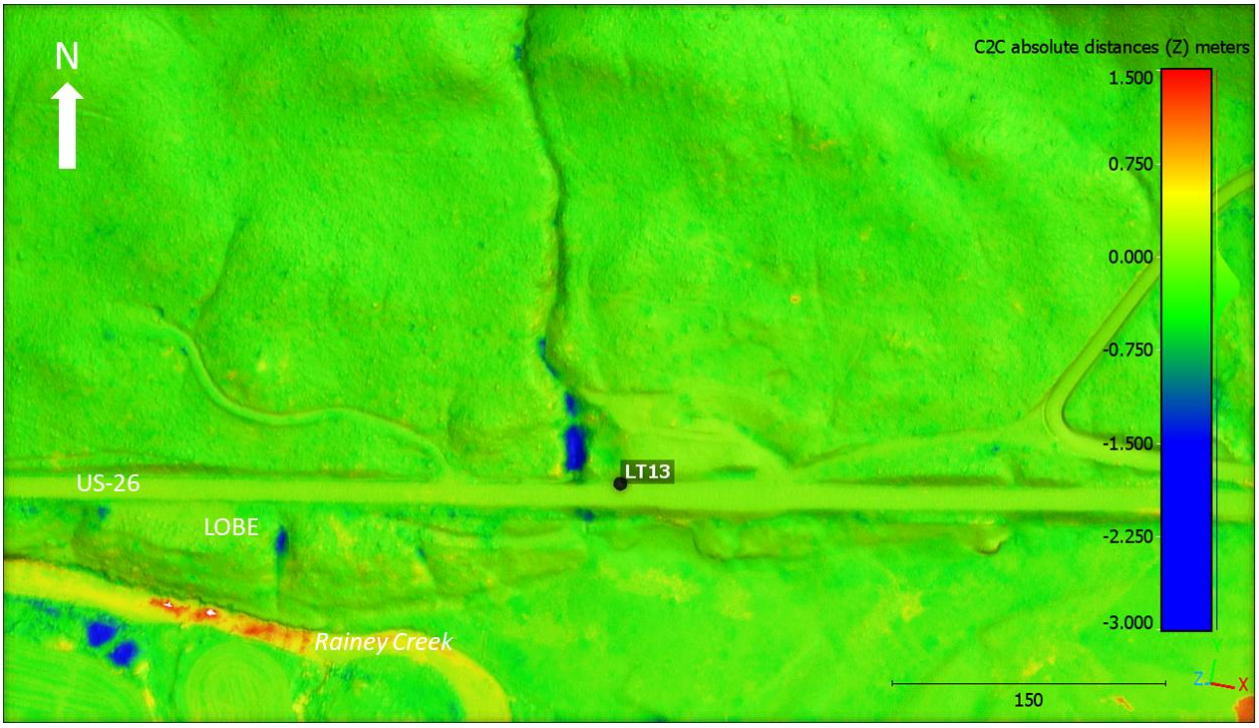

Figure 3.24 Change Detection July 2023 to Oct 2024

Gibson Geologic Profile

The Gibson Slide Area above the highway contains loess, colluvium, and extrusive igneous rock and colluvium in the following geologic units (Figure 3.25)

- Wind-blown silt (loess): QI
- Antelope Flat Basalt, rim facies: Qbar
- Huckleberry Ridge Tuff: Qyh
- Quaternary/Tertiary Colluvium: QTc
- Quaternary Alluvium: Qal

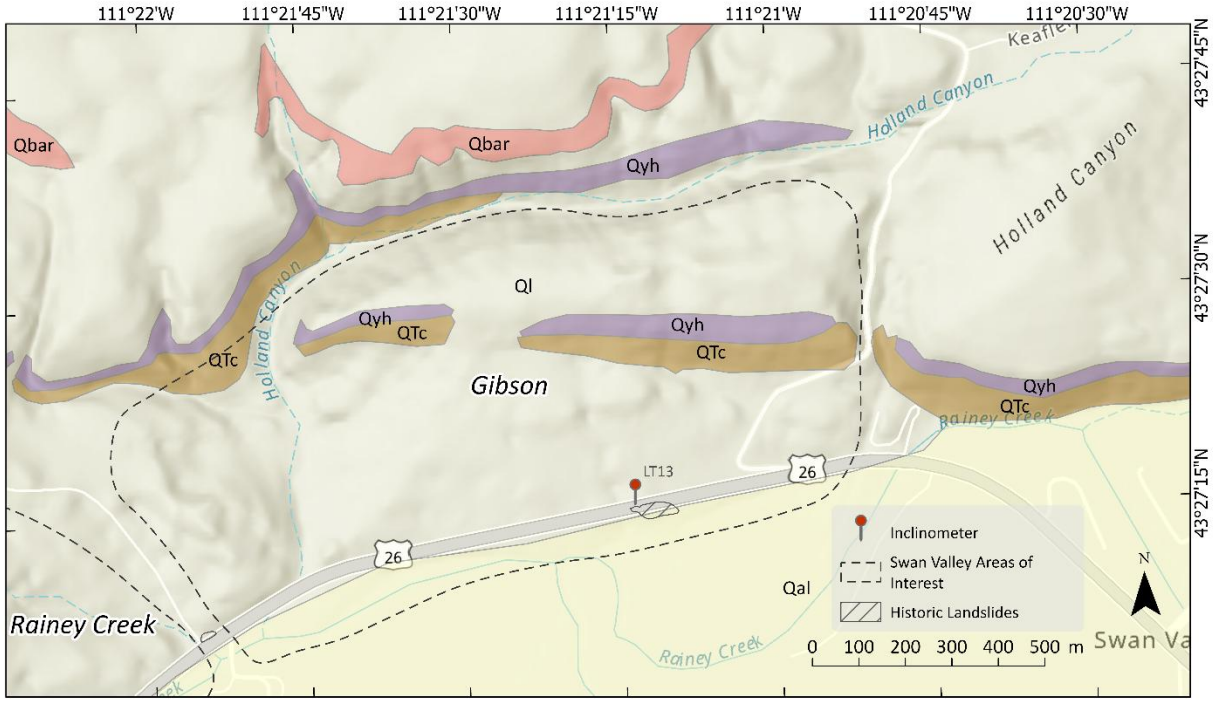

Figure 3.25 Geologic Map of the Gibson Slide Area in Swan Valley (Adapted from Dossett et al. 2012)

Gibson Instrumentation

Subsurface Profile at US-26 in a Former Landslide

Inclinometer LT-13 was installed by ITD in the Gibson Slide Area (see Figure 3.25 and Table 3.9). The inclinometer was placed along the highway where Rainey Creek channel starts to diverge to the south. LT-13 was drilled on 13 September 2017 to a depth of 50.1 ft. The subsurface profile is entirely in soil: no rock is logged in the bore hole (Figure 3.26). No descriptions of the Quaternary/Tertiary Colluvium (QTc) unit are provided in the Dossett et al (2012) Geologic Map of Swan Valley.

Table 3.9 Inclinometer Location and Status in the Gibson Slide Area

Inclinometer	Location (Lat/Long)	Ground Surface Elevation	Total Depth	Status
LT-13	43.454302 / -111.353814	5317 ft / 1621 m	48 ft / 15 m	Operational

LT-13 Boring Log

The log of Boring LT-13 shows 7 ft of FILL, 26 ft of COLLUVIUM above 17 ft of SAND (Figure 3.26). The FILL is described as a brown, dry, gravelly SAND (SW) with a trace of silt and rounded gravel up to 1.5 in. in size. The Standard penetration test N-value at the bottom of the layer is 10 blows/ft. The fill is underlain by COLLUVIUM: a brown, moist, high plasticity, silty CLAY (CH) having a mottle texture. N-values in the clay range between 6 and 12 blows/ft: most values are less than 10 blows/ft and are consistent with the past slope movement shown in the inclinometer. Water contents range between 30 and up to 55%.

The basal sand layer at a depth of 33 ft is described as a very dense, gray, wet, slightly silty SAND (SW) with numerous decomposed rock fragments. Refusal blow counts (50/1 in. to 50/3 in.) were recorded in the middle and bottom sections of the hole.

Inclinometer Results in LT-13

Inclinometer LT-13 was installed by ITD on 13 September and first read on 25 September 2017. The lateral movement data show increased displacement during the 7-year monitoring period. The movement pattern is laterally uniform between the ground surface and a depth of 12 ft. Between 12 to 14 ft, the soil movement involves lateral shear of the inclinometer casing. Most of the slope movement occurred during the 6 July 2023 and 31 May 2024 time period (Figure 3.26). Lateral displacement at the ground surface in LT-13 was less than 0.44 in. (<2.0 cm) during the monitoring period and is below the threshold for measurable displacement in the Rainey Creek LiDAR survey (Figure 3.27).

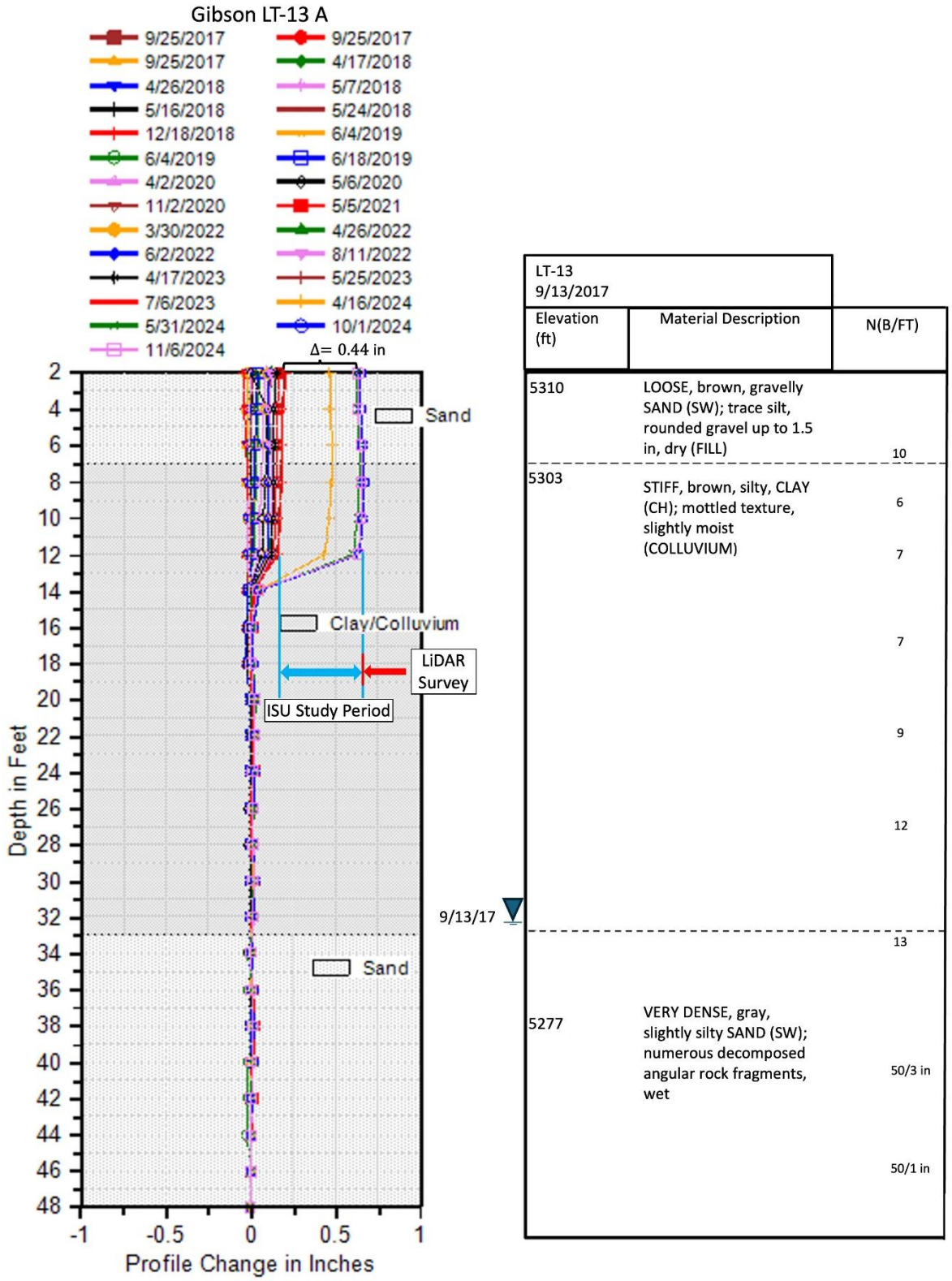

Figure 3.26 Inclinometer Displacements and Corresponding Log of Boring LT-13 in the Gibson Slide Area

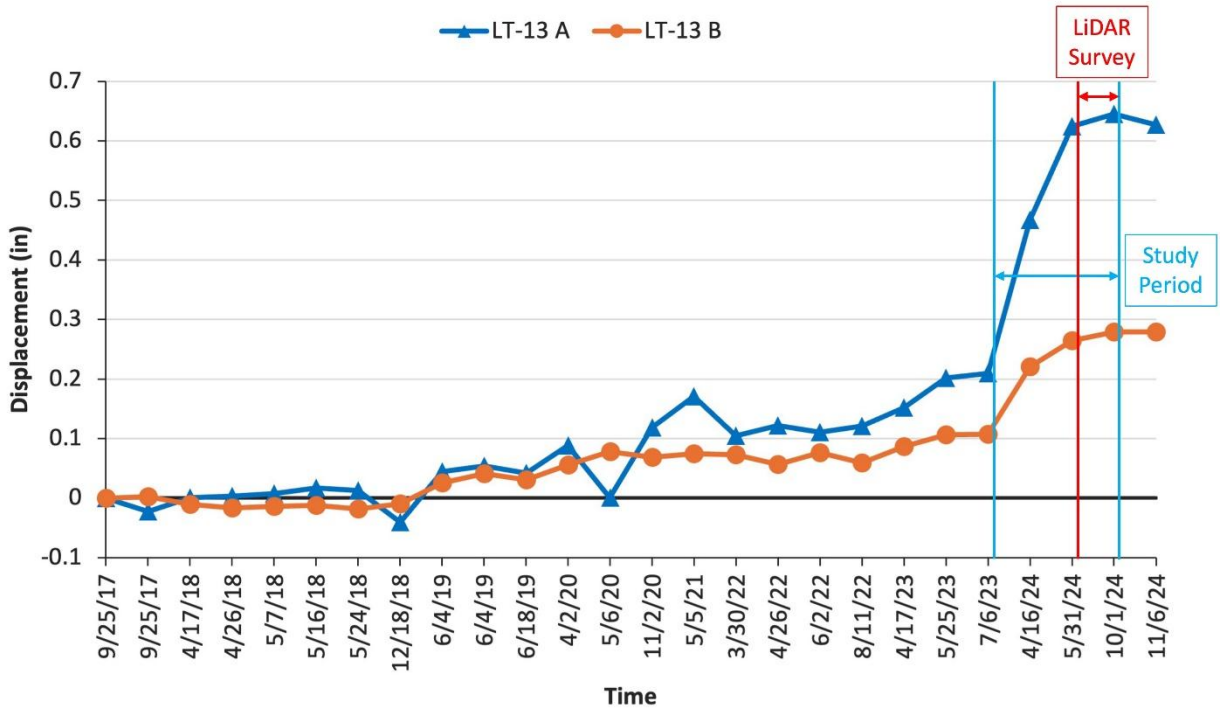

Figure 3.27 Near Surface Displacement-time Plot of Gibson Inclinometer LT-13. Red line with arrows indicates the study period.

Indian Creek Complex

Overview

The Indian Creek Landslide Complex is located in the Eastern Snake River Plain along US-26 on the east side of Palisades Reservoir (Figure 3.28). The section lies between mile markers 397.9 and 399.0. The study area is approximately 1.4 km^2 (0.55 mi^2) in size and lies between longitudes 111°06'40" W and 111°05'40" W and latitudes 43°15'04" N and 43°14'01" N. The topography includes northwest/southwest-facing slopes and an approximate east-west trending ridgeline. The upland vegetation on the northwest side of the ridge is characterized by dense coniferous and deciduous forests. On the southwest side of the ridge, the vegetation is also dense but with open areas of past slope movement and rock outcrops. Elevation ranges between 1707 and 1938 m (5600 and 6358 ft). Evidence of past hillslope movement and landslide activity is visible along slopes both above and below the highway. A large area of past hillslope movement is present in the north side of the ridge. Recent but limited slope movement below and including US-26 is evident on both sides of the ridge. ITD installed three 75 to 120 ft deep inclinometers (LT-31, LT-33 and LT-40) along US-26 in the Indian Creek area to monitor slope movement at depth in the complex area.

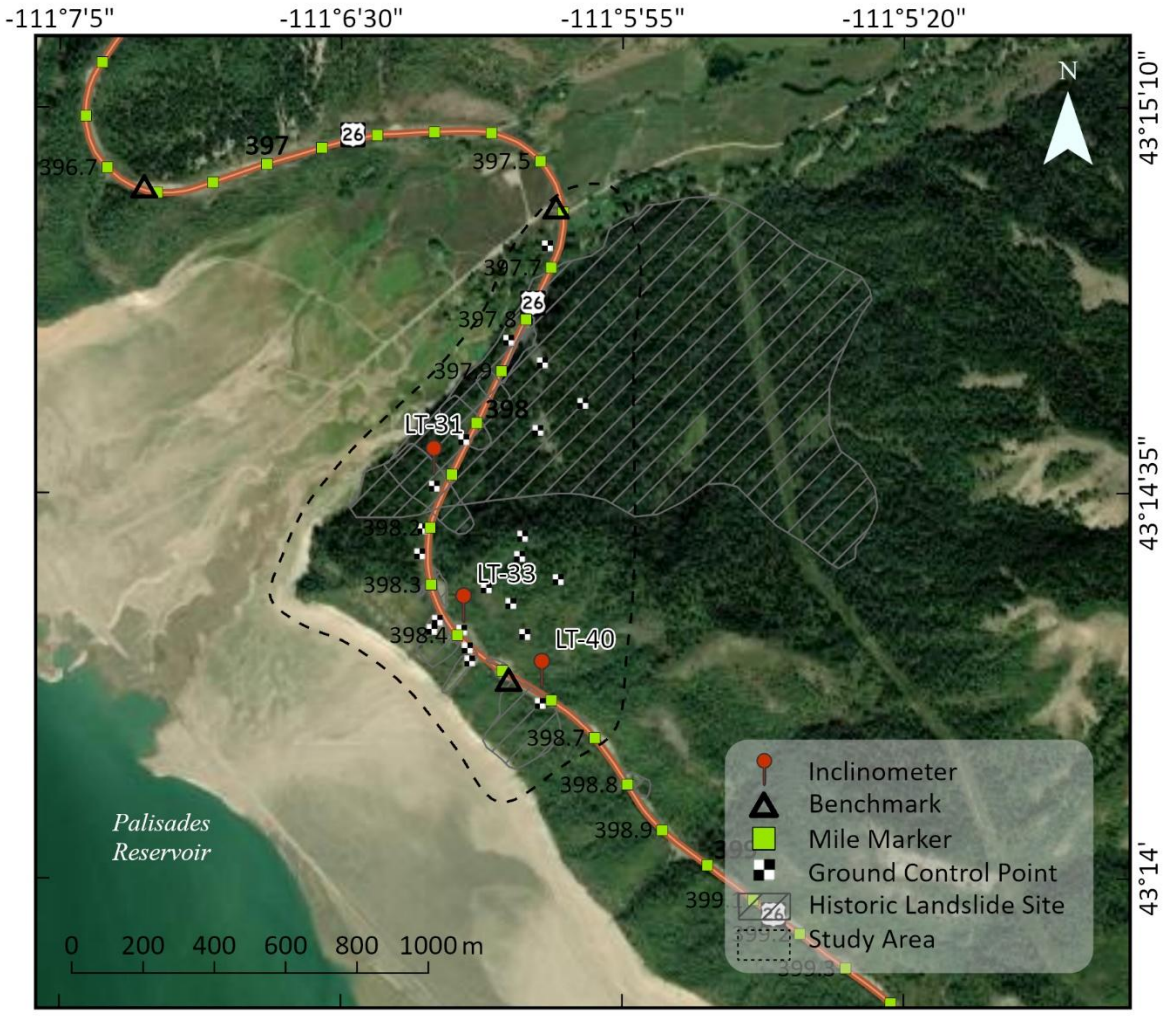

Figure 3.28 Location and Identification of Indian Creek Complex Study Area along US-26

UAS Survey of Indian Creek Complex

The ISU Department of Geosciences surveyed the entire Indian Creek Complex three times during the study investigation period (Table 3.10). The initial UAV survey was performed on 16 October 2023 and the last survey on 26 October 2024. Twenty-two ground control points (GCPs) were placed by ISU staff for the aerial surveys (Figure 3.27). A combination of five permanent ground control points (GCPs) and seventeen temporary GCPs were utilized in the UAV surveys. Two benchmarks located on the north and south ends of the slide area were utilized as control points. GCPs were recorded using an Emlid Reach RS2 Base and Rover GPS system sensitive to 2 cm (0.8 in) horizontal and 3 cm (1.2 in) vertical.

Table 3.10 Dates and Sensors of ISU - UAS Surveys in the Indian Creek Complex

Sensor	Date
D2M – Oblique Camera	10-16-2023
Q240 – LiDAR	06-07-2024
Q240 – LiDAR	10-26-2024

Site Characteristics

LiDAR surveys with and without the trees are given in Figure 3.29 and Figure 3.30, respectively. Inclinometer locations (LT-31) and US-26 are shown in the figures. Clearly, the tree cover is dense except in isolated exposed areas on the hillsides, many of which are the result of slope movement and/or surface erosion.

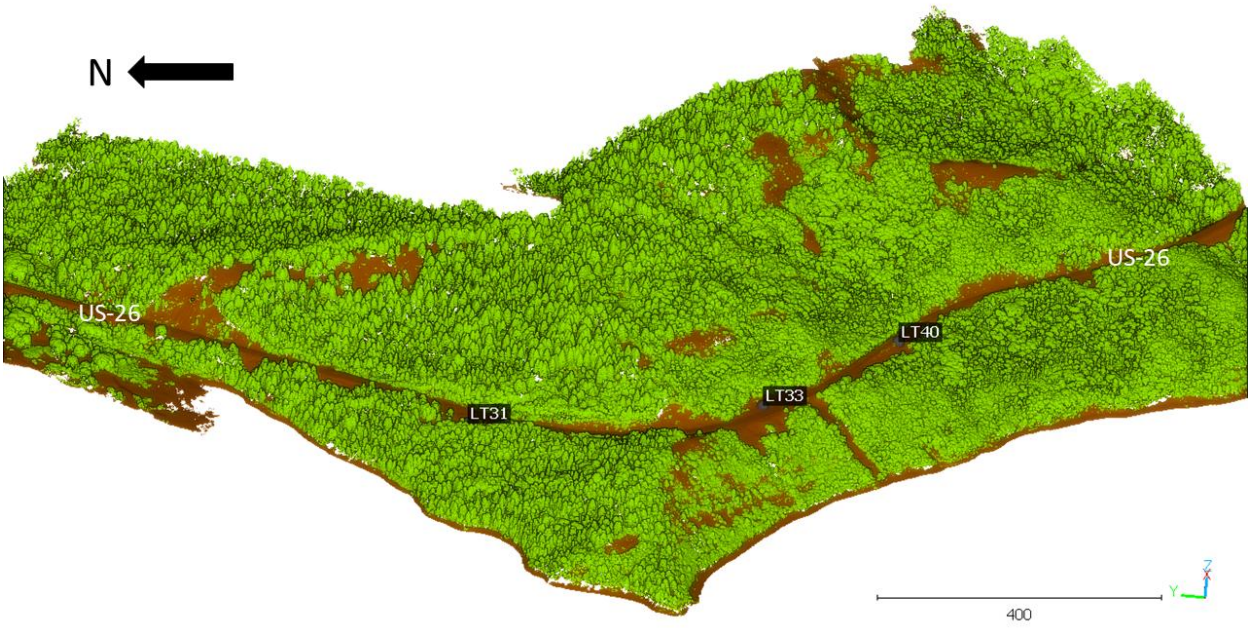

Figure 3.29 October 2024 LiDAR Survey of Indian Creek

The LiDAR survey with stripped vegetation shows a hillside area cut by a series of youthful streams primarily on the southwest side of the ridge. Limited areas of recent slope movement are noted along the upslope side of the road such as above the turn-out area (Figure 3.29). One open strip south of Inclinometer LT33 extends west from the road down to the reservoir. The ground surface in the strip appears to be a combination of slope instability immediately below US-26 and snow avalanche/erosion on the remainder of the slope.

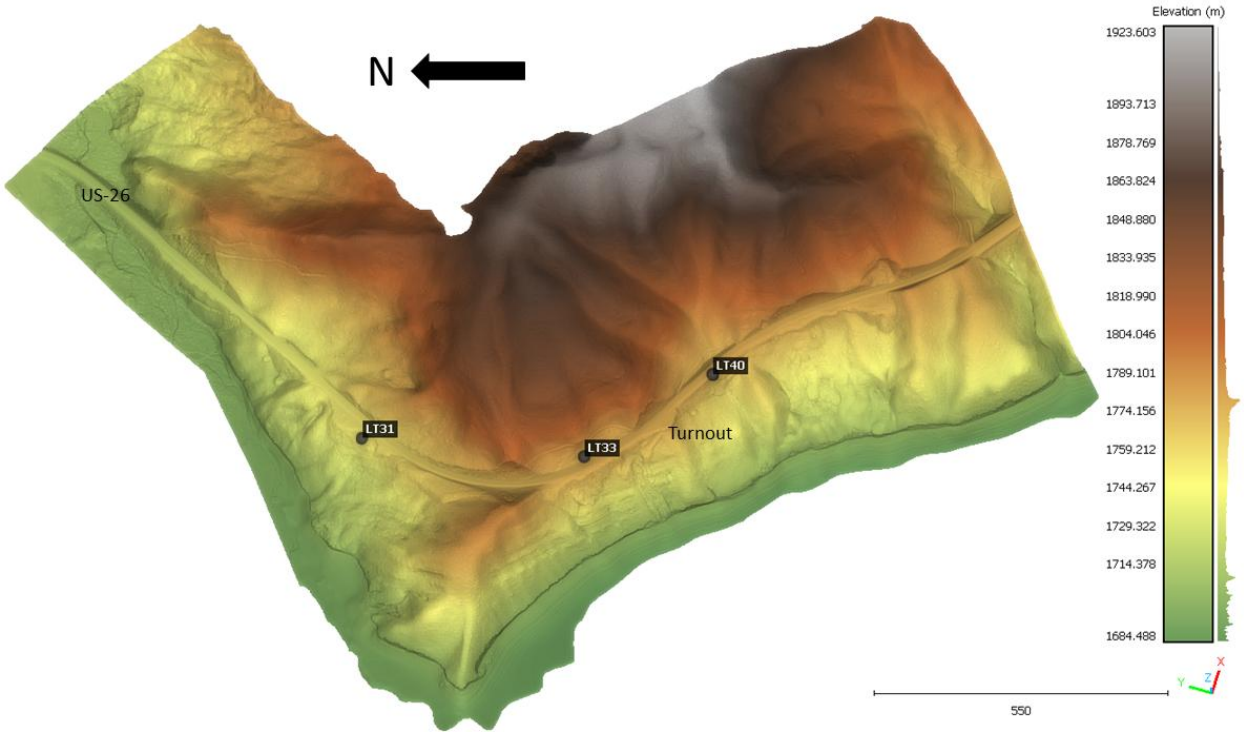

Figure 3.30 Oct 2024 LiDAR Survey with Trees Removed

Indian Creek Landslide Terrain and Change Detection

The UAS surveys of October 2023 (D2M camera/photogrammetry) and June 2024 (LiDAR) were used to estimate change detection maps for the Indian Creek study area (Figure 3.31 and Figure 3.32). Much of the area was masked by the large, dense tree vegetation that was impenetrable by the photogrammetry processed D2M camera. Unfortunately, the LiDAR sensor was not available in 2023 for surveys of Indian Creek. However, the comparison of the June to October 2024 LiDAR surveys (Figure 3.32) clearly show little to no landslide/erosion activity during the short study period. The LiDAR surveys do provide baseline ground surfaces for evaluating the future performance of the slopes and the roadway. Additional diagrams of ground surface elevation changes in the Indian Creek study area are provided in Appendix B of this report.

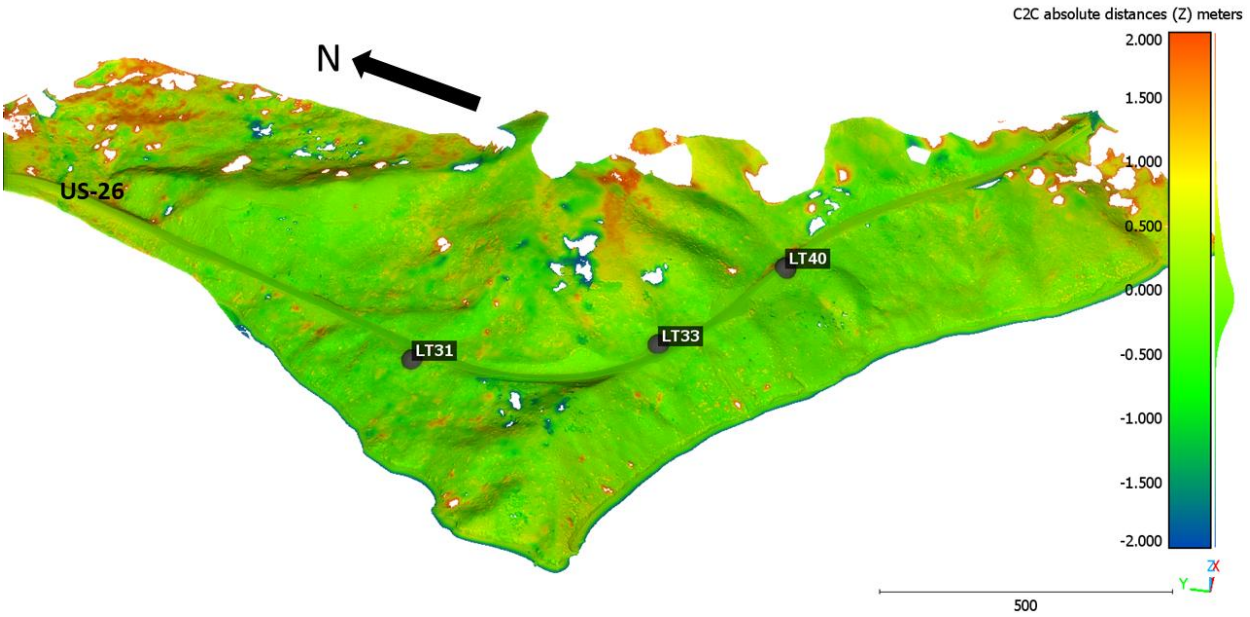

Figure 3.31 Change Detection October 2023 (D2M camera) to June 2024 (LiDAR). Orange colored areas and white gaps indicate densely treed areas because the 2023 flights captured with a camera and processed using photogrammetry methods instead of using LiDAR.

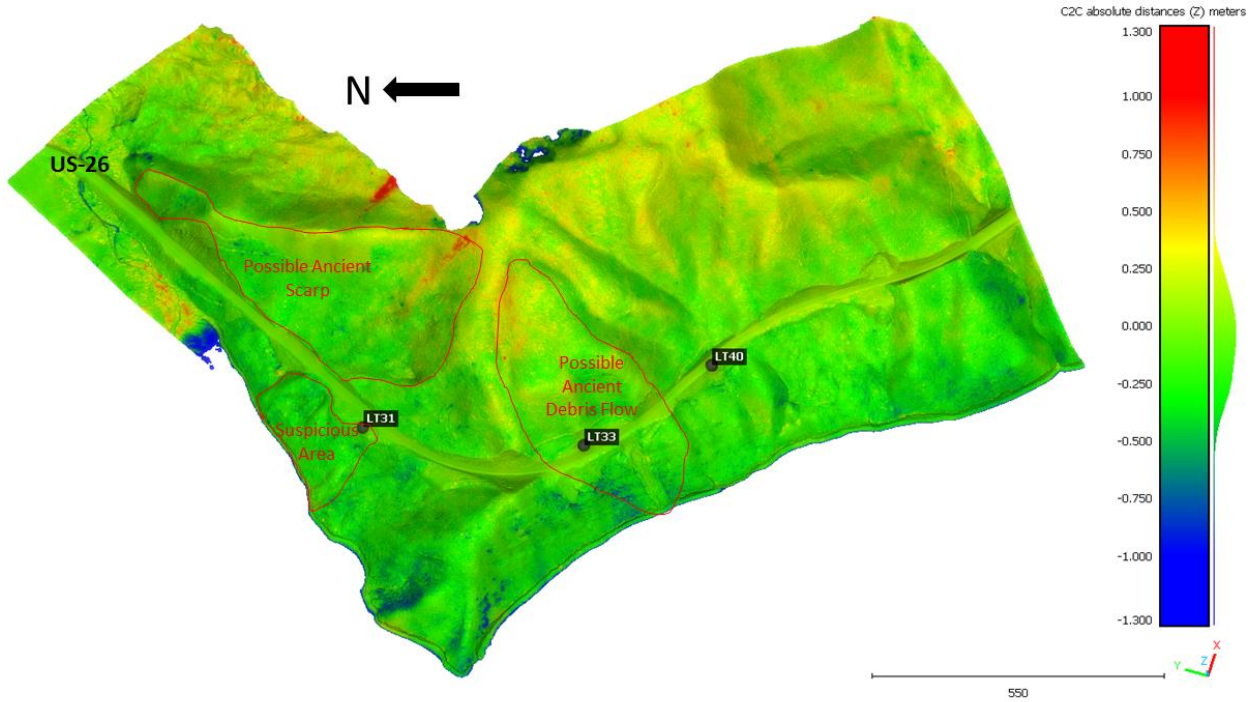

Figure 3.32 June 2024 LiDAR versus September 2024 LiDAR (red: dense trees/blue: slope erosion)

Indian Creek Geologic Conditions

Quaternary Alluvium (Qal), Colluvium (Qc), and Tertiary Huckleberry Ridge Tuff (Ttc) are identified in the Indian Creek Complex area (Figure 3.33). The alluvium in the valley north of the study area is up to 40 ft thick. Colluvium (Qc) is present throughout the slopes and contains siltstone, claystone, tuff, and pumicite and conglomerate particles. The colluvium is underlain by a volcanic rock identified as the Huckleberry Ridge Tuff. The unit is made up of welded, devitrified, rhyolitic as-flow tuff Columnar jointing is common. The section below the road and above the reservoir contains bedded layers in unmapped exposures of the Huckleberry Ridge Tuff.

Geologic structures in proximity to the site consist of normal faults. The north-northwest/south-southeast trending Grand Valley Fault is the closest major fault to the study area and was mapped approximately 300 m (980 ft) east of the major slide area. The Palisades Valley occupies a seismically active graben between two fault systems on the east and west sides of the reservoir. Schleicher (1975) suggests that water level changes in the Palisades Reservoir appear to trigger earthquakes with Richter magnitudes of 3 or less when water level fluctuations cause increases in porewater pressures in the fault zones. During the spring, earthquakes occur when reservoir water levels abruptly rise, producing excess pore water pressures in the adjacent slopes. Earthquakes are also triggered in the fall when reservoir water levels drop and produce residual groundwater levels in the adjacent slopes.

Indian Creek Instrumentation

Inclinometers

In September 2017, three inclinometers (LT-31, LT-33 and LT-40) were installed by ITD along the US-26 corridor in the Indian Creek Complex (Table 3.11). Initial measurement dates were 25 and 26 September 2017. The inclinometers were placed in and above active slide areas. ITD inclinometer designations, location/elevations, and depths are summarized in Table 3.11.

Table 3.11 Summary of Indian Creek Landslide Complex Inclinometers

Inclinometer	Location (Lat/Long)	Ground Surface Elevation	Total Depth	Status
LT-31	43.243264 / -111.105125	5755 ft	73 ft	Operational
LT-33	43.239545 / -111.104095	5870 ft	79 ft	Operational
LT-40	43.237896 / -111.101389	5755 ft	116 ft	Operational

LT-31 was installed on the south end of the large unstable area on the north side of the Indian Creek Complex (Figure 3.33). Bore holes for the inclinometers were drilled to depths of 75.9 ft, 80.8 ft, and 120.7 ft, respectively. The inclinometers are located between US-26 mile markers 396.2 and 397.3.

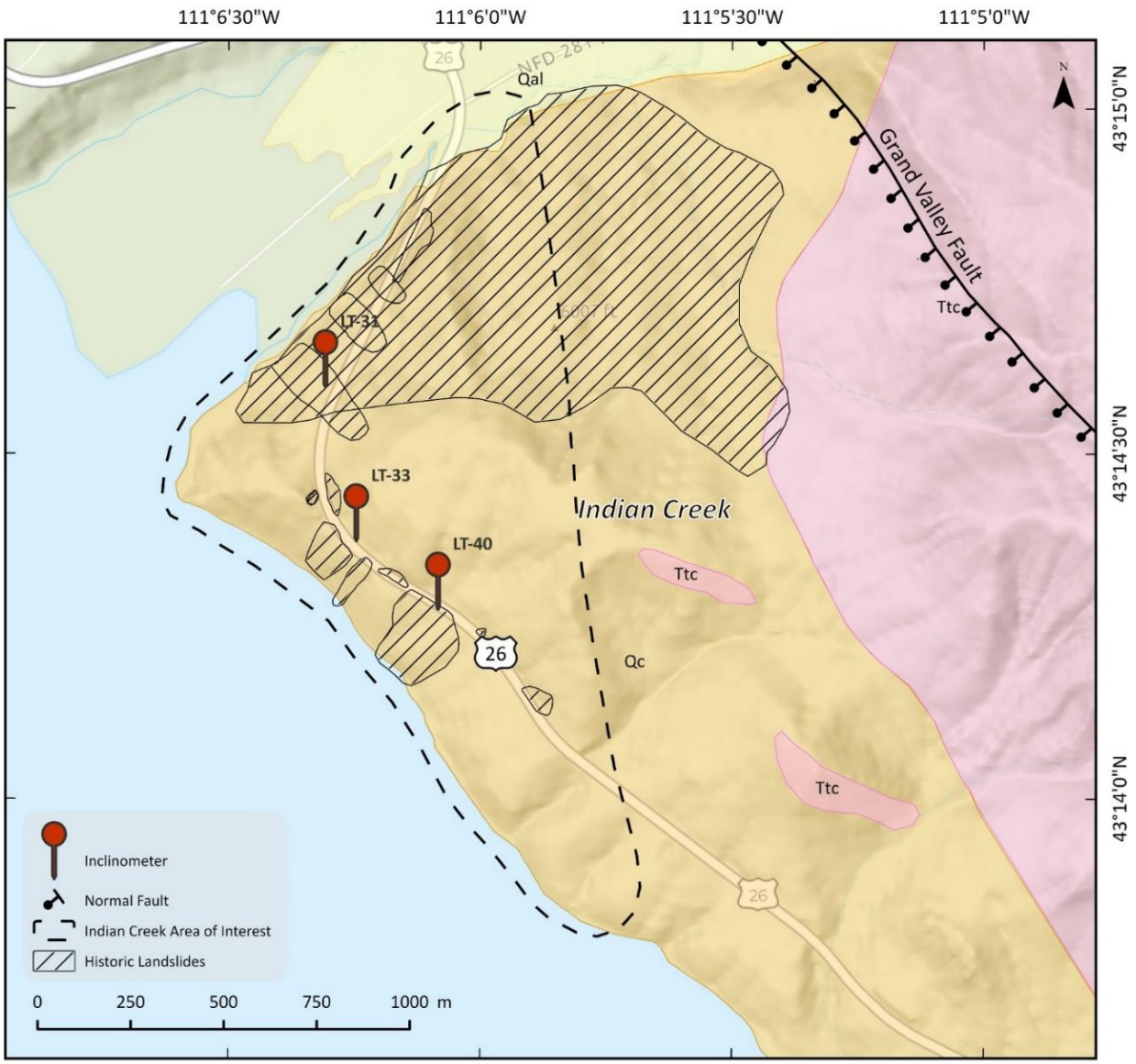

Qal – Alluvium: Unconsolidated, well sorted silt, sand, and gravel deposits along stream courses.

Qc – Colluvium: Siltstone, claystone, tuff, pumicite, and conglomerate divisible into an upper conglomerate, a middle tuff and pumicite, and a lower claystone and siltstone; up to 1500+ m thick.

Ttc – Huckleberry Ridge Tuff: Light gray to grayish-pink crystal rich welded devitrified rhyolitic ash-flow tuff with well-developed eutaxitic fabric. Columnar jointing is common. Non-flattened white and pink pumices are present in some localities. As much as 24 m thick.

Figure 3.33 Geologic Map of the Indian Creek Complex (Adapted from Albee and Cullins 1975)

Inclinometer Boring Logs

Geotechnical boring logs were prepared by Landslide Technology of Portland Oregon for the inclinometer installations similar to the bore holes in the Swan Valley Complex. Two-inch standard split spoon samples were taken at 5 ft intervals. Blow counts are recorded for each 6 in. interval of drive for a sample length of 18 in. Soil descriptions include color, moisture and origin for the limited coarse-grained soils encountered in Bore Hole LT-40. Visual percentages of grain size, grain shape, density and cementation are also provided in the log. Plasticity, consistency (strength) and the presence of sand, gravel and organics were described for the fine-grained soils. Samples were visually classified under the Unified Soil Classification System (USCS) and interpretations made on the origins of the layers. Water contents are provided in graphical format for the soil samples. Groundwater levels and dates recorded during and after drilling are also provided in the logs. Rock type, color, cementation and moisture are given in the log of LT-40 where rock was encountered in the bore hole. The sandstone and claystone encountered at a depth of 72 ft were drilled with a hollow stem auger and sampled with a 2-in. diameter standard split spoon. No rock was encountered in Borings LT-31 and LT-33.

Subsurface Profiles in LT-series Borings

In LT-31, FILL is described in the boring log from the ground surface down to a depth of 43 ft (Figure 3.34). ITD geotechnical personal opine that the FILL is actually LANDSLIDE DEBRIS (Enright Personal Communication, 2025). The FILL/LANDSLIDE DEBRIS is described as a brown, slightly moist, soft to medium stiff, slightly sandy, slightly clayey to clayey SILT (ML) with occasional organics and wood debris. A specific notation of wood debris is given in the log between depths of 30 to 31.5 ft. Standard Penetration Test values in the FILL/LANDSLIDE DEBRIS supporting the road were low and ranged from a minimum of 2 to a maximum of 12 blows/ft. Ground water levels during September to December 2017 were in the FILL/ LANDSLIDE DEBRIS at depths of 35 to 38.2 ft below the ground surface. A zone of significant movement has and is occurring in LT-31 at a depth of 45 ft just below the fill-colluvium contact. No FILL was encountered in Boring LT-33.

The colluvium below the FILL in Boring Hole LT-31 and below the ground surface in LT-33 is described as a brown to gray, very stiff to hard, silty CLAY with a trace of fine sand to slightly sandy, occasional organics and slightly moist. Sandy silt lenses were encountered in Boring LT-31 and occasional rock fragments up to 1.5 inches in size in Boring LT-33. Standard Penetration N-values in the CLAY range from a minimum of 26 blows/ft to refusal - 50 blows for less than 6 in. of drive. LT-31 bottoms out in the CLAY COLLUVIUM at a depth of 75.9 ft

The CLAY COLLUVIUM in LT-33 is underlain by a thick stratum of SILT starting at a depth of 32 ft and extending 80 ft down to the bottom of the bore hole at elevation 5831 ft. The SILT is described in the log as gray and slightly sandy/slightly clayey. The top of the layer at 32 ft is dry and then moist to wet at a depth of 57 ft. Groundwater levels were measured at approximate depths of 60.3 ft and 32.7 ft on 23 September (at time of drilling) and 10 December 2017 after the hole was completed, respectively. Refusal Standard Penetration N-values 96/9 in. to 50/3 in. were recorded through the full depth of the COLLUVIUM.

Boring LT-40 was drilled in the US-26 roadway on the south side of the Indian Creek Complex. The upper 32 ft is identified as FILL with road aggregate and gravel in the upper 8 ft and soft to medium stiff, slightly sandy, slightly clayey and clayey SILT (ML) between 8 and 32 ft. The Standard Penetration N-values in the granular fill is 12 blows/ft and 7 to 15 blows/ft in the underlying silt. The water content ranges between 8 and 28% and the FILL is described as dry to moist. The inclinometer installed in LT-40 underwent small lateral displacements in the fill within 8 ft of the ground surface during the 2017 to 2024 monitoring period. Landslide debris underlies the fill down to a depth of 72 ft. The debris is described as a brown, soft to medium stiff, slightly sandy, slightly clayey to clayey SILT (ML) with a trace of gravel-sized rock up to 1.5 inches in size, occasional organics and wood debris. N-values in the silt range between 6 and 14 blows/ft. One groundwater level was recorded at a depth of 56.5 ft in December 2017, 3 months after the hole was drilled.

The LANDSLIDE DEBRIS in LT-40 is underlain by 7 ft of SANDSTONE above 40 ft of CLAYSTONE to the bottom of the hole at elevation 5634.3 ft. The SANDSTONE is described as a very dense silty, fine to medium SAND. The CLAYSTONE is a reddish-brown, silty CLAY with a mottled texture and dry. N-values in the rock were at refusal 94 blows/10 in. to 50 blows/2 in. No cores were taken in the rock units.

Inclinometer Measurements

Slope Indicator Inc. inclinometers were installed by ITD in all three LT-series boreholes in the Indian Creek Complex. Inclinometer tubes were placed to depths of 73 to 120 ft and were grouted from the end caps to the ground surface. Baseline readings at 2-ft depth intervals were taken by ITD personnel starting on 25 and 26 September 2017. Subsequent readings were made on the following dates during the ITD-ISU investigation period:

- 29 November 2023
- 16 April 2024
- 06 June 2024
- 01 October 2024 and
- 06 November 2024

Inclinometers LT-33 and LT-40 are located in and adjacent to a historic 1960 slide area but do not show significant lateral displacement during the one-year observation period. The absence of measurable movement is consistent with the displacement vectors obtained in the LiDAR surveys.

Lateral displacement down to a depth of 45 ft was recorded in Inclinometer LT-31 located on the south end of the massive landslide area prior to and during the study period (Figure 3.34). The displacement depth profile shows a total rigid body, lateral displacement of 1.28 in. (3.25 cm) down to a depth of 41 ft followed by lateral shear between 41 to 45 ft. During late November 2023 to early November 2024, the additional surface displacement was approximately 0.18 in. (0.46 cm). As observed at other sites, such

as in the Swan Valley Complex, the displacements have not reached the 2 to 3 cm differential measurement thresholds for detection of slope movement in the LiDAR surveys (Figure 3.35).

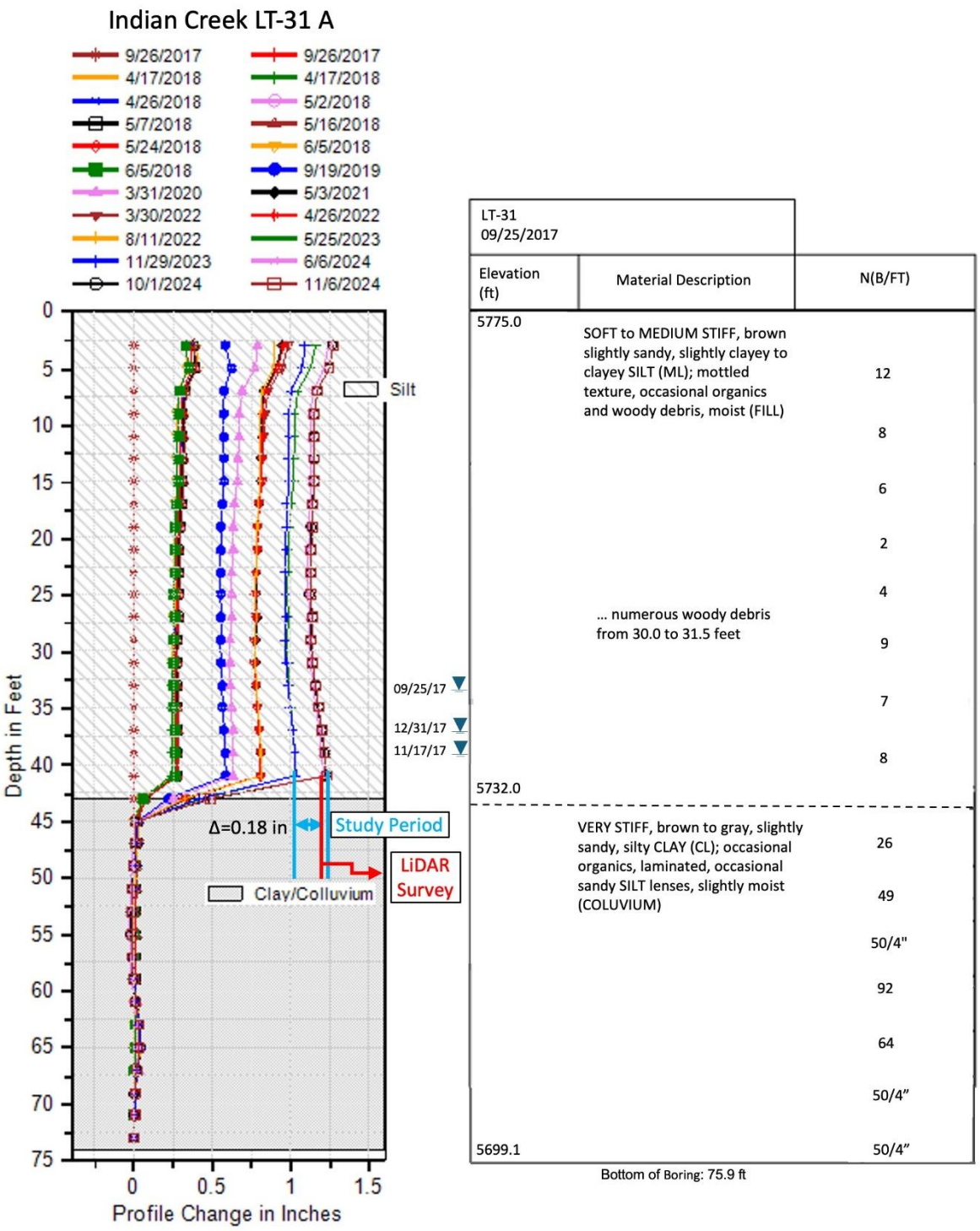

Figure 3.34 Inclinometer displacements and corresponding log of Boring LT-31 in the Indian Creek Study Area.

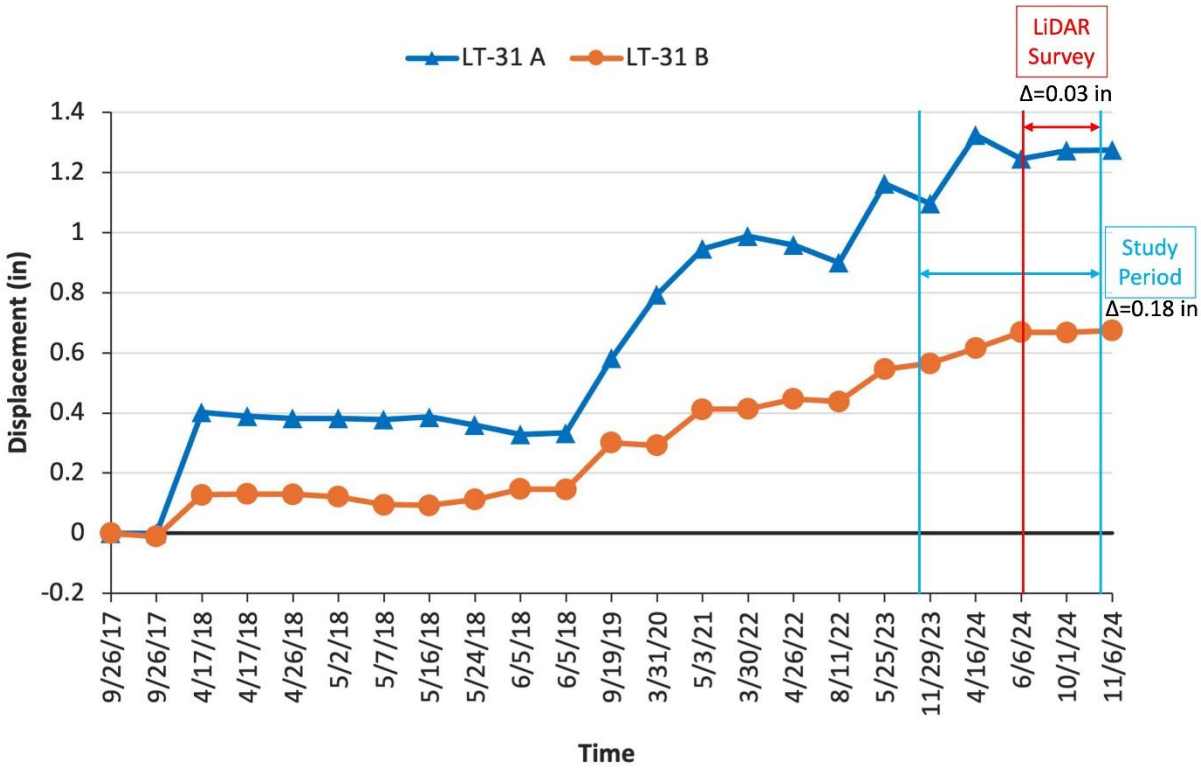

Figure 3.35 Near-surface Displacement-Time at Inclinometer LT-31

Pine Bar Landslide Area

Overview

The Pine Bar study area, also called Tincup, is located along SH-34 in west central Caribou County, Idaho (Figure 3.36). The site is an area of past landslide activity on the northwest side of Tincup Creek. The slope has limited vegetation cover except in local areas adjacent to the road along the base of the slide. The landscape is characterized by a mixture of trees and grasses reflective of its natural, forest environment. Soil is exposed in the upper part of the hillside which indicates some level of past and active movement. The study area is approximately 1.26 km^2 (0.49 mi^2) in size and is located between longitude 111°12'09" W and 111°12'41" W and latitude 42°58'19" N and 43°14'03" N. The elevation ranges between 1908 and 2005 m (6260 to 6578 ft). The downslope side of the road contains sections in which past slope movements have caused lateral displacement of the creek. ITD has installed four inclinometers (LT-1, LT-2, LT-3 and B-4) in a line on the east side of the landslide area. Pine Bar Campground is located just west of the study area.

Figure 3.36 Pine Bar Landslide Area along US 36 in Caribou County Idaho

Tincup Creek runs below the highway and serves as the primary hydrological feature affecting the stability of the slopes. Evidence of other past and present landslide activity are pervasive along other hillslope sections of SH-34.

Pine Bar UAS Surveys

The Pine Bar study area was aerially surveyed five times during the two-year investigation period (Table 3.12). The initial aerial survey was performed on 20 October 2023 and the last on 15 September 2024. One permanent benchmark located in the Pine Bar Campground was used for control in this study. Twenty-five additional ground control points were placed throughout the slide area. Additionally, the inclinometers LT1, LT2, LT3, and B4 were used for ground control. X-Y-Z coordinates of GCP locations were determined with a GPS sensitive to 2 cm horizontal and 3 cm vertical. Coordinate locations for the instruments were obtained from ITD.

Table 3.12 Dates of ISU Research Team Surveys in Pine Bar

Sensor	Date
D2M - Oblique	10-20-2023
Q240 - LiDAR	10-30-2023
Phantom 4 Pro	08 - 15 & 16 - 2024
Q240 - LiDAR	06-06-2024
Q240 – LiDAR and Sony RXI RII	09-15-2024

Change Detection

The ISU drone flights, air photos, and LiDAR surveys indicate a minor area of slope movement (shown in Blue) on the south side of the highway above Tincup Creek (Figure 3.37 and Figure 3.38). A small area of upward displacement (heave) shown as red/orange is present at the base of the slope just above the creek bed (Figure 3.38). Based on the survey, the affected area is approximately 90 ft (28 m) wide, 70 ft (21 m) downslope and only 32 ft (10 m) from the south edge of the road. Gaps in data (dark holes) within the LiDAR survey are tree locations.

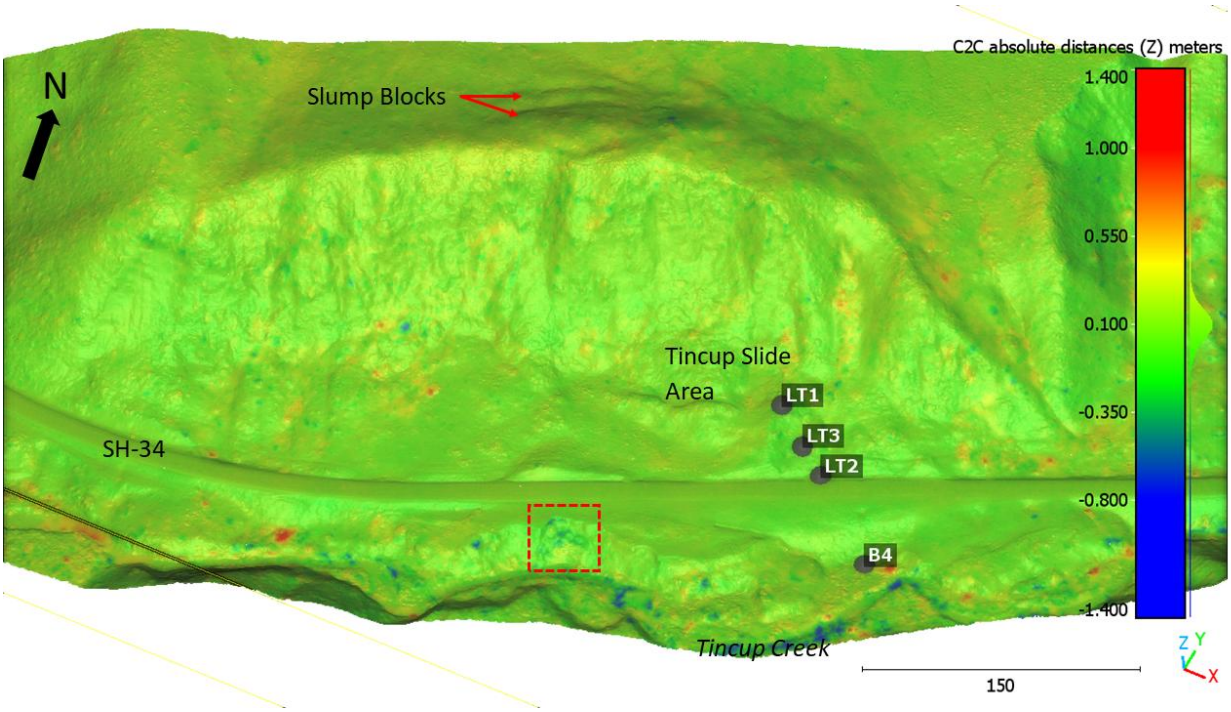

Figure 3.37 ISU LiDAR Survey Displacements in the Pine Bar Study Area during the 30 October 2023 to 15 September 2024 Monitoring Period

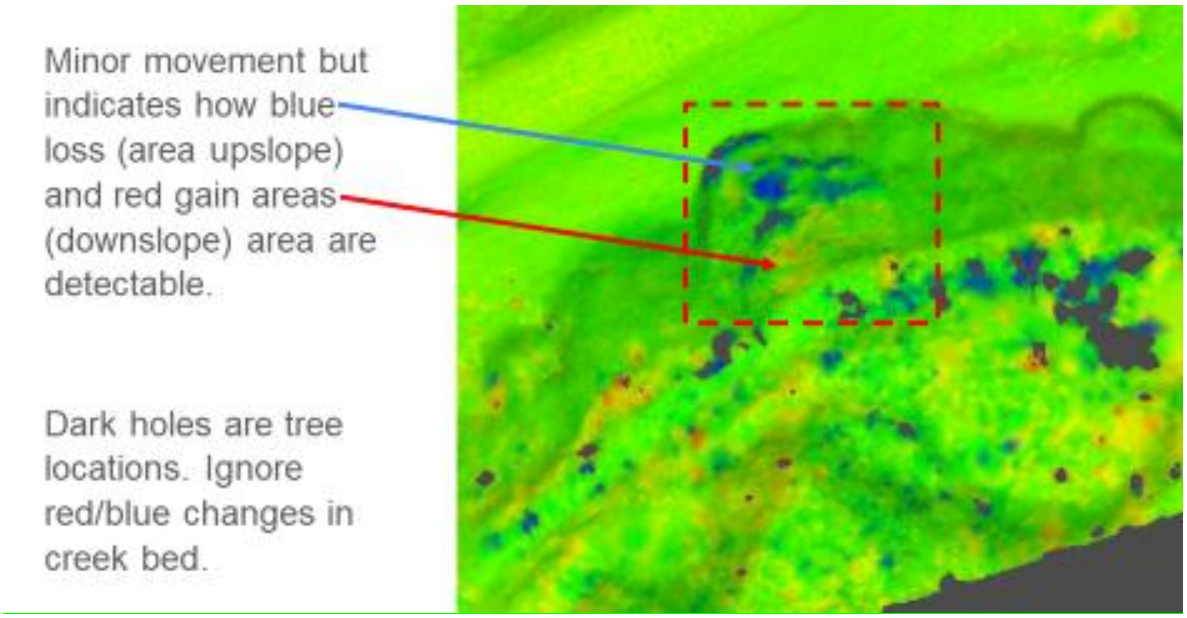

Figure 3.38 Area of Minor Slope Movement Identified in Drone Surveys in the Pine Bar Study.

Pine Bar Geologic Conditions

The bedrock geology in the Tincup slide area is derived from a portion of the USGS Preston Quadrangle geologic map and the Geological map of the Driggs quadrangle, Idaho (Mitchell and Bennett 1979; Oriel and Platt 1980). The map (Figure 3.39) shows that the specific site is located in the Cretaceous Draney Limestone and Bechler Conglomerate (Kgu). The Bechler Conglomerate underlies the Draney Limestone and consists of mudstone, sandstone, and conglomerate (Eyer 1969). Microfossils can be found in calcareous nodules within the mudstone. The Draney Limestone is comprised of interbedded shales and muds with thinly bedded limestones in the upper section and a massive limestone unit in the lower section. North northwest-east southeast trending, high angle normal faults are present on both sides of the slope and a major thrust fault is located east of the study area.

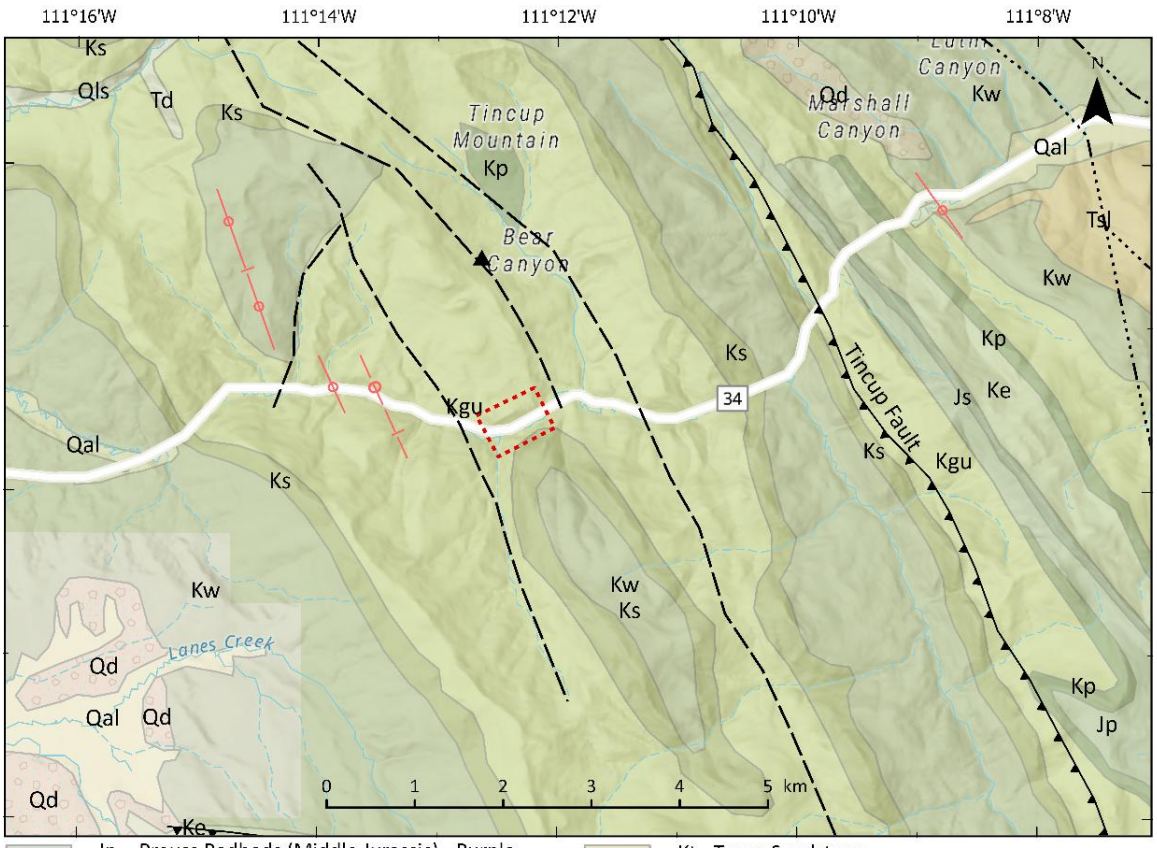

Jp - Preuss Redbeds (Middle Jurassic) - Purple, maroon, and reddish-gray sandy siltstone and claystone; halite, alum, and gypsum, in irregular zones. Thins eastward from 500 to 110 m

Js - Stump Formation (Upper and Middle Jurassic) - Glauconitic siltstone, sandstone, and limestone. Thins eastward from 100 to 50 m

Jsp - Stump Formation and Preuss Redbeds (Upper and Middle Jurassic)

Ke - Ephraim Conglomerate - Red and maroon mudstone and chert-peddle conglomerate; cross bedded tan to brown sandstone. Thins eastward from 1,000 to 150 m

Kgu - Unnamed red unit, Draney Limestone, Bechler Conglomerate

Kp - Peterson Limestone - Light-gray limestone and pastel colored calcareous mudstone. About 70 m thick

Ks - Smith's Formation (Lower Cretaceous) - Ferruginous black shale and tan to brown sandstone. Thins westward from 260 m to about 90 m

Kt - Tygee Sandstone

Kw - Wayan Formation (Lower Cretaceous) - Variegated red, purple, yellow, and gray mudstone, siltstone, and sandstone; minor porcelanite, bentonite, and coal. About 1,200 m thick

Qal - Alluvioum - Well to poorly sorted, unconsolidated gravel, sand, and silt in channels and flood plains. As much as 20 m thick

Qd - Colluvium- Unconsolidated and unstratified angular debris on hillsides

Tsl - Salt Lake Formation (Pliocene and Miocene) - White, gray, and green tuff, calcareous siltstone, sandstone, and conglomerate; grades into red-weather diamictite near exposures of older rocks.

Pine Bar Study Area of Interest

Anticline

High Angle Fault

Syncline

Thrust Fault

Thrust Fault Concealed

Adapted from: Oriel, S.S. and Platt, L.B. 1980; Mitchell, V.E.and Bennett, E.H. 1979

Figure 3.39 Geologic Map of the Pine Bar Project Area

Rainfall Activity During the 2023-2024 Investigation Period

Precipitation records for the Pine Bar study area were obtained from the NOAA station at Somsen Ranch, Idaho (Figure 3.38). The station is located within 15 miles of the site. The data show four periods of 0.9 in. rainfall between 30 June to 10 August 2024. The last survey in September 2024 was just before a 1.3 in. storm event. The LT-1, LT-2 and B-4 inclinometer boring logs show a thick sequence of clay in the upper part of the soil profile which would have limited infiltration during these widely spaced rainfall events.

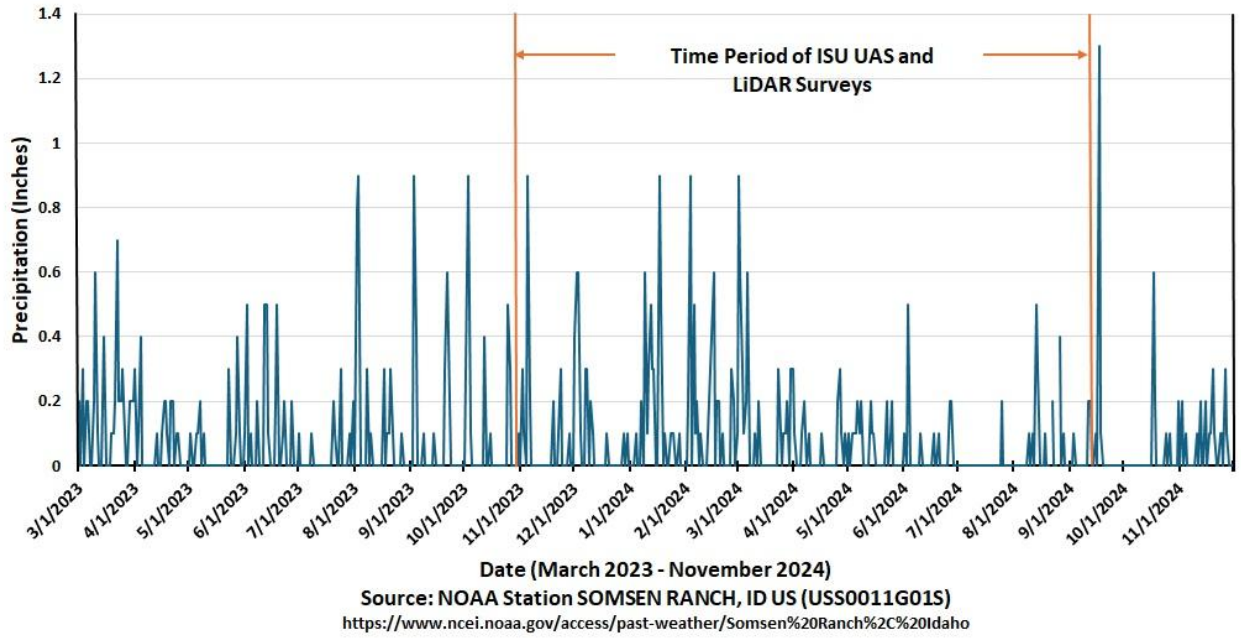

Figure 3.40 Precipitation Record during the Pine Bar Landslide Investigation Period

Pine Bar Inclinometers

Three inclinometers were installed by Landslide Technology along an upslope-downslope profile in the Pine Bar slide area (Figure 3.37). Inclinometers (LT-1, LT-2 & LT-3) are located on the upslope side of the highway. An older inclinometer (B-4) placed on the downslope of the highway is also used to record slope movement. Vibrating wire piezometers were placed in sanded sections of the LT-series grout columns to monitor ground water levels. The initial survey dates of the LT-series boreholes were 24 and 25 September 2019. The initial B-4 inclinometer survey data is 09 May 2016. LT-1 and LT-2 were last read on 11 September 2024 and LT-3 and B-4 on 30 May 2024. ITD inclinometer designations, station locations/elevations, and depths are summarized in Table 3.13. Based on aerial photos, ITD has carried out remedial stability work on the downslope side of SH-34 in the area of the inclinometer locations.

Table 3.13 Summary of ITD Inclinometer Installations in the Pine Bar Study Area

Inclinometer	Location (Lat/Long)	Approximate Ground Surface Elevation	Total Depth	Status
LT-1	42.9743/ -111.2044	6305 ft / 1922 m	107 ft / 32.6 m	Operational
LT-2	42.9741 / -111.2039	6256 ft / 1907 m	60 ft / 18.3 m	Operational
LT-3	42.9741 / -111.2041	6276 ft / 1913 m	55 ft / 16.8 m	Operational
B-4	42.9738 / -111.2034	6210 ft / 1893 m	50 ft / 15.2 m	Operational

Boring Logs

Geotechnical boring logs were prepared by Landslide Technology for the Pine Bar inclinometer drill holes. Bore hole depths range between 50 and 107 ft with the deepest holes on the upslope side of the past movement area. Two-inch OD standard split spoon samples were taken at 5-ft intervals. Blow counts were recorded for each 6-in. interval of drive for a total sample length of 18-in. Coarse grained soil descriptions included color and moisture; visual percentages of grain size, particle shape and density. Plasticity, consistency (strength), minor sand and/or gravel percentages and moisture were provided for the fine-grained soils. Samples were visually classified under the Unified Soil Classification System (USCS) and interpretations made on the origins of the individual layers. Water contents were provided in the logs using a graphical format across from the corresponding soil samples. Some groundwater levels and dates recorded during drilling were also provided in the logs. Spilt spoon and continuous HQ-triple tube cores were taken where rock was encountered in the bore hole. Rock type, color, degree of weathering and strength (described using hardness terms) were given in the logs. Joint properties include spacing, planarity, staining and mineral filling. Core recovery and Rock Quality Designation (RQD) were provided in graphical format for each core run. Core photos were attached to the some of the reports.

The inclinometer boring logs of two holes (LT-1 and LT-2) located on the upslope side of the road show similar subsurface conditions down to the top of LIMESTONE. In Boring LT-1, the COLLUVIUM described in the log is a red-brown to grey, stiff to hard, plastic, lean CLAY (CL) with fine to coarse sand and subangular gravel-sized limestone fragments (Figure 3.41). The soil is slightly moist to wet. A three-ft boulder was encountered at a depth of 11 to 14 ft. Standard Penetration N-values in the colluvium range between 11 and 33 blows/ft. Water levels were recorded at approximate depths of 18.5 and 32.2 ft below the top of the bore hole. Highly to slightly weathered limestone in the Draney Formation was encountered at a depth of 49 ft (approximate elevation: 1906.7 m or 6256 ft). All measurable slope displacement in LT-1 which started in September 2019 occurred above a depth of 22 ft in colluvium (Figure 3.41).

Boring LT-2 on the north side of SH-34 also encountered COLLUVIUM but only down to a depth of 21 ft (top of Draney Limestone at approximate elevation 6229 ft). The COLLUVIUM was similarly described as

in Boring LT-1, however, the N-Values were lower (6 to 20 blows/ft). The Draney Formation below the COLLUVIUM was described as a red-brown, decomposed LIMESTONE: hard, lean CLAY (CL), slightly moist with weak cementation. Ground water was not encountered during or after advance of the bore hole. A standard penetration test value of 1 blow/ft was recorded in the limestone at a depth of 24 ft just below the soil-rock contact. Based on the inclinometer measurements, some differential lateral displacement extends down to a depth of 24 to 26 ft where the limestone is very soft.

The log of Bore Hole LT-3 located between LT-1 and LT-2 shows a stratified sequence of fine and coarse-grained soils. Loose SAND and GRAVEL containing 0 to 20% silt is present in the upper 10 ft of the borehole. The layer is USCS-classified as SM-GM, has an N-value of 6 blows/ft at a depth of 5 ft and is assigned a mixed COLLUVIUM/ALLUVIUM origin. The COLLUVIUM below the surface layer is a wet, very stiff, lean CLAY (CL) with 30 to 50% sand and gravel. Granular colluvial deposits underlie the clay between depths of 14 and 29 ft. The upper layer was described as a wet, medium dense GRAVEL (GC) with sand in a clayey matrix. The lowest soil unit in the profile is a loose, well-graded SAND (SW-SC) with gravel and clay. A standard penetration N-value of 6 blows/ft was recorded at a depth of 20 ft. All four soil layers in LT-3 were described as wet, however no water levels were recorded in the log. The Draney LIMESTONE below the colluvium was described as grey, slightly to moderately weathered with high to moderate frequency irregular joints. Based on the N-values and soil descriptions in LT-2 and LT-3, conditions are favorable for slope movement at or near the soil/rock contact (depth of 20 to 26 ft) in the area where the ITD remedial work was performed.

Inclinometer Measurements

The inclinometers placed in Borehole LT-1 (Figure 3.41) and B-4 (Figure 3.42) on the east end of the SH-34 study area show slope movement at depths of 22 and 12 ft, respectively below the ground surface during 30 October 2023 to 15 September 2024 drone surveys. LT-1 underwent differential lateral displacement of 0.25 to 0.4 in. (0.64 to 1.3 cm) at the ground surface and roughly 0.2 in. (0.51 cm) at a depth of 18 ft. Shear displacement occurred between 18 and 22 ft at the base of the movement zone. Inclinometer B-4, located downslope of the 2006 ITD stabilization work, underwent an additional lateral displacement of 0.37 in. (0.94 cm) from the surface to a depth of 8 ft (2.4 m) during the September 2023 to May 2024 time period (Figure 3.42). (No inclinometer measurements were taken at B-4 in September 2024). The shear displacement extended down to a maximum depth of 12 ft. Overall, the B-4 inclinometer data indicate some minor additional displacement downslope of the previous ITD remedial work. Lateral displacement at the two other inclinometer locations (LT-2 and LT-3) was less than 0.10 in. and 0.31 in. (0.25 to 0.79 cm), respectively, down to depths of less than 10 ft (3.05 m) during the drone survey study period. Ground surface displacement-time plots on the LT-1 and B-4 inclinometer data are given in Figure 3.43 and Figure 3.44. Measured lateral/vertical displacements at the ground surface in the inclinometer locations appear to be at or just above drone survey sensitivity. The incremental slope movements did not reach the 2 cm (0.8 in.) horizontal and 3 cm (1.2 in.) vertical thresholds for measurable displacement in the Pine Bar LiDAR survey.

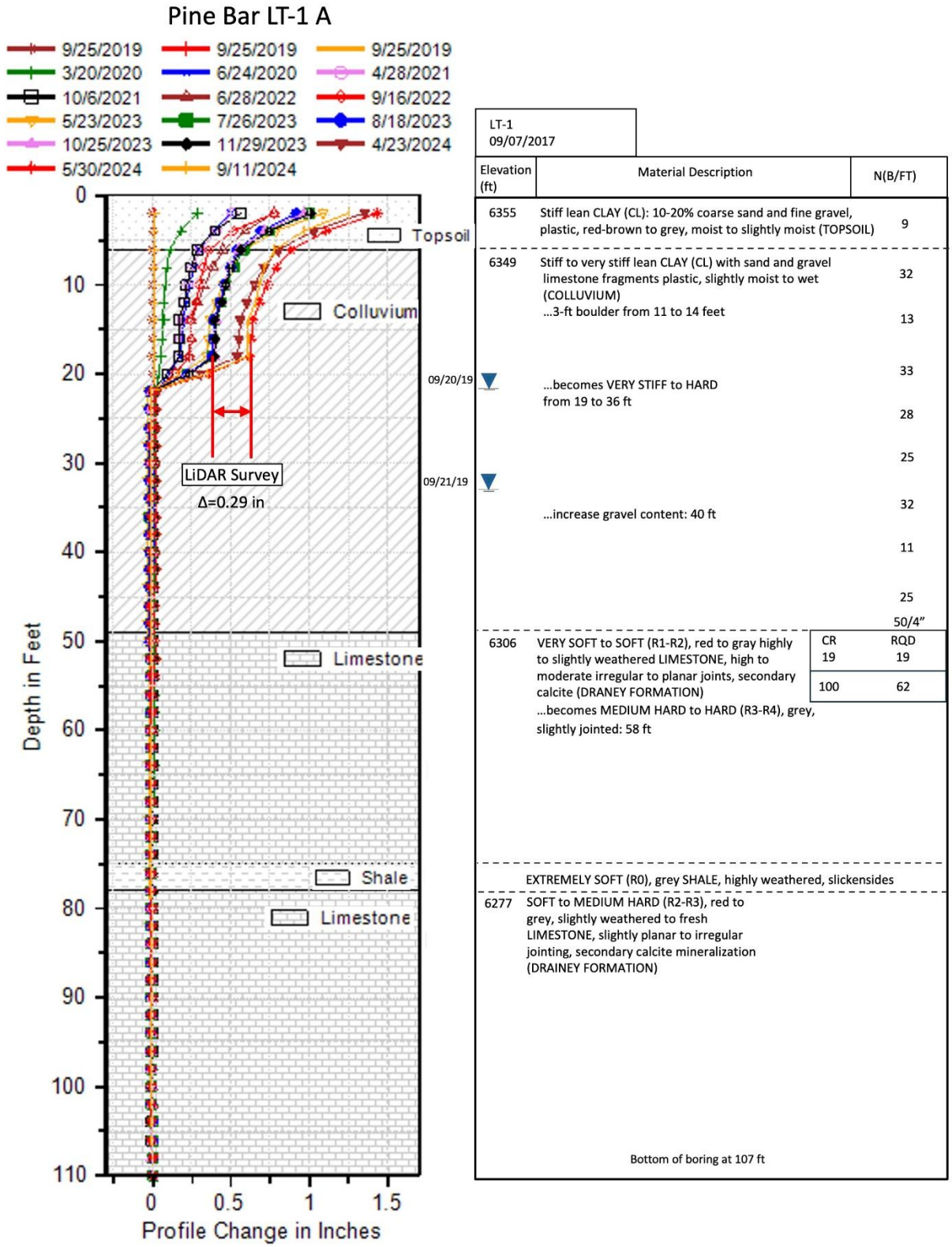

Figure 3.41 LT1 Pine Bar Inclinometer Readings and Boring Log

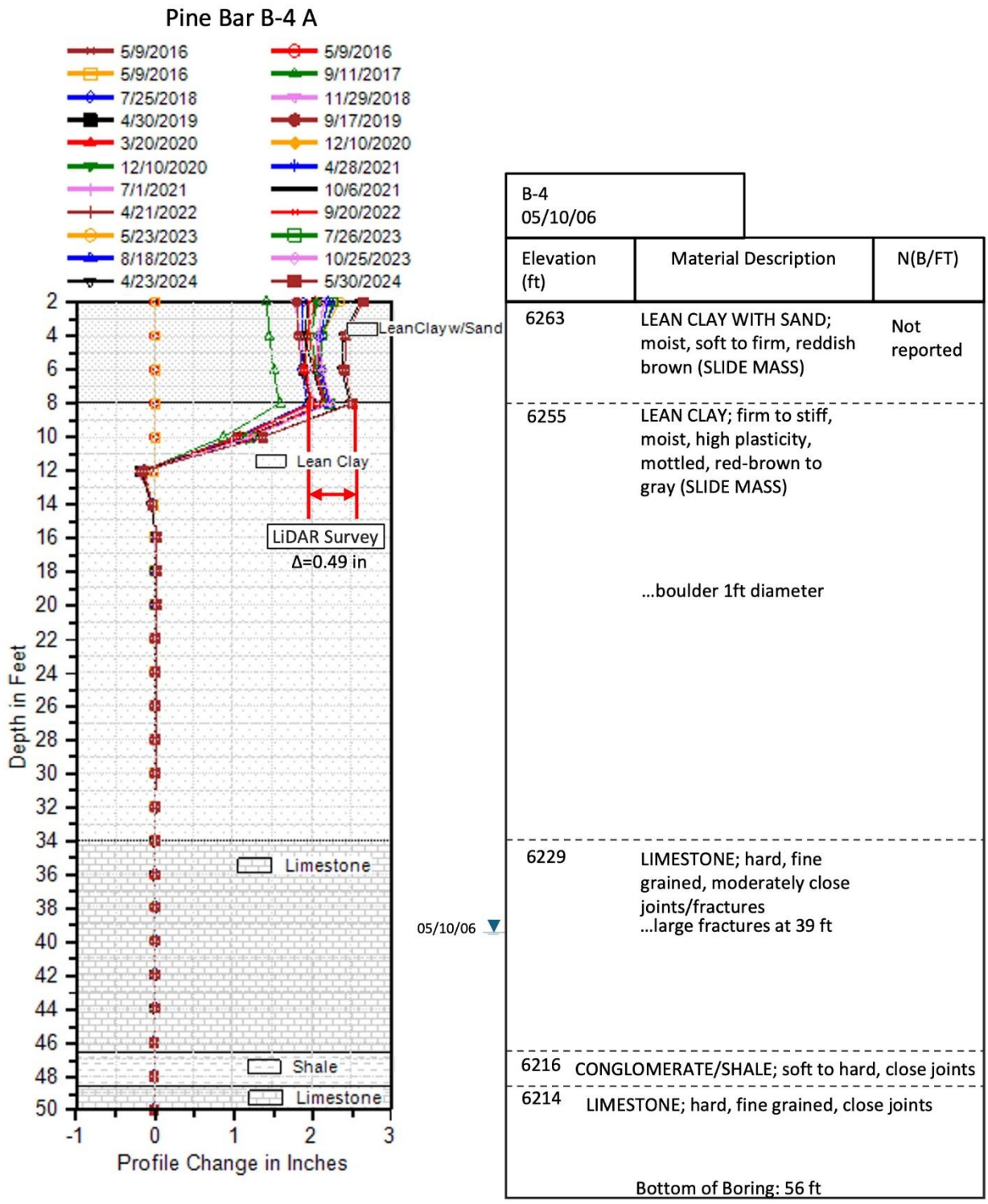

Figure 3.42 Pine Bar A-axis Inclinometer and Boring Log Data at B-4

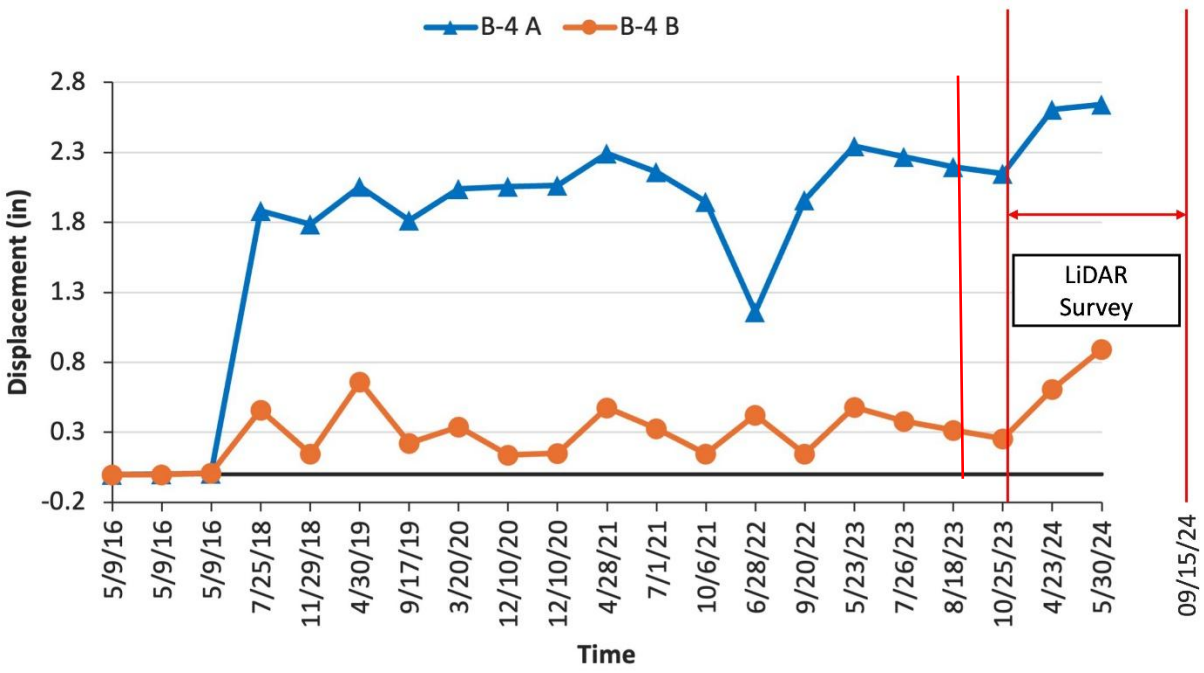

Figure 3.43 Displacement-Time Plot of Surface Movement at Inclinometer B-4

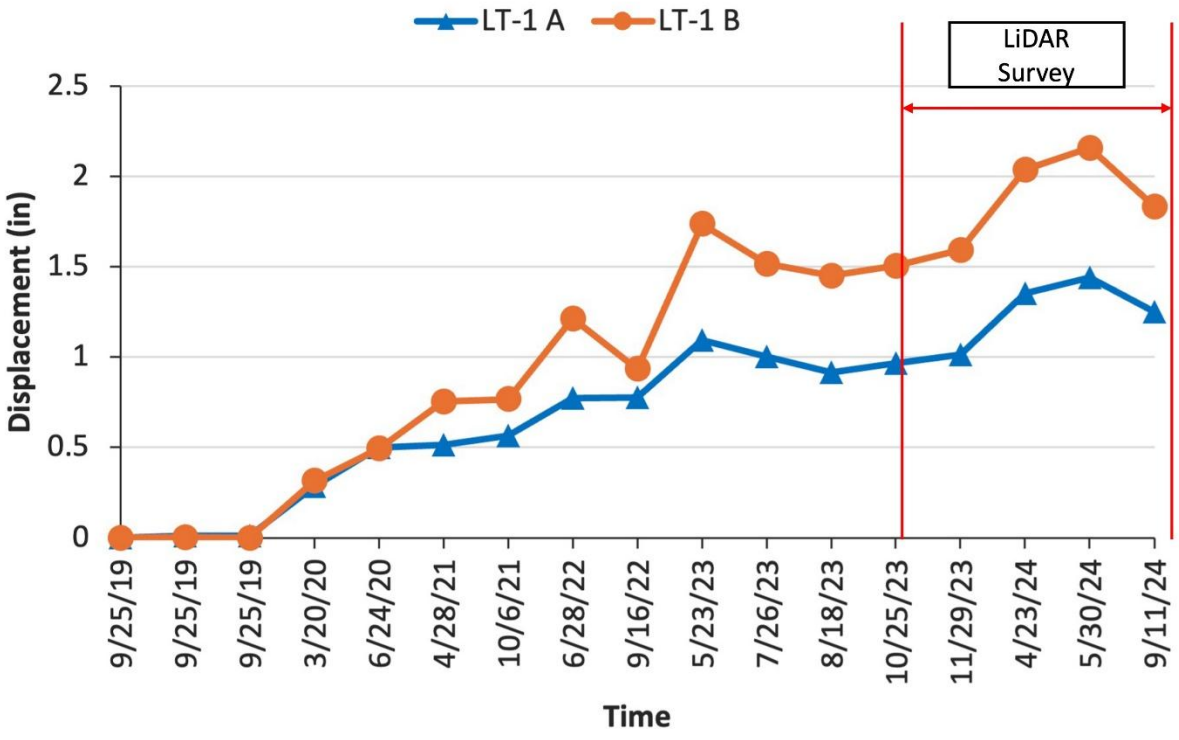

Figure 3.44 Displacement-Time Plot of Surface Movement at Inclinometer LT-1

Bud Peck Landslide Area

Overview

The Bud Peck study area is located between Interstate I-15 on the west and old Highway 191 on the east (Figure 3.45). The property is approximately 3 miles south of Malad Summit between I-15 mile markers 22 and 23. The site has an area of approximately 0.77 km^2 (0.30 mi^2) and is geographically located between longitudes 112°12'36" W and 112°13'30" W and latitudes 42°19'20" N and 42°18'51" N.

The Bud Peck property is located at the base of a broad ridge between two drainages which flow into Devil Creek: one north of the site and one south. The buildings are sited beneath a steep, approximate 30-ft high slope immediately below the interstate. The surrounding landscape consists of agricultural land, grassy fields and sparse residential areas, reflecting the rural character of the region.

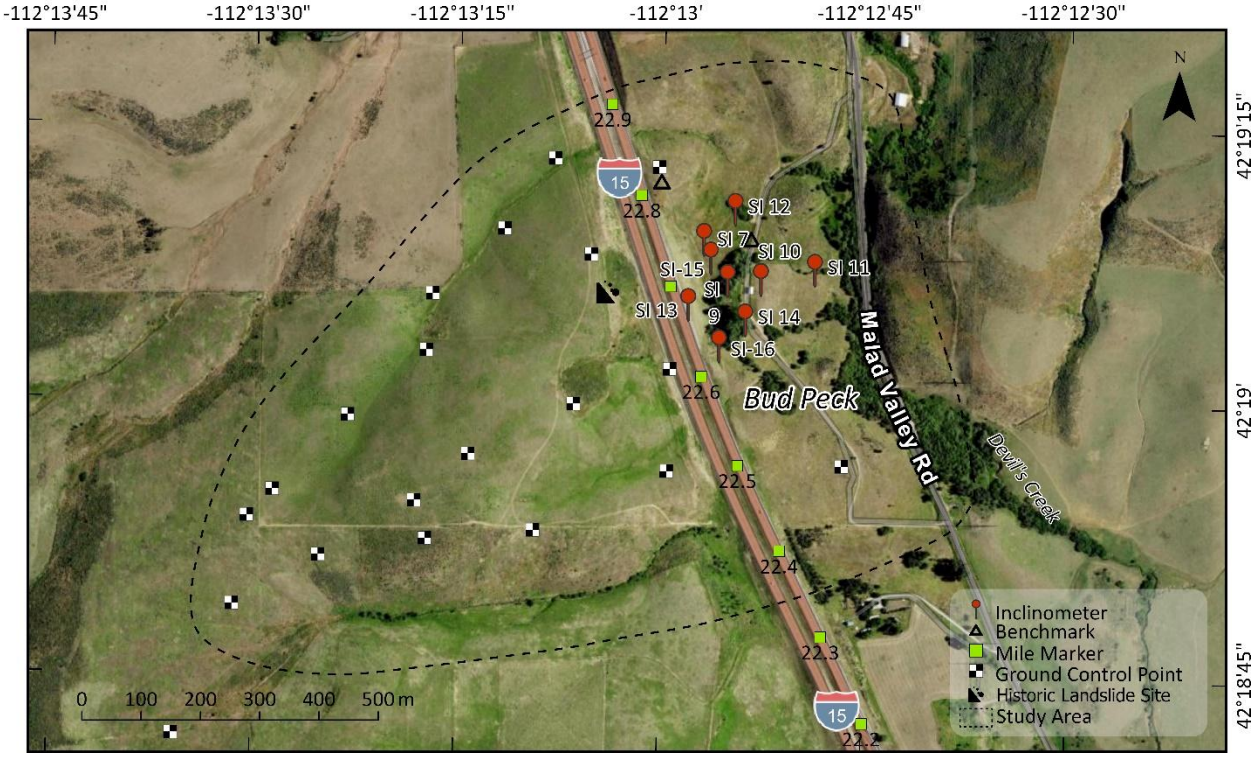

Figure 3.45 Bud Peck Study Area located in ITD District 5 along Interstate I-15 in southeast Idaho

UAS Surveys

The ISU Department of Geosciences surveyed the Bud Peck landslide area three times during the 16 September 2023 to 26 October 2024 investigation period (Table 3.14). ISU placed 20 temporary ground control markers at the site (Figure 3.45). X-Y-Z coordinates of the points were determined using a GPS sensitive to 2 cm horizontal and 3 cm vertical.

Table 3.14 UAS Survey Dates for the Bud Peck Landslide Area

Sensor	Date
D2M - Oblique	09-16-2023
Q240 - LiDAR	06-20-2024
Q240 – LiDAR	10-26-2024

Survey Results and Change Detection

The October 2024 LiDAR survey results show the ground surface topography at Bud Peck slide area (Figure 3.46). The vegetation was removed to reveal the configuration of the terrain. The ridge between the east-west stream valleys is distinctly highlighted in the LiDAR survey. Further, the steep slope on the east side of I-15 as well as the hummocky topography below the road are visible in the UAV survey.

Comparison of the September 2023 and October 2024 LiDAR surveys indicate local areas of very slight downward movement (less than 1 cm [0.4 in.]) along the slopes bordering SH-191 (blue-shaded spots) east and south of the Bud Peck property (Figure 3.47). Sparse vertical movement was also detected in the lower portion of the steep fill slope on the east side of I-15. As of 26 October 2024, no longitudinal, north-south cracks were observed in the I-15 pavement and shoulder above the Bud Peck Property. Very dense vegetation is represented by the white areas in the comparison surveys.

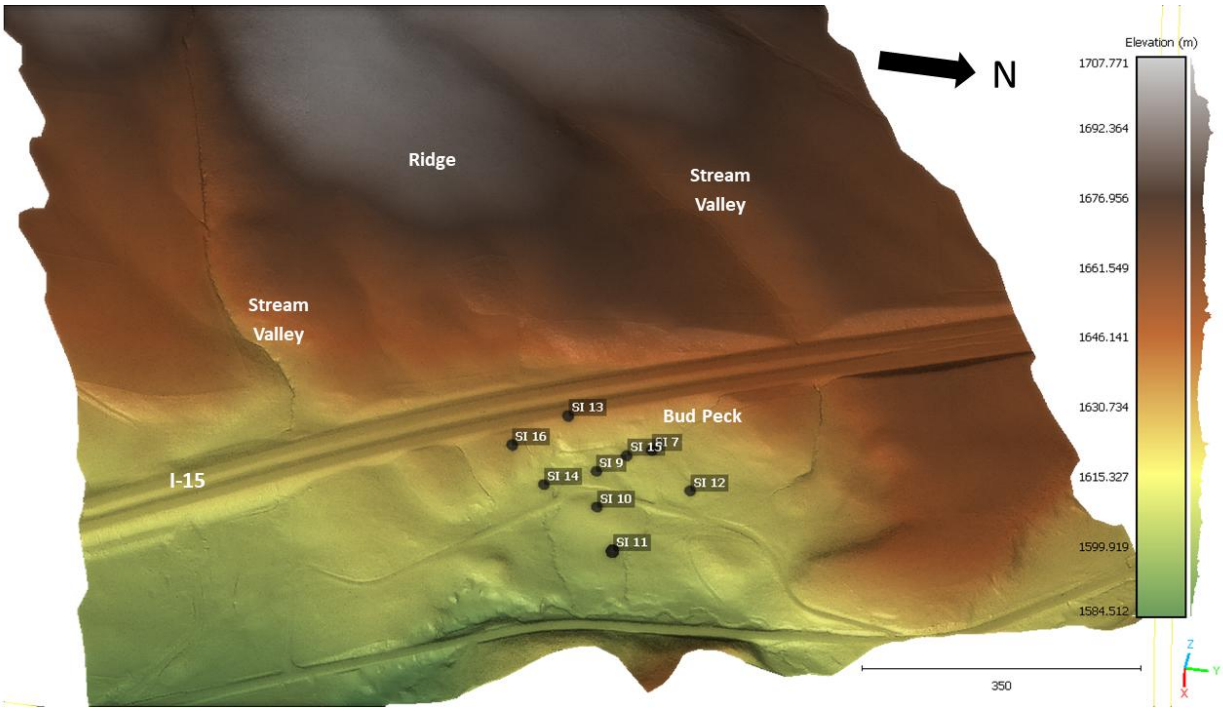

Figure 3.46 October 2024 LiDAR Survey of Bud Peck Landslide Site – Vegetation Removed

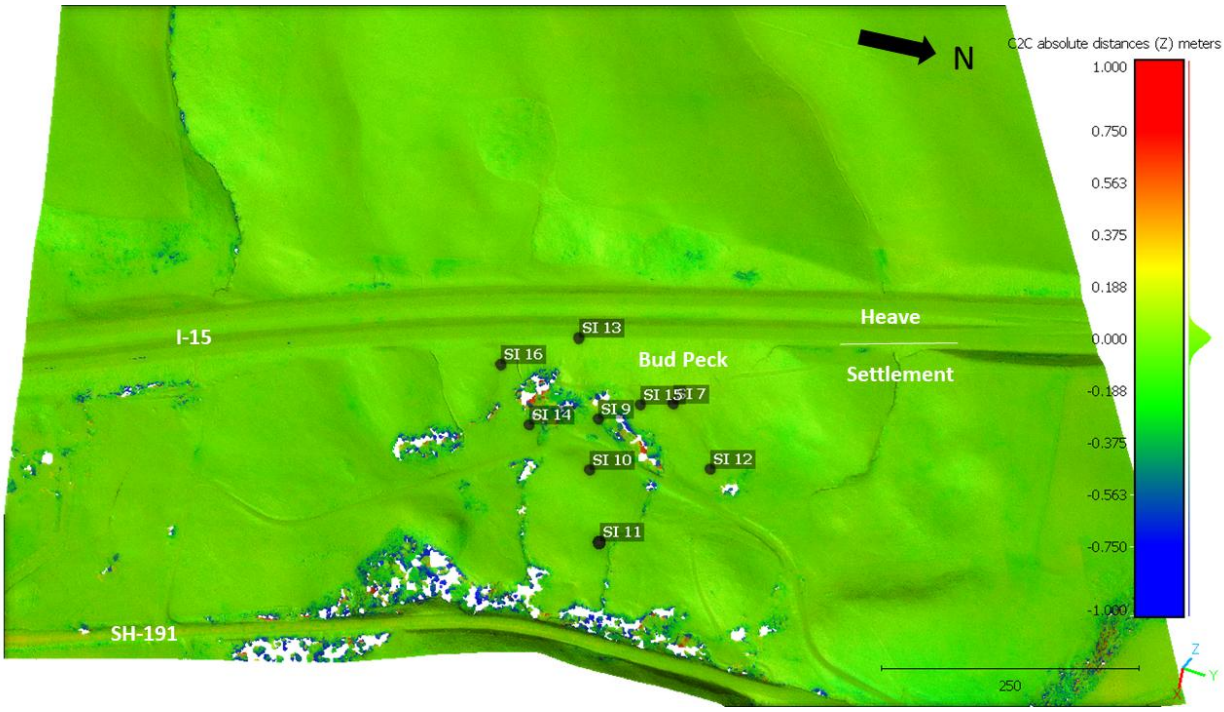

Figure 3.47 Ground Surface Displacements Between the ISU September 2023 and October 2024 UAS Surveys

Bud Peck Geologic Profile

The geology at the Bud Peck site and along I-15 consists of an alluvial fan deposit (Qaf) containing poorly sorted, unconsolidated sand and gravel up to 330 ft (100 m) thick (Figure 3.48). Alluvial sand and gravel are also present in the Devil Creek valley east of the fan deposit. The area is underlain by sedimentary and volcanic rocks within the Basin and Range physiographic province. North northwest – south southeast trending normal faults border the area.

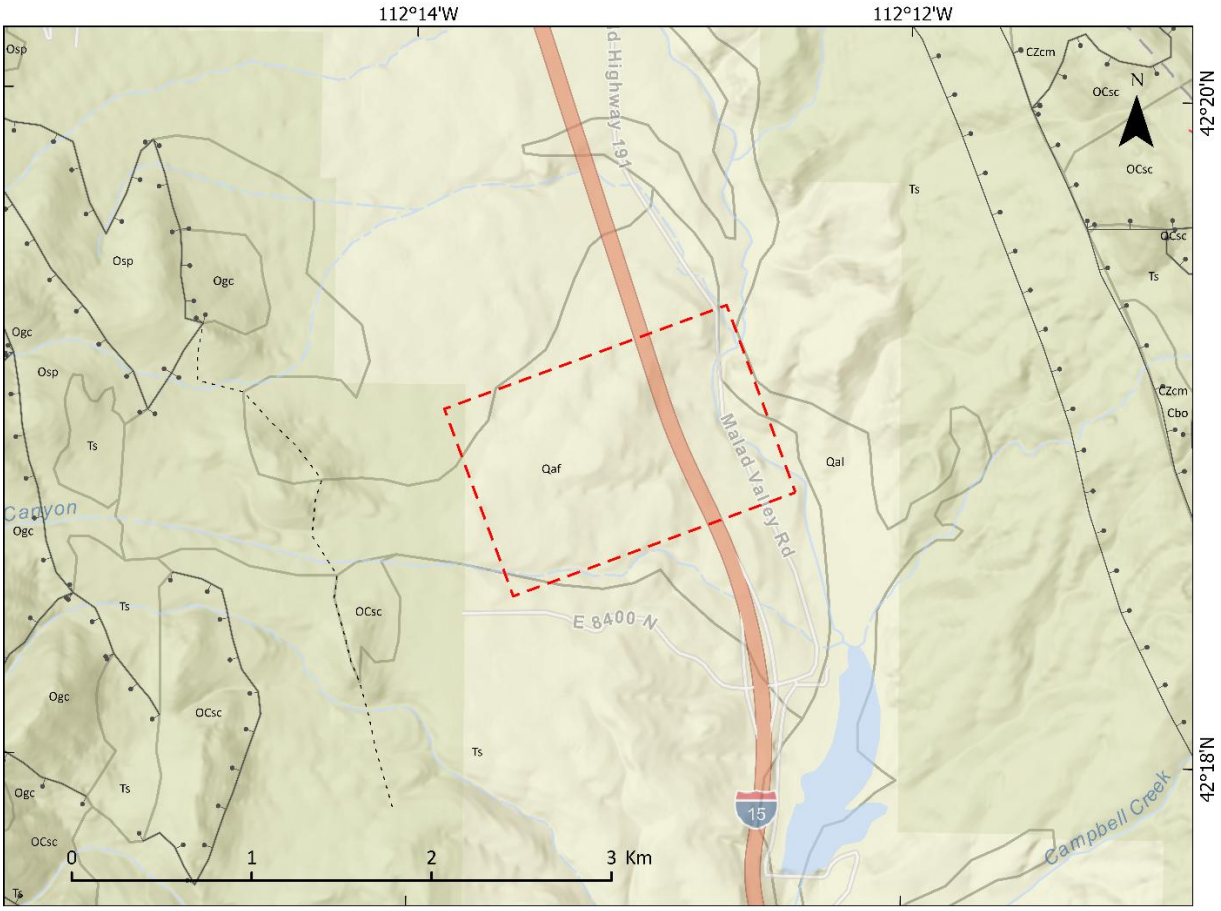

Qal - Alluvial deposits (Holocene to Pleistocene?) - Moderately-to well-sorted gravel, sand, silt, and clay, deposited in stream channels, terraces, and floodplains; up to about 30 ft (9 m) thick.

Qaf - Alluvial-fan deposits (Holocene to Pleistocene) - Moderately-to poorly-sorted clay, silt, sand, gravel, and boulders, deposited by debris-flow and sheet-wash processes; forms fan-shaped bodies at the mouths of drainages; thickness variable, up to 100 ft (30 m) thick.

Ts - Salt Lake Formation, undifferentiated (Pliocene? to Middle Miocene) - Includes gray, tan, and brown, and locally green sandstone, conglomerate, diamictite, tuffaceous sandstone, siltstone, and mudstone, rare lacustrine dolomite and limestone, and water-lain tuff deposited in alluvial fan and lacustrine environments.

Osp - Swan Peak Quartzite (Middle Ordovician) - White, massive, cliff-forming, locally bioturbated, vitreous quartzite, with brown micaceous siltstone and shale at base; 492-1150 ft (150-350 m) thick.

Adapted from: Long S.P. and Link, P.K. 2007

Ogc - Garden City Formation (Middle and Lower Ordovician) - Lower section consists of medium-gray, medium-bedded, fossiliferous limestone, with common tan silty partings and intraformational conglomerate.

OCsc - Saint Charles Formation (Lower Ordovician to Upper Cambrian) - Lower section - a very fine-grained, tan arkosic sandstone, with distinctive white feldspar grains, upper section consists of mottled, medium-gray, silty dolomite and limestone, locally rich in gray to brown chert nodules and stringers, 1045 ft (320 m) thick.

CZcm - Camelback Mountain Quartzite (Lower Cambrian to Neoproterozoic) - White to tan, vitreous, thick-bedded, medium-to coarse-grained, locally conglomeratic quartzite, up to 1570 ft (479 m) thick.

Bud Peck Study Area of Interest

Anticline

Normal Fault

Thrust Fault

Normal Fault Concealed

Figure 3.48 Geologic Map in and around the Bud Peck Site (Adapted from Long and Link 2007)

Rainfall Activity During the 2023-2024 Investigation Period

Precipitation records for the Bud Peck study site were obtained from the NOAA station in Malad City, Idaho (Figure 3.49). The station is located within 15 miles of the site. The data shows long periods between short duration precipitation events.

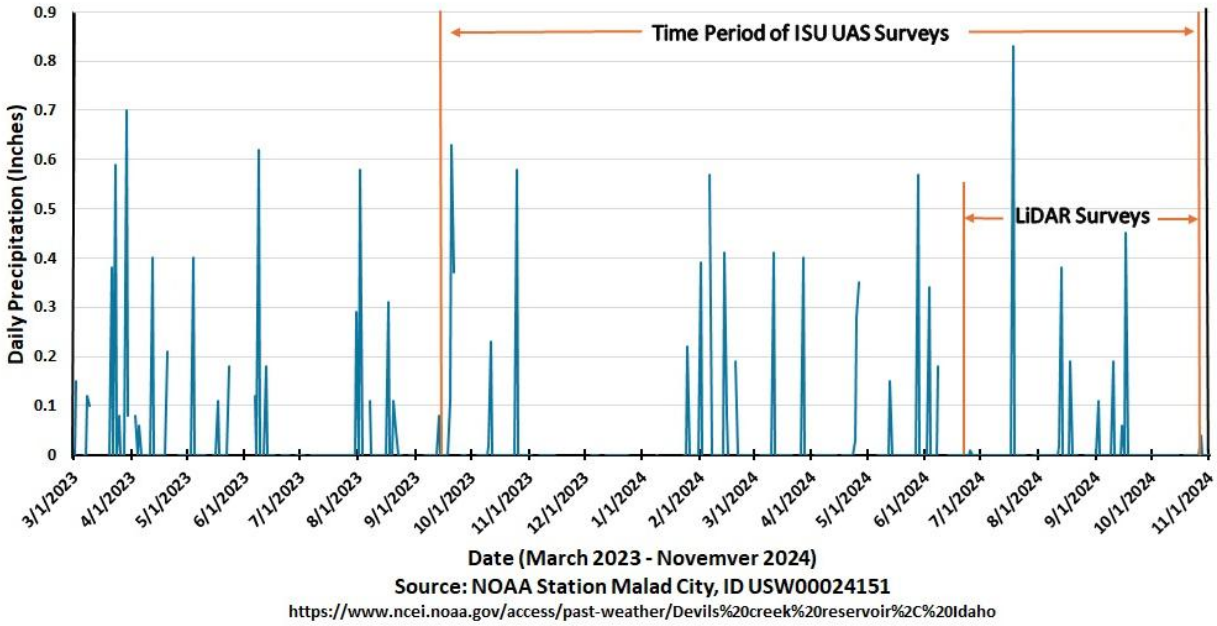

Figure 3.49 Precipitation Record for Bud Peck Landslide Area during the Project Investigation Period

Bud Peck Instrumentation

Inclinometers

Nine inclinometers were placed by ITD in the Bud Peck slide area (Figure 3.50). Based on ITD boring logs, at least five of the inclinometer casings were installed between 1982 to 1987 (Table 3.15). Initial slope displacement measurements provided by ITD in the nine inclinometers were taken in September or October in either 2016 or 2017. Three sets of inclinometer readings were provided during the 2023-2024 ITD-ISU Bud Peck study period.

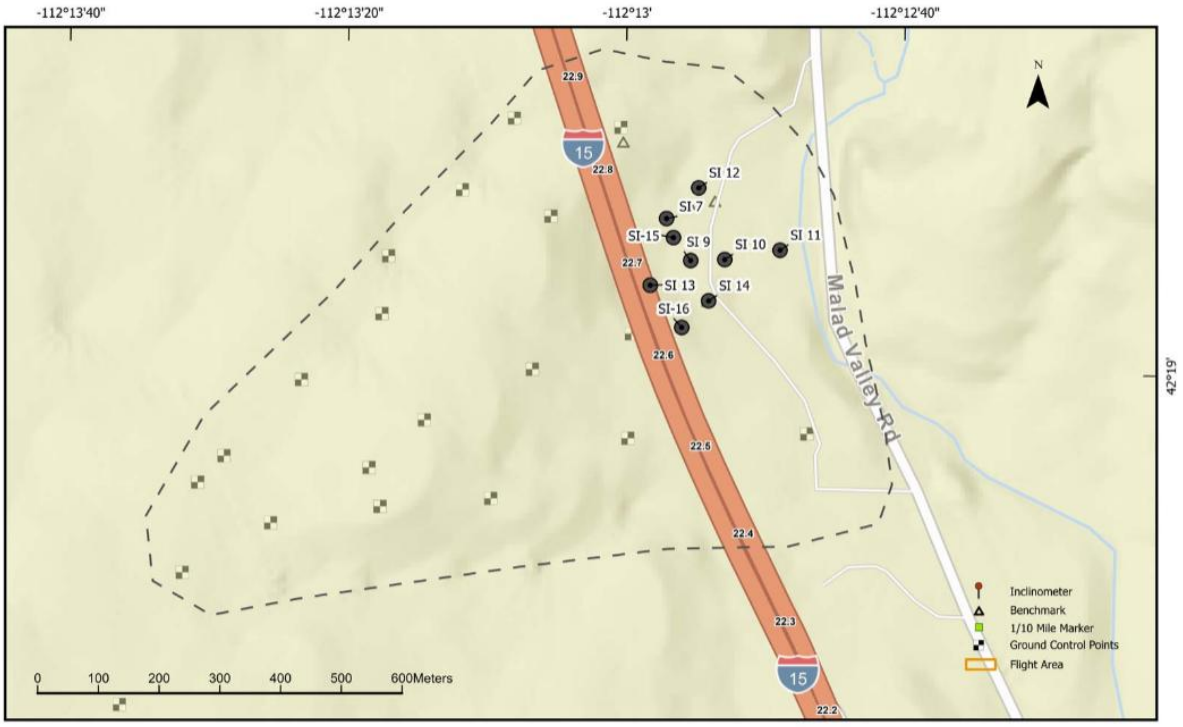

Figure 3.50 Plan Locations of Bore Holes and Inclinometer in the Bud Peck Landslide Study Area

Boring Logs

Six boring logs prepared by the geotechnical section of District 5 were available for the Bud Peck site. Four logs (SI-10, SI-11, SI-12 and SI-13) were provided for bore holes drilled to place inclinometers. The bore holes were advanced using either auger or tri-cone drilling methods and logs prepared from drill cutting returns. The available logs of bore holes drilled at the Bud Peck site show minimal in-place samples. Visual soil descriptions provided in the logs include color, grain size/visual percentage, moisture/water where present, lost circulation, presence of calcium carbonate and soil consistency. No descriptions of in-place rock were given in the available logs. Where encountered, ground water levels were recorded at the time of drill hole advance. Some lab tests were provided in the ITD documents.

Table 3.15 Summary of Bud Peck Inclinometer Bore Hole/Measurement Dates and Corresponding ITD-ISU UAS Surveys

Inclinometer	Bore Hole Data	Initial Reading Date	Dates During UAV Surveys[1]
SI-7	-	12 Sep 2017	2 May - 9 Oct 2024
SI-9	-	27 Oct 2016	17 Jun - 9 Oct 2024
SI-10	26 Sep 1983	13 Sep 2017	27 Oct 2023 - 9 Oct 2024
SI-11	29 Sep 1983	13 Sep 2017	2 May - 9 Oct 2024
SI-12	12 Oct 1983	13 Sep 2017	2 May - 9 Oct 2024
SI-13	30 Sep 1987	21 Oct 2016	2 May - 9 Oct 2024
SI-14		13 Sep 2017	2 May - 9 Oct 2024
SI-15		27 Oct 2016	17 Jun - 9 Oct 2024
SI-16		20 Oct 2016	27 Oct 2023 - 2 May 2024

[1] ISU UAV survey dates: 20 Jun 2024 and 26 Oct 2024

Subsurface Profiles and Displacements in Bud Peck Inclinometers

The bottoms of the nine inclinometer casings placed in the Bud Peck study area range between 38 and 145 ft below the ground surface. Based on the inclinometer boring logs, the subsurface conditions on the east side of I-15 consist mostly of red-brown/dark brown and light gray, soft to hard, non-calcareous to calcareous, CLAY and silty CLAY with some SAND and/or GRAVEL layers typically in the lower part of the soil profile. The descriptions in the logs indicate much finer soil conditions than depicted in the descriptions of the same geologic formation mapped in southeast Idaho (Figure 3.48). Where present, the ground water table encountered during drilling was located at depths of 10 to 53 ft below the ground surface. Lone artesian conditions were found at a depth of 25.8 ft in Boring SI-12. The log of Bore Hole SI-13 located along the east edge of the I-15 northbound lane contains roughly 27 ft of gray pumice FILL below the roadway surface.

Drill logs of Boring Nos 7, 9, SI-7 and SI-10 to SI-13 in the Bud Peck slide area were provided by ITD for this study. Inclinometer data were available for the 9 SI bore holes. Two of the logs and inclinometer measurements (SI-7 and SI-13) present in the former slide area represent the subsurface conditions/recent ground movements at the site and are provided in Figure 3.51 and Figure 3.53.

Bore Hole/Inclinometer SI-13

Bore hole/Inclinometer SI-13 is located on the east shoulder of I-15 above the Bud Peck site (Figure 3.50). Figure 3.51 shows the upper 26.8 ft of the subsurface profile consists of white pumice FILL. The FILL is underlain by 26 ft of brown to orange-brown CLAY with lenses of sand and gravel; some of the

gravel lenses contain clay. The remainder of the profile below 52.8 ft consists primarily of clayey GRAVEL or gravelly CLAY; a 3.5-ft thick gravelly SAND layer was found between depths of 67 to 70.5 ft below the ground surface. Below 78 ft, the materials are described in the log as partially cemented to cemented sandy and clayey GRAVEL. No ground water levels were reported in the boring log.

All past measured displacement at SI-13 occurred below the road in the pumice FILL. The displacement pattern indicates a bulge with a maximum total horizontal movement of approximately +0.2 in. (0.51 cm) near the center of the layer. No measurable movement was recorded in the inclinometer during the ITD-ISU UAS survey period consistent with the lack of longitudinal/transverse cracks in the I-15 asphalt above the study area.

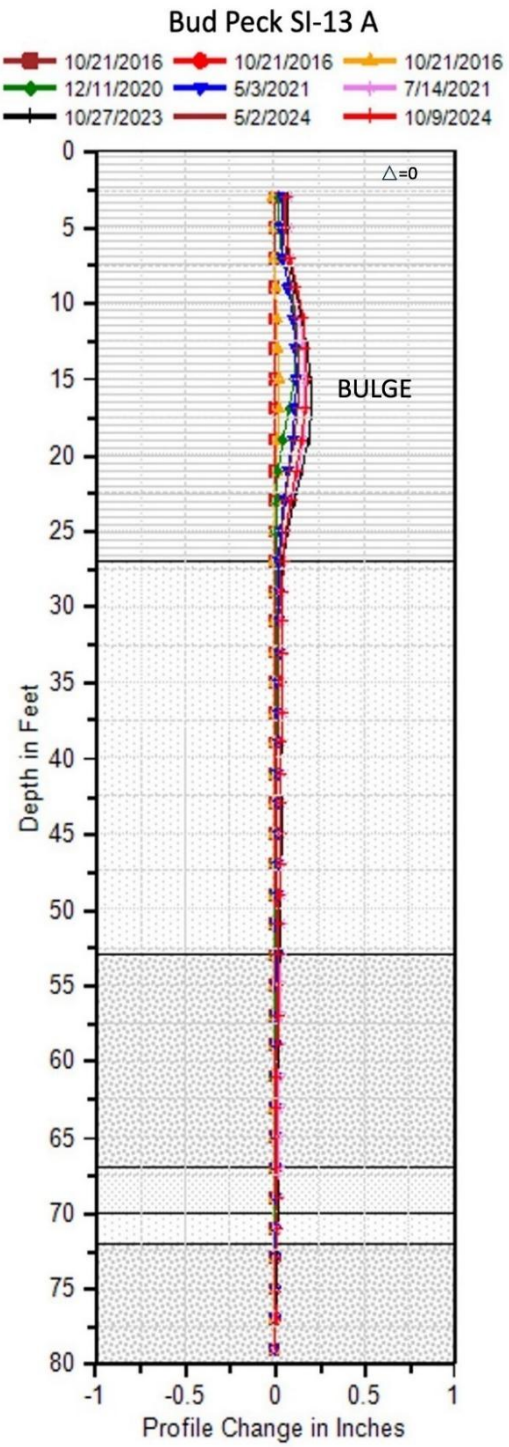

SI-13
09/30/1987

Elevation (ft)	Material Description
5415.9	Gray-white Pumice FILL, very hard, lost circulation at 5ft, softer/smaller grain size below 5ft
5389.1	Brown to orange-brown CLAY with thin, widely scattered lenses of clayey gravel, sand and gravel; lost circulation at 28.9 ft
5363.1	Very hard, brown clayey GRAVEL to gravelly CLAY
5348.9	Gravelly SAND
5345.4	CLAY/clayey GRAVEL
5326.2	Orange-brown, partially cemented to cemented, sandy to clayey GRAVEL
	Bottom of Boring: 89.7 ft

Figure 3.51 SI-13 Inclinometer Displacement and Corresponding Boring Log in the Shoulder of I-15

Inclinometer SI-7

Bore Hole/Inclinometer SI-7 is located in the landslide area near the bottom of the I-15 embankment (Figure 3.50). The exploratory bore hole was drilled to a depth of 40.5 ft and used to install a 38-ft long inclinometer.

The log of Bore Hole SI-7 has a 4-ft thick wet organic SILT just below the ground surface (Figure 3.53). The greatest lateral displacement although small is in the SILT. The remainder of the soil profile is made up primarily of light brown, reddish brown and green CLAY and sandy CLAY with and without gravel. A 3-ft thick layer of clayey SAND was encountered at a depth of 23 to 26 ft and a 5-ft thick layer of cemented brown gravelly SAND was logged at the bottom of the hole. One ground water level at a depth of 8.9 ft was recorded prior to drilling on the morning of 5 October 1982 when the hole was at a depth of 14.5 ft.

The lateral displacement recorded from Inclinometer SI-7 at the ground surface was approximately +0.14 in (outward rotation) during the June 2024 to October 2024 drone survey monitoring period (Figure 3.52). All of the recorded displacement is in the upper silt and clay layers within 8 ft of the ground surface (Figure 3.53).

Artesian conditions were encountered in borings SI-14 and SI-15 in the conglomerate below depths of 95 ft (Enright personal communication, 2025).

Study Period Displacement in the Remaining Bud Peck Inclinometers

The horizontal ground surface displacement in the other eight inclinometers ranged between -0.20 to +0.09 in. (Table 3.16). The meaning of the positive and negative inclinometer readings with respect to slope movement is illustrated in Figure 3.52. All lateral movement during the UAV survey period is below the 0.78 in. (2.0 cm) vertical and 1.2 in. (3.0 cm) horizontal LiDAR survey thresholds.

Table 3.16 Summary of Inclinometer Surface Displacement Measurements During the UAS Study Period

Inclinometer	Approximate Incremental Displacement (in) [1]
SI-9	+0.09
SI-10	+0.04
SI-11	-0.05
SI-12	-0.11
SI-13	+0.01
SI-14	-0.20
SI-15	-0.09
SI-16	+0.06

[1]Postive value is outward horizontal displacement.

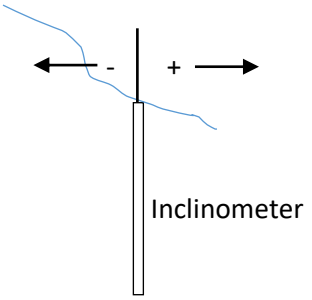

Figure 3.52 Interpretation of Positive and Negative Inclinometer Readings. Blue Line Represents the Slope

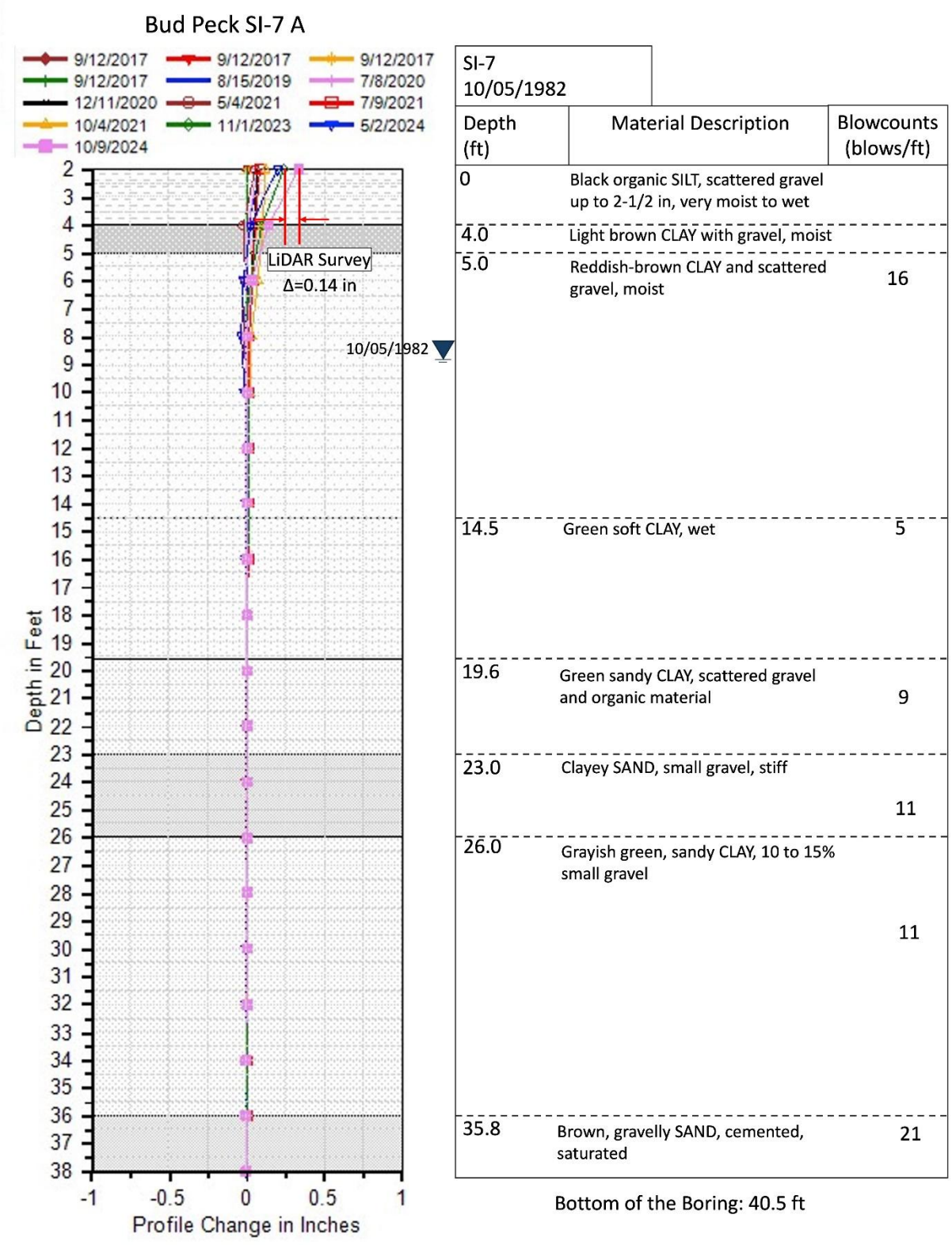

Figure 3.53 SI-7 Inclinometer displacement and corresponding boring log in the east slope of I-15 at the Bud Peck site

SH-33 Bike Path and State Line Landslide Areas

Overview

Idaho State Highway 33 (SH-33) landslide area is in a mountainous and heavily forested region of eastern Idaho at the Wyoming Border (Figure 3.54). SH-33 runs between Victor, Idaho and Jackson, Wyoming and has a history of landside/snow slide activity. The most recent large landslide occurred in Teton Pass, Wyoming between 6 and 8 June 2024 along SH-22 (continuation of SH-33) that closed the road for several weeks (Figure 3.55). Just after the Teton Pass landslide event, ITD asked the ISU Geosciences Department to perform a UAS LiDAR survey in the State Line area along SH-33 where present/past landslide activity has occurred along two sections of the highway near the turnouts (Bike Path on the west end and State Line on the east end). The ISU LiDAR survey was performed on 25 June 2024. ITD made a UAS photogrammetric (RGB camera) survey on 26 June 2024.

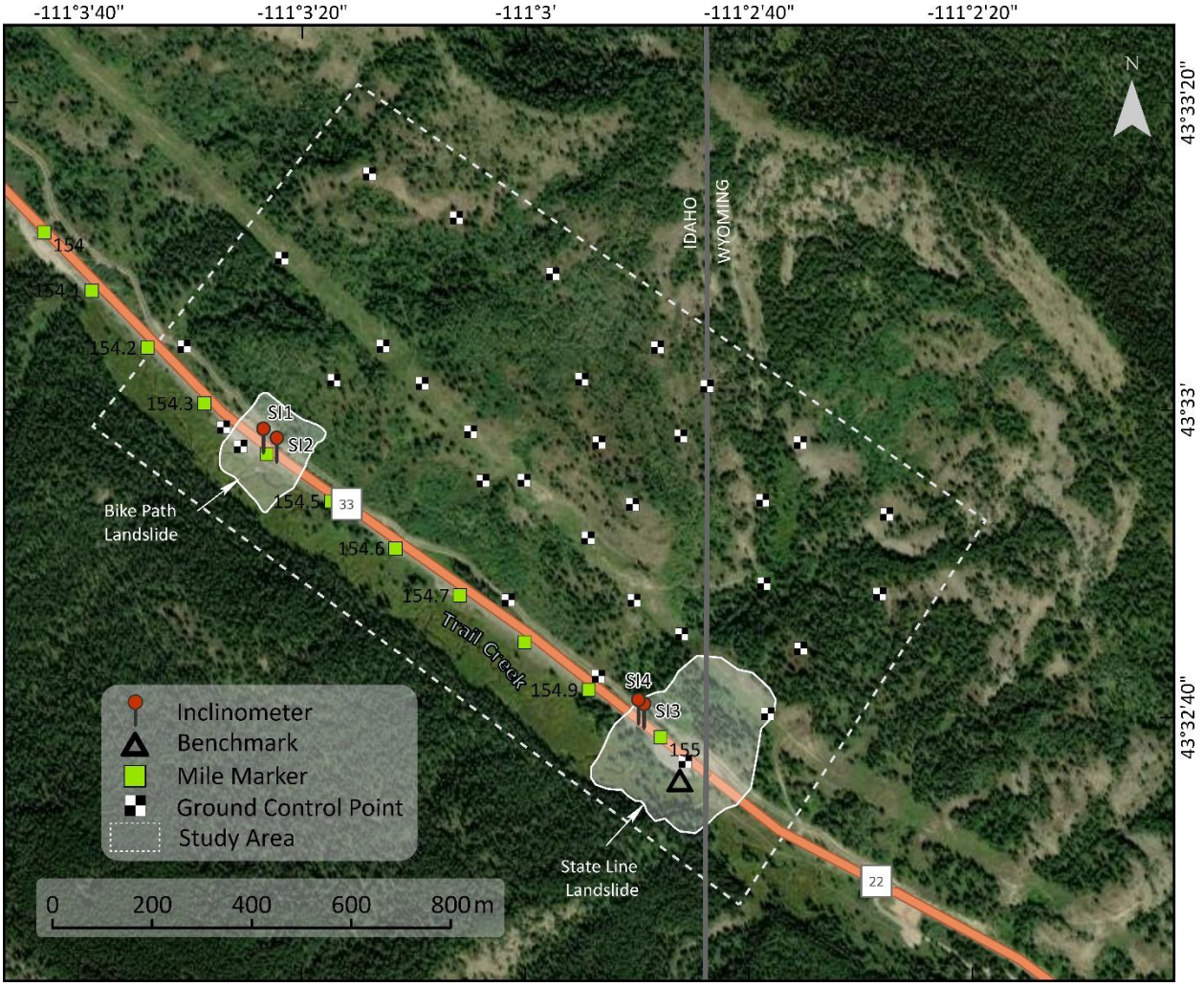

Figure 3.54 SH 33 Bike Path and State Line Landslide Study Areas along the Idaho-Wyoming Border

Figure 3.55 June 6 to 8, 2024 Teton Pass Landslide along the SH-22 in Wyoming (photo taken from Petley 2024).

The past and recent SH-33 landslides are located between mile-markers 154.3 to 155 in Idaho and extend across the Idaho-Wyoming border to mile marker 17.4 in Wyoming on SH-22 (State Line Landslide) and between mile-markers 154.3 to 154.5 on SH33 in Idaho (Bike Path Landslide). The entire study site has an area of approximately 1.46 km^2 (0.56 mi^2) and is geographically located between longitudes 111°03’35” W and 111°02’18” W and latitudes 43°32’27” N and 43°33’21” N. Trail Creek is below the road on the southwest side of the highway and a recently constructed bike path was built approximately 30 ft above on the north side of the road and across the toe of the slope. ITD drilled and installed four inclinometers on the southeast and northwest ends of the study area to monitor slope movements (Figure 3.54). The surrounding landscape consists of pine forests and grasslands.

UAS Survey at SH 33 Bike Path and State Line Landslide Areas

The ISU LiDAR survey shows the ground surface topography along SH-33 northwest of the Wyoming border (Figure 3.56). The vegetation has been removed in the figure to display the bare earth topography.

The LiDAR image clearly reveals past landslide activity along SH-33. Two areas of hummocky topography border the highway; one at the state line and the second near the middle of the study area. A third location with hummocky ground and an upper scarp is present part way up the slope on the west end of the bare earth model. The bike path on the northeast side of the road which cuts across the debris flow and the center landslide is visible in the figure (Figure 3.57). A debris flow which previously crossed the highway is located just west of the State Line turnout (Figure 3.58).

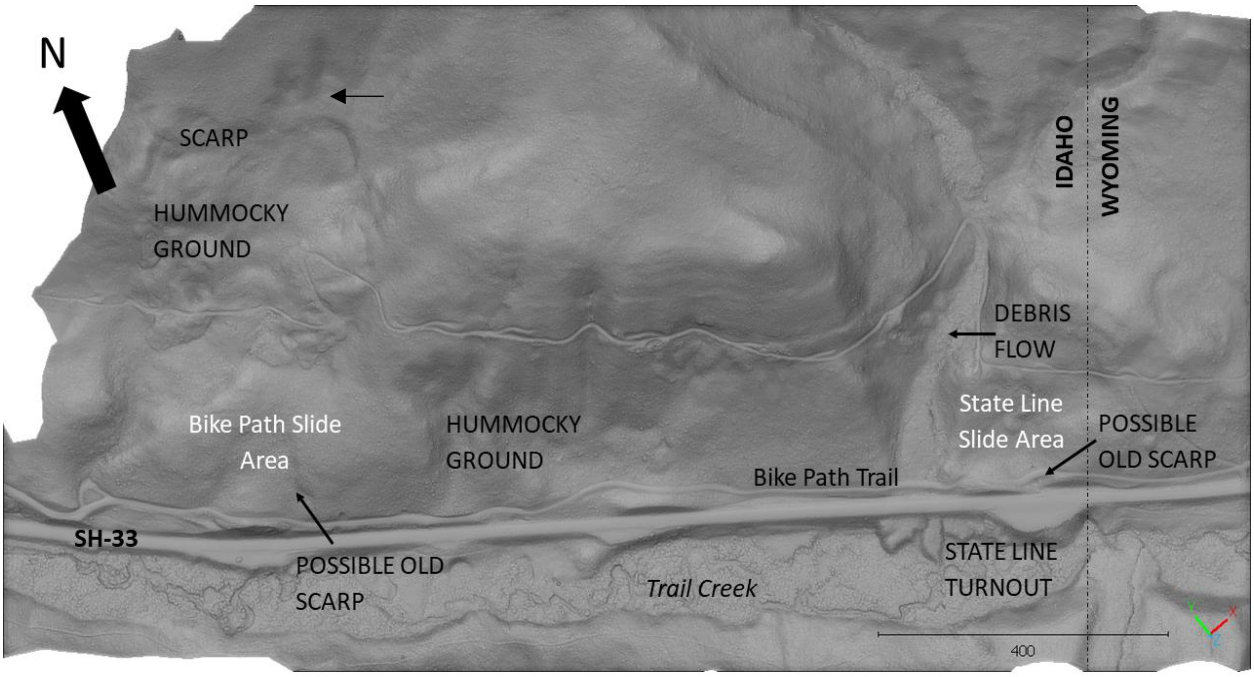

Figure 3.56 June 25, 2024 ISU LiDAR survey of the SH-33 Bike Path and State Line Landslide Sites

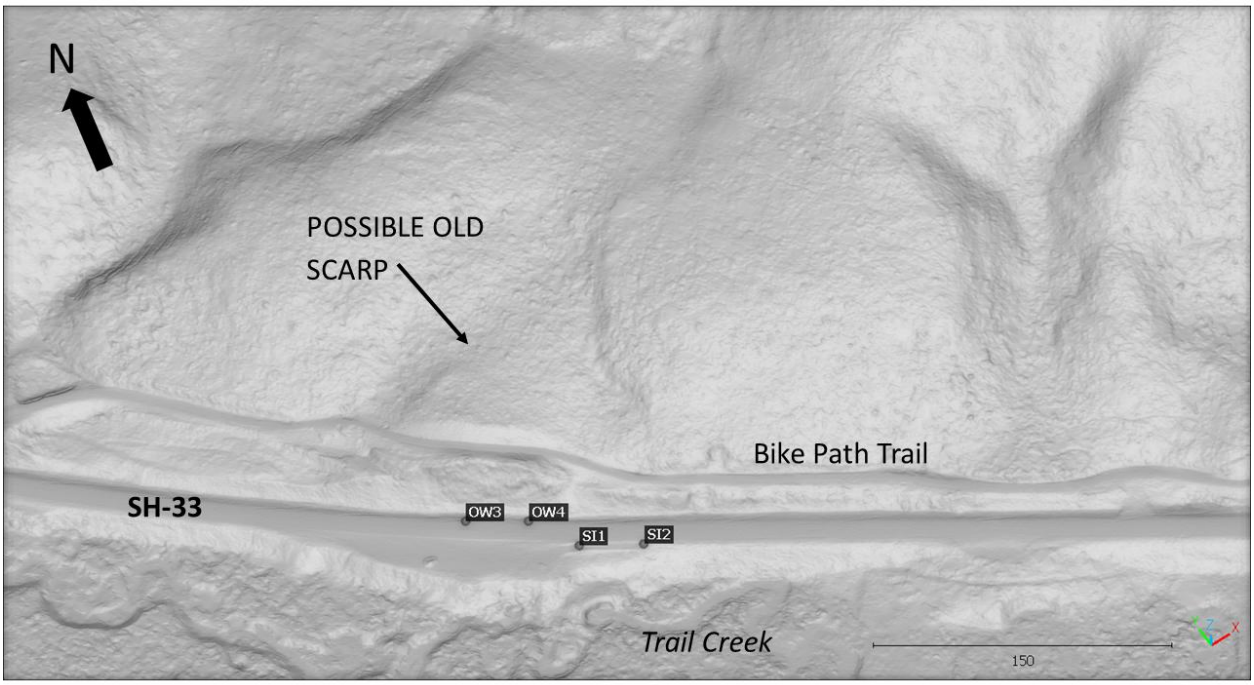

Figure 3.57 Bike Path Landslide Area

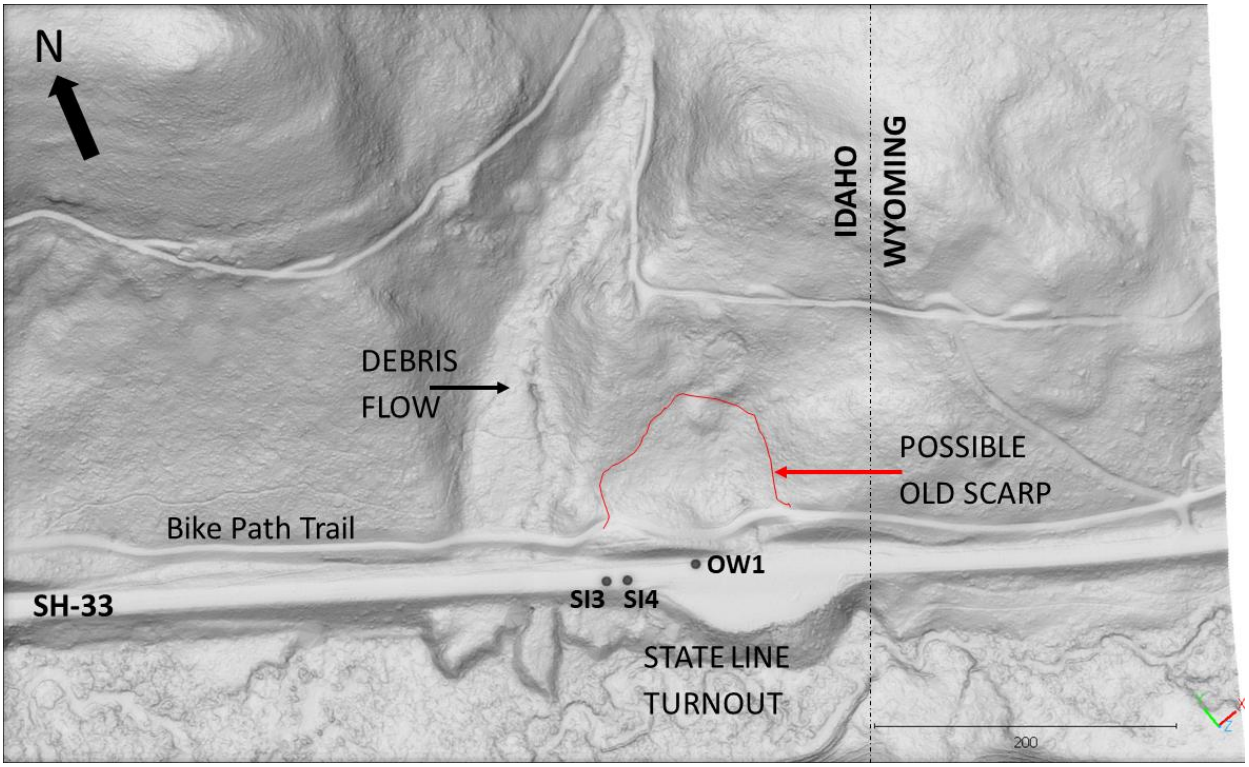

Figure 3.58 State Line Landslide Area

Geologic Conditions

The geology along SH-33 in and near the study area consists of a very complex sequence of extrusive igneous and older sedimentary rocks with overlying Quaternary colluvial soil (Figure 3.59). The sedimentary rocks in the southeastern half of the area include folded Jurassic age (Jt/Js) glauconitic, calcareous sandstone; arenaceous limestone; shaley sandstone and siltstone; shaley limestone and limestone. The younger Cretaceous rocks (Ke/Kgu) in the center of the plunging syncline are primarily siltstone, sandstone, and limestone with limited quartzite bands on a conglomerate base. The rocks in the syncline closest to the road dip to the northeast away from the highway. The northwestern portion of the study area near the road has Tertiary age (Tk) rhyolitic tuff and is present within the Bike Path slide area. The soils present throughout most of the area are mapped as Quaternary age (Qt) colluvium. Quaternary and recent alluvial soils (Qal) are present in the Trail Creek floodplain.

The most striking structural geologic feature is the major, linear thrust fault running along the base of the slope in the Trail Creek floodplain. The thrust fault trends N50W and parallels SH-33. One, short, northwest trending normal fault is mapped in the older sedimentary rocks near the center of the plunging syncline.

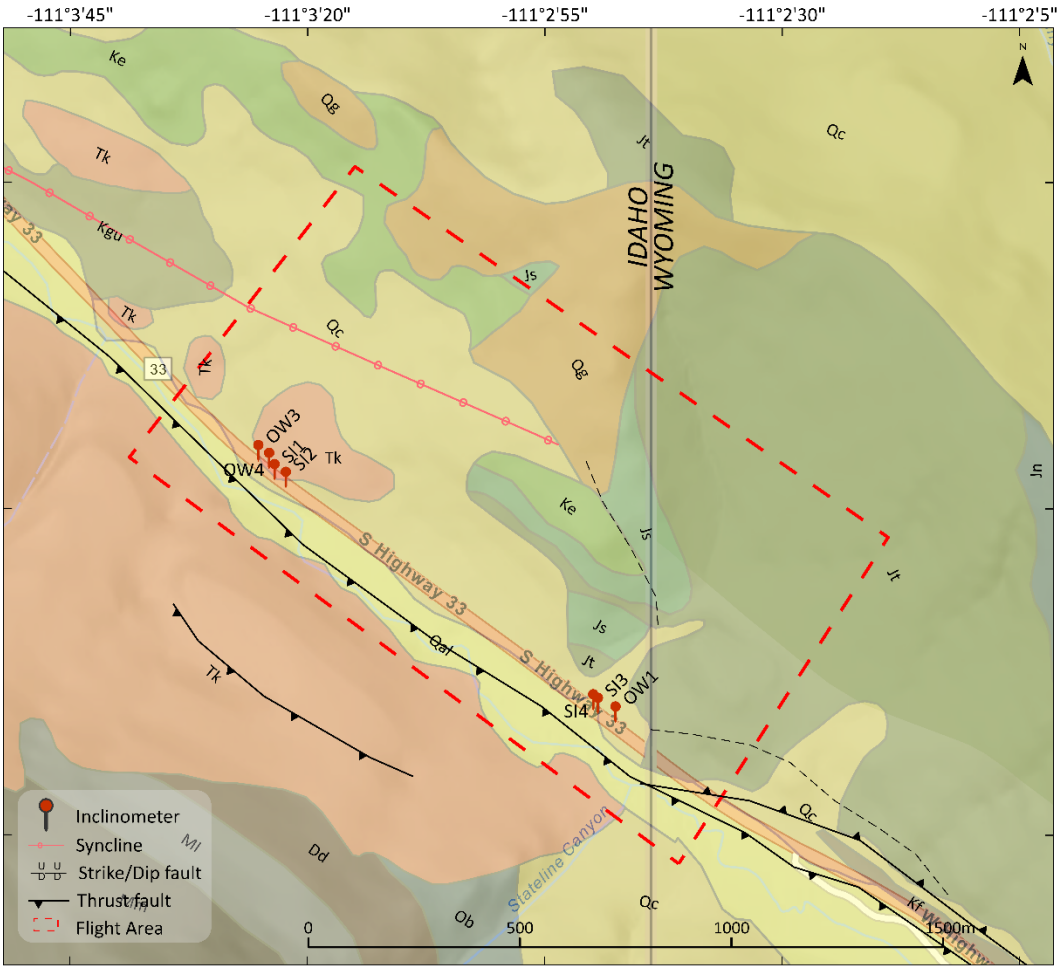

Qc - Colluvium

Tk - Mainly pinkish to yellowish-gray compact rhyolitic vitric-crystal tuff.

Qg - Older gravels; Poorly sorted moderately well cemented coarse gravel in the Teton Range. Locally includes deposits of glacial origin.

Ob - Bighorn Dolomite White to light - gray fine - to medium - grained massive cliff-forming dolomite; light - gray mottling commo; about 440 feet thick.

Dd - Darby Formation; Calcareous siltstone and sand stone with interbeds of silty yellow- brown limestone in upper part; gray fine-grained limestone and dolomite in lower part.

Ml - Lodgepole Limestone; Mainly dark-gray thin bedded fine grained limestone; brownish - and buff-weathering dolomitic limestone beds near top; lower 5 to 10 feet.

Mm - Light- to dark-gray thick-bedded to massive cherty limestone and dolomite; massive cliff-forming beds of brecciated limestone containing thin laminae of red and yellow silt in upper part.

TRa- Hematitic-red to reddish-purple calcareous siltstone and shale with scattered interbeds of gray and pinkish-gray aphanitic limestone; siltstone commonly has white polka-dot mottling at certain zones.

Js - Stump and Preuss Sandstones. Stump Sandstone, cross bedded greenish – to brownish – gray fine – to medium – grained glauconitic calcareous sandstone or arenaceous limestone with fossiliferous, oolitic, and conglomeratic limestone near top.

Kf- Frontier Formation; Interbedded very fine grained calcareous sandstone and dusky- yellow to yellowish - gray scale. Contains coal and carbonaceous lenses. Base marked by a massive noncalcareous locally conglomeratic sandstone.

Kgu - Upper part: in descending order consists of very light gray fine-grained to aphanitic limestone, the Draney Limestone; red shale and siltstone inter-bedded with thin beds of red limestone, the Bechler Shale; and very light gray fine-grained medium-bedded limestone, the Peterson Limestone.

Qal - Alluvium

Jn- Nugget Sandstone Moderate- reddish – orange to orange – pink very fine grained ridge – forming quartz sandstone.

Ke - Ephraim Conglomerate; mainly hematitic -red to purplish – red siltstone and sandstone and thin beds of light – gray cross bedded quartzite; gray to purplish – red limestone beds near top and a lenticular dark-colored resistant pebble conglomerate at base.

Jt -Twix Creek Limestone; upper half is light – gray shaly limestone that characteristically fractures into pencil-shaped fragments; lower half from top to bottom has the following rock types; red siltstone, light-brownish-gray thin-bedded in limestone, medium- gray lithographic limestone, light-gray shaly limestone, white brecciated limestone, and light-brownish-gray thin-bedded oolitic limestone.

Adapted from E.H. Pampeyan et al. 1967.

Figure 3.59 Geologic Map of the ID-33/WY-22 Bike Path and State Line Landslide Areas (adapted from Pampeyan et al. 1967)

Weather Conditions during the 2024 Investigation Period

The landslide that occurred in the Teton Pass area along WY-22 on 6-8 June 2024 was likely caused by elevated groundwater levels related to high temperatures associated rapid snowmelt and preceding days of heavy rainfall (Merzbach 2024). Precipitation and maximum temperature records for the Bike Path / State Line study site were obtained from the NOAA station identified as Phillips Bench, Wyoming. The station is located within 20 miles east of the site. The precipitation data show a period of > 1 in. persistent rainfall (Figure 3.60) prior to the June 6-8 landslide event at Teton Pass. Rising temperatures which likely melted a residual snowpack were also recorded before June 7th (Figure 3.61). The timing of observed pavement damage along SH-33 in the State Line area appears to coincide with the large landslide at Teton Pass (Figure 3.62).

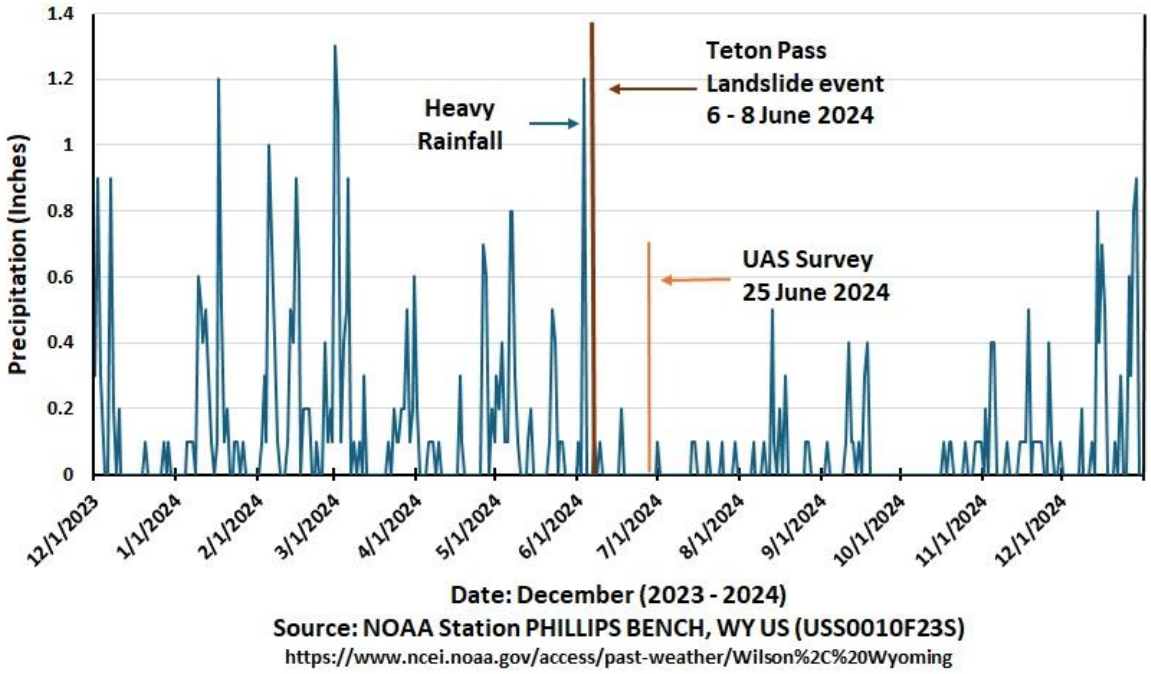

Figure 3.60 Precipitation Record for the State Line and Bike Path Landslide Areas

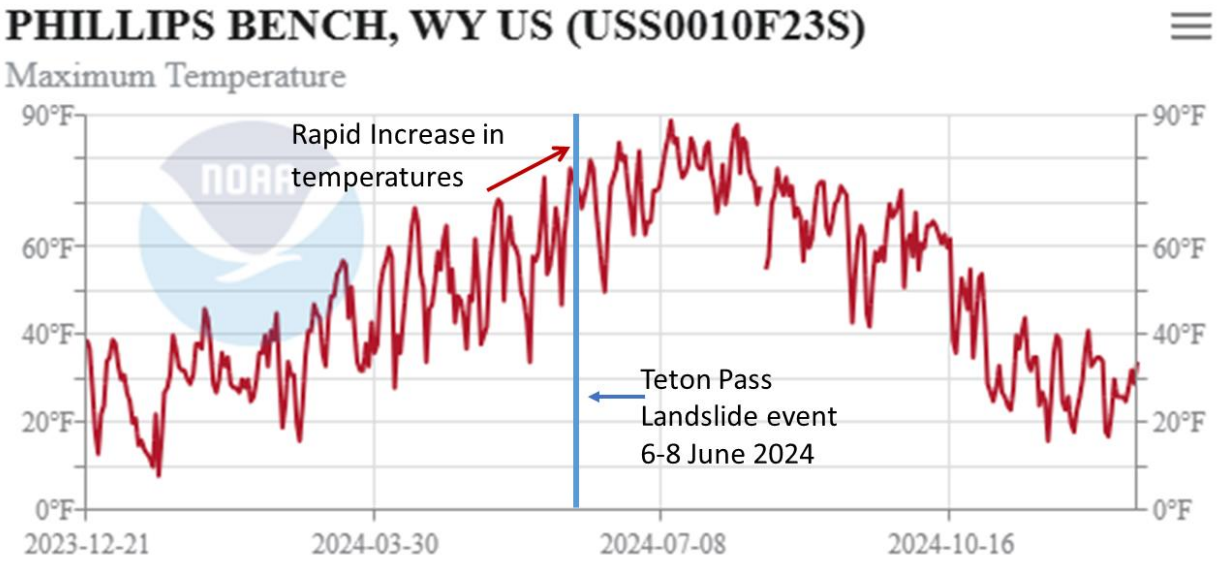

Figure 3.61 Temperature Record for the Bike Path and State Line Landslide Areas

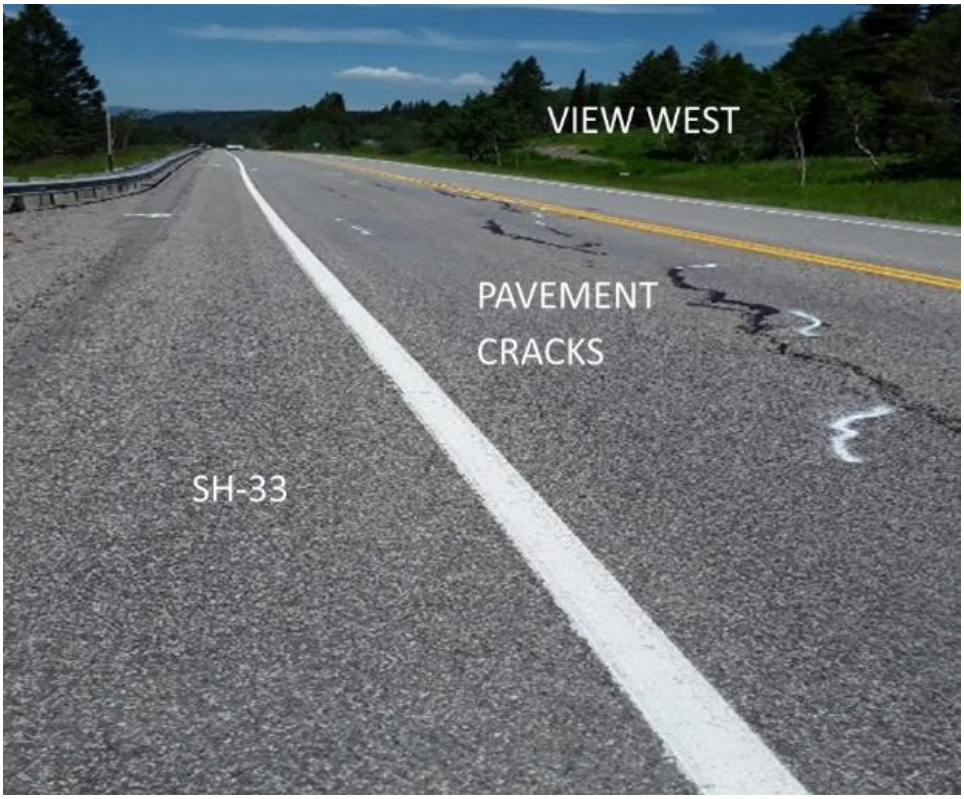

Figure 3.62 Longitudinal Cracks in SH-33 Pavement by the State Line Turnout Caused by Slope Movement between the Road and Trail Creek (photo: Shawn Enright, June 2024)

Recent Landslide Activity and ITD Instrumentation in the Study Areas

In spring and early summer 2024, ITD staff observed and monitored landslide activity on the northwest (Bike Path) and southeast (State Line) ends of the study area. The landslides were located between Trail Creek and the highway and caused cracks and offsets in the pavement (Figure 3.63 and Figure 3.64). ITD carried out a subsurface investigation and installed four inclinometers (SI-1 to SI-4) in and adjacent to the slide areas and an observation well (OW1) near the State Line turn-out (Figure 3.59). Only one ISU UAS-LiDAR survey was flown in the area on 25 June 2024 after the pavement damage was observed. The survey provides ITD with a baseline digital ground surface for future UAS monitoring of landslide activity along SH-33 at the Wyoming border. In Section 4 of this report, a comparison is made between the ISU 25 June 2024 LiDAR survey and a Teton County 2020 manned aircraft LiDAR survey obtained from the Idaho LiDAR Consortium website. Discussion of the differences between the 2020 and 2024 LiDAR surveys is given in Section 4 of this report.

Project Inclinometers

A summary of the inclinometer bore hole depths and the bottoms of the inclinometer casings is in Table 3.17:

Table 3.17 SH 33 State Line and Bike Path Landslide Area Bore Holes and Inclinometers

Slide Area	Designation	Bore Hole Depth	Inclinometer Depth
Bike Path	SI-1	28 ft	26 ft
Bike Path	SI-2	42 ft	39 ft
State Line	SI-3	51 ft	42 ft
State Line	SI-4	59.5 ft	58 ft

Initial slope displacement measurements recorded by ITD staff for Inclinometers SI-1/SL-2 were taken on 30 May 2024 and later in Inclinometers SI-3/SI-4 on 19 and 20 June 2024, respectively. Subsequent measurements were made on the Inclinometer pairs in June 2024 just prior to the LiDAR survey with the last set of measurements taken on 1 October 2024 (Appendix A).

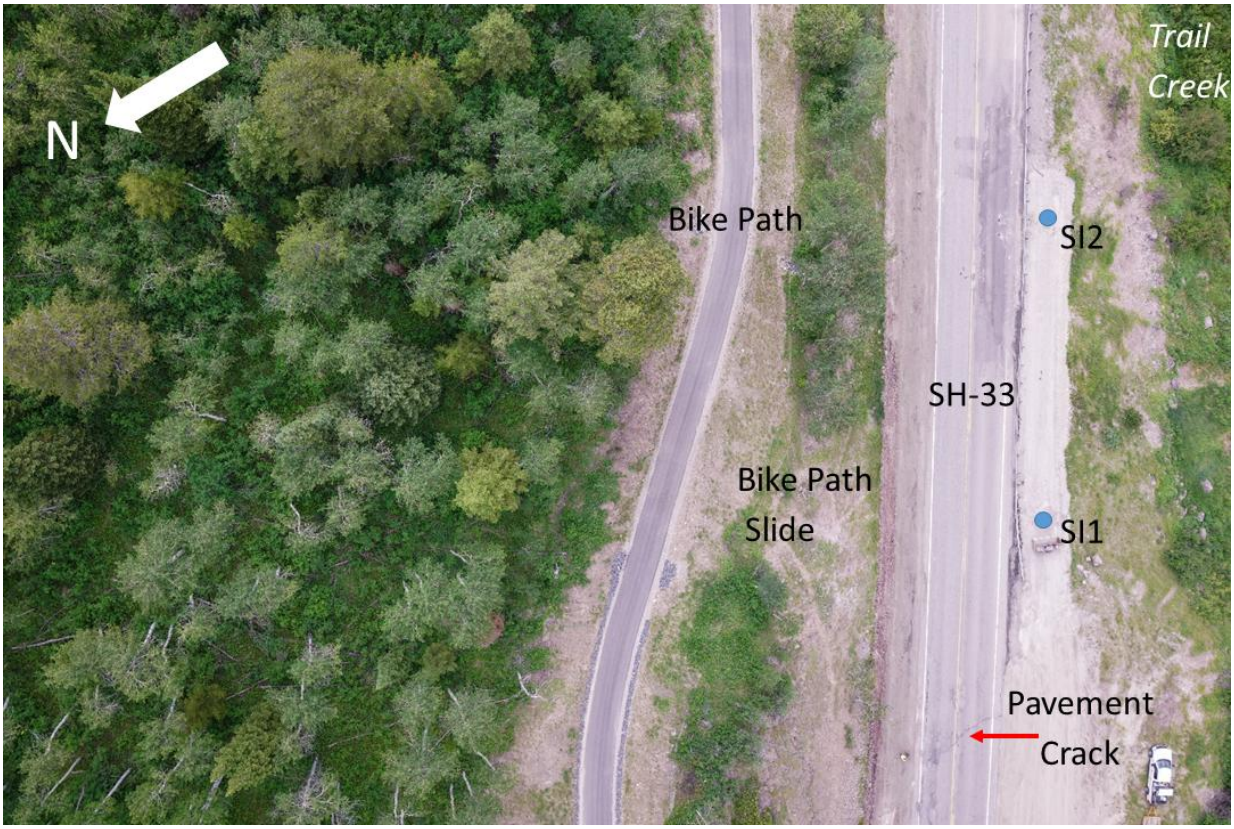

Figure 3.63 Photo of Bike Path Slide Area with SI-1 and SI-2 Inclinometer Locations (Photo provided by ITD)

Close-up views of the inclinometer locations in the two slide areas are given Figure 3.63 and Figure 3.64. Inclinometers SI-1 and SI-2 on the west end of the site are located on the south side of the road and were installed after the slope movement occurred.

SI-3 and SI-4 are located in the State Line slide area were placed by ITD staff on the south shoulder of the road inside the slide area (Figure 3.64). Linear pavement cracks caused by the lateral movement are visible in the highway asphalt.

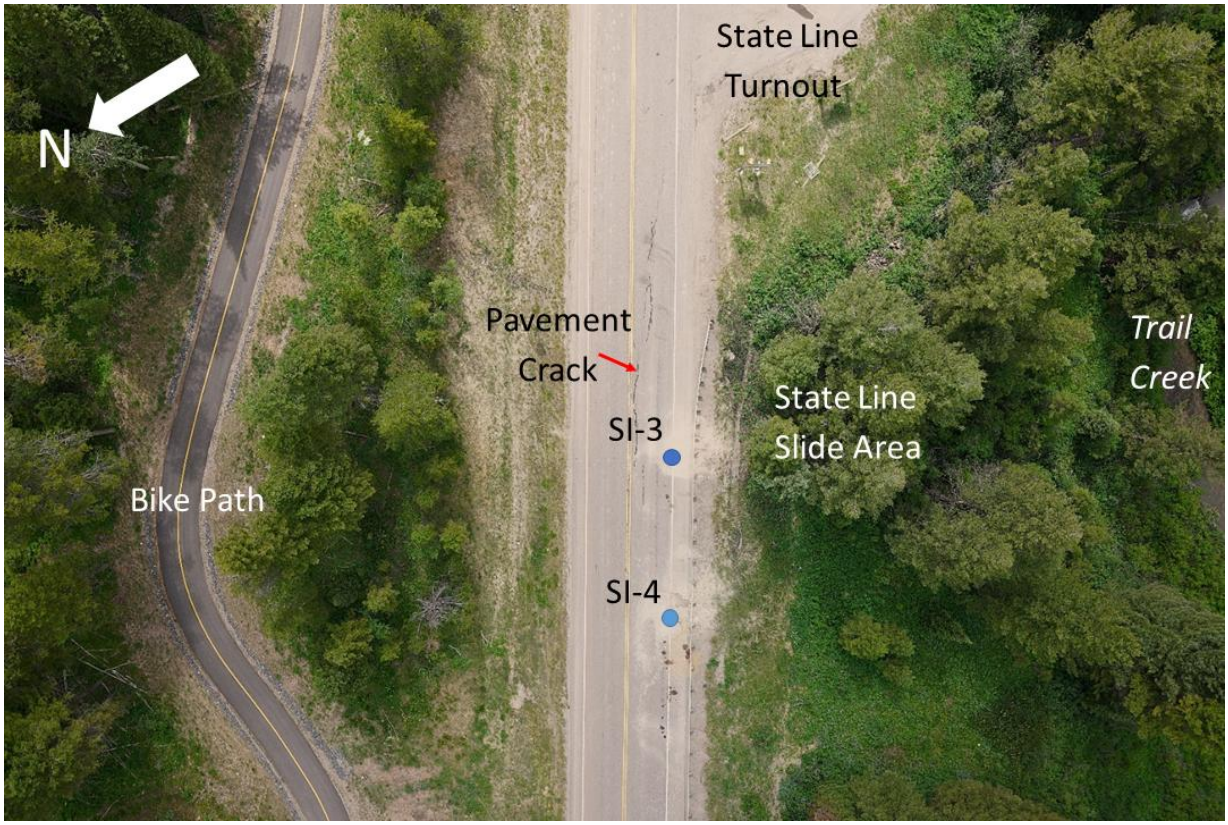

Figure 3.64 Photo of State Line Slide Area with SI-3 and SI-4 Inclinometer Locations (Photo provided by ITD)

Boring Logs

Geotechnical bore holes were drilled and sampled by ITD in order to determine the subsurface conditions and place in the inclinometers. Logs of the borings prepared by ITD staff were provided to the researchers.

Bike Path Bore Holes/Inclinometers SI-1 and SI-2

The upper 1.5 ft of Borehole SI-1 is described as silty GRAVEL and GRAVEL. The soil below the upper layer is a gravelly CLAY down to a depth of 18 ft below the ground surface. The upper 4.5 ft of the gravelly CLAY contains fine to coarse sand. Between 8 and 18 ft, the log indicates that the soil may be a welded volcanic ash. Standard Penetration N-values reported in the log range between 14 and 32 blows/ft. Between 18 and 27 ft, the log describes a dark gray and light greenish yellow CLAYEY BRECCIA interpreted to be broken fault gouge in a shear zone of the Jackson Thrust Fault. The BRECCIA is underlain by a highly weathered clayey TUFF. Groundwater levels at the time of exploration were recorded at 19.3 and 20 ft. The ITD log of Bore Hole SI-2 shows 17.5 ft of soil above 24.5 ft of high

weathered bedrock. The upper 4.4 ft of the soil profile is described as GRAVEL (GM) with little cobbles. Gravelly CLAY with cobbles, sandy CLAY and high plasticity CLAY underlie the upper GRAVEL down to a depth of 17.5 ft. The sandy CLAY between 9 and 13 ft is described as possible slide material and CLAY between 13 and 17.5 ft as a "probable bad player". The underlying high plasticity CLAY between 17.5 and 25 ft is appears to be highly weathered bedrock. Uncorrected Standard Penetration Test N-values range between 2 and 10 blows/ft down to a depth of 20 ft. A 5-ft thick layer of interbedded clayey SHALE and silty SANDSTONE was encountered at 25 ft. The remainder of the bore hole down to 42 ft is highly weathered SANDSTONE. Groundwater levels recorded during drill hole advance were measured at 9.3 and 3.8 ft below the surface. Both borings were logged by Shawn Enright of ITD District 6.

State Line Bore Hole/Inclinometer SI-4

Bore hole/Inclinometer SI-4 is located on the west shoulder in the State Line section of SH-33 (Figure 3.4963). The bore hole was drilled using an 8-12-in. diameter hollow stem auger and split spoon samples taken in 18-in. intervals every 5 ft staring at 10 ft below the ground surface. No blowcounts were provided in the log. The bore hole was advanced entirely in soil down to a depth of 59.5 ft (Figure 3.5064). Nearly all of the profile is made up of lean to fat CLAY (CH and CL) and silty CLAY (CL-ML) in layers 2 to 19.5 ft thick. Fill below the pavement is 3.4 ft thick and is described as lean CLAY and SANDY CL. A 4.3-ft thick layer of hard, dry silty SAND was encountered at a depth of 15 ft below the pavement surface. At a depth of 21.3 ft, the soil is logged as landslide debris and is classified as a slightly moist, lean CLAY (CL). The profile below a depth of 40 ft is labeled a hard, light reddish orange, non-plastic, slightly damp, silty CLAY (CL) which may be weathered rock (Figure 3.64). Groundwater was encountered at a depth of approximately 48.9 ft.

Inclinometer Measurements

Three of the four inclinometers placed by ITD in the two landslide areas (SI-1, SI-2 and SI-3) show essentially no lateral displacement during the May-June and October 2024 monitoring period (Appendix A).

At SI-4, lateral displacement continued after the cracks formed in the roadway (Figure 3.61). Movement was recorded between 20 June and 1 October 2024 (Figure 3.64). The displacement pattern is downslope between the ground surface and a depth of 6 ft followed by negative or upslope rotation between 6 and 10 ft. Between 10 and 18 ft, the movement was approximately 0.27 in (0.68 cm) downslope. ITD staff opine that the sine-wave pattern of displacement could be caused by settlement of the sand backfill around the inclinometer casing (Enright personal communication 2025). The soils in the slope below 18 ft appear to be undergoing creep movement toward Twin Creek. The lateral displacement on the road surface during the measurement interval is approximately 0.07 in. (0.18 cm) well below the sensitivity of the LiDAR survey.

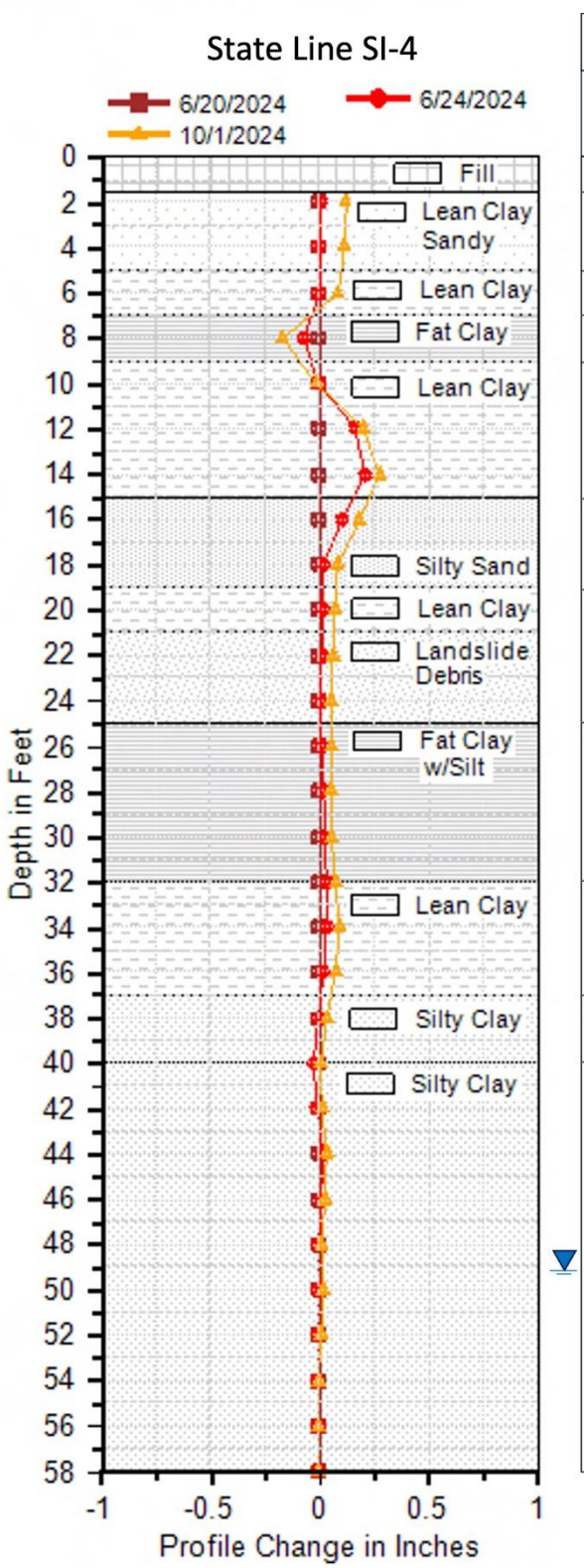

SI-4	
Depth (ft)	Material Description
0	Asphalt, FILL, dry, Poorly Graded Gravel (GP) (GP-GM)
1.6	FILL, stiff to soft, light greenish brown, medium plasticity, dry to moist, fine to medium grained, LEAN CLAY with SANDY (CL)
5	LEAN CLAY (CL), damp to moist, mixed w/multiple gravel
7	Stiff, damp, high plasticity, FAT CLAY (CH)
9	High plasticity, damp to moist, LEAN CLAY (CL) Medium stiff, high plasticity, slightly moist, LEAN CLAY (CL) Vane shear at 11 ft. Peak 26 kpa, residual 10 kpa.
15	Residuum, loose, non plastic, dry, SILTY SAND (SM) Hard, dry, SILTY SAND (SM)
19.3	Stiff to soft, dark brown, slightly moist, LEAN CLAY (CL) Landslide debris, stiff, slightly moist, LEAN CLAY (CL)
25	Hard, dark brown to dark orangeish brown, medium plasticity, dry, fine to coarse grained, angular, gravelly FAT CLAY with SILT (GC-GM)
32	Dark brownish orange and light reddish yellow, damp, fine to medium grained LEAN CLAY (CL)
37	Firm to hard, light tan, low plasticity, dry to coarse grained, angular to subrounded, SILTY CLAY (CL-ML)
40	Hard, light reddish orange, non plastic, slightly damp, fine grained, subangular to rounded, SILTY CLAY (CL-ML), may be weathered bedrock Drilling change alternating hard to medium hard 40 minutes to drill 5 feet

BOTTOM OF BORING: 58 FT

Figure 3.65 Displacement-Depth Measurements and Corresponding Boring Log at SI-4

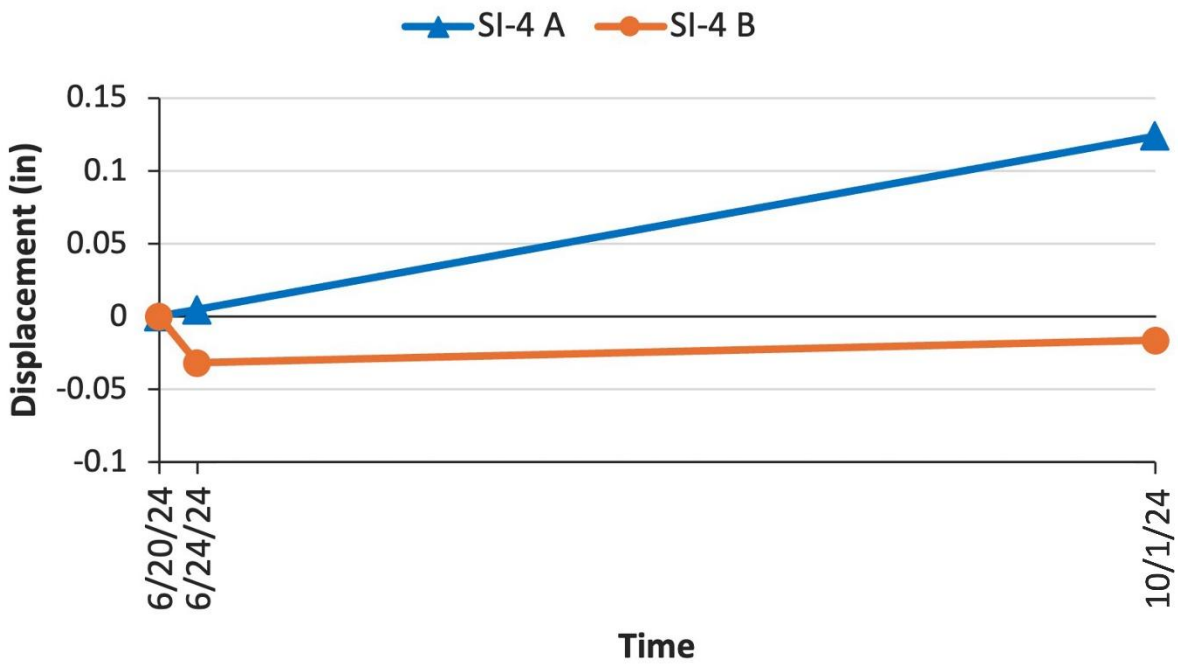

Figure 3.66 SI-4 Displacement-Time Plot (draft)

4. Change Detection Comparisons at Landslide Study Areas with Prior Manned Aircraft Datasets

Overview

To extend the capabilities of the present ISU-UAV study, the Geoscience Team analyzed past manned aircraft LiDAR surveys in the project areas and compared the results with the present UAS surveys. The ISU landslide study areas have past (2017-2020) LiDAR survey coverage that is available to the public (Table 4.1). The past LiDAR is at quality levels QL1 or QL2, depending on location. QL1 or QL2 indicates a point cloud resolution with a range of 2 to ≥ 8 pts/m^2 whereas the ISU LiDAR data is ≥ 50 pts/m^2. It should be noted the 10 cm vertical accuracy in the past surveys is much lower than the vertical sensitivity of the ISU surveys (2 cm).

Approach/Methods

Past manned LiDAR data for each study site was downloaded either through the Idaho LiDAR Consortium's website (https://www.idaholidar.org/existing-lidar-data/) or through the USGS 3DEP LiDAR Explorer application (https://apps.nationalmap.gov/lidar-explorer/#/). The ISU team identified the tiles needed for each of the study sites and merged them together using LAStools' lasmerge command (rapidlasso GmbH, version 241210). LAStools is available from https://rapidlasso.com. To accurately place the datasets into the same projected horizontal and vertical coordinate systems, NOAA's vertical datum transformation software (https://vdatum.noaa.gov/) was used to transform the past LiDAR data from NAD83 (2011), NAVD88, Geoid12B (or Idaho State Plane) to WGS84 UTM 12N with WGS84(1762).

At the start, not all past LiDAR datasets were available for the study sites. In future studies, the new statewide LiDAR datasets would be used as the base reference instead of converting them to the coordinate system for processing the ISU UAS LiDAR datasets. To assess changes in the LiDAR point clouds, Cloud Compare (version 2.14 alpha, 2025) software was used with a cloud-to-cloud (C2C) comparison which provides absolute X, Y, XY, and Z distances. The highest quality UAS LiDAR dataset was used with the most recent, publicly available LiDAR data. XY and Z distances can reveal mass hillside movements between the datasets. For all point clouds, C2C was used for change detection to develop Z and XY values. A multi-cloud to multiscale model-to-model cloud comparison (M3C2) was also used to further evaluate the point clouds. In this section, the results with visualizations are provided that highlight any elevation changes between ITD past and present ISU surveys.

Table 4.1 Recent Manned Aircraft LiDAR Surveys by Landslide Study Area

Landslide Study Area	Date Acquired	Quality Level	Vertical Accuracy / pts/m²	ASPRS LAS Version	Horizontal Coordinate System	Vertical Coordinate System
Swan Valley Complex [1]	2019-11-16	**QL1** ≤ 0.35 m nominal pulse spacing	10 cm ≥ 8 pts/m²	LAZ 1.4	NAD83(2011) UTM 12N (meters)	North American Vertical Datum (NAVD) 1988 Geoid 12B
Indian Creek [2]	2020-09-23	**QL2** ≤ 0.71 m nominal pulse spacing	10 cm ≥ 2 pts/m²	LAZ 1.4	NAD83(2011) UTM 12N (meters)	North American Vertical Datum (NAVD) 1988 Geoid 12B
Pine Bar [3]	10/1/2017 - 11/8/2017	**QL1** ≤ 0.35 m nominal pulse spacing	10 cm ≥ 8 pts/m²	LAZ 1.4	NAD83(2011) UTM 12N (meters)	North American Vertical Datum (NAVD) 1988 Geoid 12B
Bud Peck [4]	2019-10-03	**QL2** ≤ 0.71 m nominal pulse spacing	10 cm ≥ 2 pts/m²	LAZ 1.4	NAD83(2011) UTM 12N (meters)	North American Vertical Datum (NAVD) 1988 Geoid 12B
SH-33 State Line and Bike Path [5]	2020-08-28	**QL1** ≤ 0.35 m nominal pulse spacing	10 cm ≥ 8 pts/m²	LAZ 1.4	Idaho State Plane, East Zone. NAD83 (2011). US Survey Foot	North American Vertical Datum (NAVD) 1988 Geoid 12B

1. Swan Valley Complex Data Source/Citation: U.S. Geological Survey, 20240427, USGS Lidar Point Cloud ID_SouthernID_2018_D19. Tiles: 12TVP680105, 12TVP695105, 12TVP710105, 12TVP725105: U.S. Geological Survey.

2. Indian Creek Data Source/Citation: U.S. Geological Survey, 20231227, USGS Lidar Point Cloud ID_SouthernID_2018_D19. Tiles: 12TVN905865, 12TVN905880, 12TVN920865, 12TVN920880: U.S. Geological Survey.

3. Pine Bar Data Source/Citation: Quantum Spatial, Blackfoot & Portneuf, Idaho Delivery 2 LiDAR Technical Data Report. Tiles: 12TVN8257, 12TVN8258, 12TVN8357, 12TVN8358: Prepared for Boise State University.

4. Bud Peck Data Source/Citation: U.S. Geological Survey, 20231114, USGS Lidar Point Cloud ID_SouthernID_2018_D19. Tiles: 12TUM990845, 12TUM990860: U.S. Geological Survey.

5. SH-33 State Line and Bike Path Data Source/Citation: U.S. Geological Survey, 300225, USGS Lidar Point Cloud, ID Southern ID_2018_D19. Tiles: Teton_53-32, Teton_53-31, Teton_54-32, Teton_53-31: U.S. Geological Survey.

A comparison of the point cloud resolutions between manned aircraft LiDAR surveys and ISU photogrammetry and LiDAR datasets is provided in Table 4.2. The alignment error between the data sets is analyzed.

Table 4.2 Point Cloud Alignment Accuracy

Landslide Study Area	Manned LiDAR pts/m² (Ground)	ISU LiDAR/Photogrammetry pts/m² (Ground)	XY RMS error (m)	Z RMS error (m)
Pine Bar	4	82.9	0.12	0.025
Indian Creek	4	LiDAR 73.5 D2M 61.7	0.110 (LiDAR) 0.134 (D2M)	0.013 (LiDAR) 0.067 (D2M)
Bud Peck	3	240	0.14	0.03
Rainey Creek	6.8	2023 D2M Photogrammetry 2024 October Q240 LiDAR: 36.7	0.14-0.26	0.034
Swan Valley East	6.8	2023 D2M Photogrammetry: 2024 October Q240 LiDAR: 36.7	0.14-0.26	0.034
Gibson	6.9	58.29	0.14-0.26	0.038
SH33 State Line and Bike Path	7.45	76.18	0.03	0.021

Landslide Change Detection

Pine Bar Landslide Area

Four tiles were merged from the 2017 LiDAR survey (Table 4.1) using LAStools (rapidlasso GmbH) and the coordinate system transformed to WGS84 UTM 12N with NOAA vdatum. For this comparison the team utilized the UAS Q240 LiDAR data acquired on 30 October 2023. This dataset was captured when leaf-off conditions were ideal and provided the best ground returns. Once the datasets were in the same coordinate system the alignment accuracy was checked (Table 4.2).

For the comparison between the 2017 and 2023 LiDAR datasets, an XY and Z absolute distance comparison provided the best results for assessing slope change. In Figure 4.1, elevation change reveals slight areas of loss that are notable along the river bank and along areas of the steep slopes near the top

of the ridgeline above the highway. Recorded movement was < 0.75 m. Some areas of change may be attributed to dense vegetation. Low-lying vegetation below inclinometer B4 was incorrectly classified as ground surface in the 2017 LiDAR, thus showing as a loss in the cloud to cloud comparison.

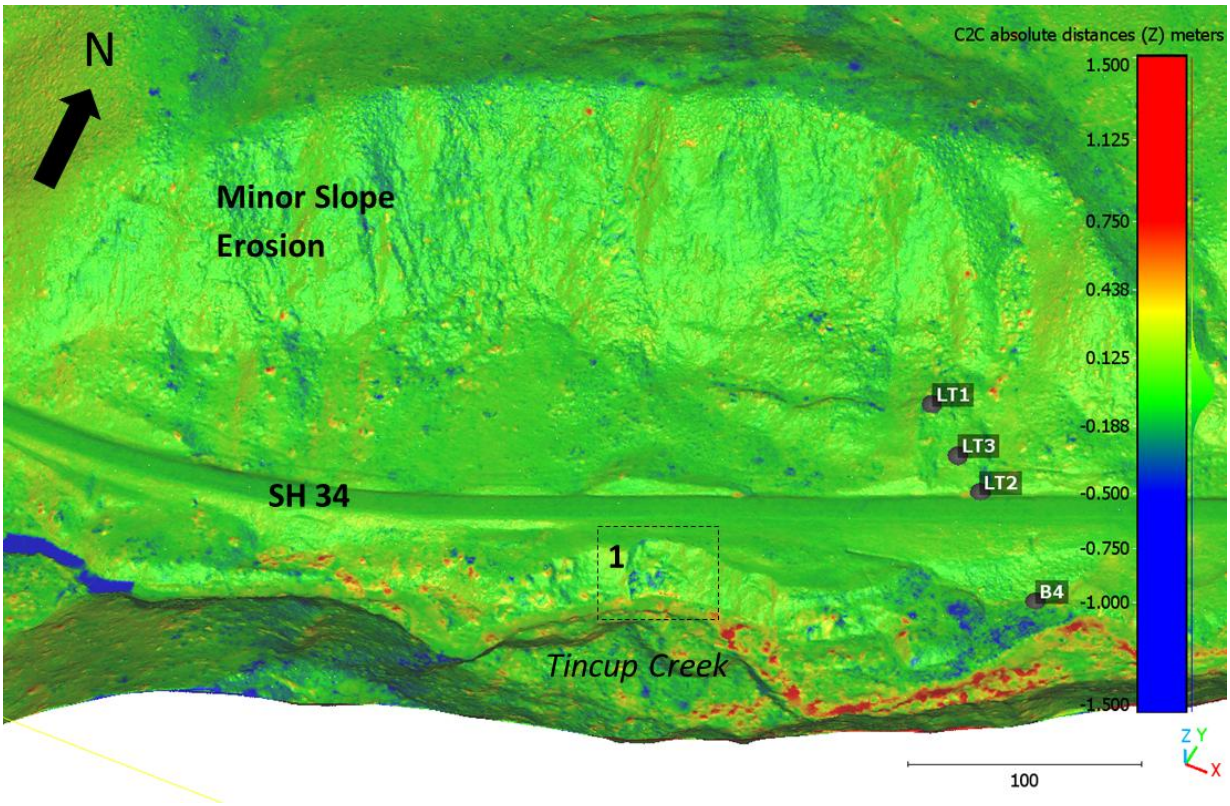

Figure 4.1 Z ITD LiDAR Survey Displacement in the Pine Bar Study Area during October-November 2017 and 30 October 2023

Between 2017 and 2023 minor ground loss was taking place below the road in Area 1 with corresponding ground heave in the flood plain below. In only one year (2023 and 2024), slope movement/erosion appears to have increased significantly and encroached closer to the south edge of the road. Similar to comparisons between the 2023 to 2024 ISU LiDAR collections for this site, some minor vertical loss was detected below the highway as indicated in Figure 4.2. Continued river incision by Tincup Creek could continue to undermine this slope (Egholm, Knudsen, and Sandiford 2013).

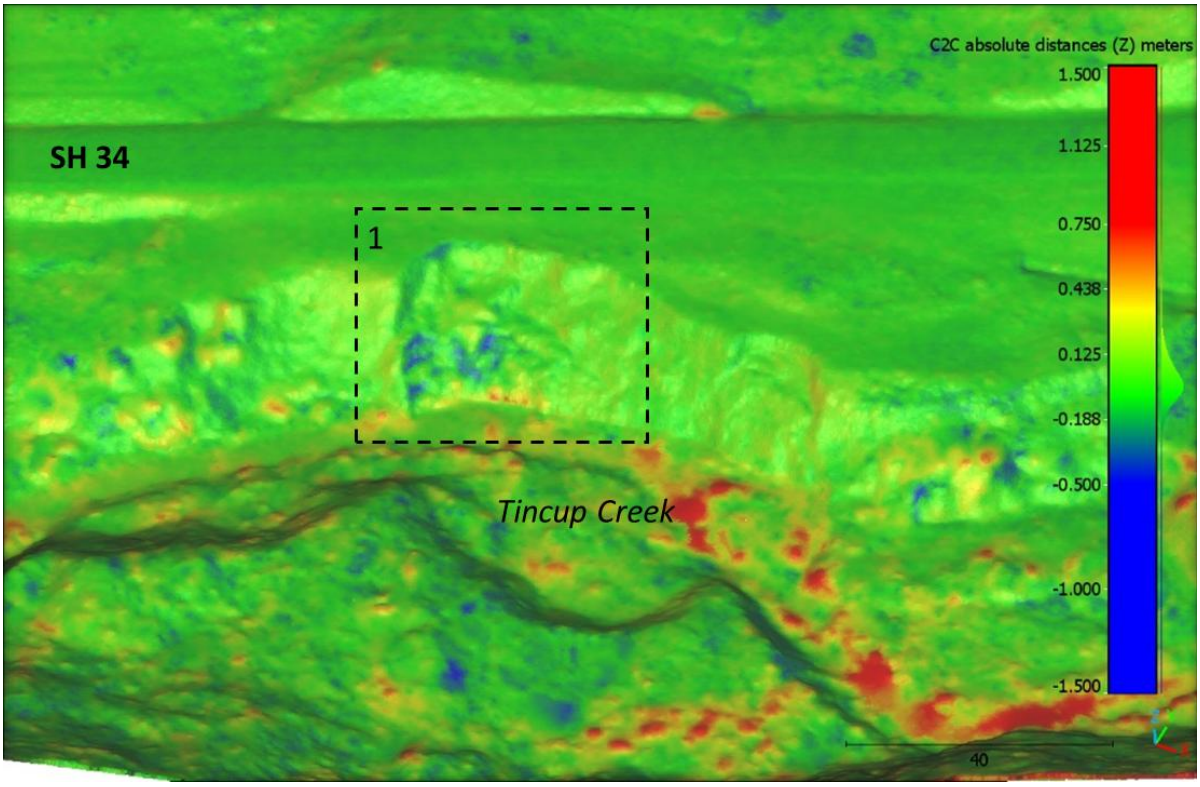

Figure 4.2 Z Slope Movement in Pine Bar Area 2 between the 2017 and 2023 LiDAR Surveys

Bud Peck Landslide Area

Two LiDAR tiles were merged from a 2019 ITD LiDAR survey of Bud Peck and compared for change against the 26 October 2024 LiDAR survey (Figure 4.3). The presence of white in the former landslide area means that the 2019 LiDAR survey was unable to penetrate the tree cover and may have concealed any additional slope movement adjacent to the highway. The comparison of the two surveys does indicate greater erosion in the intermittent stream south of the site during the 2019 to 2023 time period.

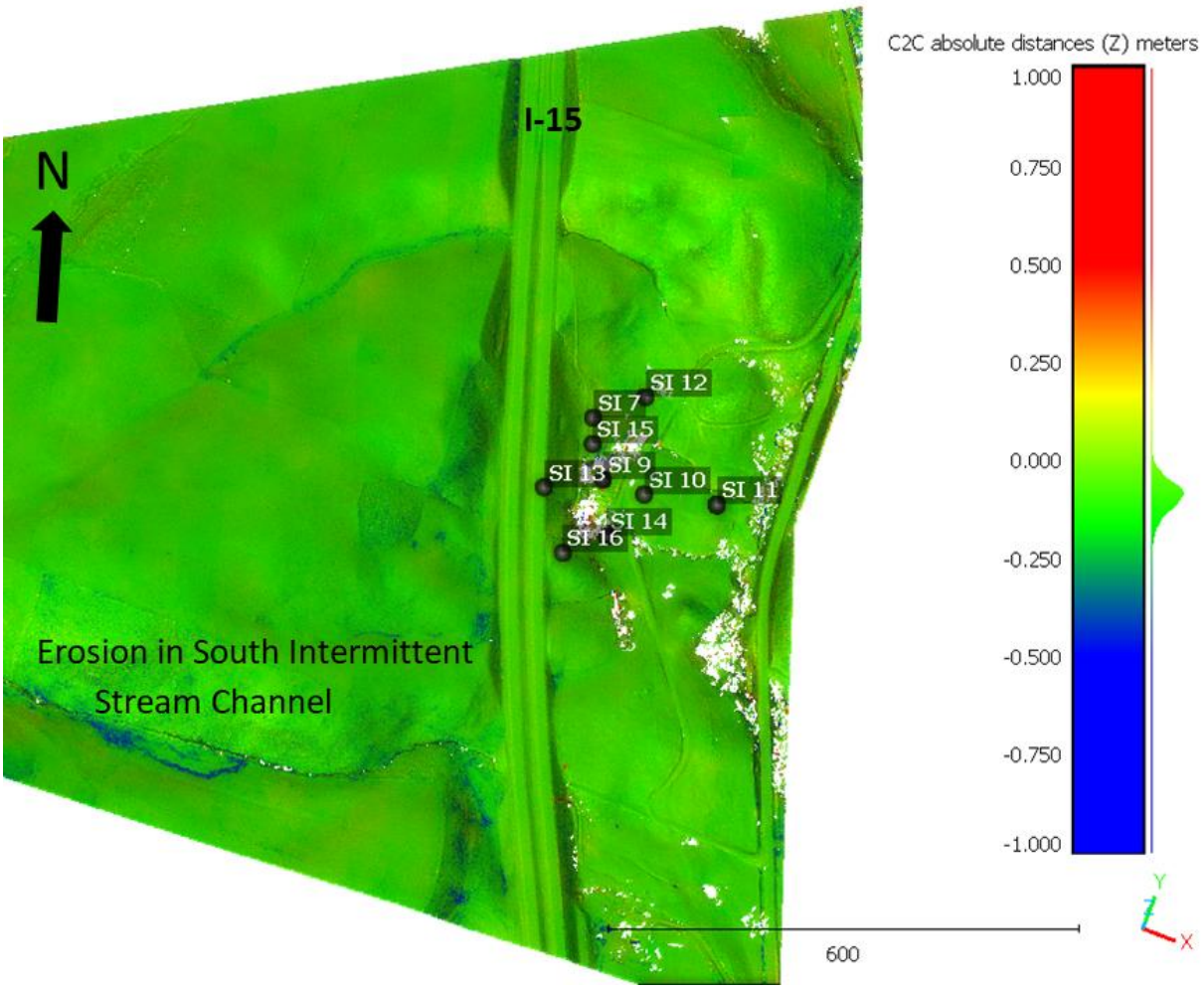

Figure 4.3 Manned Aerial LiDAR 2019 Compared with the 26 October 2024 UAS LiDAR Survey in the Bud Peck Landslide Area

Indian Creek Landslide Complex

Four tiles from the 2020 Manned Aircraft survey in the Indian Creek area were compared with the ISU 26 October 2024 LiDAR dataset. Three areas of interest were identified in Figure 4.4 with closeups in Figure 4.5 and Figure 4.6.

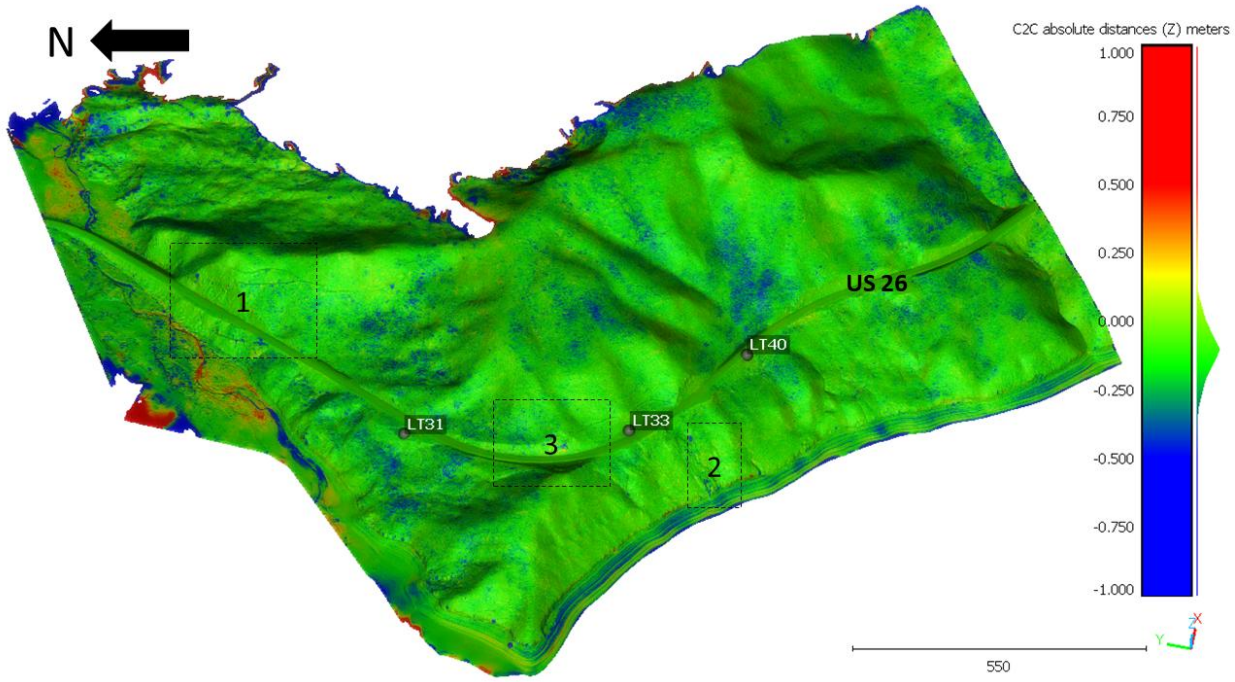

Figure 4.4 Indian Creek 2020 LiDAR Comparison with 26 October 2024 LiDAR.

In Area 1, the combined surveys show erosion (in blue) on the slope above US-26 with deposition of soil (in red) in the ditch at the base of the slope on the east side of the road (Figure 4.5). In Area 2, erosion with likely slope movement has taken place below the west side of SH-26 and just above Palisade Reservoir. The survey results in Area 3 (Figure 4.6) show additional movement in a past landslide on the east side of the highway (downward movement in blue above upward movement in red) similar to the pattern of displacement in the East Swan Valley site. No slope movement occurred in Area 3 during the ISU 2023-2024 LiDAR surveys.

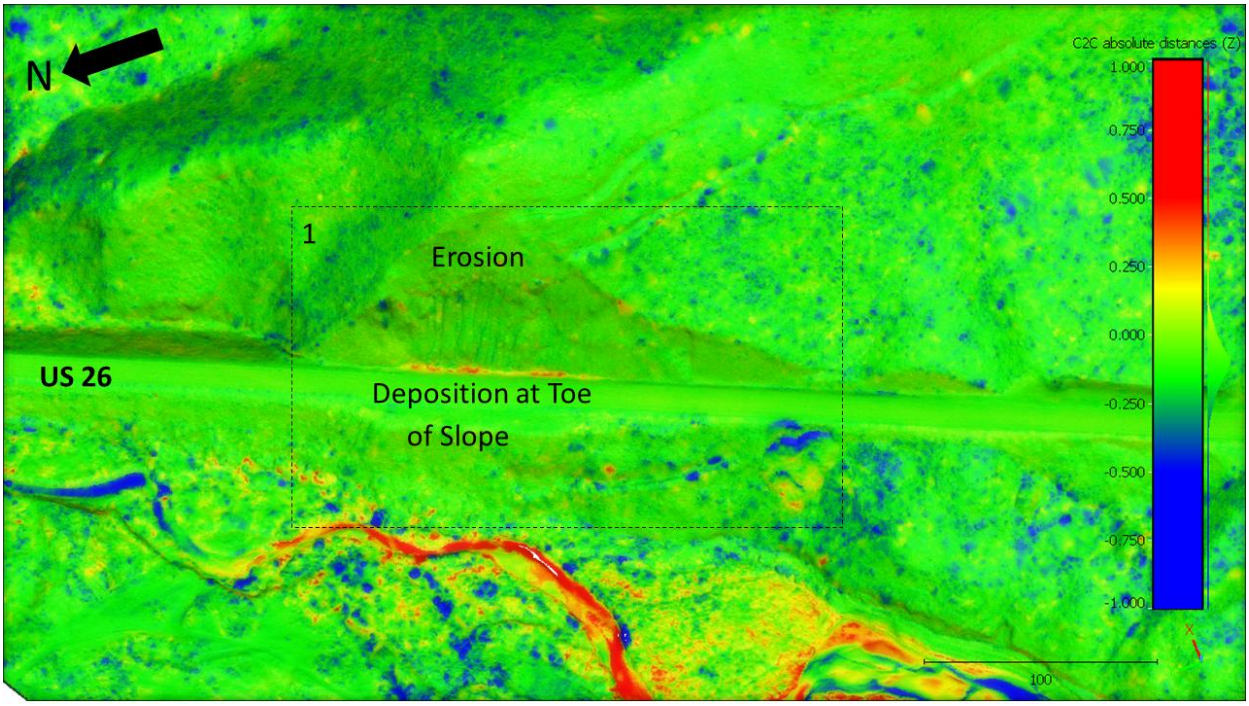

Figure 4.5 Indian Creek Area 1 – Erosion Above and Deposition Below the Slope on the East Side of US-26.

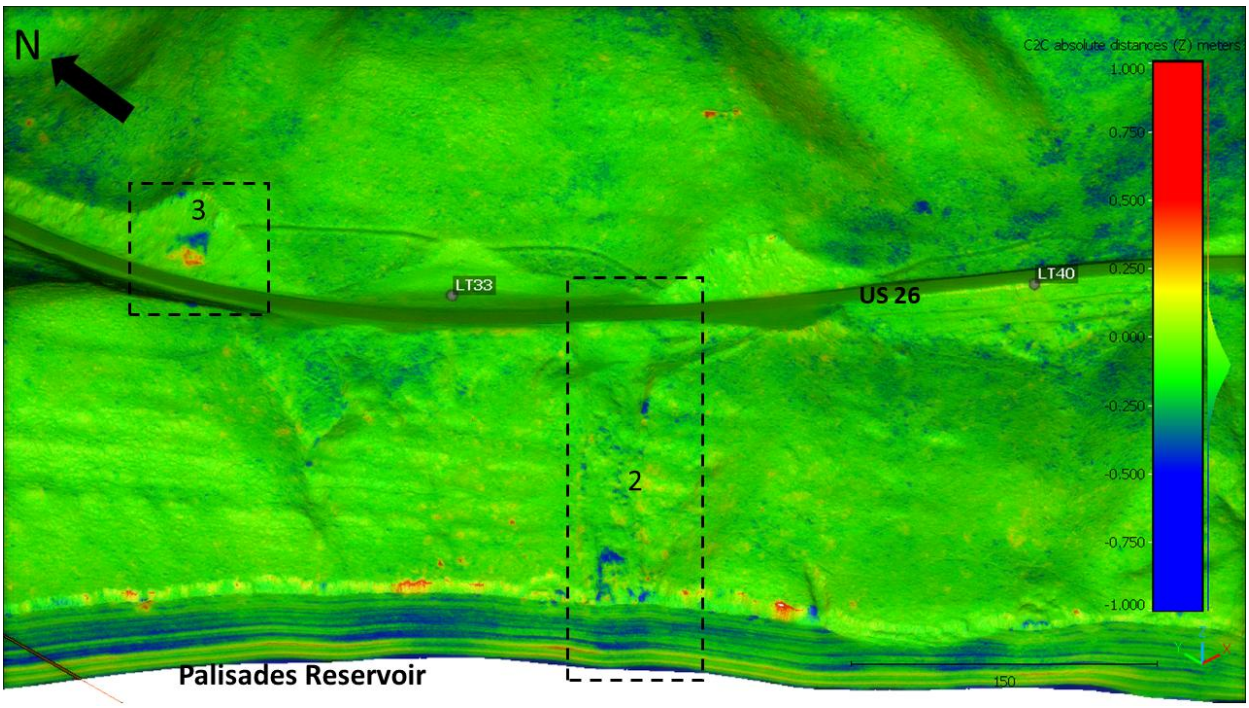

Figure 4.6 Indian Creek Movement Areas 2 and 3. Area 2 has undergone erosion in the slope above the Palisades Reservoir and Area 3 has experienced landslide movement.

Swan Valley East Landslide Area

Four tiles were merged for the manned aircraft 2019 LiDAR to compare with the 2023 D2M photogrammetry data and the October 2024 ISU LiDAR data. The intent was to show the development of the landslide on the east side of inclinometer LT4. In Figure 4.7, the elevations differences show very small settlement/heave upslope of US-26 prior to 2023. The upslope settlement/downslope heave fits the landslide model, however given the intensity of displacement, the movement would not cause immediate concern in 2023 for landslide development above the road.

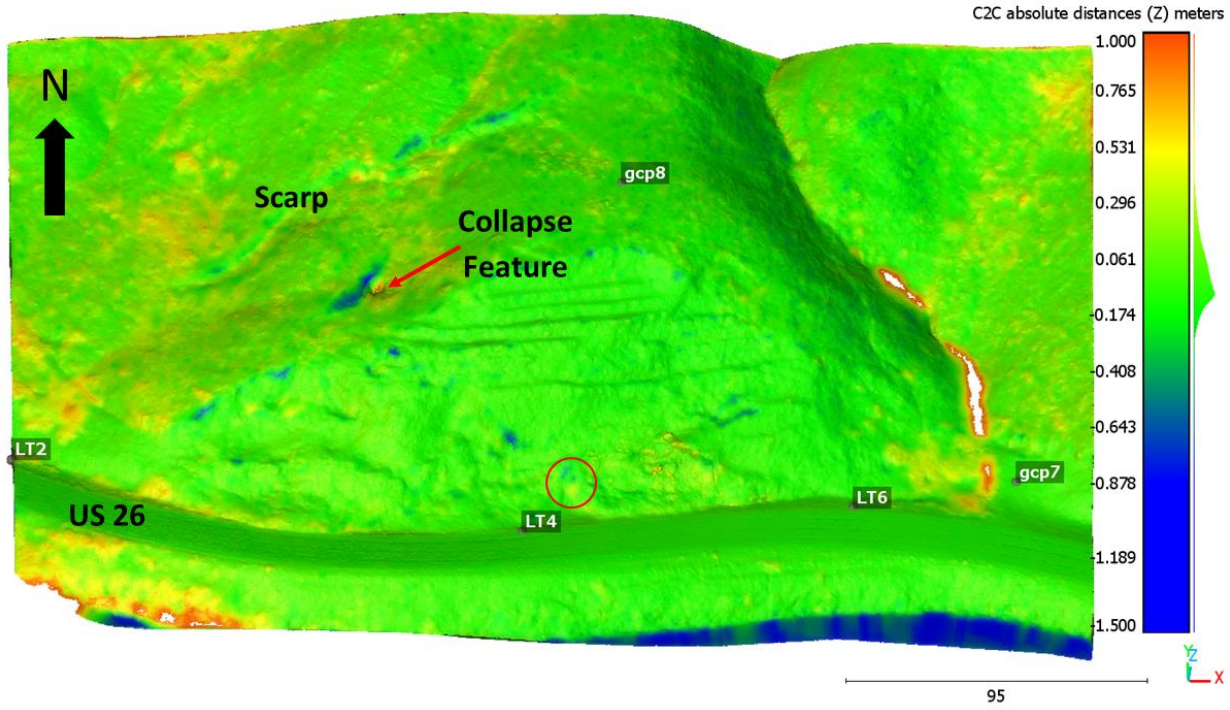

Figure 4.7 Swan Valley East Active Slide Area. Manned Aircraft LiDAR 2019 versus D2M 2023 Photogrammetry Point Cloud

In Spring 2024, the same area developed into a landslide/mudflow which did not reach the road (Figure 4.8). Clearly, this example by itself demonstrates capability of the UAS LiDAR system in monitoring ITD highway assets. Because of the displacement pattern, 2024 landslide activity, ground surface depression and presence of a long scarp high on the hillside, this would be an area to monitor for future movement that could affect the roadway.

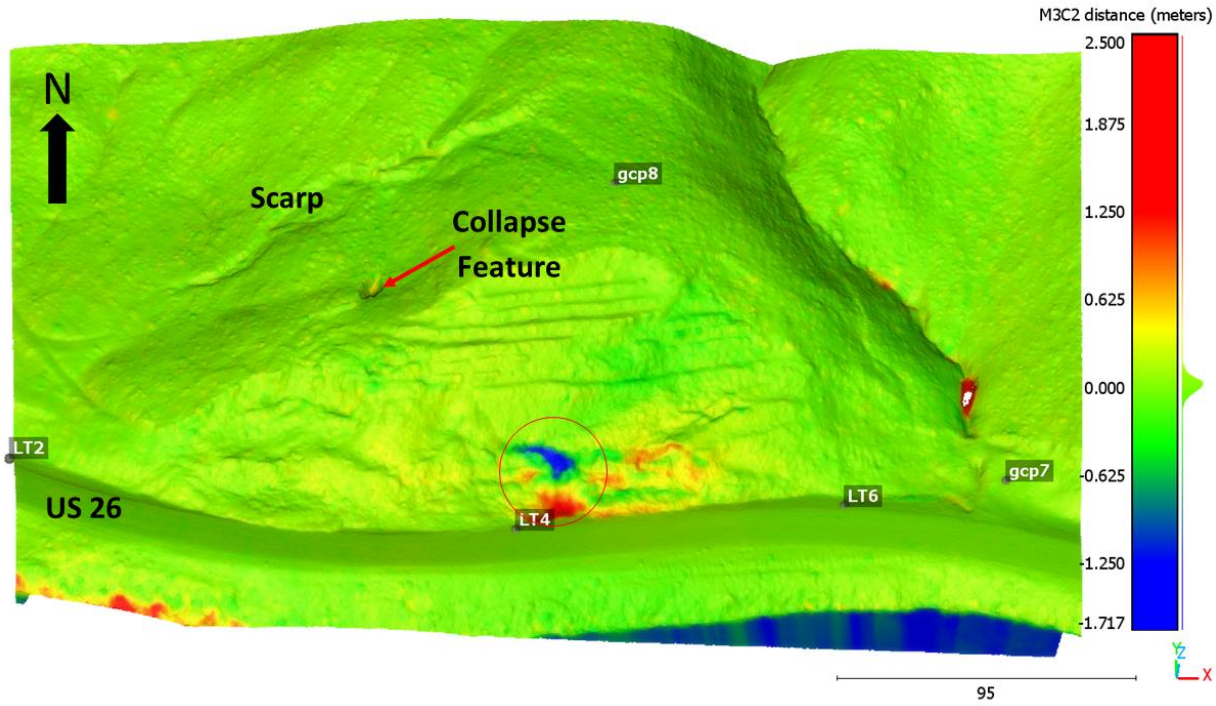

Figure 4.8 Swan Valley East Active Slide Area on US-26. Manned Aircraft LiDAR 2019 versus ISU LiDAR October 2024.

ITD provided ISU researchers with aerial imagery captured on 05 November 1987. These large scale (1:3600) aerial images were scanned, georeferenced, and processed into 3D models using Agisoft Metashape (Figure 4.9). The 1987 dataset was aligned to 2020 and 2024 models for comparative analysis (Figure 4.10, Figure 4.11, and Figure 4.12). The development of the hillside collapse feature on the east end of the Swan Valley East study area between the 1987 and 2024 the LiDAR surveys is shown in Figure 4.13.

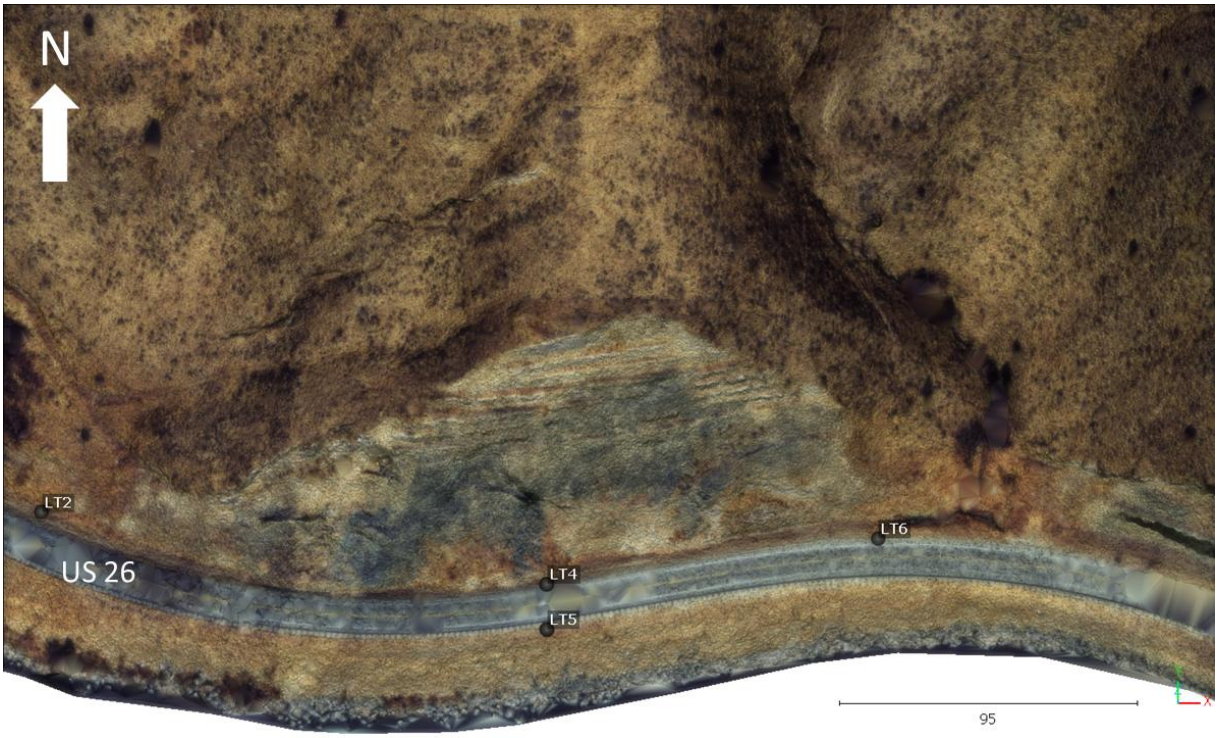

Figure 4.9 1987 Aerial Photograph Model on the East End of the Swan Valley East Study Area

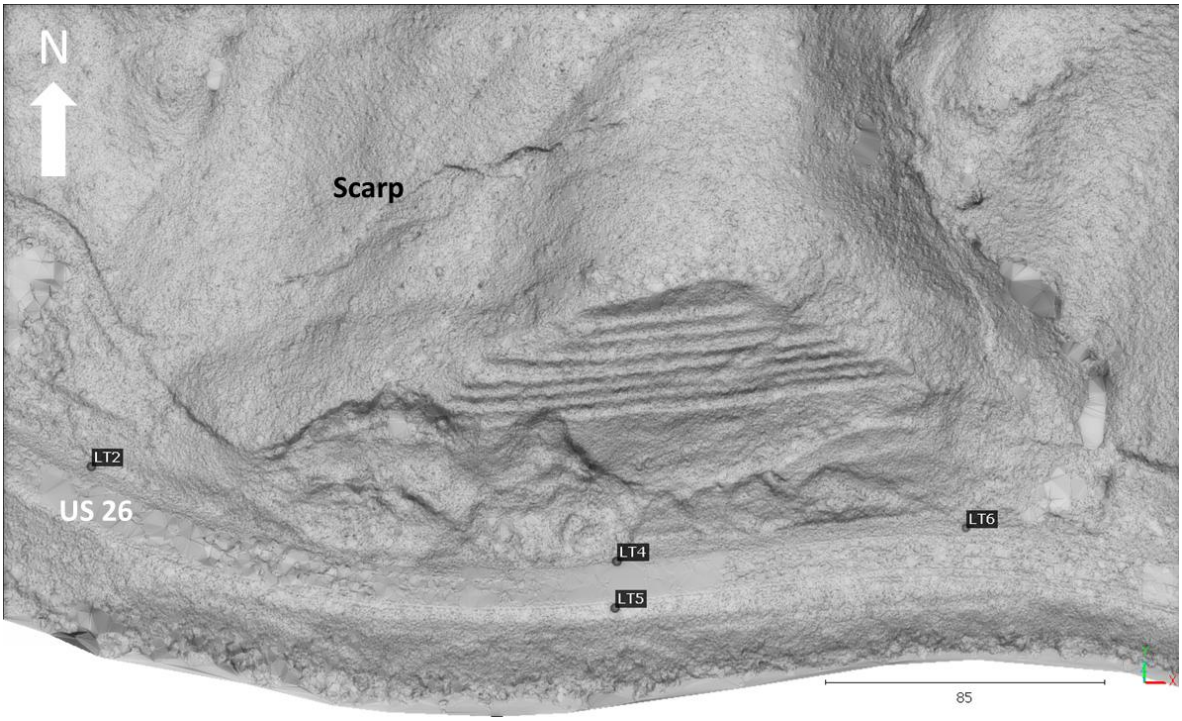

Figure 4.10 1987 Terrain Model – Swan Valley East

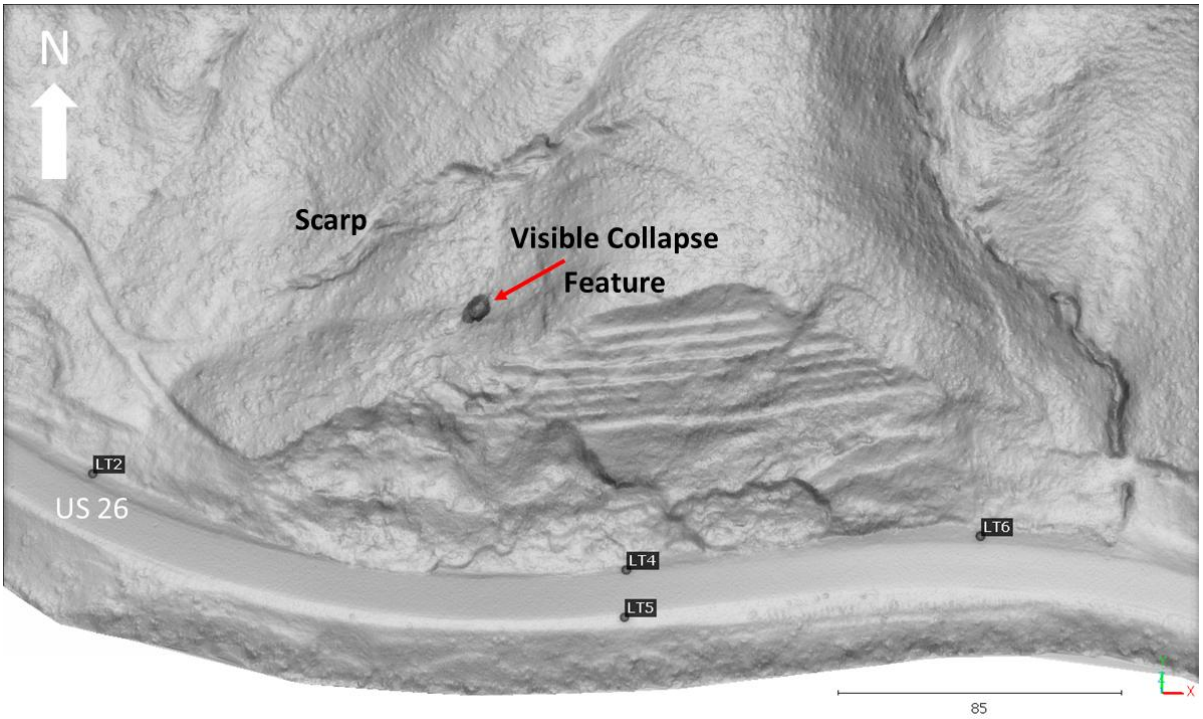

Figure 4.11 2020 Terrain Model-Depression Visible above Swan Valley East Landslide Area

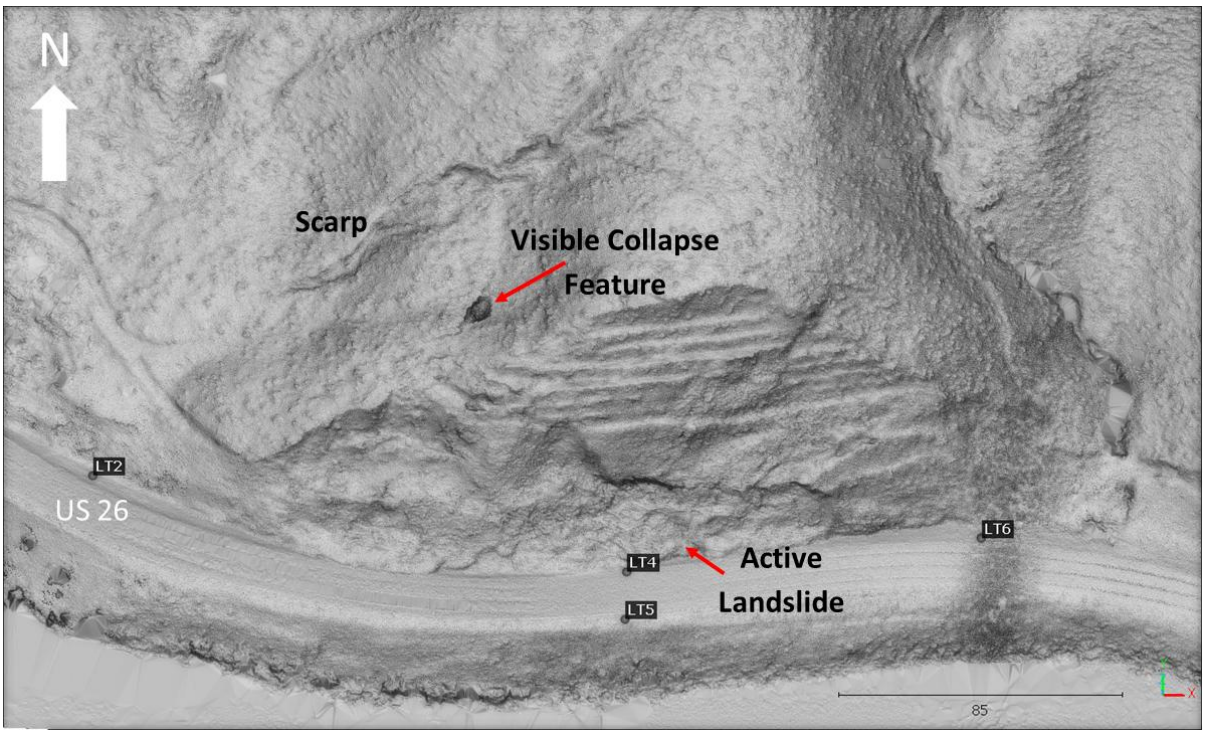

Figure 4.12 2024 ISU LiDAR Survey – Active Landslide

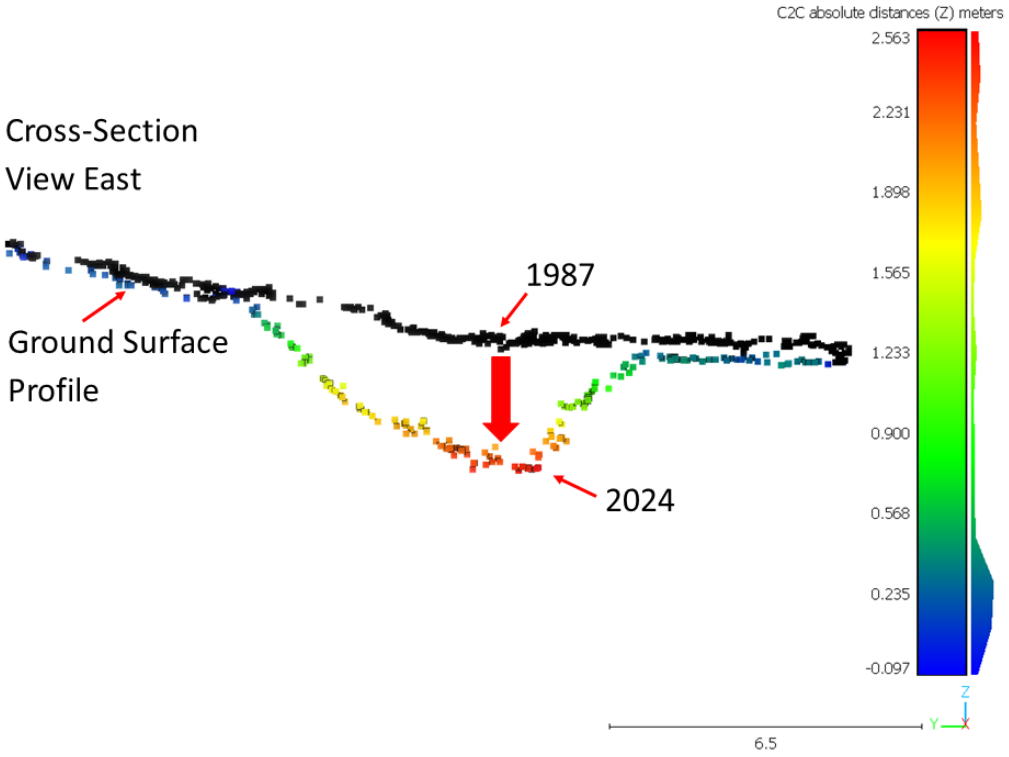

Figure 4.13 Collapse Feature Growth Above Swan Valley East Landslide between 1987 and 2024

SH-33 Bike Path Landslide Area

In the SH-33 Idaho-Wyoming State Line Landslide Complex, the manned 2020 LiDAR survey was compared with the 2024 ISU UAS survey (Figure 4.15 and Figure 4.16). In 2020, the bike path was still under construction, but had been completed at the time of the 2024 ISU survey. Comparison of the two surveys show movement along the bike path: small areas of soil accumulation in red and ground loss in blue (Figure 4.16 to Figure 4.18). The causes of the ground elevation changes can be explained by bike path construction and potential instability caused by excavation along the toe of a previous landslide clearly indicated by the hummocky ground in the slope above the bike path.

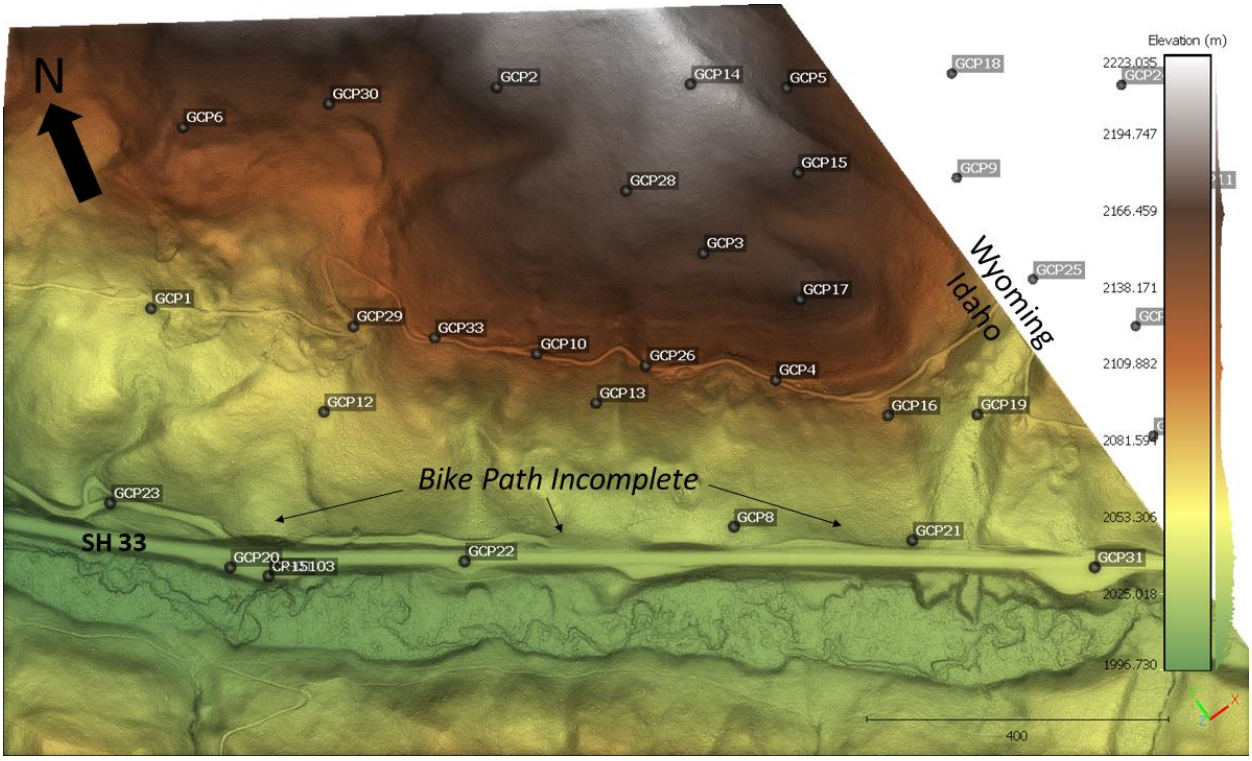

Figure 4.14 SH-33 Bike Path LiDAR 2020 Manned LiDAR Survey

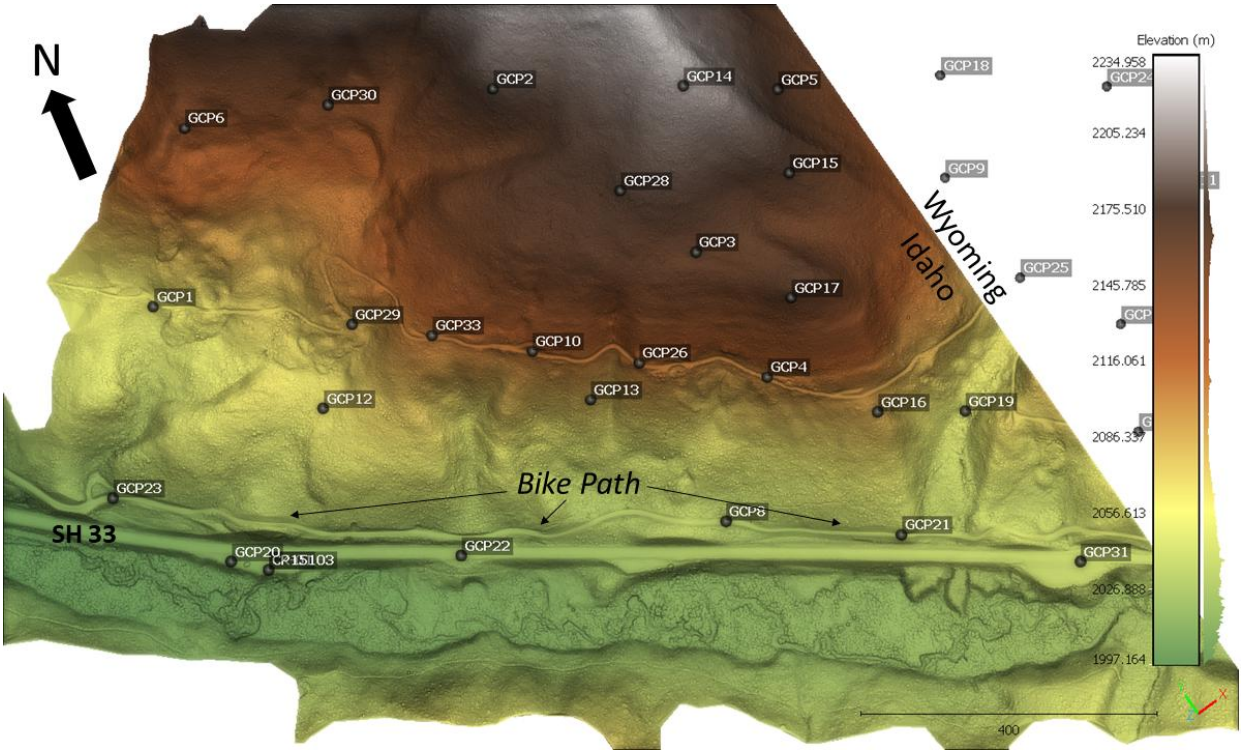

Figure 4.15 SH-33 Bike Path ISU UAS LiDAR 2024

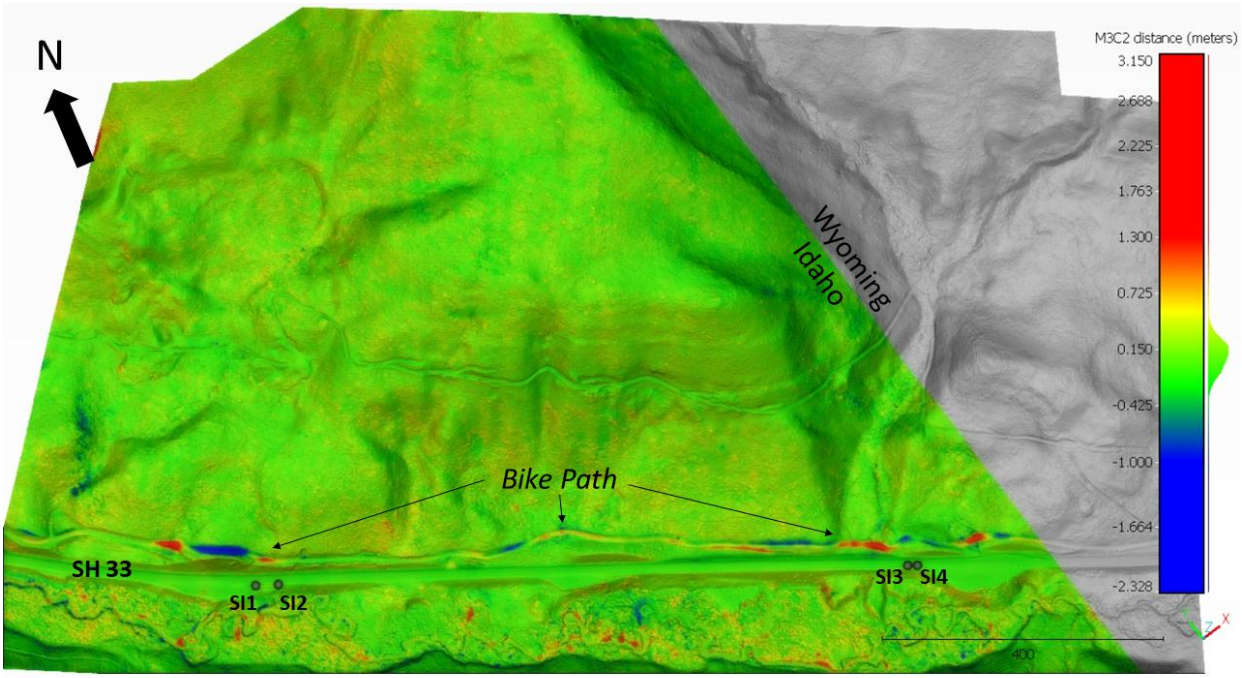

Figure 4.16 SH-33 Bike Path Landslide Area Change Detection – Manned LiDAR 2020 vs. ISU LiDAR 2024

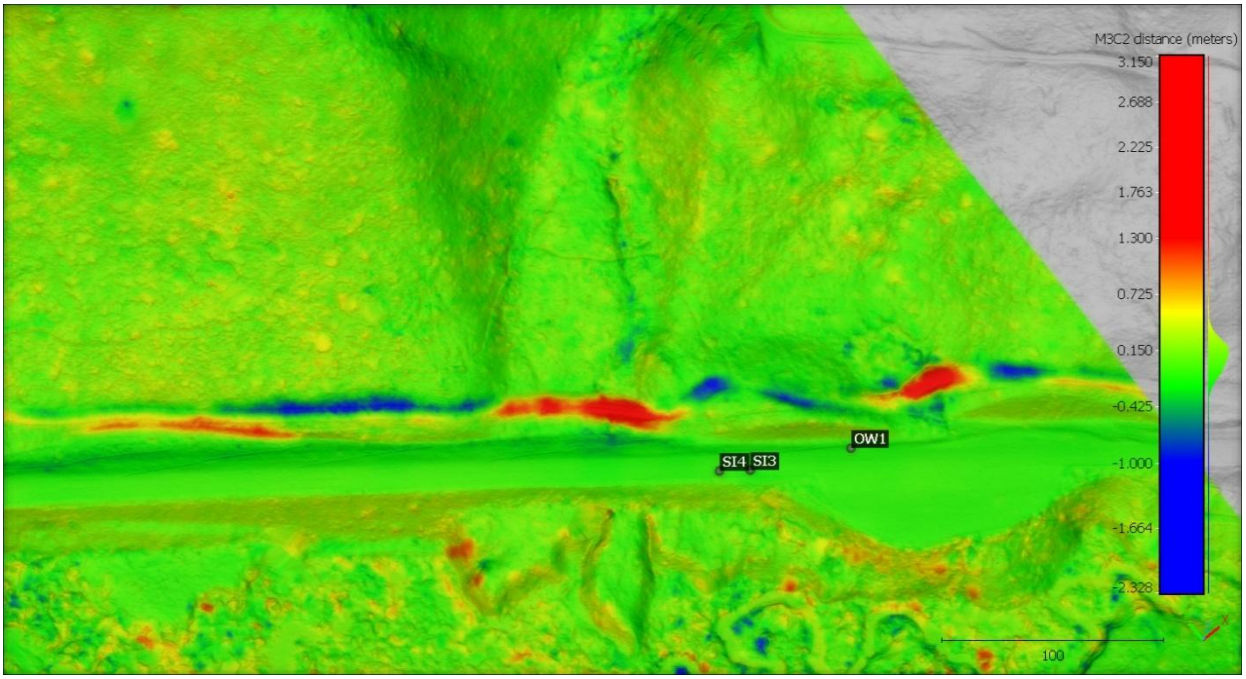

Figure 4.17 State Line Landslide Area Change Detection – 2020 to 2024

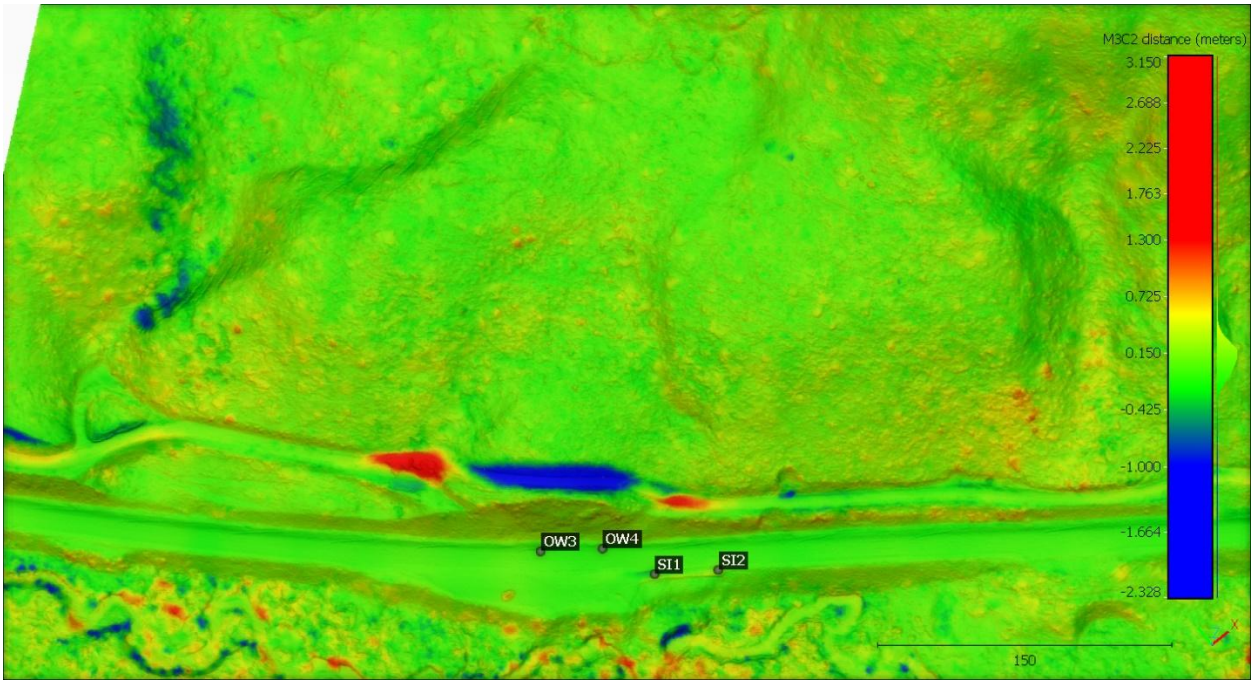

Figure 4.18 Bike Path Landslide Area Change Detection – 2020 to 2024

5. Interpretation and Recommendations of Best Practices

This section provides a summary of best practices and recommendations for remote sensing-based change detection analysis with in-situ measurements.

1. Type of remote sensing data to use for a given set of landslide conditions.

Fixed-Wing (VTOL) UAS Photogrammetry – **Optical Camera**

- Cover: Bare ground, low density shrub and/or forb/grass
- Area: < 3 mi^2
- Terrain: smooth to rugged (optical camera), steep (multi-angle camera)

Fixed-Wing UAS **LiDAR**

- Cover: Lightly treed to heavily forested or dense shrub cover
- Area: < 3 mi^2
- Terrain: smooth to rugged (70° FOV LiDAR), steep (>120° FOV LiDAR)

Multi-copter UAS Photogrammetry – **Optical Camera**

- Cover: Bare ground, low density shrub and/or sparse forb/grass
- Area: < 0.5 mi^2
- Terrain: smooth to rugged (optical camera), steep (multi-angle camera)

Multi-copter UAS **LiDAR**

- Cover: Light treed and heavily forested or dense shrub cover
- Area: < 0.5 mi^2
- Terrain: smooth to rugged (70° FOV LiDAR), steep to overhanging (360° FOV LiDAR)

Manned Aircraft LiDAR Survey

- Cover: Any
- Area: > 40 mi^2
- QL 1 or 2, meets USGS LiDAR Base specifications, LAS 1.4, classified
- Estimated cost per mi^2: $170-$200

2. Timing and frequency for collection of suitable types of remote sensing data.

For LiDAR data acquisition in heavily forested or dense shrub areas, spring or late fall conditions are preferable for optimal “leaf-off” conditions. Misinterpretations are possible at study sites when leaf-off conditions are compared to leaf-on conditions. At sites with sparse cover, timing of flights is less critical as it is easier to obtain bare earth models.

For subsequent monitoring, yearly UAS surveys are recommended in landslide areas along with companion inclinometer measurements and water level readings. More frequent readings would be made in areas of active landslide movement. It is apparent in this study that the LT-4, LT-5 and LT-6 inclinometer measurements in Swan Valley East alone did not provide the needed data on the active landslide which developed between 2023 and 2024. This study also shows that initial aerial surveys with past manned LiDAR surveys at QL levels 0-2 provide reasonable baselines for monitoring slopes with future UAV LiDAR readings. Consideration should be given to obtain UAS baseline and follow-on readings in all of the ITD assets where landslide activity has been observed.

3. Methods for varied ground and vegetative cover.

To distinguish between ground and vegetative cover, several methods are available for classifying point clouds to make this separation. Depending on the character of the land cover we use different software approaches can be used. R software with the LiDR package has toolkits that are well suited to remove low-lying dense vegetative cover. Minor corrections of misclassified vegetation/ground are easily corrected in LAStools. ArcGIS Pro also has automated point cloud classification tools to separate bare earth from vegetation.

4. Approximate accuracy thresholds for monitoring landslide movement with remote sensing tools.

Optimal accuracy thresholds for monitoring landslide movement is 2 cm vertical and 3 cm horizontal, depending on land cover and steepness of terrain.

5. Landslide Concerns in East Swan Valley

A significant area of potential instability in the Swan Valley East study area has been identified in the ISU-ITD LiDAR surveys east of the SH-26/South Fork Bridge. The area contains three progressively higher scarps the farthest of which extends more than 850 ft upslope above the road. The breadth of the potentially unstable area extends between the east and west drainages and is more than 1000 ft laterally along the slope. At this time, the east side of the upper scarp is discontinuous but is intermittent and can easily coalesce with further downslope displacement. Further, the depression in the intermediate scarp serves as a source of groundwater infiltration which increases pore water pressures acting along the surface of sliding. At present there are no dewatering wells in the slope to dissipate the excess pressures. The infiltration is responsible for the mudslide which stopped short of the roadway between the 2023 and 2024 measurement period. The situation not only shows the benefits of UAS LiDAR/photogrammetry surveys but also identifies a potential public safety hazard. Yearly UAS LiDAR and photogrammetry monitoring is recommended.

6. Future ITD Landslide Investigation

In discussions with ITD Shawn Enright, the ITD-ISU team recommends the following sequence of activities in evaluating future landslides along ITD assets:

- obtain geologic/topographic maps of the landslide area

- conduct UAS flights with photogrammetry

- establish ground control and perform LiDAR/photogrammetry surveys including infrared sensors

- map damage and place/monitor control points along roadway surface inside and outside the movement area

- strategically locate and drill exploratory bore holes. Obtain continuous split spoon samples in soil and core where rock is encountered.

- install inclinometers: slot casings to monitor ground water levels. Survey tops of inclinometer casings.

- install multi-anchor horizontal extensometers in the slope using the ODEX drilling system

The estimated cost for performing one complete UAS survey not including analysis is approximately $65-$100 per acre, depending on the access and complexity of the area. For example, densely forested areas require additional and closer together flight passes than areas with less dense vegetative cover.

6. Cited Works

Agisoft. 2024. “Aerial Data Processing (with GCPs) - Orthomosaic & DEM Generation.” Agisoft Helpdesk Portal. 2024.

Agisoft LLC. 2023. “Discover Intelligent Photogrammetry with Metashape.” https://www.agisoft.com/.

Albee, H.F., and H.L. Cullins. 1975. “Geologic Map of the Alpine Quadrangle, Bonneville County, Idaho, and Lincoln County, Wyoming.” *Geologic Quadrangle Map*. US Geological Survey.

Alexander, David. 1992. “On the Causes of Landslides: Human Activities, Perception, and Natural Processes.” *Environmental Geology and Water Sciences* 20 (3): 165–79. https://doi.org/10.1007/BF01706160.

Andresen, Christian G., and Emily S. Schultz-Fellenz. 2023. “Change Detection Applications in the Earth Sciences Using UAS-Based Sensing: A Review and Future Opportunities.” *Drones*. MDPI. https://doi.org/10.3390/drones7040258.

Awasthi, Basant, Shashank Karki, Pratikshya Regmi, Deepak Singh Dhami, Shangharsha Thapa, and Uma Shankar Panday. 2020. “Analyzing the Effect of Distribution Pattern and Number of GCPs on Overall Accuracy of UAV Photogrammetric Results.” In *Proceedings of UASG 2019: Unmanned Aerial System in Geomatics 1*, 339–54. Springer.

BayesMap Solutions LLC. 2020. “BayesStripAlign 2.1.”

Bernard, Thomas G., Dimitri Lague, and Philippe Steer. 2021. “Beyond 2D Landslide Inventories and Their Rollover: Synoptic 3D Inventories and Volume from Repeat Lidar Data.” *Earth Surface Dynamics* 9 (4): 1013–44. https://doi.org/10.5194/esurf-9-1013-2021.

Booth, Adam M., Justin C. McCarley, and Joann Nelson. 2020. “Multi-Year, Three-Dimensional Landslide Surface Deformation from Repeat Lidar and Response to Precipitation: Mill Gulch Earthflow, California.” *Landslides* 17 (6): 1283–96. https://doi.org/10.1007/s10346-020-01364-z.

Booth, Adam M., Justin McCarley, Jason Hinkle, Susan Shaw, Jean Paul Ampuero, and Michael P. Lamb. 2018. “Transient Reactivation of a Deep-Seated Landslide by Undrained Loading Captured With Repeat Airborne and Terrestrial Lidar.” *Geophysical Research Letters* 45 (10): 4841–50. https://doi.org/10.1029/2018GL077812.

Campforts, Benjamin, Charles M. Shobe, Irina Overeem, and Gregory E. Tucker. 2022. “The Art of Landslides: How Stochastic Mass Wasting Shapes Topography and Influences Landscape Dynamics.” *Journal of Geophysical Research: Earth Surface* 127 (8): 1–22. https://doi.org/10.1029/2022JF006745.

Carey, Jordan A., Nicholas Pinter, Alexandra J. Pickering, Carol S. Prentice, and Stephen B. Delong. 2019. “Analysis of Landslide Kinematics Using Multi-Temporal Unmanned Aerial Vehicle Imagery, La Honda, California.” *Environmental and Engineering Geoscience* 25 (4): 301–17. https://doi.org/10.2113/EEG-2228.

Cignoni, P., C. Rocchini, and R. Scopigno. 1998. “Metro: Measuring Error on Simplified Surfaces.” *Computer Graphics Forum* 17 (2): 167–74. https://doi.org/10.1111/1467-8659.00236.

CloudCompare. 2015. “2.5D Volume.” CloudCompareWiki. 2015. https://www.cloudcompare.org/doc/wiki/index.php/2.5D_Volume.

———. 2016. “Align.” CloudCompareWiki. 2016. https://www.cloudcompare.org/doc/wiki/index.php?title=Align.

Cooper, Hannah M., Charles H. Fletcher, Qi Chen, and Matthew M. Barbee. 2013. “Sea-Level Rise Vulnerability Mapping for Adaptation Decisions Using LiDAR DEMs.” *Progress in Physical Geography* 37 (6): 745–66. https://doi.org/10.1177/0309133313496835.

Corsini, Alessandro, Cristina Castagnetti, Eleonora Bertacchini, Riccardo Rivola, Francesco Ronchetti, and Alessandro Capra. 2013. “Integrating Airborne and Multi-Temporal Long-Range Terrestrial Laser Scanning with Total Station Measurements for Mapping and Monitoring a Compound Slow Moving Rock Slide.” *Earth Surface Processes and Landforms* 38 (11): 1330–38. https://doi.org/10.1002/esp.3445.

Cucchiaro, Sara, Eleonora Maset, Marco Cavalli, Stefano Crema, Lorenzo Marchi, Alberto Beinat, and Federico Cazorzi. 2020. “How Does Co-Registration Affect Geomorphic Change Estimates in Multi-Temporal Surveys?” *GIScience and Remote Sensing* 57 (5): 611–32. https://doi.org/10.1080/15481603.2020.1763048.

Daehne, Alexander, and Alessandro Corsini. 2013. “Kinematics of Active Earthflows Revealed by Digital Image Correlation and DEM Subtraction Techniques Applied to Multi-Temporal LiDAR Data.” *Earth Surface Processes and Landforms* 38 (6): 640–54. https://doi.org/10.1002/esp.3351.

Davidson, L., J. P. Mills, I. Haynes, C. Augarde, P. Bryan, and M. Douglas. 2019. “Airborne to Uas Lidar: An Analysis of Uas Lidar Ground Control Targets.” *International Archives of the Photogrammetry, Remote Sensing and Spatial Information Sciences - ISPRS Archives* 42 (2/W13): 255–62. https://doi.org/10.5194/isprs-archives-XLII-2-W13-255-2019.

DiFrancesco, Paul Mark, David Bonneau, and D. Jean Hutchinson. 2020. “The Implications of M3C2 Projection Diameter on 3D Semi-Automated Rockfall Extraction from Sequential Terrestrial Laser Scanning Point Clouds.” *Remote Sensing* 12 (11). https://doi.org/10.3390/rs12111885.

Dossett, T. S., T. H. Reed, S. L. McILrath, D. K. Moore, and G. F. Embree. 2012. “Geologic Map of the South Fork of the Snake River Between Swan Valley and Ririe, Idaho.” *Technical Report* T-12-5.

Egholm, David L., Mads F. Knudsen, and Mike Sandiford. 2013. “Lifespan of Mountain Ranges Scaled by Feedbacks between Landsliding and Erosion by Rivers.” *Nature* 498 (7455): 475–78. https://doi.org/10.1038/nature12218.

Eitel, Jan U.H., Bernhard Höfle, Lee A. Vierling, Antonio Abellán, Gregory P. Asner, Jeffrey S. Deems, Craig L. Glennie, et al. 2016. “Beyond 3-D: The New Spectrum of Lidar Applications for Earth and Ecological Sciences.” *Remote Sensing of Environment* 186: 372–92. https://doi.org/10.1016/j.rse.2016.08.018.

Eker, Remzi, Abdurrahim Aydın, and Johannes Hübl. 2018. “Unmanned Aerial Vehicle (UAV)-Based Monitoring of a Landslide: Gallenzerkogel Landslide (Ybbs-Lower Austria) Case Study.” *Environmental Monitoring and Assessment* 190 (1): 28. https://doi.org/10.1007/s10661-017-6402-8.

Esposito, Giuseppe, Riccardo Salvini, Fabio Matano, Marco Sacchi, Maria Danzi, Renato Somma, and

Claudia Troise. 2017. “Multitemporal Monitoring of a Coastal Landslide through SfM-Derived Point Cloud Comparison.” *Photogrammetric Record* 32 (160): 459–79. https://doi.org/10.1111/phor.12218.

Eyer, J.A. 1969. “Gannett Group of Western Wyoming and Southeastern Idaho.” *Bulletin*. Vol. 53.

Fotsing, Cedrique, Nafissetou Nziengam, and Christophe Bobda. 2020. “Large Common Plansets-4-Points Congruent Sets for Point Cloud Registration.” *ISPRS International Journal of Geo-Information* 9 (11). https://doi.org/10.3390/ijgi9110647.

Frazier, Tim, and Lisa Nichols. 2015. “Enhancing the Resilience of Idaho’s Transportation System to Natural Hazards and Climate Change.” https://rosap.ntl.bts.gov/view/dot/29418.

Froude, Melanie J., and David N. Petley. 2018. “Global Fatal Landslide Occurrence from 2004 to 2016.” *Natural Hazards and Earth System Sciences* 18 (8): 2161–81. https://doi.org/10.5194/nhess-18-2161-2018.

Girardeau-Montaut, D., M. Roux, R Marc, and G Thibault. 2005. “Change Detection on Points Cloud Data Acquired W Ith a Ground.” *International Archives of Photogrammetry Remote Sensing and Spatial Information Sciences* 36 (part 3): 30–35. http://www.danielgm.net/phd/isprs_laserscanning_2005_dgm.pdf.

Gressin, Adrien, Clément Mallet, Jér Ôme Demantké, and Nicolas David. 2013. “Towards 3D Lidar Point Cloud Registration Improvement Using Optimal Neighborhood Knowledge.” *ISPRS Journal of Photogrammetry and Remote Sensing* 79: 240–51. https://doi.org/10.1016/j.isprsjprs.2013.02.019.

H.R.2670 - 118th Congress. 2024. *National Defense Authorization Act (NDAA) for Fiscal Year 2024*. USA: Library of Congress. https://www.congress.gov/bill/118th-congress/house-bill/2670.

Highland, Lynn M., and Peter Bobrowsky. 2008. “The Landslide Handbook — A Guide to Understanding Landslides.” *Reston, Virginia, U.S. Geological Survey Circular 1325*, 129.

Hung, C. L.J., C. W. Tseng, M. J. Huang, C. M. Tseng, and K. J. Chang. 2019. “Multi-Temporal High-Resolution Landslide Monitoring Based on Uas Photogrammetry and Uas Lidar Geoinformation.” In *International Archives of the Photogrammetry, Remote Sensing and Spatial Information Sciences - ISPRS Archives*, 42:157–60. International Society for Photogrammetry and Remote Sensing. https://doi.org/10.5194/isprs-archives-XLII-3-W8-157-2019.

Jaboyedoff, Michel, Thierry Oppikofer, Antonio Abellán, Marc-Henri Derron, Alex Loye, Richard Metzger, and Andrea Pedrazzini. 2012. “Use of LIDAR in Landslide Investigations: A Review.” *Natural Hazards* 61 (1): 5–28. https://doi.org/10.1007/s11069-010-9634-2.

James, M. R., S. Robson, S. d’Oleire-Oltmanns, and U. Niethammer. 2017. “Optimising UAV Topographic Surveys Processed with Structure-from-Motion: Ground Control Quality, Quantity and Bundle Adjustment.” *Geomorphology* 280: 51–66. https://doi.org/10.1016/j.geomorph.2016.11.021.

Kaushal, Sahil, Jiyadh Thanveer, Shah Masud ul Islam, Arun Negi, Aryan Dhanshyan, Yuvika Beetan, Srikrishnan Siva Subramanian, K S Sajinkumar, and Ali P Yunus. 2025. “Unveiling the Amplifying Impact: Anthropogenic Activities and the Two-Fold Surge in Landslides in the Lesser Himalayas.” *CATENA* 250: 108771. https://doi.org/https://doi.org/10.1016/j.catena.2025.108771.

Kjekstad, Oddvar, and Lynn Highland. 2009. “Economic and Social Impacts of Landslides BT - Landslides –

Disaster Risk Reduction." In , edited by Kyoji Sassa and Paolo Canuti, 573–87. Berlin, Heidelberg: Springer Berlin Heidelberg. https://doi.org/10.1007/978-3-540-69970-5_30.

Kuçak, Ramazan Alper, Serdar Erol, and Bihter Erol. 2022. "The Strip Adjustment of Mobile LiDAR Point Clouds Using Iterative Closest Point (ICP) Algorithm." *Arabian Journal of Geosciences* 15 (11). https://doi.org/10.1007/s12517-022-10303-2.

Lague, Dimitri, Nicolas Brodu, and Jérôme Leroux. 2013. "Accurate 3D Comparison of Complex Topography with Terrestrial Laser Scanner: Application to the Rangitikei Canyon (N-Z)." *ISPRS Journal of Photogrammetry and Remote Sensing* 82: 10–26. https://doi.org/10.1016/j.isprsjprs.2013.04.009.

Long, S.P., and P.K. Link. 2007. "Geologic Map Compilation of the Malad City 30 x 60 Minute Quadrangle, Idaho." *Technical Report* T-07-1.

Merzbach, H. 2024. "Teton Pass Landslide May Be a Preview of What's to Come in Other Mountain Towns." *Wyoming Public Media*, June 2024. https://www.wyomingpublicmedia.org/natural-resources-energy/2024-06-25/teton-pass-landslide-may-be-a-preview-of-whats-to-come-in-other-mountain-towns.

Miao, Fasheng, Yiping Wu, Linwei Li, Kang Liao, and Longfei Zhang. 2019. "Risk Assessment of Snowmelt-Induced Landslides Based on GIS and an Effective Snowmelt Model." *Natural Hazards* 97 (3): 1151–73. https://doi.org/10.1007/s11069-019-03693-2.

Mirus, Benjamin B., Eric S. Jones, Rex L. Baum, Jonathan W. Godt, Stephen Slaughter, Matthew M. Crawford, Jeremy Lancaster, et al. 2020. "Landslides across the USA: Occurrence, Susceptibility, and Data Limitations." *Landslides* 17 (10): 2271–85. https://doi.org/10.1007/s10346-020-01424-4.

Mitchell, V.E., and E.H. Bennett. 1979. "Geologic Map of the Driggs Quadrangle, Idaho." *Geologic Map*. Idaho Geological Survey.

Mora, Omar E, M. Gabriela Lenzano, Charles K Toth, Dorota A. Grejner-Brzezinska, and Jessica V. Fayne. 2018. "Landslide Change Detection Based on Multi-Temporal Airborne LIDAR-Derived DEMs." *Geosciences (Switzerland)* 8 (1): 6–8. https://doi.org/10.3390/geosciences8010023.

Okyay, Unal, Jennifer Telling, Craig L. Glennie, and William E. Dietrich. 2019. "Airborne Lidar Change Detection: An Overview of Earth Sciences Applications." *Earth-Science Reviews* 198 (June). https://doi.org/10.1016/j.earscirev.2019.102929.

Oniga, Valeria Ersilia, Ana Ioana Breaban, Norbert Pfeifer, and Constantin Chirila. 2020. "Determining the Suitable Number of Ground Control Points for UAS Images Georeferencing by Varying Number and Spatial Distribution." *Remote Sensing* 12 (5). https://doi.org/10.3390/rs12050876.

Oriel, S.S., and L.B. Platt. 1980. "Geologic Map of the Preston 1 Degree x 2 Degrees Quadrangle, Southeastern Idaho and Western Wyoming." *Miscellaneous Investigations Series Map*. Vol. I–1127.

Pampeyan, E.H., M.L. Schroeder, E.M. Schell, and E.R. Cressman. 1967. "Geologic Map of the Driggs Quadrangle, Bonneville and Teton Counties, Idaho, and Teton County, Wyoming." *Mineral Investigations Field Studies Map*. Vol. MF-300.

Pankow, Kristine L., Jeffrey R. Moore, J. Mark Hale, Keith D. Koper, Tex Kubacki, Katherine M. Whidden, and Michael K. McCarter. 2014. "Massive Landslide at Utah Copper Mine Generates Wealth of

Geophysical Data." *GSA Today* 24 (1): 4–9. https://doi.org/10.1130/GSATG191A.1.

Quantum Systems. 2021. "Qbase 3D Mission Planning and Monitoring Software." 2021. https://quantum-systems.com/qbase-3d/.

———. 2023. "Oblique D2M Five Lens RGB Camera." 2023. https://quantum-systems.com/blog/2023/05/02/oblique-d2m-2/.

———. 2024. "Trinity Pro - Next-Generation EVTOL Fixed-Wing Mapping Drone." Quantum Systems. 2024. https://quantum-systems.com/trinity-pro/?utm_term=fixed wing drone vtol&utm_campaign=Global_Generic&utm_source=adwords&utm_medium=ppc&hsa_acc=5070149546&hsa_cam=21401070175&hsa_grp=160696950650&hsa_ad=707797936210&hsa_src=g&hsa_tgt=kwd-662095092700&hsa_kw.

Rangel, José Manuel Galván, Gil Rito Gonçalves, and Juan Antonio Pérez. 2018. "The Impact of Number and Spatial Distribution of GCPs on the Positional Accuracy of Geospatial Products Derived from Low-Cost UASs." *International Journal of Remote Sensing* 39 (21): 7154–71. https://doi.org/10.1080/01431161.2018.1515508.

Rapidlasso GmbH. 2023. "LAStools." https://rapidlasso.de/.

Rengers, Francis K., Luke A. McGuire, Nina S. Oakley, Jason W. Kean, Dennis M. Staley, and Hui Tang. 2020. "Landslides after Wildfire: Initiation, Magnitude, and Mobility." *Landslides* 17 (11): 2631–41. https://doi.org/10.1007/s10346-020-01506-3.

Resop, J, L Lehmann, and W. Cully Hession. 2019. "Drone Laser Scanning for Modeling Riverscape Topography and Vegetation: Comparison with Traditional Aerial Lidar." *Drones* 3 (2): 1–15. https://doi.org/10.3390/drones3020035.

Sarkar, S, and D P Kanungo. 2004. "An Integrated Approach for Landslide Susceptibility Mapping Using Remote Sensing and GIS." *Photogrammetric Engineering and Remote Sensing*. https://doi.org/10.14358/PERS.70.5.617.

Schaffrath, Keelin R., Patrick Belmont, and Joseph M. Wheaton. 2015. "Landscape-Scale Geomorphic Change Detection: Quantifying Spatially Variable Uncertainty and Circumventing Legacy Data Issues." *Geomorphology* 250: 334–48. https://doi.org/10.1016/j.geomorph.2015.09.020.

Schleicher, David. 1975. "A Model for Earthquakes near Palisades Reservoir, Southeast Idaho." *Journal of Research of the U.S. Geological Survey* 3 (4): 393–400. https://pubs.usgs.gov/publication/70042868.

Schuster, Robert L, and Lynn M Highland. 2001. "Socioeconomic and Environmental Impacts of Landslides in the Western Hemisphere." *Open-File Report*. https://doi.org/10.3133/ofr01276.

Schuster, Robert L, and Gerald F Wieczorek. 2018. "Landslide Triggers and Types." In *Landslides*, 59–78. Routledge.

Sidle, Roy C., and Thom A. Bogaard. 2016. "Dynamic Earth System and Ecological Controls of Rainfall-Initiated Landslides." *Earth-Science Reviews* 159: 275–91. https://doi.org/10.1016/j.earscirev.2016.05.013.

Stumvoll, M J, M Konzett, E M Schmaltz, and T Glade. 2022. "Application of UAS to Detect Infrequent

and Local Large-Scale Surficial Displacements: Critical Examples from the Fields of Landslide and Erosion Research BT - SUAS Applications in Geography." In , edited by Kory Konsoer, Michael Leitner, and Quinn Lewis, 203–33. Cham: Springer International Publishing. https://doi.org/10.1007/978-3-031-01976-0_8.

Sun, Jianwei, Guoqin Yuan, Laiyun Song, and Hongwen Zhang. 2024. "Unmanned Aerial Vehicles (UAVs) in Landslide Investigation and Monitoring: A Review." *Drones* 8 (1). https://doi.org/10.3390/drones8010030.

Swanson, F. J., and C. T. Dyrness. 1975. "Impact of Clear-Cutting and Road Construction on Soil Erosion by Landslides in the Western Cascade Range, Oregon." *Geology* 3 (7): 393–96. https://doi.org/10.1130/0091-7613(1975)3<393:IOCARC>2.0.CO;2.

Syzdykbayev, Meirman, Bobak Karimi, and Hassan A. Karimi. 2020. "Persistent Homology on LiDAR Data to Detect Landslides." *Remote Sensing of Environment* 246 (May): 111816. https://doi.org/10.1016/j.rse.2020.111816.

Tanyaş, Hakan, Tolga Görüm, Dalia Kirschbaum, and Luigi Lombardo. 2022. "Could Road Constructions Be More Hazardous than an Earthquake in Terms of Mass Movement?" *Natural Hazards* 112 (1): 639–63. https://doi.org/10.1007/s11069-021-05199-2.

Tetra Tech. 2023. "State of Idaho 2023 Hazard Mitigation Plan." Boise, Idaho. https://ioem.idaho.gov/wp-content/uploads/2023/11/2023-SHMP-State-Mitigation-Final-11_15_23.pdf.

Wachal, David J, and Paul F Hudak. 2000. "Mapping Landslide Susceptibility in Travis County, Texas, USA." *GeoJournal* 51 (3): 245–53. https://doi.org/10.1023/A:1017524604463.

Wheaton, Joseph M. 2008. "Uncertainity in Morphological Sediment Budgeting of Rivers." University of Southampton.

Yellowscan. 2021. "Quantum-Systems Introduces Geomatics Grade, High-Speed Scanning LiDAR – Powered by YellowScan." 2021. https://www.yellowscan.com/press-news/quantum-systems-introduces-geomatics-grade-high-speed-scanning-lidar-powered-by-yellowscan/.

Youd, T. Leslie. 1985. "Landslides Caused by Earthquakes: Discussion." *Bulletin of the Geological Society of America* 96 (8): 1091–92. https://doi.org/10.1130/0016-7606(1985)96<1091:LCBEDA>2.0.CO;2.

Yu, Xianyu, Kaixiang Zhang, Yingxu Song, Weiwei Jiang, and Jianguo Zhou. 2021. "Study on Landslide Susceptibility Mapping Based on Rock–Soil Characteristic Factors." *Scientific Reports* 11 (1): 1–27. https://doi.org/10.1038/s41598-021-94936-5.

Zielke, Olaf. 2024. "Lidar for Geohazard and Natural Resource Characterization BT - Remote Sensing for Characterization of Geohazards and Natural Resources." In , edited by Estelle Chaussard, Cathleen Jones, Jingyi Ann Chen, and Andrea Donnellan, 75–87. Cham: Springer International Publishing. https://doi.org/10.1007/978-3-031-59306-2_4.

Zimmerman, Taylor, Karine Jansen, and Jon Miller. 2020. "Analysis of UAS Flight Altitude and Ground Control Point Parameters on DEM Accuracy along a Complex, Developed Coastline." *Remote Sensing* 12 (14). https://doi.org/10.3390/rs12142305.

Appendix A. Inclinometer Plots with Bore Log Data

Swan Valley Inclinometer Plots

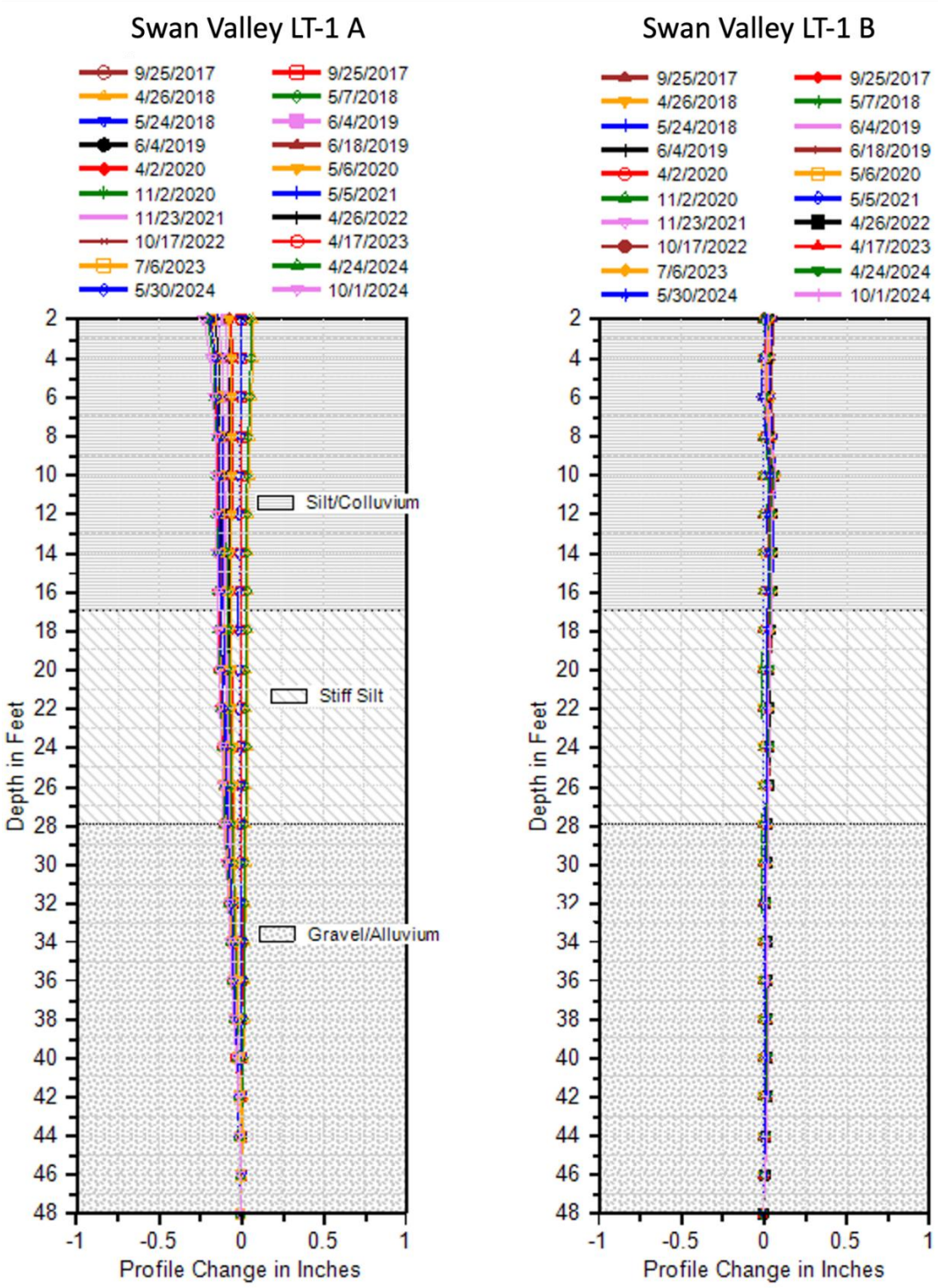

Figure A.1 Swan Valley LT-1 profile change and bore log data

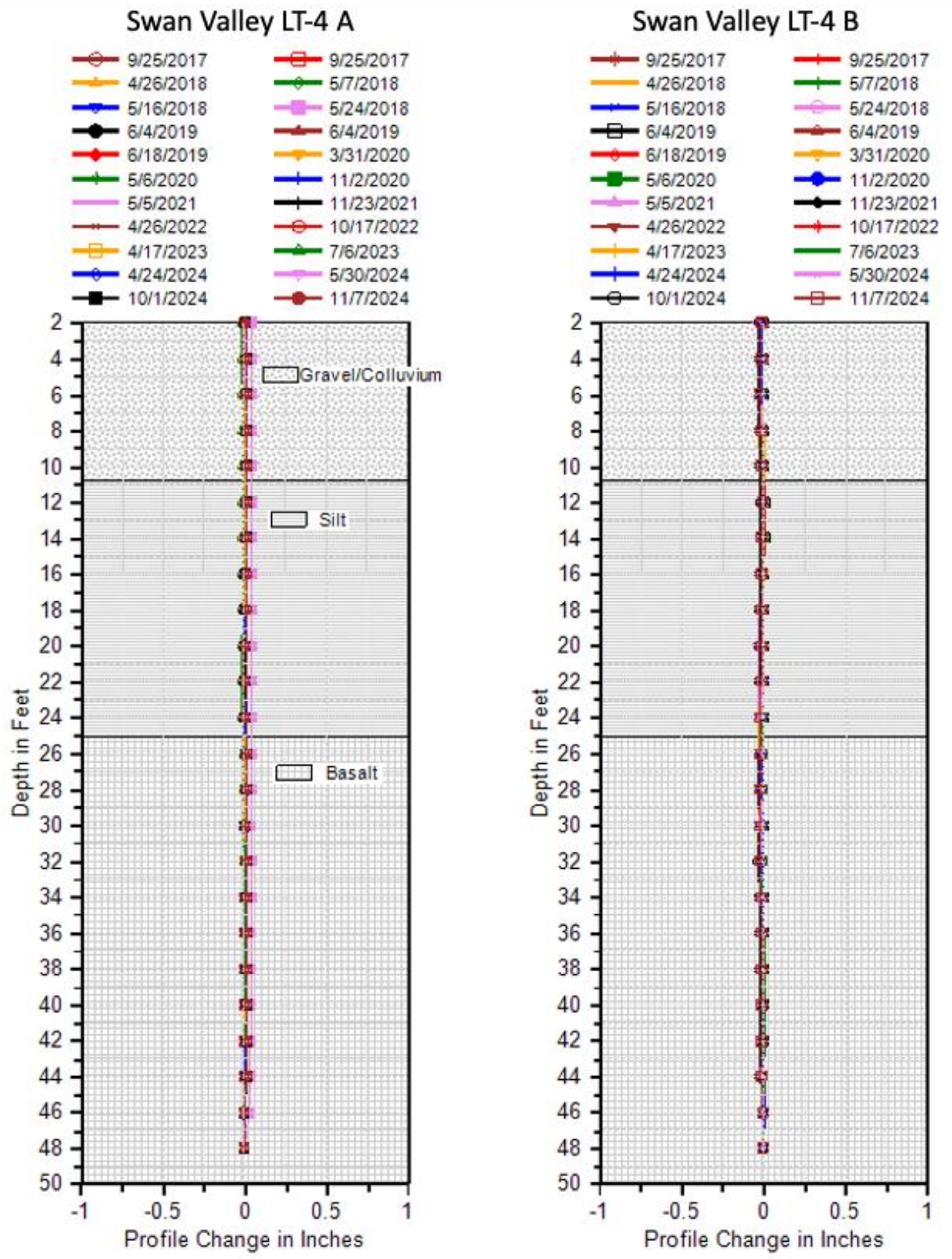

Figure A.2 Swan Valley LT-2 profile change and bore log data

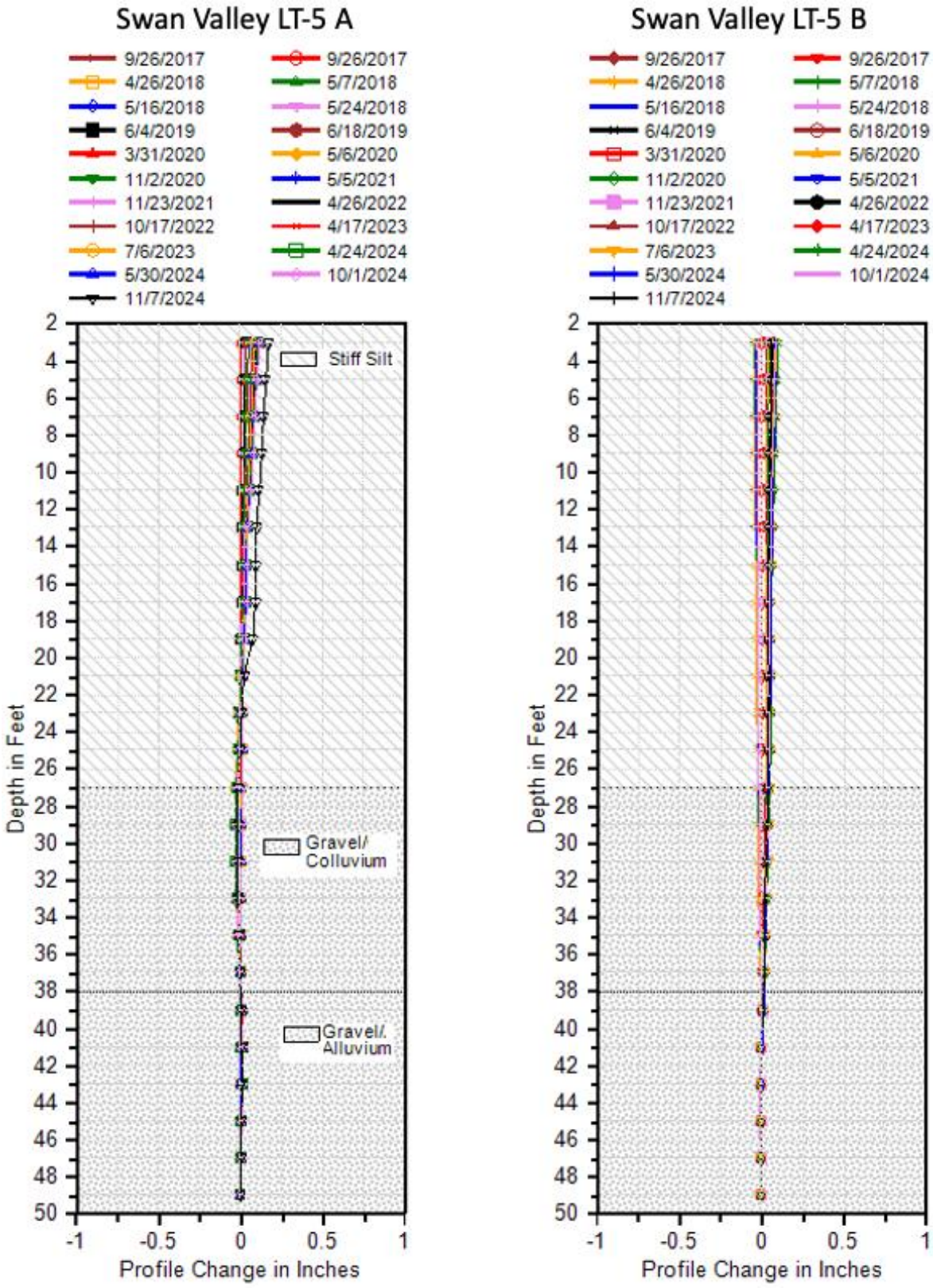

Figure A.3 Swan Valley LT-5 profile change and bore log data

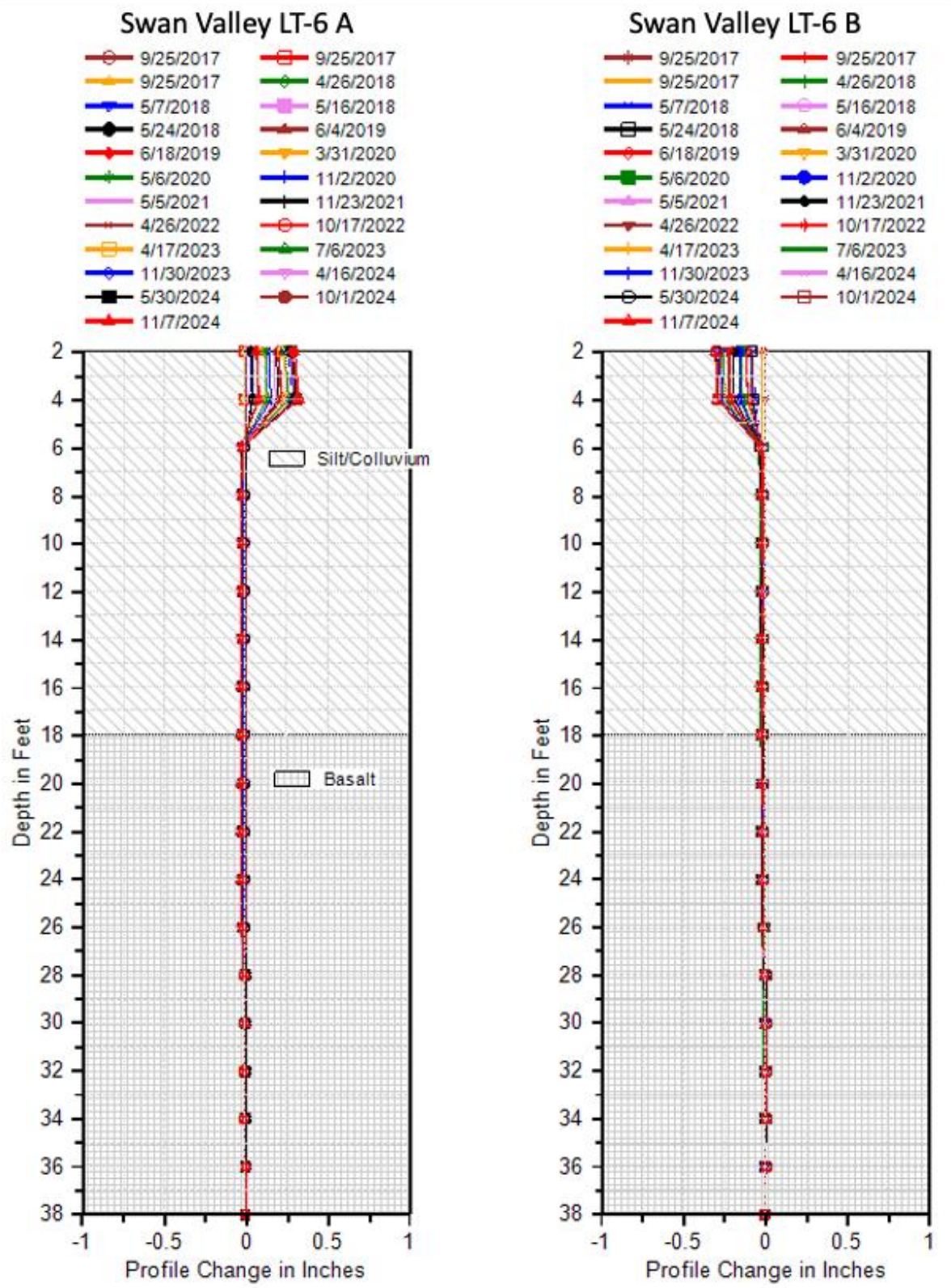

Figure A.4 Swan Valley LT-6 profile change and bore log data

Rainey Creek Inclinometer Plots

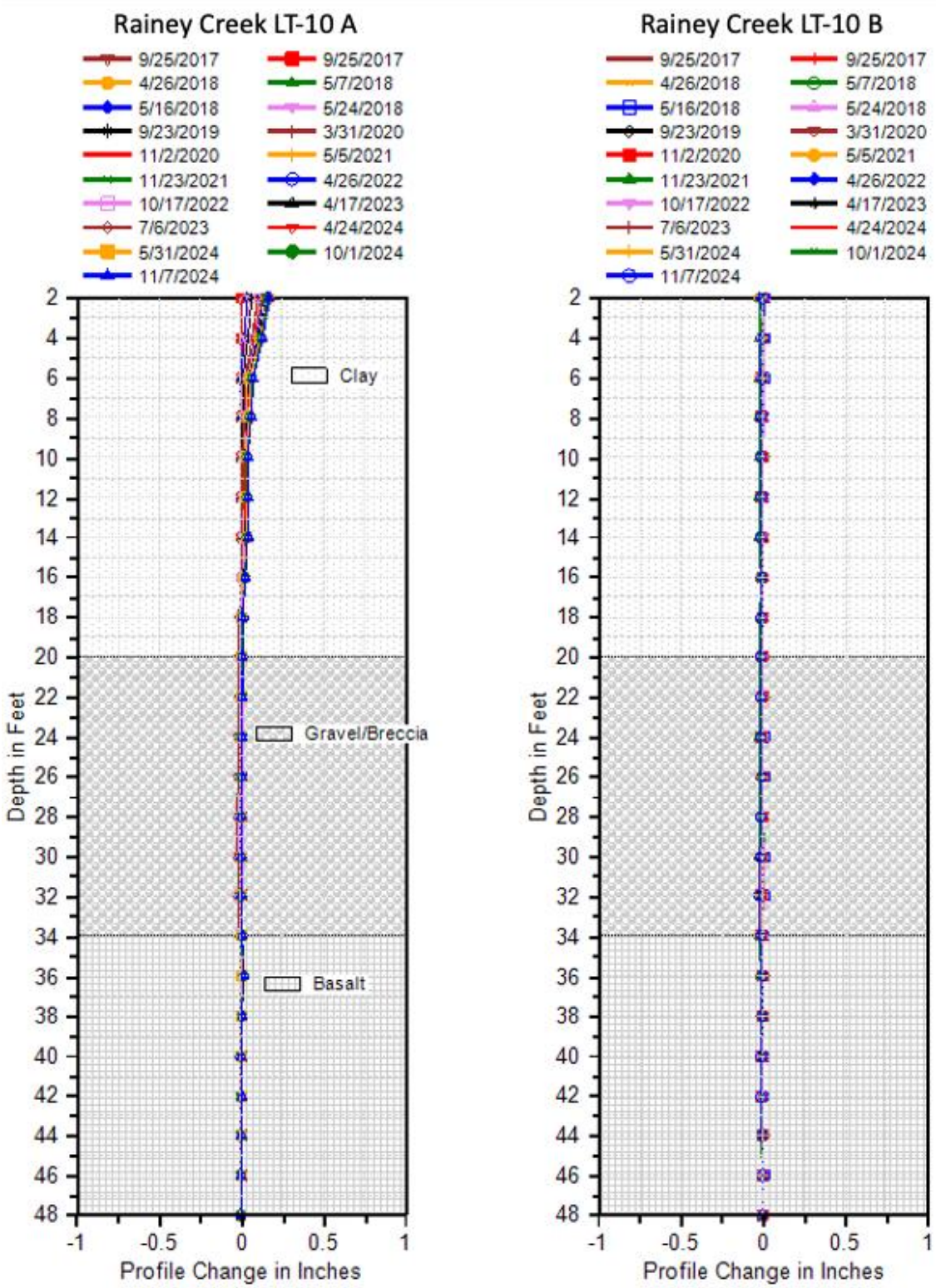

Figure A.5 Rainey Creek LT-10 profile change and bore log data

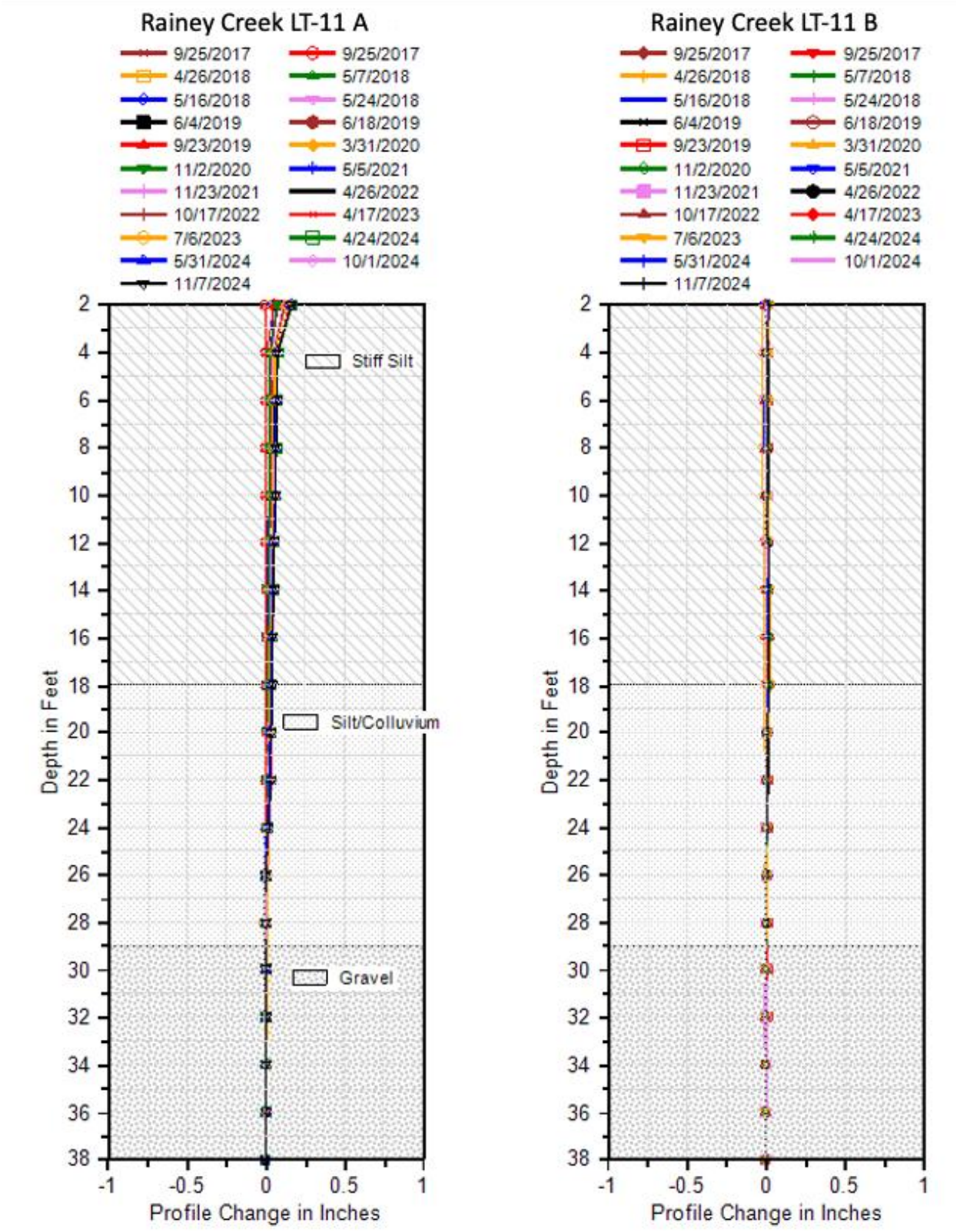

Figure A.6 Rainey Creek LT-11 profile change and bore log data

Gibson Inclinometer Plots

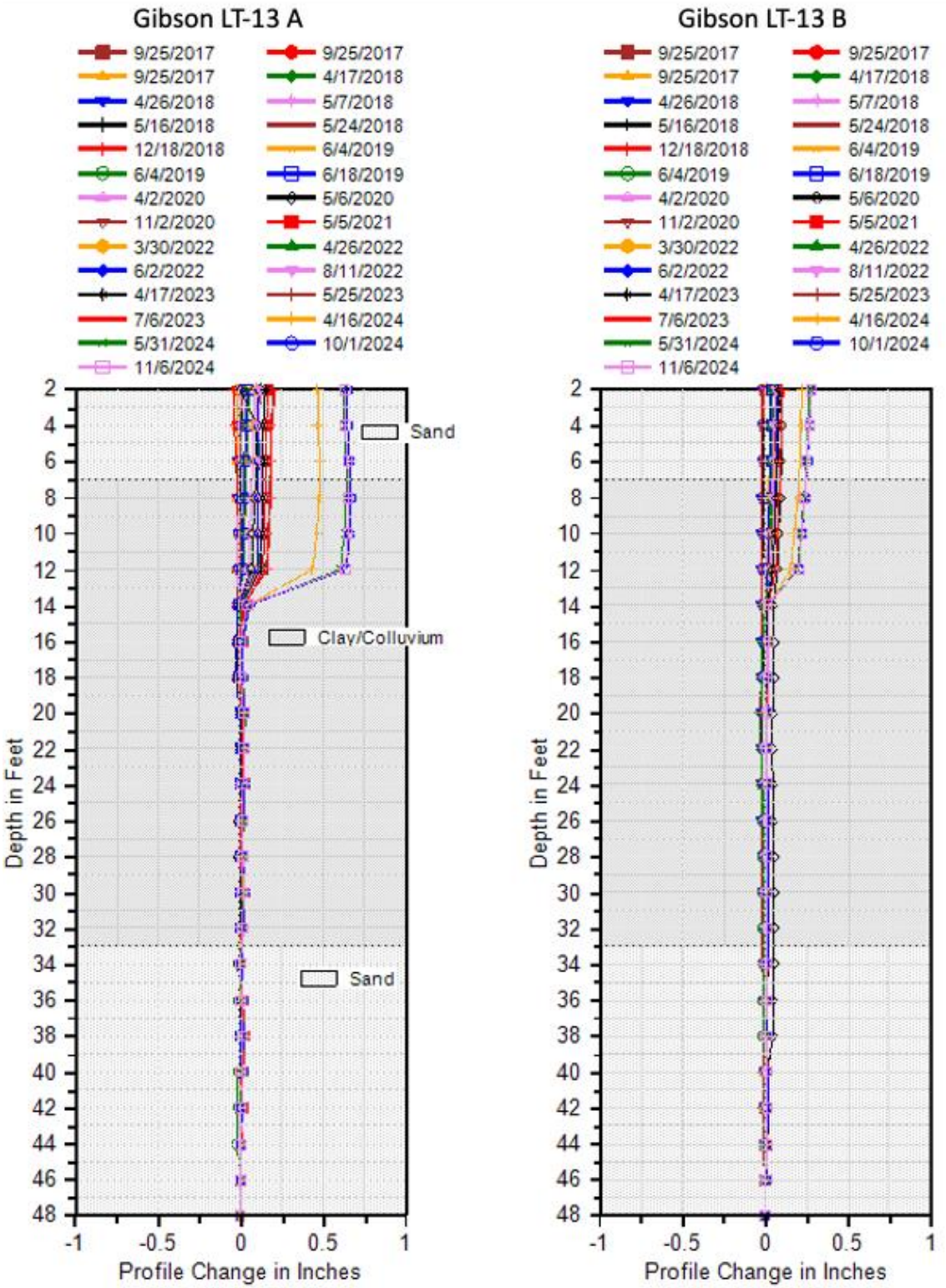

Figure A.7 Gibson LT-13 profile change and bore log data

Indian Creek Inclinometer Plots

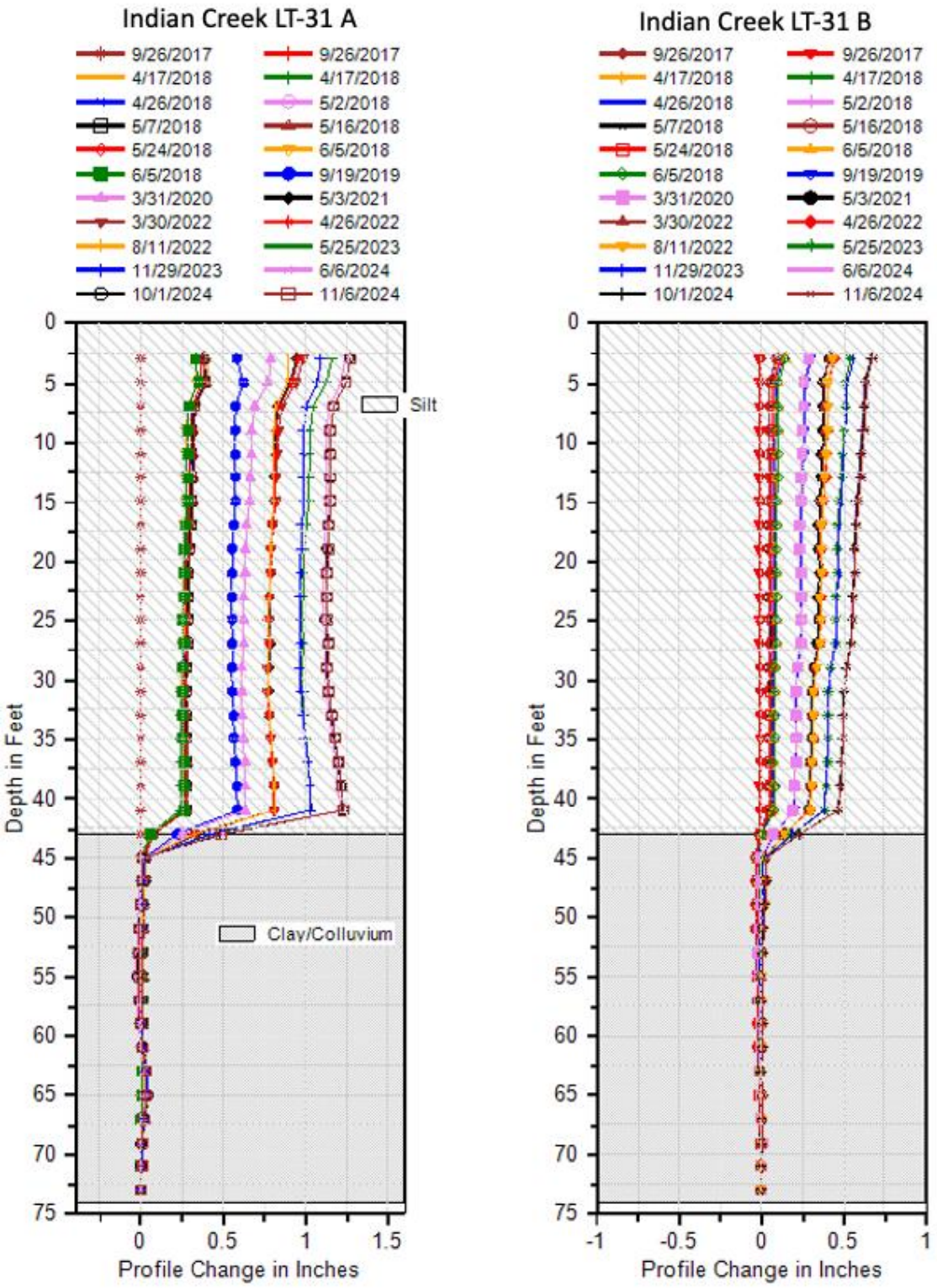

Figure A.8 Indian Creek LT-31 profile change and bore log data

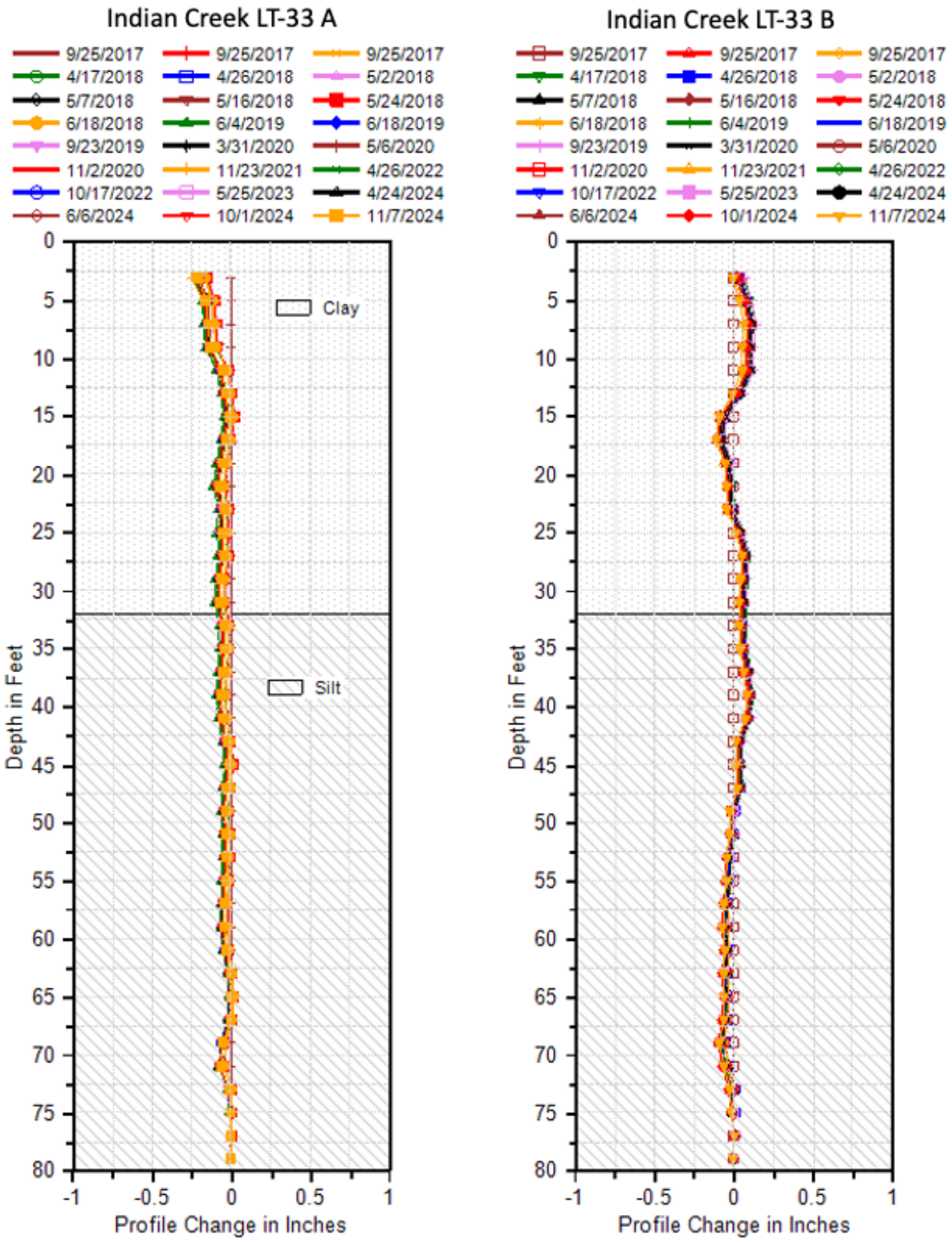

Figure A.9 Indian Creek LT-33 profile change and bore log data

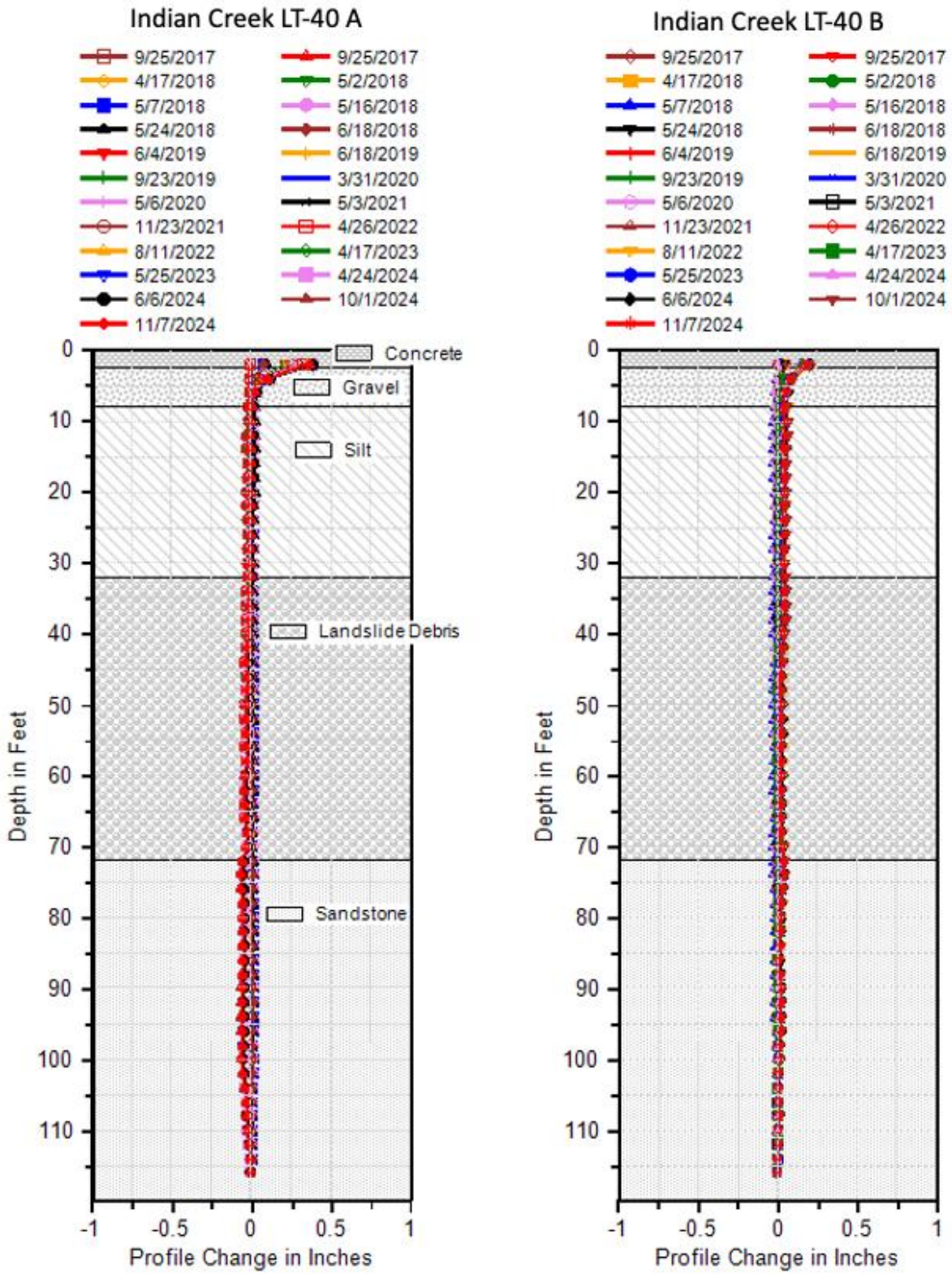

Figure A.10 Indian Creek LT-40 profile change and bore log data

Pine Bar Inclinometer Plots

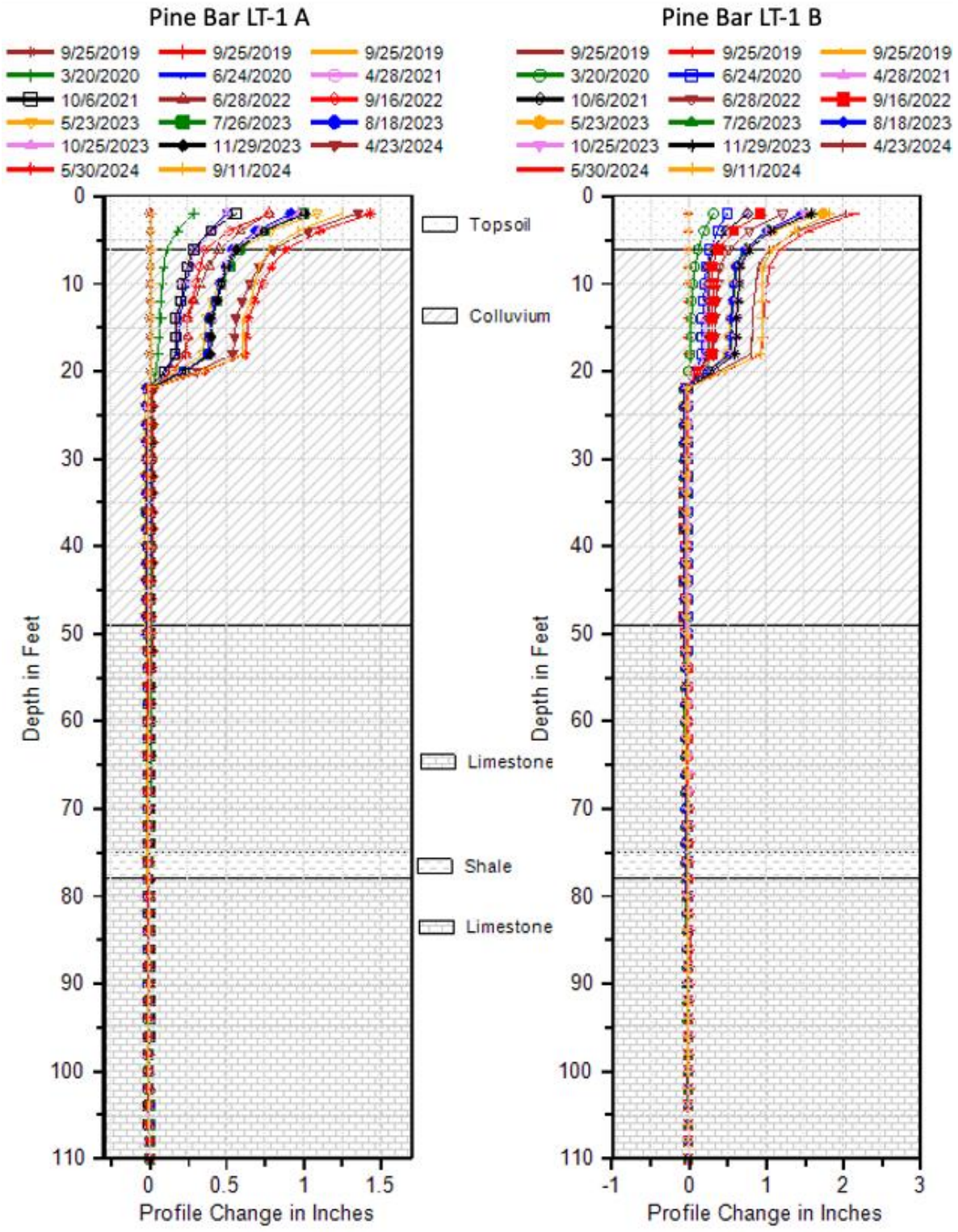

Figure A.11 Pine Bar LT-1 profile change and bore log data

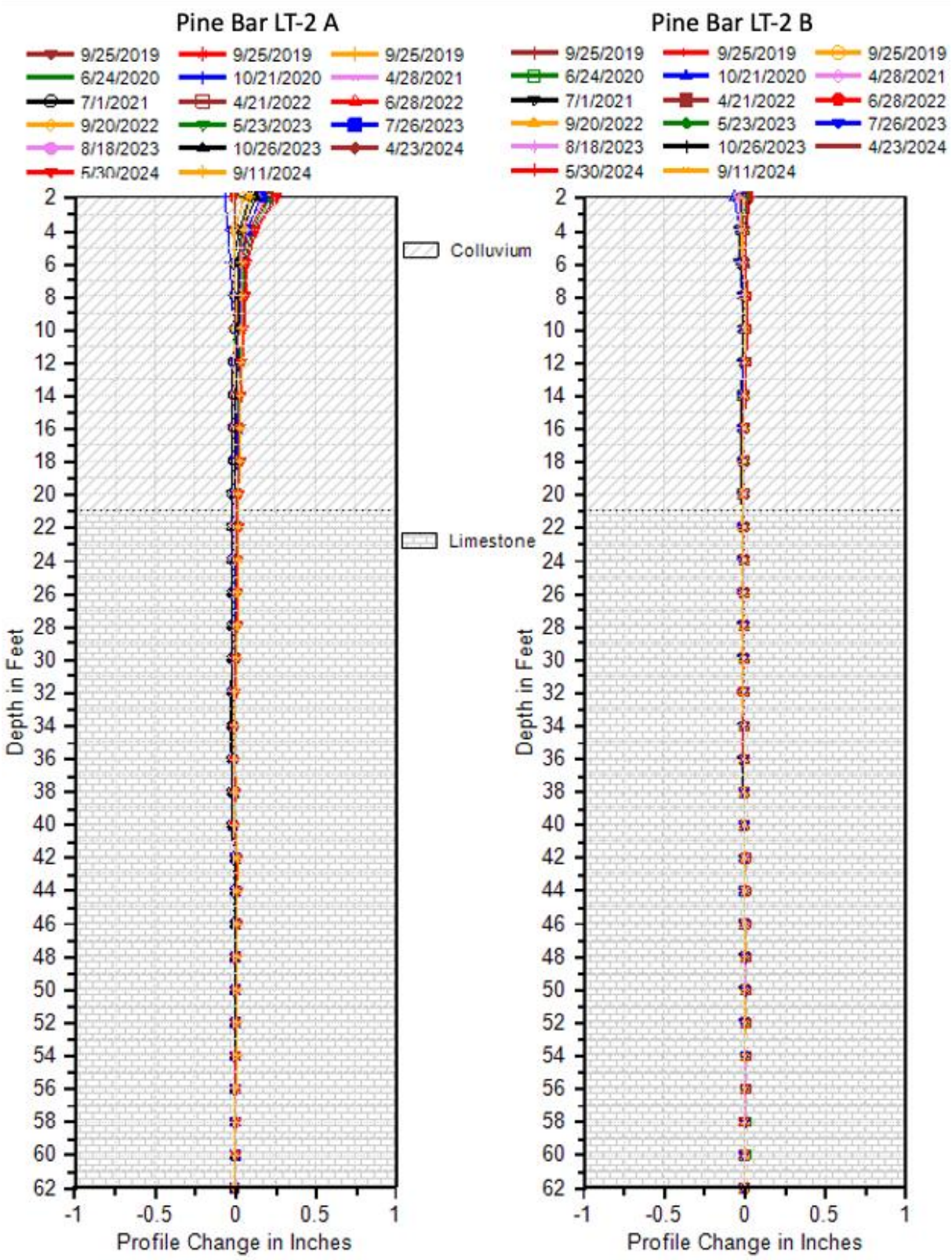

Figure A.12 Pine Bar LT-2 profile change and bore log data

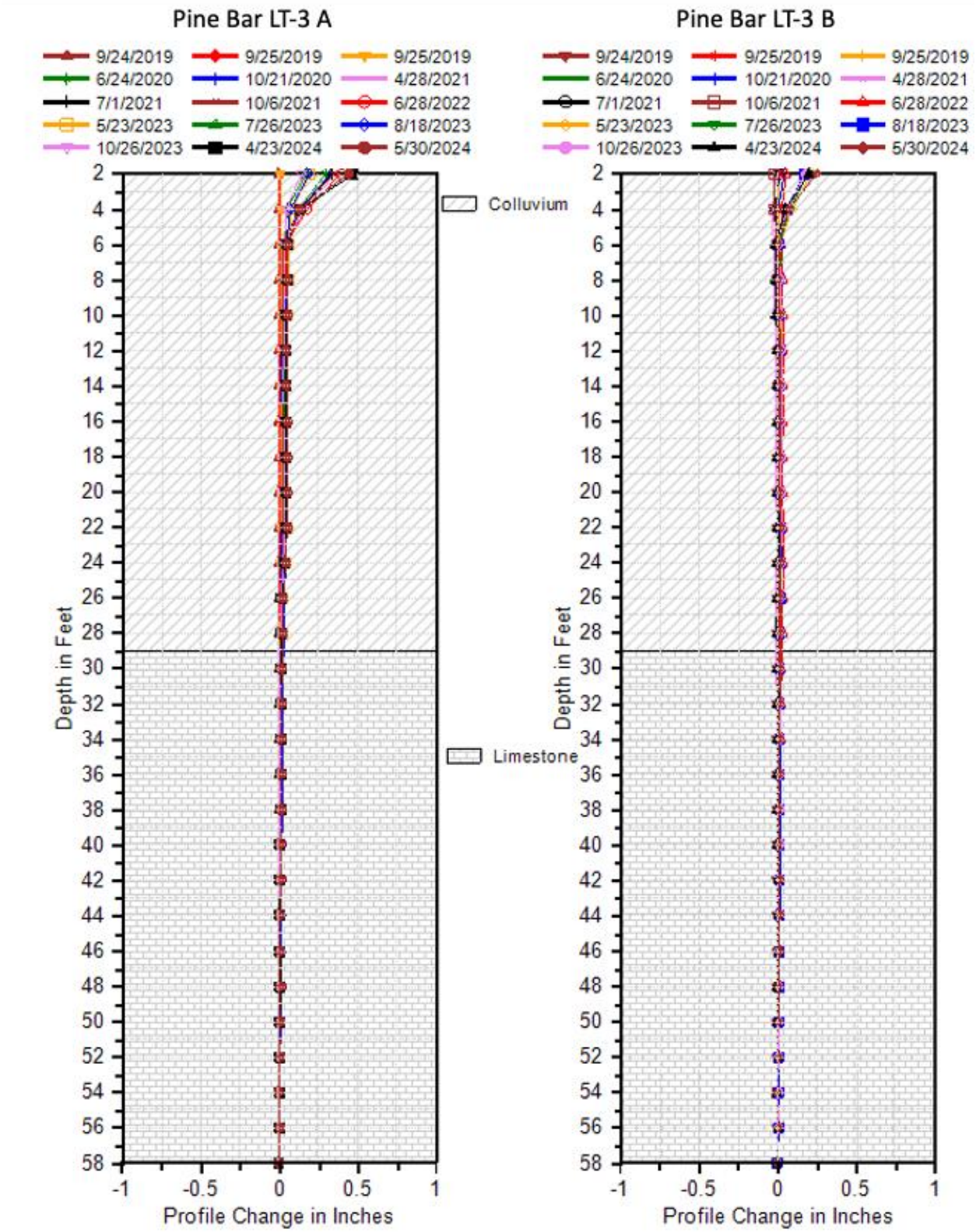

Figure A.13 Pine Bar LT-3 profile change and bore log data

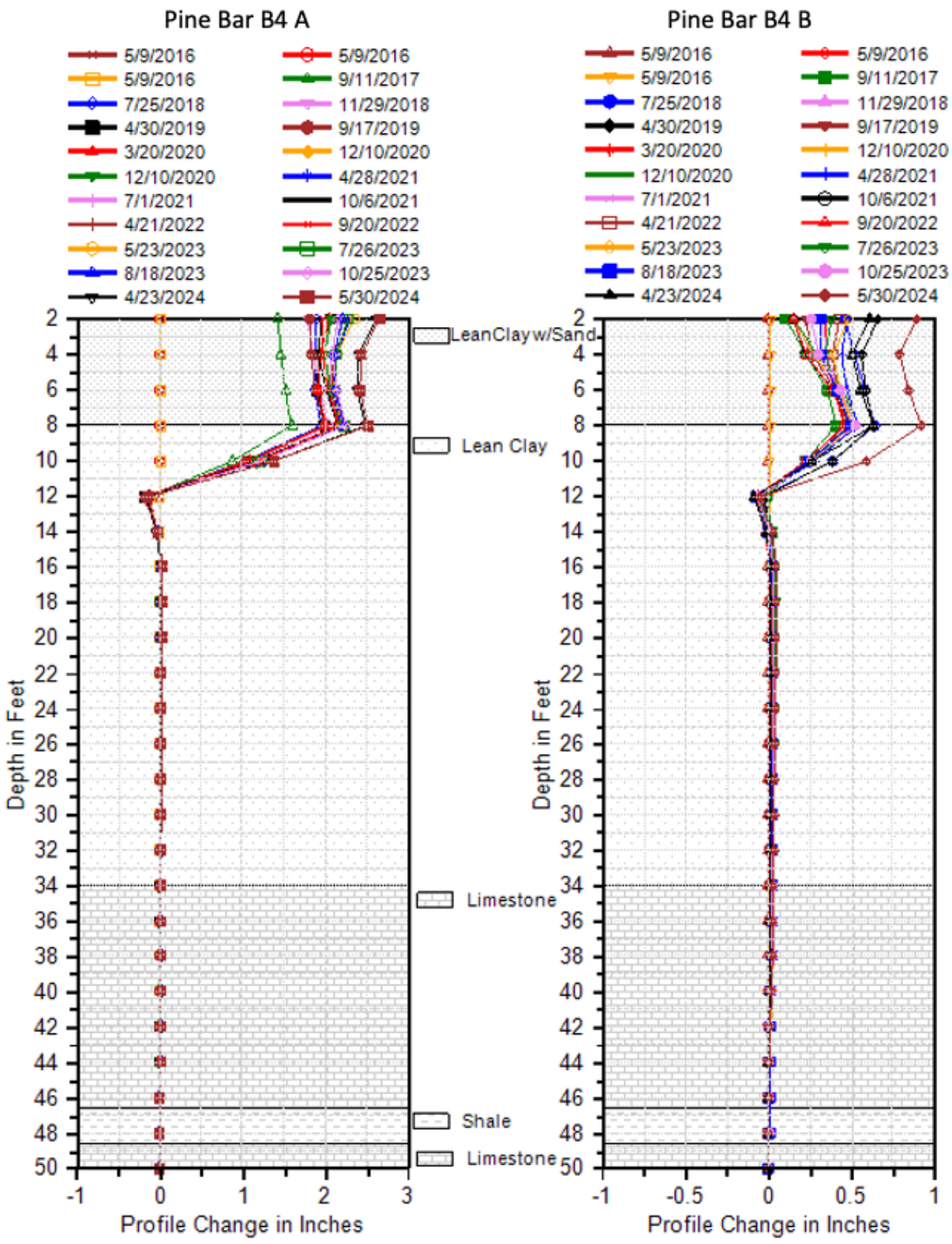

Figure A.14 Pine Bar B4 profile change and bore log data

Bud Peck Inclinometer Plots

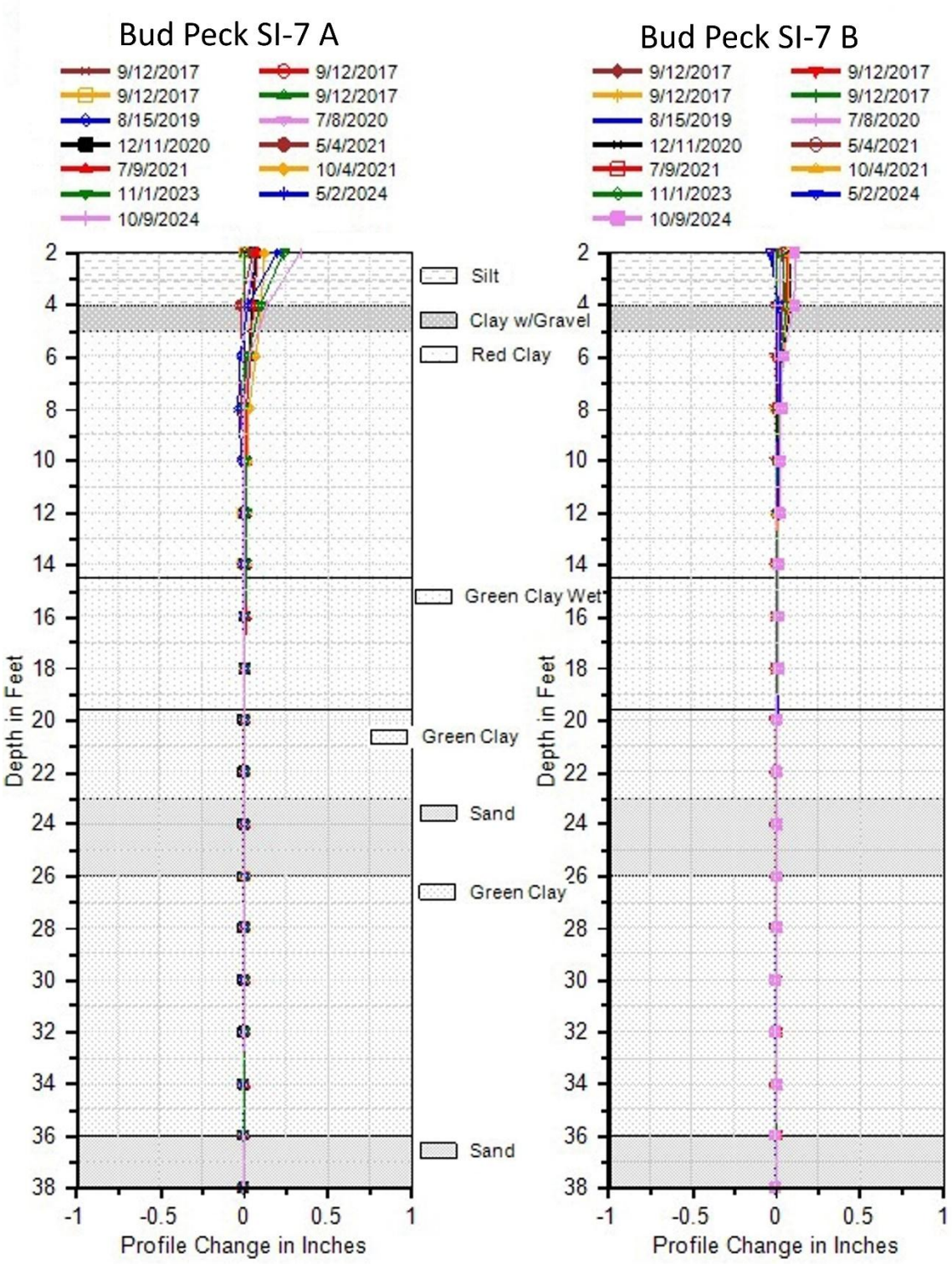

Figure A.15 Bud Peck SI-7 profile change and bore log data

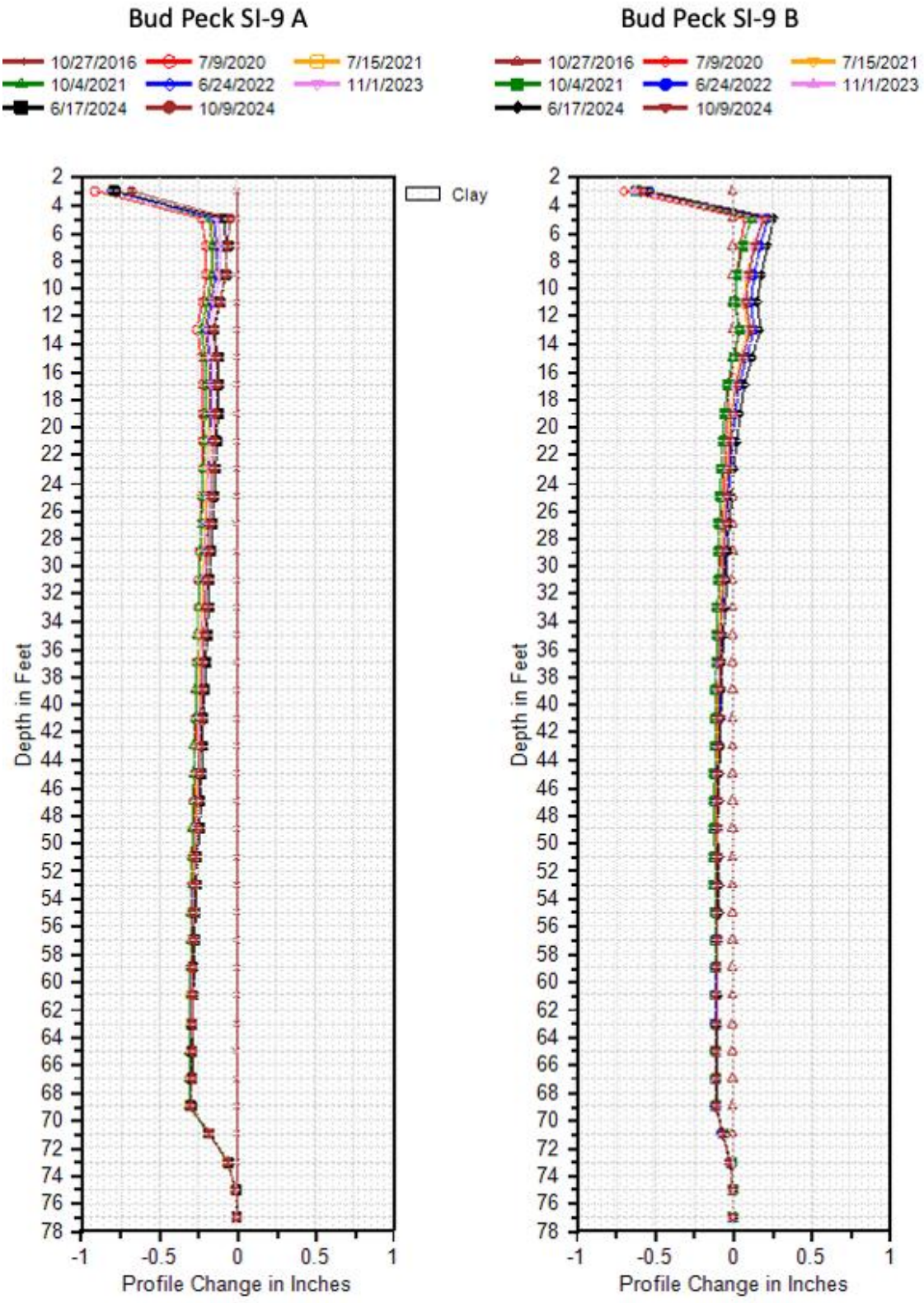

Figure A.16 Bud Peck SI-9 profile change and bore log data

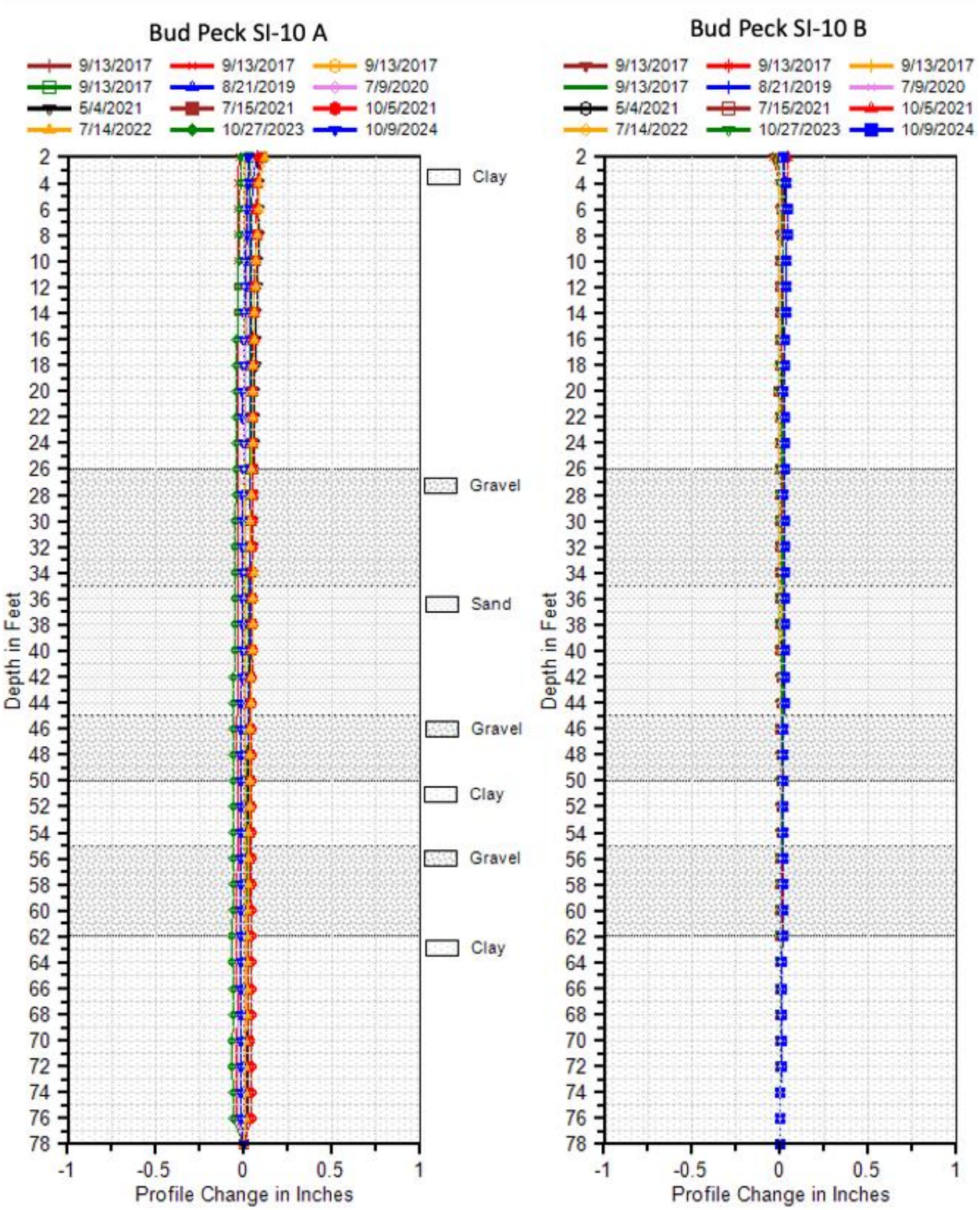

Figure A.17 Bud Peck SI-10 profile change and bore log data

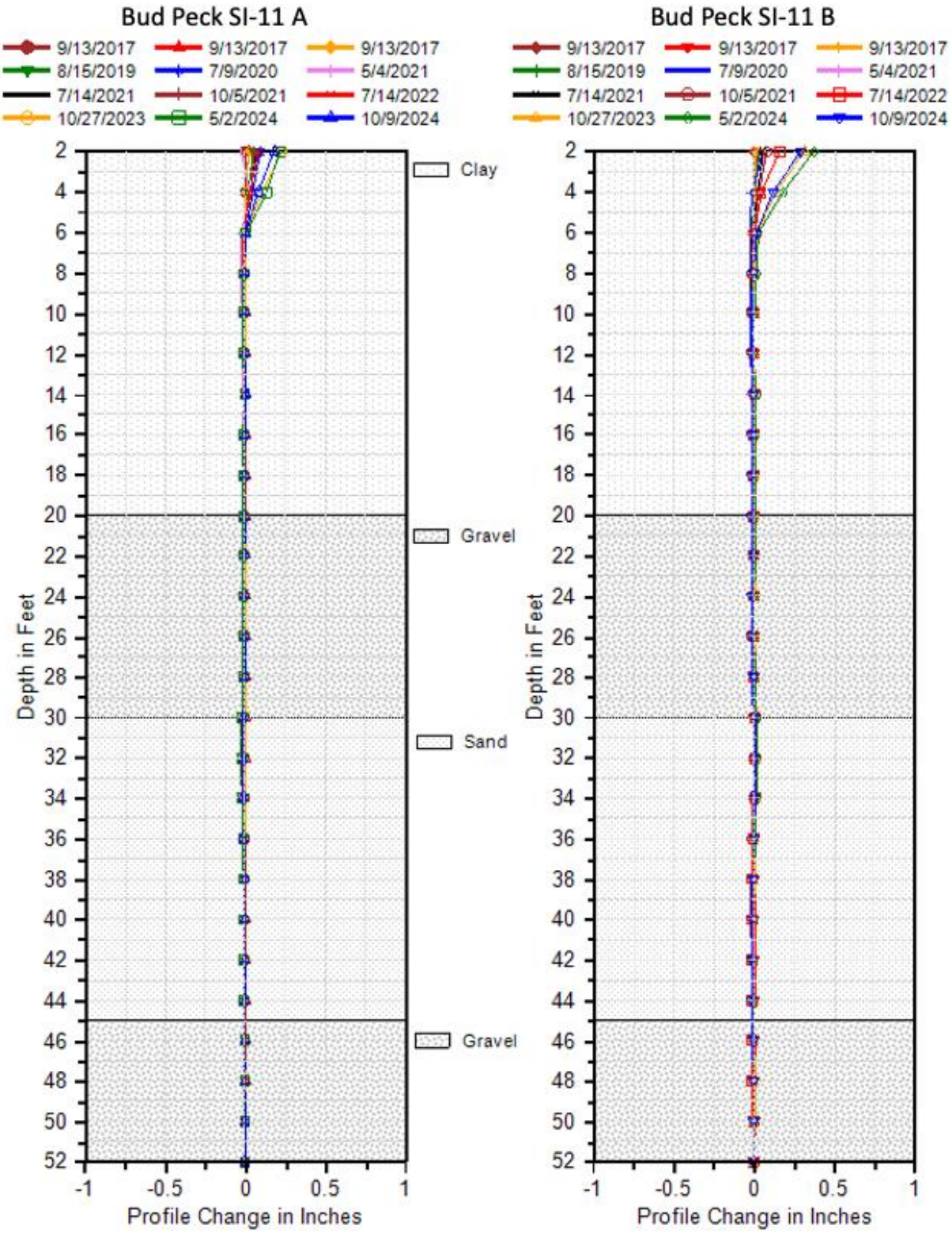

Figure A.18 Bud Peck SI-11 profile change and bore log data

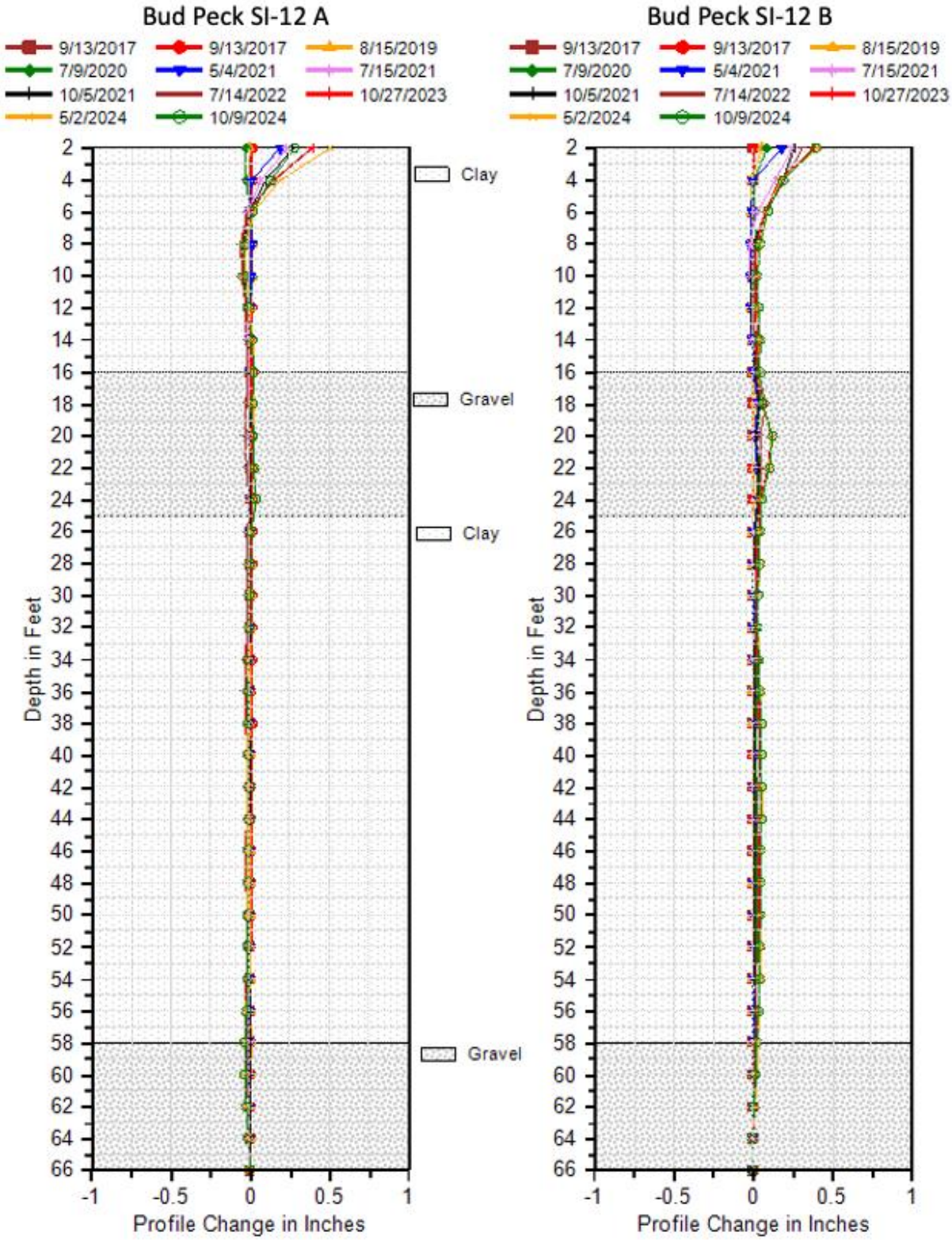

Figure A.19 Bud Peck SI-12 profile change and bore log data

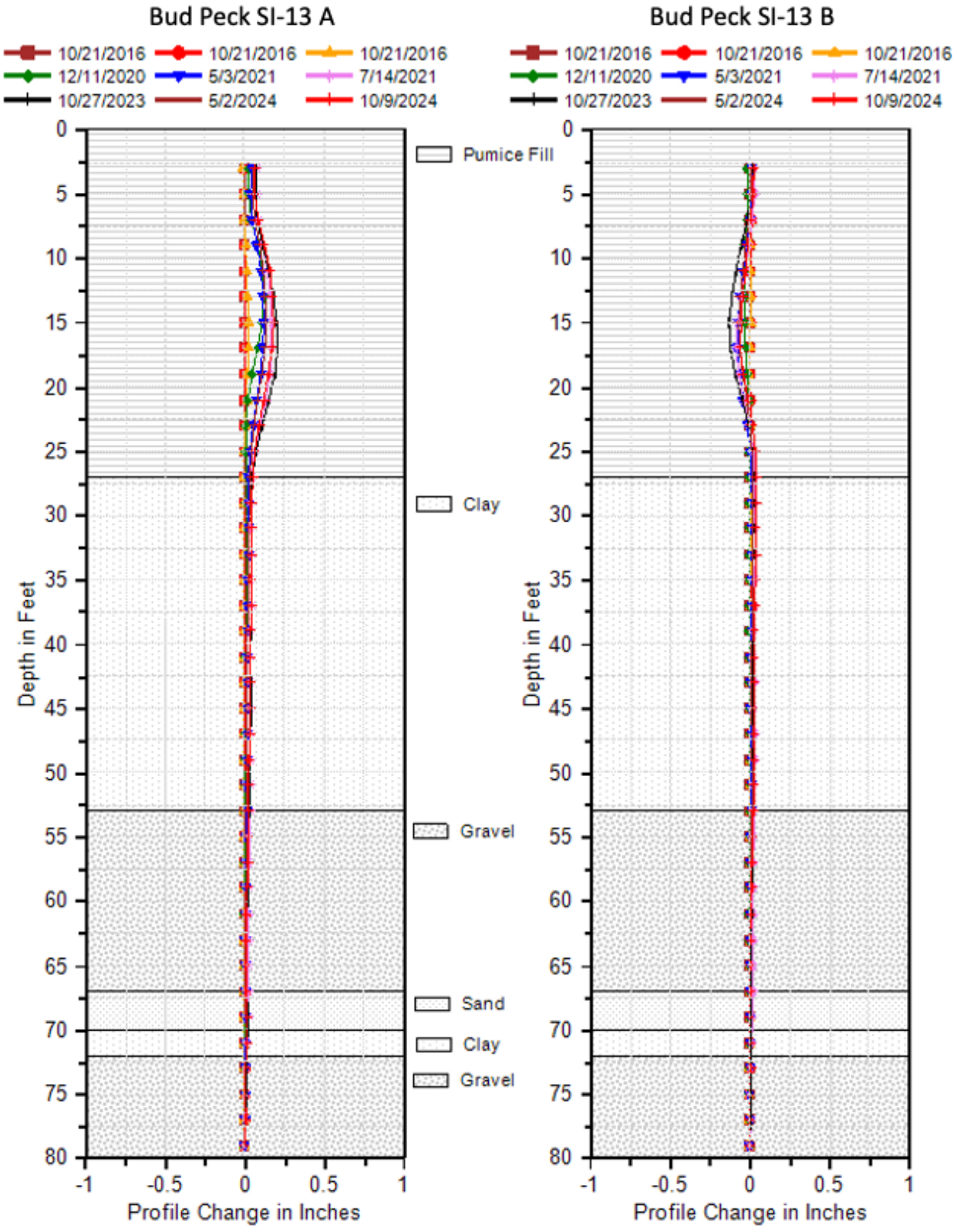

Figure A.20 Bud Peck SI-13 profile change and bore log data

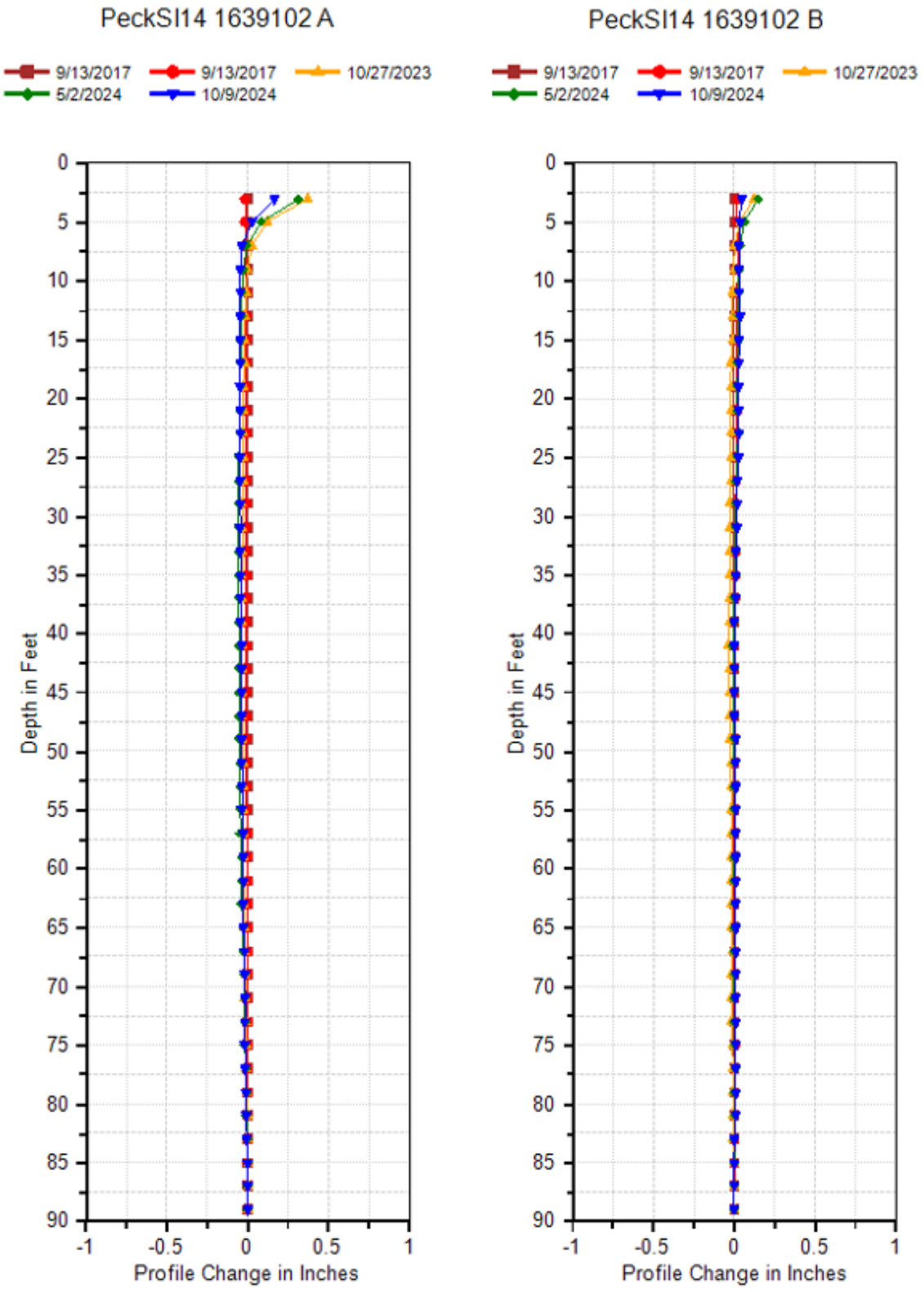

Figure A.21 Bud Peck SI-14 profile change data. Bore log data is absent

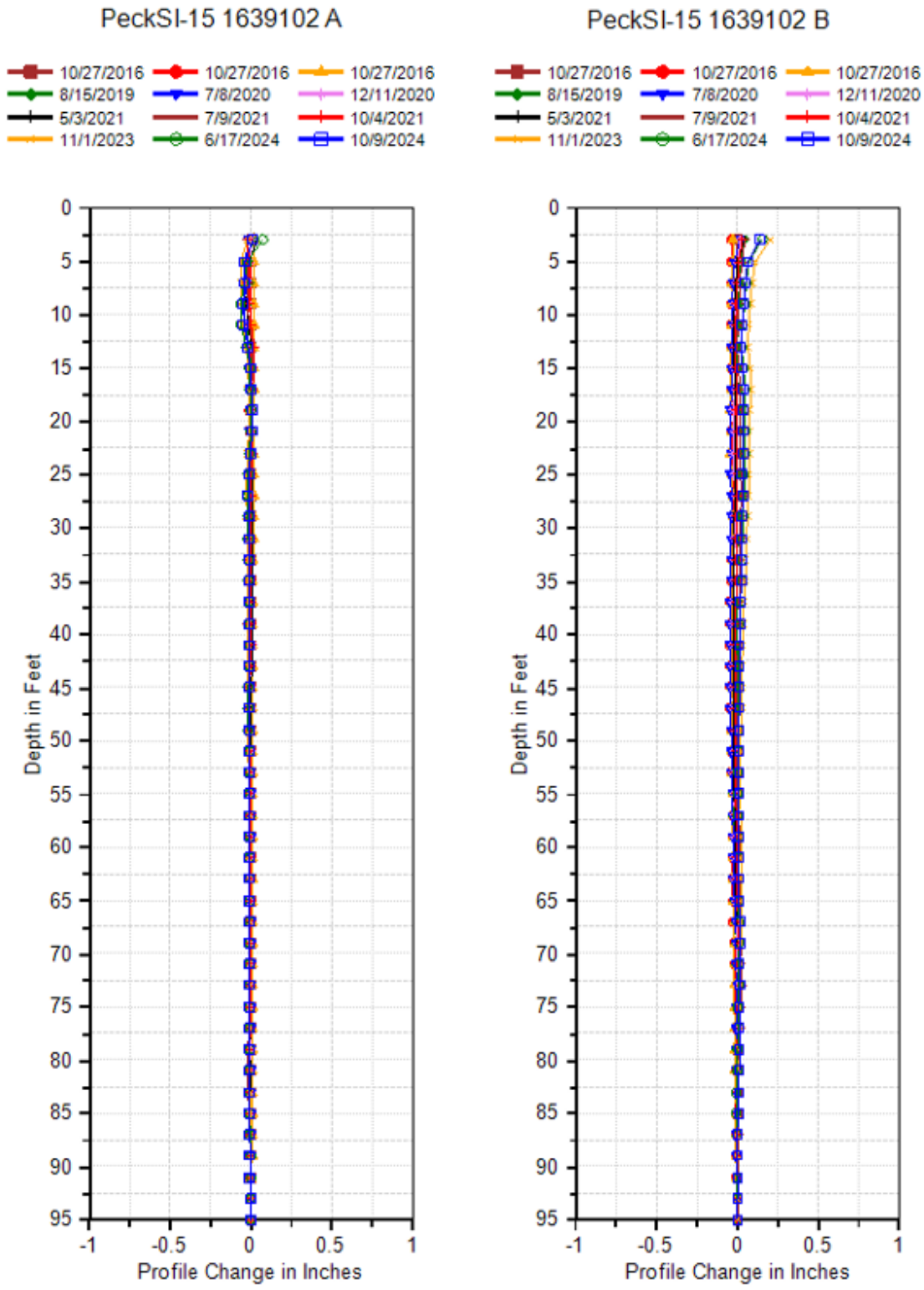

Figure A.22 Bud Peck SI-15 profile change data. Bore log data is absent

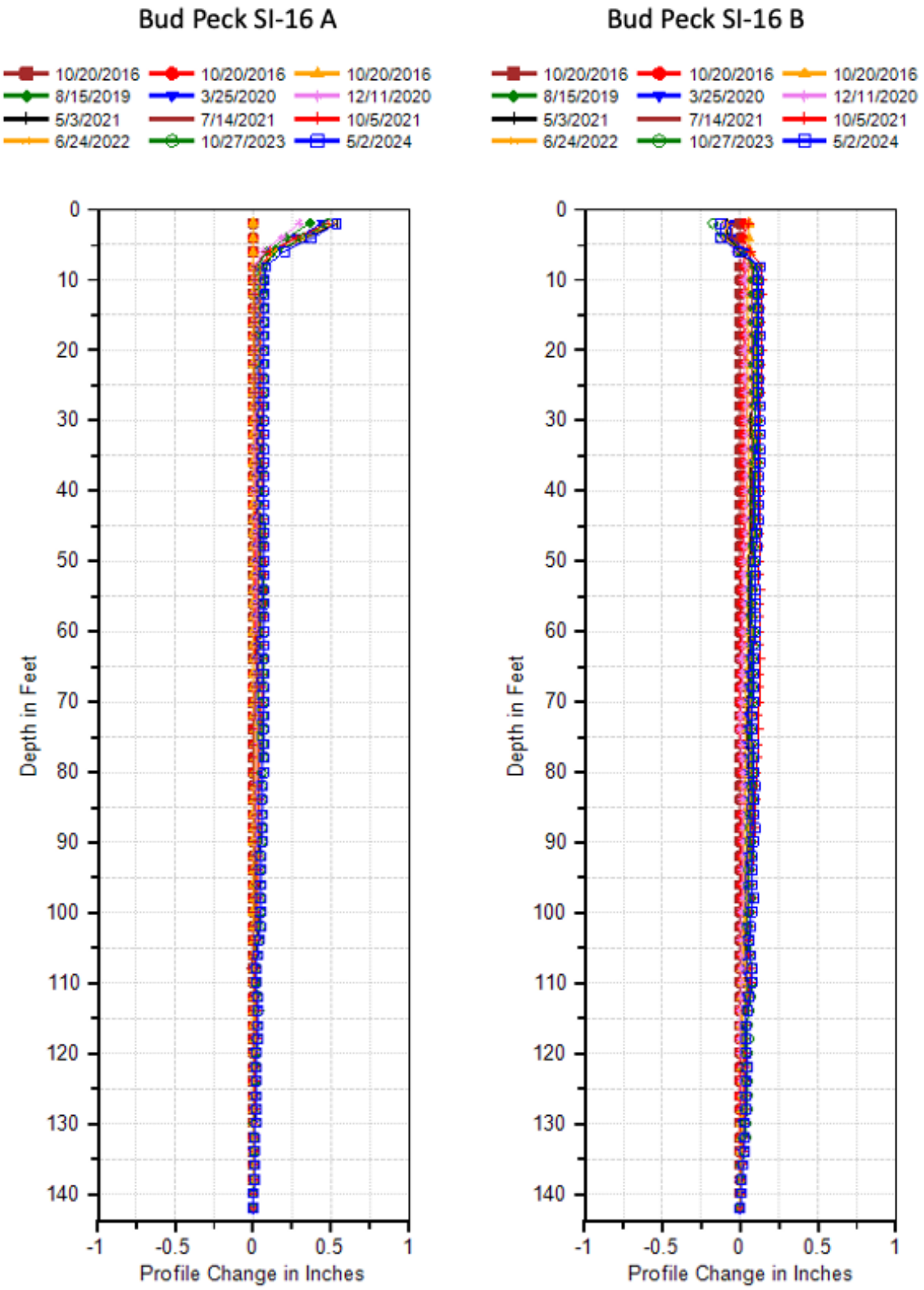

Figure A.23 Bud Peck SI-16 profile change data. Bore log data is absent

State Highway 33 Inclinometer Plots

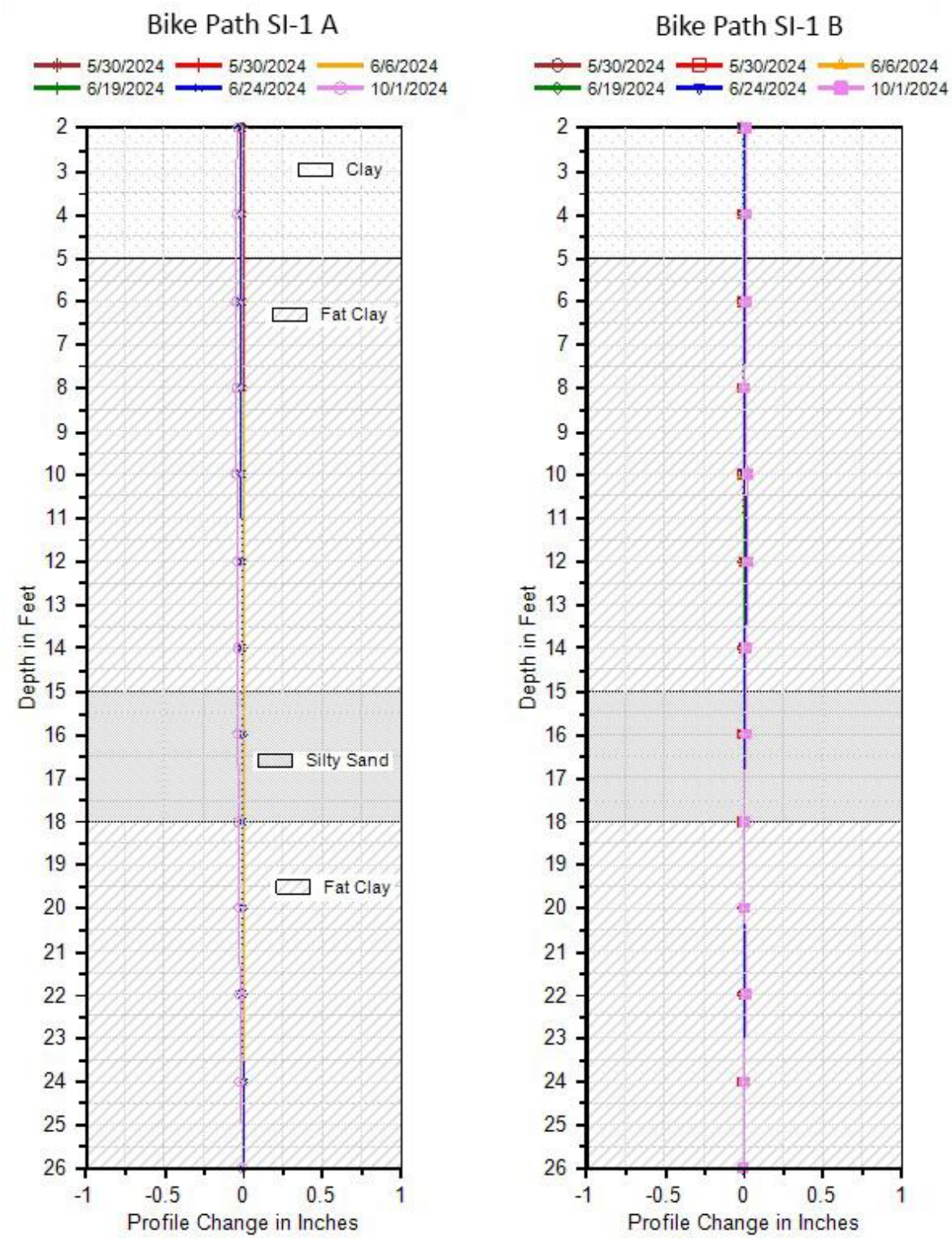

Figure A.24 State Highway SI-1A profile change and bore log data

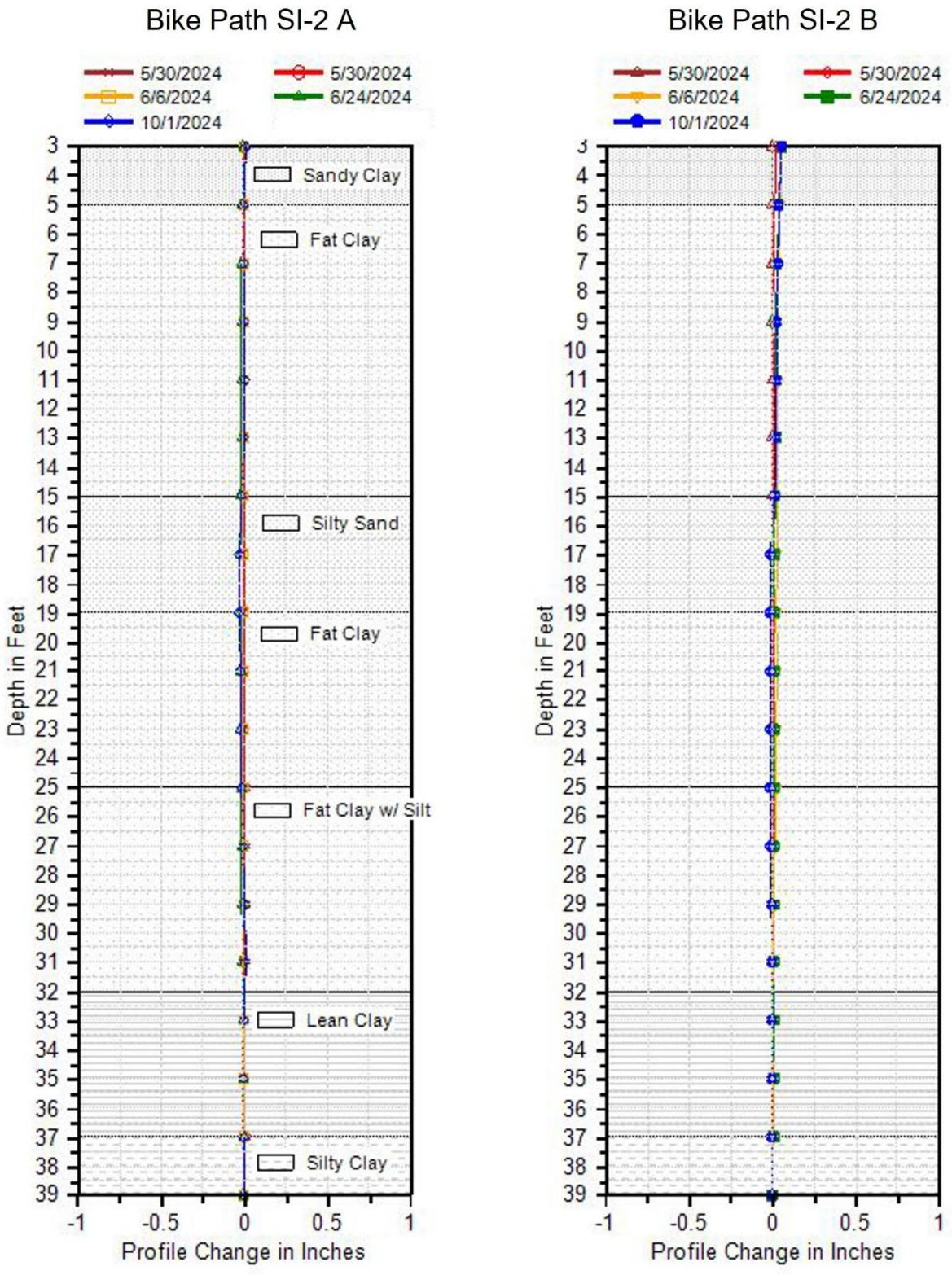

Figure A.25 State Highway 33 SI-2A profile change and bore log data

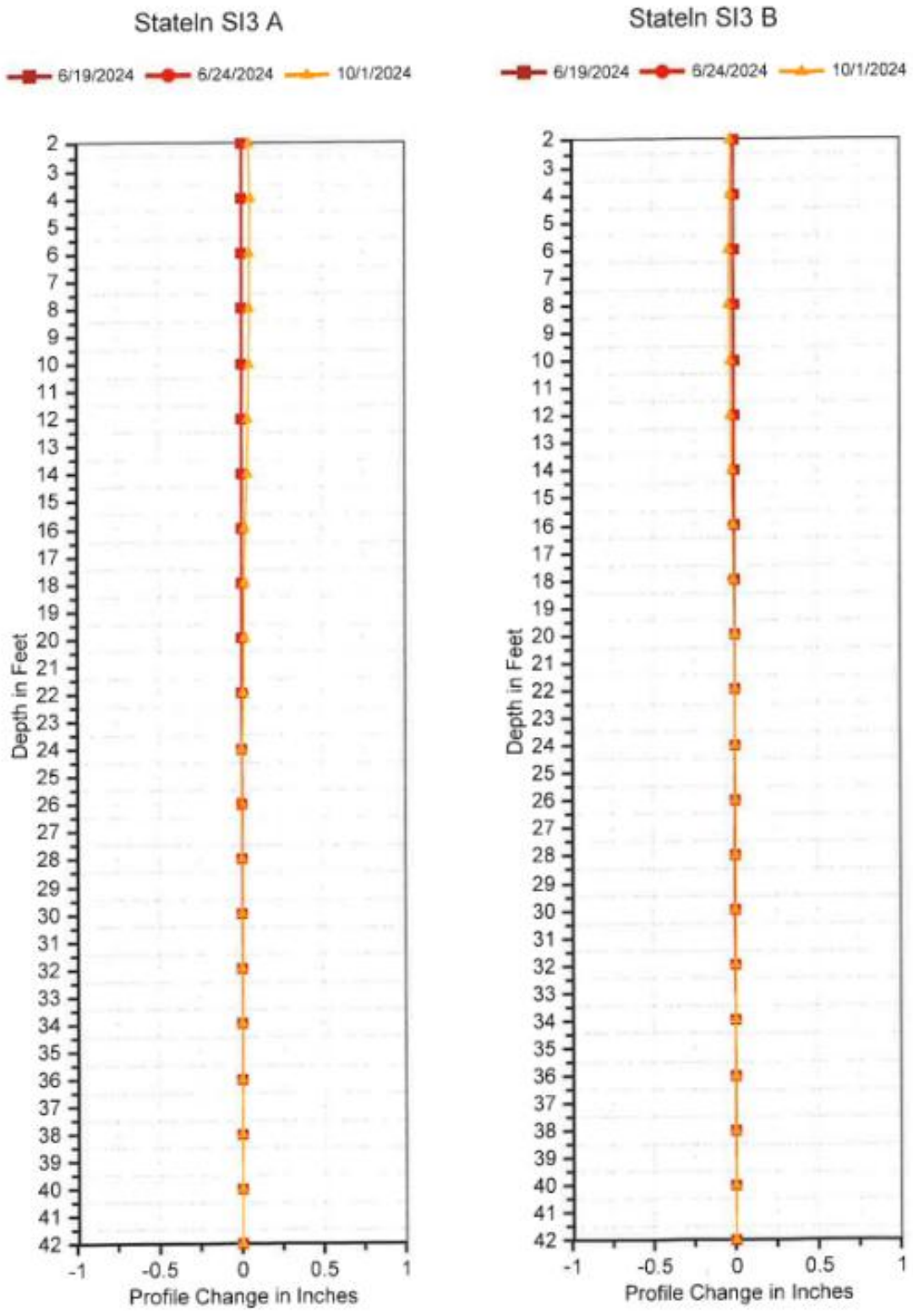

Figure A.26 SI-3 State Line Landslide Path

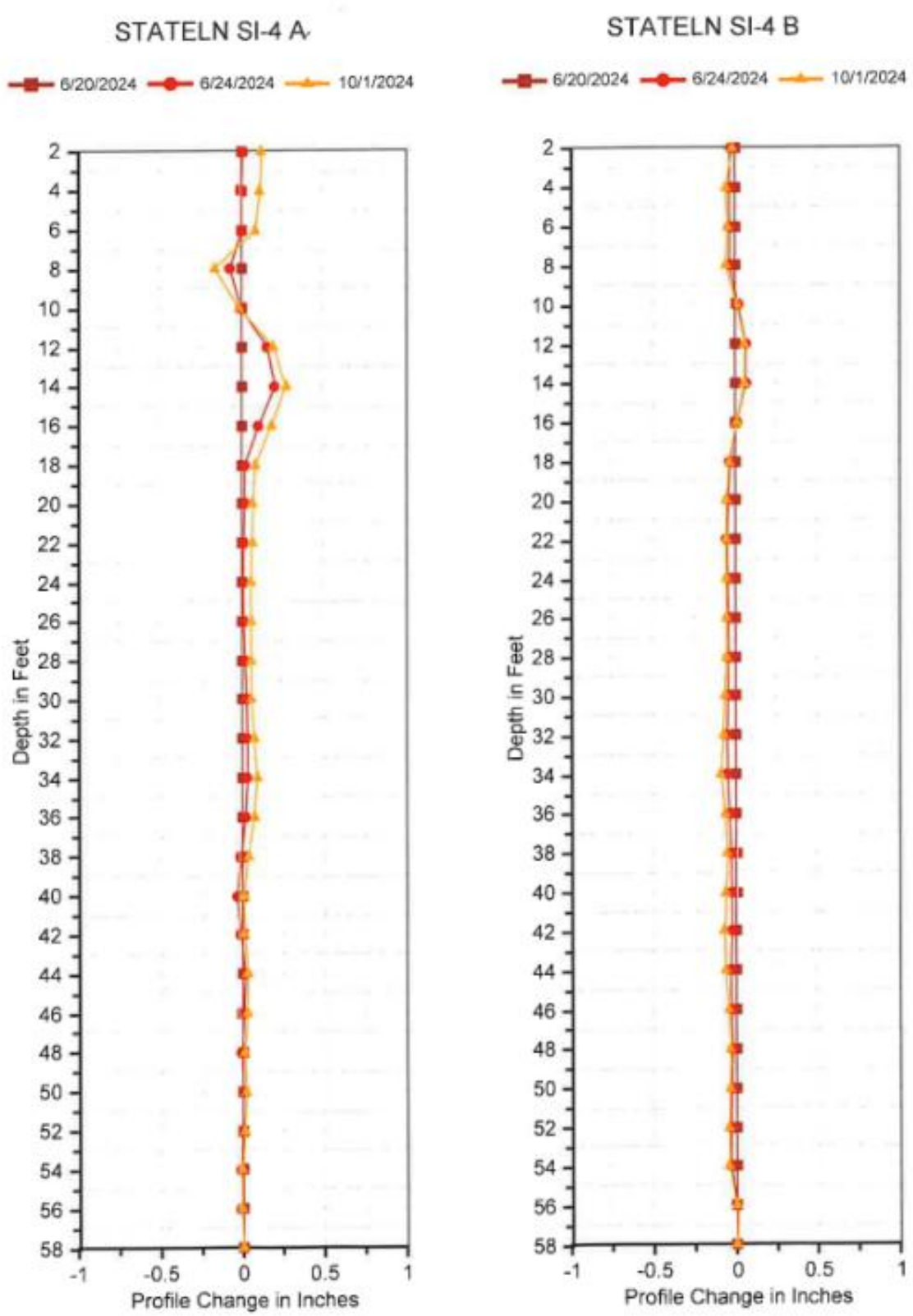

Figure A.27 SI-4 State Line Landslide Path

Appendix B. Change Detection Comparisons

Indian Creek Landslide Complex

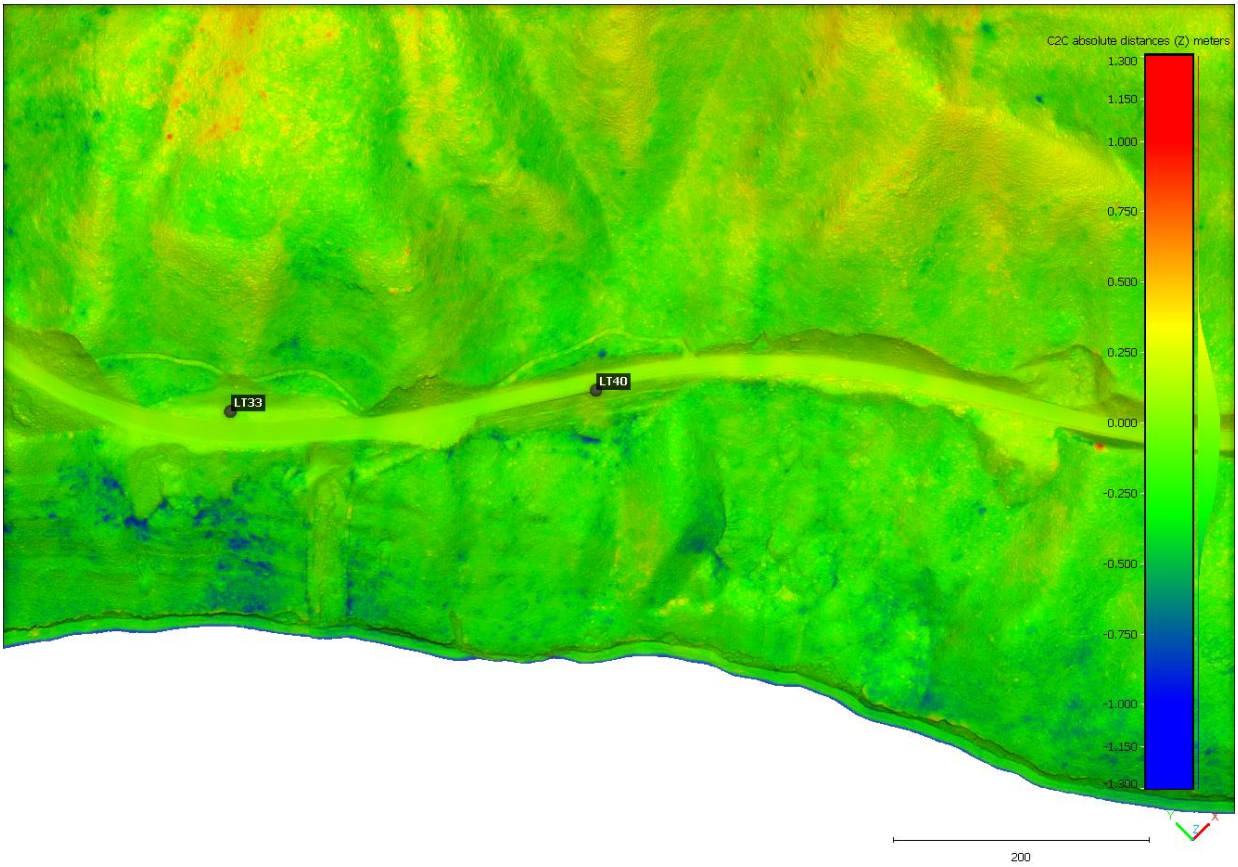

Figure B.1 LT 33 and LT40 Change Detection (LiDAR Spring 2024/Fall 2024)

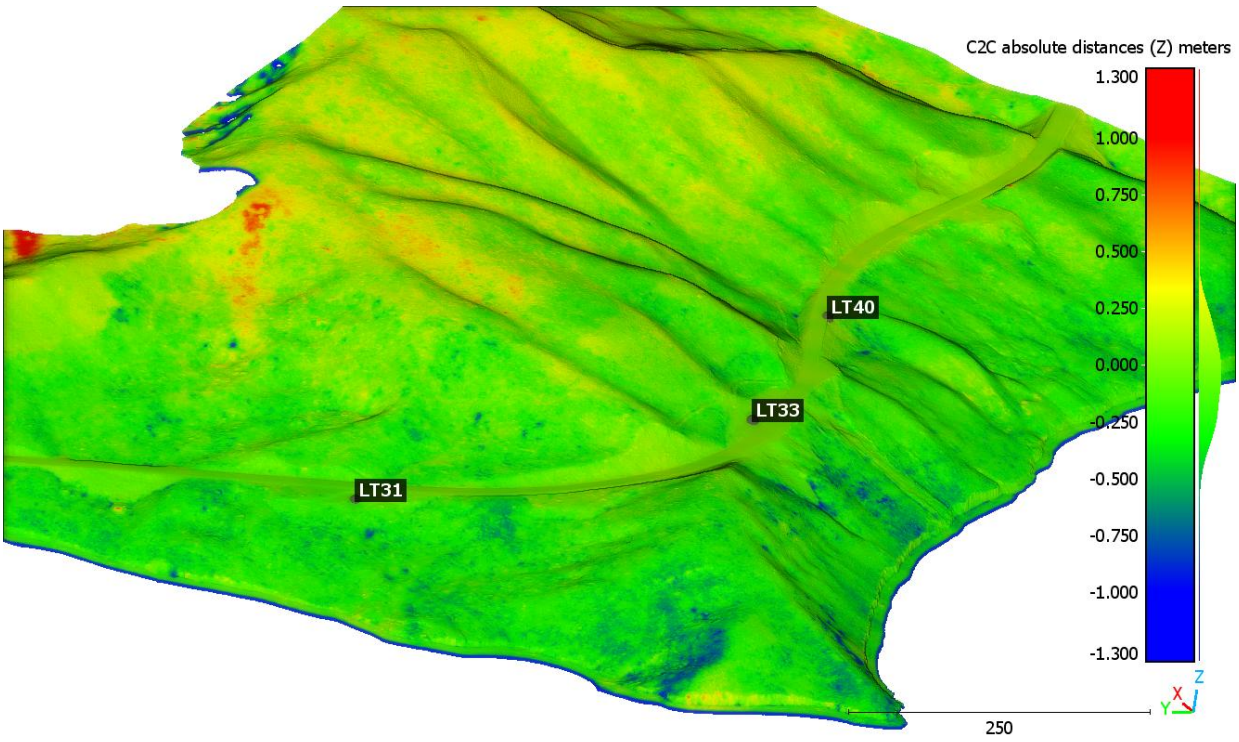

Figure B.2 Change Detection LiDAR Spring 2024/Fall 2024

Appendix C. Summary of UAS Platform, Sensor, Computer Hardware and Software used in this Study

Unmanned Aircraft System Platform for LiDAR that is NDAA compliant:

- Quantum Trinity Pro with Qube 240 LiDAR and D2M Oblique Camera

Computer Hardware:

- Intel i9 9900K CPU @ 3.6 GHz
- 256 GB RAM
- 4 TB SSD internal drive
- 20TB of server drive processing and storage
- Nvidia GeForce RTX 2080 Ti Graphics card with 16 GB RAM

Computer Software for Data Processing and Analysis:

- BayesStripAlign v. 2.25 (Bayes Solutions)
- Agisoft Metashape v. 2.2.0
- CloudCompare v. 2.13.2 (General Public License software)
- LASTools v. 2.0.2 (rapidlasso)
- ArcGIS Pro v.3.2 to 3.4 (Esri)